UNIVERSITÀ
DEGLI STUDI
DI PADOVA

Administrative unit: **University of Padova**

Department: **Land, Environment, Agriculture and Forestry (LEAF)**

---

PhD Program: **Land, Environment, Resources and Health (LERH)**

Batch: 30th

# SCALE DEPENDENCE OF HYDROLOGICAL EFFECTS FROM DIFFERENT CLIMATIC CONDITIONS ON GLACIERIZED CATCHMENTS

**PhD Programme Coordinator:** Ch.mo Prof. Davide Matteo Pettenella

**Supervisor:** Ch.mo Prof. Giancarlo Dalla Fontana

**Co-Supervisor:** Ch.mo Dott. Luca Carturan

**PhD candidate**: Fabrizio De Blasi

UNIVERSITÀ
DEGLI STUDI
DI PADOVA

Sede Amministrativa: Università degli Studi di Padova

Dipartimento: **Territorio e Sistemi Agro-Forestali (TESAF)**

---

CORSO DI DOTTORATO DI RICERCA: **Land, Environment, Resources, Health (LERH)**

Ciclo: 30°

# EFFETTO DI SCALA SULLA RISPOSTA IDROLOGICA DI BACINI GLACIALIZZATI IN DIFFERENTI CONDIZIONI CLIMATICHE

**Coordinatore:** Ch.mo Prof. Davide Matteo Pettenella

**Supervisore**: Ch.mo Prof. Giancarlo Dalla Fontana

**Co-Supervisore**: Ch.mo Dott. Luca Carturan

**Dottorand**o: Fabrizio De Blasi

# Index

## Abstract

The high altitude environments are particularly sensitive to climate change and very rapid and intense effects are affecting the Alpine cryosphere. Knowledge of the hydrological responses of high-altitude watershed is critical to manage water resources, especially in the context of current climate change, resulting in a lower percentage of solid precipitation, temporal redistribution and quantitative variations in precipitation inputs, higher temperatures, and more persistent drought conditions during the summer. Although the remaining glacial masses are still able to secure sufficient water supplies, the rate of reduction of the glaciers, however, is now very rapid. Mountain glaciers have generally experienced worldwide retreat since the second half of XIX Century, and for example in the Alps they lost about two/thirds of the initial area, with area loss rates accelerating since 2003. At this pace, the hydrological buffering effect of the glaciers will run out quickly. Several years in the last decades, which have been particularly warm and dry, have shown that glaciers can compensate scarce rainfall with a significant contribution to the runoff of rather large basins, especially in summer.

The aim of this work was to understand how different climatic and glacier cover conditions can modify the hydrological response of glacierized catchments, and to analyze the scale dependency of the hydrological response and the resulting impacts on fresh water availability.

The investigations were carried out in the Noce catchment, a 1050 $km^2$ watershed located in the Eastern Italian Alps, and in three sub-catchments of the same basin, with area ranging from 8 to 385 $km^2$ and different percent glacierization. Valuable information on past and current evolution of climate and glaciers exist in this study area. In particular, precious data series of high-altitude meteorological and hydrometric data, reconstructions of glacier fluctuations since the Little Ice Age, and measurements of glacier mass balance were available. Based on this availability, and considering the high uncertainties affecting model studies that use future projections of climate and glaciers, we decided to do a sensitivity analysis based on past observations. This approach has the advantage of analyzing the sensitivity of the glacio-hydrological system of the study area under actually observed climatic and glacier cover conditions, likely reducing the main source of error caused by model approaches based on future projections. Moreover using real observations has the potential of increasing the internal consistency of the glacio-hydrological model employed in this sensitivity analysis, during calibration and validation. A drawback of this method is that it does not take into consideration future change in climate and glacier cover. For this reason, we analyzed also a condition with complete absence of glaciers, and recent ‘extreme’ years, like 2003, that has been frequently referred to as a possible example of future climatic conditions during summer in the Alps.

The results of this study confirm previous research that indicate a progressive transition from a glacial to a nival hydrological regime in the analyzed catchments, with a tendency to a strong decrease in runoff after the seasonal snow has melted, in the second half of summer. The runoff peak tends to shift from mid- to early summer. Different glacier cover scenarios (LIA, current and absence of glaciers) have highest impacts in August runoff, during periods of glacier wastage as in the 1940s and in the 2000s, and in the smaller catchments with high

percent glacierization. Compared to the absence of glaciers, current glaciers still ensure higher runoff during summer, in all climatic conditions considered. However, this glacier damping effect is largely decreased if compared to the LIA conditions, and this decrease is directly related to catchment area. If smaller and highly glacierized catchment still preserves ~50% of the initial damping effect in August, the larger catchments keep only 25-30% of it. The glacier contribution to late summer runoff decreases obviously from headwater to lower and larger catchments. However, the decreasing rate tends to flatten for catchment area larger than 80 $km^2$, and for the larger analyzed catchment it still reaches 26%. Most importantly, the current glacier contribution to late summer runoff in the larger catchment reaches ~60% in extremely warm and dry summers, like in 2003. However, increased runoff due to glacier wastage in 2003 occurred only in the headwater and most glacierized catchment, whereas using the LIA glacier cover would have ensured increased runoff in all analyzed catchments. This suggests that the expected peak in runoff under warming climate, attributable to glacier melt, has already passed in the study area.

## Riassunto

Gli ambienti d'alta quota sono particolarmente sensibili ai cambiamenti climatici ed effetti molto rapidi ed intensi interessano la criosfera alpina. La conoscenza della risposta idrologica dei bacini d'alta quota è un aspetto chiave nella gestione della risorsa idrica, specialmente nell'attuale contesto di variazione climatiche. Attualmente assistiamo ad una minor percentuale di precipitazioni solide, una redistribuzione temporale e variazione nelle quantità delle precipitazioni, temperature più alte e periodi di siccità estiva più frequenti. Nonostante i rimanenti ambienti nivo-glaciali riescano ancora a garantire sufficienti apporti idrici, il tasso di riduzione dei ghiacciai attuali è molto rapido. I ghiacciai d'alta quota a livello mondiale hanno cominciato a ritirarsi dalla seconda metà del XIX secolo. Le Alpi, ad esempio, hanno perso circa due terzi della superficie glaciale iniziale, accelerando il tasso di perdita dal 2003. A questo ritmo la capacità dei ghiacciai di tamponare le fluttuazioni del regime idrologico, determinate dal clima, si esaurirà rapidamente. Negli ultimi decenni, diversi anni particolarmente caldi e secchi hanno dimostrato come i ghiacciai possano compensare le scarse precipitazioni con un significativo contributo ai deflussi in bacini piuttosto estesi specialmente in estate.

Il duplice obbiettivo di questo lavoro è quello di capire come condizioni climatiche ed estensioni glaciali differenti possano modificare la risposta idrologica di bacini alpini glacializzati, e analizzare l'effetto di scala della risposta idrologica nonché l'impatto sulla disponibilità idrica.

Le indagini sono state effettuate nel bacino idrografico del fiume Noce, uno bacino di 1050 $km^2$ situato nelle Alpi italiane orientali, e in tre sottobacini del medesimo spartiacque con aree comprese tra 8 e 385 $km^2$ e differenti percentuali di glacializzazione. Relativamente a quest'area esistono informazioni preziose sull'evoluzione passata e attuale sia dal punto di vista climatico che glaciale. In particolare, sono disponibili rare serie di dati meteorologici ed idrometrici ad alta quota, ricostruzioni delle oscillazioni dei ghiacciai sin dalla Piccola Era Glaciale (PEG) e misure di bilancio di massa glaciale. Sulla base di questi dati, e considerando le elevate incertezze degli studi modellistici che utilizzano scenari futuri di evoluzione del clima e dei ghiacciai, abbiamo effettuato un'analisi di sensibilità basata sulle osservazioni passate. Questo approccio ha il vantaggio di analizzare la sensibilità del sistema glacio-idrologico dell'area di studio in condizioni climatiche e di copertura glaciale effettivamente osservate, riducendo così la principale fonte di errore causata da approcci modellistici che si basano su proiezioni future. Inoltre, sfruttando osservazioni reali, questo approccio è in grado di aumentare la coerenza interna della modellazione glacio-idrologica qui implementata sia in fase di calibrazione che di validazione. Un inconveniente di questo metodo è che non tiene in considerazione i cambiamenti futuri del clima e delle estensioni glaciali. Per sopperire a questa mancanza, abbiamo deciso di analizzare anche una situazione di completa assenza di copertura glaciale, nonché alcuni anni recenti considerati meteorologicamente "estremi", come ad esempio il 2003 che è stato spesso indicato come possibile esempio di condizioni climatiche future durante l'estate.

I risultati di questo studio confermano le precedenti ricerche che indicano una progressiva transizione dei bacini analizzati da un regime glaciale a uno nivo-idrologico, con una tendenza di rapida decrescita dei deflussi nella seconda parte dell'estate dopo la fusione

della neve stagionale. I risultati dimostrano inoltre che il picco di deflusso tende ad essere anticipato, spostandosi da metà a inizio estate. Durante i periodi di maggior fusione dei ghiacciai, come negli anni ’40 e 2000, e nei bacini più piccoli con elevata percentuale di glacializzazione, i diversi scenari di copertura glaciale (PEG, attuale e assenza di ghiacciai) hanno forti impatti nei deflussi nel mese di agosto. Rispetto ad un’assenza di copertura glaciale, i ghiacciai attuali garantiscono ancora elevati deflussi durante l’estate in ogni condizione climatica considerata.

Tuttavia, questo effetto tampone dei ghiacciai è in gran parte diminuito se confrontato con le condizioni di estensione durante la PEG, e questa diminuzione è direttamente correlata con l’estensione dei bacini considerati. Sebbene il bacino più piccolo e più glacializzato conservi ancora il 50% dell’effetto tampone iniziale in agosto, i bacini più grandi ne mantengono solo il 25-30%. Evidentemente, il contributo glaciale al deflusso tardo estivo diminuisce progressivamente passando dal bacino di testata ai bacini a quota inferiore ed estensione maggiore. Tuttavia, il tasso di decrescita tende ad appiattirsi per estensioni più grandi di 80 $km^2$, e raggiunge il 26% nel bacino più esteso tra quelli analizzati. Se si analizzano estati estremamente calde e secche, come il 2003, è particolarmente interessante notare che l’attuale contributo glaciale al deflusso tardo estivo del bacino più grande raggiunge il 60%. Tuttavia, un aumento del deflusso a causa della fusione glacio-nivale in condizioni come il 2003, si è verificato solo nel bacino di testata con la percentuale di glacializzazione più elevata, mentre l’estensione dei ghiacciai durante la PEG avrebbe assicurato, con le medesime condizioni meteorologiche, un aumento dei deflussi in tutti i bacini analizzati. Questo suggerisce che nell’area di studio il picco di portata attribuibile alla fusione dei ghiacciai, sotto l’influsso dell’attuale riscaldamento globale, si è già verificato.

# 1. Research synopsis

## 1.1. Research background and justification

The alpine cryosphere has high sensitivity to climatic variations, and response times are different in relation to different fields. Seasonal snow cover responds almost instantly to climatic variations, both in terms of thickness and duration. Glaciers have longer response times, and significant changes in their areal extent and volume usually indicate persistent climate change. The response of alpine permafrost is considerably more variable because its coverage is discontinuous and controlled by specific microclimatic conditions, especially if we consider the terrain near the lower limit of this phenomenon. In any case, the reaction times of permafrost are normally longer than those of glaciers. These three components (snow cover, glaciers and permafrost) stand as "intermediaries" between climate forcing and the hydrological responses of alpine catchments. This high sensitivity to climatic fluctuations and the many feedbacks that affect snow- and ice-dominated alpine watersheds can drastically affect the regimes of downstream rivers (Levermann et al., 2012; Gurtz et al., 2005).

Knowledge of the hydrological responses of high-altitude watershed is critical to manage water resources (Barnett et al., 2005; European Environment Agency, 2009; Beniston, 2010), especially in the context of current climate change, resulting in a lower percentage of solid precipitation, temporal redistribution and quantitative variations in precipitation inputs, higher temperatures, and more persistent drought conditions during the summer. These phenomena can reduce the extent of glaciers and the accumulation and duration of seasonal snow and change the thermal regime of permafrost (Solomon et al., 2007). At the moment, any remaining glacial masses can still ensure sufficient water supplies for human needs. The reduction rate of glaciers, however, is accelerating (Solomon et al., 2007), and effects on the runoff will soon become noticeable (Levermann et al., 2012; Gurtz et al., 2005). Recent years, which have been particularly warm and dry, have shown that the cryosphere can buffer scarce rainfall with increased runoff during the summer, even within relatively large basins. Consequently, we should analyse this “buffer” ability of the cryosphere under conditions of poor water availability.

Runoff regimes from mid-latitude mountain catchments, such as those in the European Alps, are dominated by the storage of snow during the cold season and runoff release during the spring and summer. The distinct modification of streamflow by glaciers is well-documented in the literature (Meier and Tangborn, 1961; Stenborg, 1970; Fountain and Tangbborn, 1985; Lang, 1986; Braithwaite and Olesen, 1988; Chen and Ohmura, 1990; Collins and Taylor, 1990; Hopkinson and Young, 1998). Hock et al. (2005) identified five characteristics of glacier discharge: i) unit discharge, ii) seasonal variations, iii) diurnal variations, iv) yearly variability and v) runoff correlation.

About unit discharge, Hock et al. (2005) noted that the total streamflow is reduced in years of positive glacier net balance, when water is withdrawn from the annual hydrological

cycle and stored in glaciers. The opposite occurs in years of negative glacier mass balance because water is released from long-term glacier storage, thereby increasing streamflow.

About seasonal variation, Hock et al. (2005) reported that most of the annual runoff in climatic regions that are subject to distinct accumulation and ablation periods is concentrated during the summer melting season, while runoff is negligible during the winter, when most precipitation is stored as snow. Kuhn and Batlogg (1998) found that the ratio of the maximum monthly runoff to the mean monthly runoff linearly increases with increasing glacierization above a 5% level. In contrast to snow-covered basins, which are subject to spring meltwater peaks, the seasonal glacier–meltwater runoff peak is delayed because of refreezing and firn saturation at the onset of melting. In addition, melt rates are generally higher during the summer because of the Sun's larger altitude angles, higher air temperatures and the lower albedo of ice compared to that of snow. Kaser (2007) found that higher glacierization ratios produce higher and later summer runoff peaks. From a hydrological perspective, glacier retreat indicates a negative storage change in the glacierized catchments, which correspondingly increases the flow of glacier-fed streams. However, if glacier retreat is sustained over a sufficient length of time, the streamflow regime shifts from a glacial regime to a more snowmelt-dependent regime, with a lower runoff peak that occurs earlier during the summer (Gurtz et al., 2005).

About diurnal variation of glacier discharge, Hock et al. (2005) noted that diurnal variations in glacier discharge are characterized by large diurnal fluctuations that are caused by the pronounced diurnal cyclicity in meltwater production. Daily peak discharges increase by up to several hundred percent of the daily minimum flows during precipitation-free days.

About year-to-year runoff variability, Hock et al. (2005) reported that glaciers tend to dampen annual streamflow variations, which is generally referred to as the glacier compensation effect (Lang, 1986), where ablation variations offset precipitation variations. Approximately 10% to 40% glacierization reduces the year-to-year variability to a minimum. This variability becomes larger at both higher and lower glacierization levels.

Finally, about runoff correlation, Hock et al. (2005) reported that runoff tends to be positively correlated with the temperature and negatively correlated with the precipitation with increasing glacierization, while glacier-free basins show a positive correlation between runoff and precipitation. Thus, glacier meltwater predominates over precipitation as a contributor to runoff in highly glacierized basins.

Distributed (or semi-distributed) modelling of the seasonal snow cover, glacier mass balance, and subsequent hydrological response at the basin scale presents some key challenges that must be adequately considered to realistically interpret responses to climatic variations. Some of the most significant issues include i) the genesis and evolution of the seasonal snow cover, ii) the role of wind and gravitational redistribution during accumulation, iii) the spatial distributions of rainfall and temperature, and iv) the extension of and variations in snow and ice cover.

In particular, implementing a specific hydrological model that can simulate the regimes of downstream rivers in snow- and ice-fed basins that are subject to different meteorological conditions with different ice-cover scenarios, is important because of the high

climate sensitivity of the components of the cryosphere (Barry, 2006; Haeberli, 2006; Haeberli et al., 2007) and the significant climate changes that are expected over the next several decades (IPCC, 2013; WGMS, 2012). One aspect that requires further investigation is the analysis of the relationship between changes in the cryosphere and runoff in basins with different sizes, altitudes and spatial distributions of its cryosphere components.

## **1.2.** State of knowledge on the research topic

High-altitude environments are particularly sensitive to climate change, and very rapid and intense effects affect the alpine cryosphere. Glaciers are the component of the cryosphere that are experiencing the most evident variations. Alpine glaciers are estimated to have lost 35% of their surface between 1850 and the 1970s, while another 22% was lost by the end of the 1990s (Paul et al., 2004; Zemp et al., 2008). Subsequent estimations quantified a further surface loss of approximately 9% from 1999 to 2010 (Paul et al., 2011). The deglaciation rate has been accelerating since 1980 with further intensification after 2003 (Huss et al., 2008; Farinotti et al., 2009). In many cases, the "dynamic" retreat to higher elevations have been replaced by “in situ” dissolution and the rapid fragmentation of the remaining glacial masses, which have been reduced to patches of dead ice (Paul et al., 2004; Carturan and Seppi, 2007; Carturan et al., 2015). This deglaciation process was not homogeneous, and differences have been observed even for glaciers within the same mountain group (e.g., Arck and Escher 1997; Chueca et al., 2007).

The topic of this PhD programme is to study the different climatic and glacier-cover conditions that can modify the hydrological response of glacierized catchments with increasing area. The state of knowledge on the research topic covers the following arguments:

a) Collection and management of nivo-meteorological and topographic datasets
b) Glacial mass-balance methods
c) Nivo-hydrological modelling
d) Climatic variations and cryosphere

In the next section, we summarize the state of the art of the above arguments.

### *1.2.a. Collection and management of nivo-meteorological and topographic datasets*

#### 1.2.a.1. Meteorological dataset

According to the WMO (IPCC, 2013), several steps must be taken during the collection and processing of meteorological data. These steps include i) the retention of information regarding how the data have been processed, validated and transmitted to the regional or central office from every single station, ii) quality-control procedures and iii)

homogeneity tests. These steps are vital to ensure both the accuracy of the observations and the validity of the resulting time series.

The most important step is to check the homogeneity of the time-series data. Homogenization involves making a time series homogeneous using a technique to remove artificial bias (IPCC, 2013). According to the WMO (IPCC, 2013), homogeneity testing should be performed to ensure that any time fluctuations in the data are only caused by vagaries in the weather and climate. The temporal homogeneity of a climate record is essential in climatological research, particularly when data are used to validate climate models and satellite estimates or assess climate change and its associated environmental and socio-economics impacts.

Currently, about ten techniques exist for inhomogeneity detection and homogenization. Peterson et al. (1998) summarized the most widely used techniques.

Craddock (1979) developed the Craddock test. This test requires a homogeneous reference series, although sufficiently long homogeneous sub-periods are sometimes sufficient. The Craddock test accumulates the normalized differences between the test series and the homogeneous reference series according to the following formula:

*Equation 1*

$$s_i = s_{i-1} + a_i * (b_m/a_m) - b_i$$

where $a$ is the homogenous reference series, $b$ is the time series to be tested and $a_m$ and $b_m$ are the time series' means over the entire period.

Expert judgement by an experienced climatologist (Jones et al., 1986; Rhoades and Salinger, 1993) has been an important tool in many adjustment methodologies because this approach can modify the weights of various inputs based on many factors that are too labourious to programme. Expert judgement can be particularly helpful in an initial inspection of the stations' data and when the reliability of certain inputs (e.g., metadata) varies.

The Caussinus-Mestre method (Caussinus and Lyazrhi, 1997; Caussinus and Mestre, 1996; Mestre and Caussinus, 2001) simultaneously detects an unknown number of multiple breaks and generates reference series. This method is based on the premise that a time series is homogeneous between two breaks and that these homogeneous sections can be used as reference series. Each series is compared to others within the same climatic area by creating difference (temperature or pressure) or ratio series (precipitation). These difference or ratio series are tested for discontinuities. When a detected break remains constant throughout a set of comparisons between a candidate station and its neighbours, the break is attributed to the candidate station's time series. Recently, these authors developed a new technique that was based on a comparison among several perturbed series instead of comparing a series to an artificial reference. A two-factor linear model (time x series) was introduced for all series at any time, and a penalized likelihood procedure was created to select the best model. A stepwise approach was adopted to facilitate computation.

Another homogenization technique involves multiple analyses of series for homogenization (MASH). MASH (Szentimrey, 1996, 1999, 2000) does not assume that the reference series are homogeneous. Possible break points and shifts can be detected and

adjusted through mutual comparisons of series within the same climatic area. The candidate series is chosen from the available time series, and the remaining series are considered to be reference series. The roles of the various series repeatedly change during this procedure. Additive or multiplicative models are applied depending on the climatic elements. A newly developed multiple-break-point-detection procedure considers the problems of significance and efficiency. This test obtains the estimated break points and shift values and their corresponding confidence intervals. One advantage of this method is its ability to simultaneously homogenize monthly, seasonal and annual series. This method can automatically utilize metadata information, such as the probable dates of break points.

The multiple-linear-regression technique (Gullett et al., 1991; Vincent, 1998) is based on the application of four regression models to determine whether the tested series is homogeneous and has a trend, a single step, or trends before and/or after a step. The dependent variable is the series of the tested station and the independent variables are the series of a number of surrounding stations. The third model is successively applied for different locations in time to identify the position of a step, and the result with the minimum residual sum of squares represents the most likely position in time of a step in the tested series. This procedure consists of the successive application of four models (Vincent, 1998).

Potter's method (Plummer at al. 1995; Potter, 1981) is a likelihood ratio test between the null hypothesis that the entire series has the same bivariate normal distribution and the alternate hypothesis that the population before the tested year has a different distribution than the population after the year in question. This bivariate test closely resembles double-mass-curve analysis. One component of the tested statistic depends on all the points in a time series, while another component depends only on the points that precede the year in question. The highest value of the tested statistic is located in the year that precedes a change in the mean of the candidate station's time series. Potter (1981) applied this technique to ratio series of a candidate station's precipitation and a composite reference series.

The standard normal homogeneity test, or SNHT (Alexandersson and Moberg, 1997; Alexandersson, 1986; Hanssen-Bauer and Forland, 1994), is a likelihood ratio test. This test is performed on a ratio or difference series between the candidate station and a reference series. First, this series is normalized by subtracting the mean and dividing by the standard deviation. In its simplest form, SNHT contains variations to consider more than one discontinuity, test for inhomogeneous trends rather than only breaks, and include change invariances.

The stop-trend method (Kobysheva and Naumova, 1979) is a non-parametric test. Data are sorted by date and consecutive ranks are assigned. Next, the time series is split into $k = n^{0.5}$, where $n$ is the number of observations with size $l = (max - min)/k$, where max and min are the maximum and minimum values in the dataset. If the difference between consecutive ranks within each interval exceeds a critical level based on the Kolmogorov coordination criterion, the observation that corresponds to the first rank is labelled with "A" and the second with "B". Once all of the intervals have been evaluated, the "A" observation defines a breakpoint if two adjacent observations in the overall time series are flagged with "A" and "B".

Solow (1987) described a technique for detecting changes in the trend of a time series by identifying the change point in a two-phase regression, where the regression lines before and after the tested year are constrained to meet at that point. Changes in instruments can cause step changes; therefore, Easterling and Peterson (1995a, b) developed a variation of the two-phase regression method in which the regression lines are not constrained to meet and where a linear regression is fitted to the component of the (candidate-reference) difference series before the tested year and another after. This test is repeated for all the years in the time series (with a minimum of 5 years in each section), and the year with the lowest residual sum of squares is considered the year of a potential discontinuity.

Other tests to detecting inhomogeneities are the Mann-Kendall trend test (Mann, 1945; Kendal, 1970) and the Pettit test (Pettit, 1979). However, these tests does not provide a correction to apply to the raw inhomogeneous series First test is a non-parametric way to detect a trend in a series of values, and the second test is commonly applied to detect a single change-point in hydrological series or climate series with continuous data.

The above-mentioned techniques are currently the most widely used homogenization methods.

Managing meteorological data in snow- and ice-dominated alpine watersheds requires an additional processing step. According to Carturan et al. (2012), estimating precipitation inputs over high-altitude ungauged areas is a key issue for many fields that investigate mountainous catchments. Systematic measurement errors at precipitation gauges mainly result from the influence of wind. Under high wind speeds, which are common in mountainous settings, precipitation gauges disrupt the boundary-layer atmospheric flow, causing frozen precipitation to preferentially blow over and around, rather than into, the gauge (Goodison et al., 1998). Liquid precipitation is less susceptible to this under-catching problem because it is denser and has a higher falling velocity. Estimates of snowfall under-catching for some types of gauges are as high as 70% or greater (Yang et al., 1998, 2000). Other systematic errors when measuring precipitation include evaporation/sublimation, wetting losses from water that stakes inside the gauge, blowing snow, and the tendency of observers to ignore trace events (Sevruk, 1982; Legates, 1987; Hood et al., 1999). All of these systematic biases cause the underestimation of precipitation, with the exception of blowing snow, which can be recorded as “false” precipitation. Adam and Lettenmaier (2003) provided a useful summary of the relative magnitudes of these systematic errors. According to Sevruk (1985), the corrected amount of precipitation $P_k$ is given by

*Equation 2*

$$P_k = k\left(P_g + \Delta P_{wl}\right)$$

where $k$ is the correction factor from the wind-field deformation above the gauge orifice, $P_g$ is the measured amount of precipitation and $\Delta P_{wl}$ are the wetting losses. The wetting losses depend on the ratio between the surface of the inner walls of the gauge collector and the orifice area $(S_w / S_0)$. The value of the parameter $k$ depends on the monthly wind speed, temperature, fraction of snow in the total precipitation, number of days with precipitation and

degree of gauge-site exposure. Based on these data, researchers can obtain the monthly values of correction factors for rain and snow, which are indicated as $K_{rain}$ and $K_{snow}$, respectively. This procedure was assessed by Carturan et al. (2012), who compared the calculated $K_{snow}$ at the Careser dam weather station (TN) to a $K_{snow\_we}$ (mean winter-season precipitation correction factor for snow) value that was derived from comparisons of raw gauge data with snow-water-equivalent observations at the same site:

*Equation 3*

$$K_{snow\_we} = \frac{\sum_{i=1}^{n} we_i}{\sum_{i=1}^{n} P_i}$$

where $n$ is the number of days with solid precipitation during the winter, $we_i$ is the i-th daily fresh-snow water equivalent (calculated from the fresh snow depth by means of the snow density based on Equation 4) and $P_i$ is the daily solid precipitation that is measured by the gauge. According to Carturan et al. (2012), the snow density can be calculated using the following relationship by La Chapelle (1961):

*Equation 4*

$$\rho(T) = 50 \quad with\ T \leq -15^{\circ}C$$

$$\rho(T) = 6.67\,T + 150 \quad with\ T > -15^{\circ}C$$

where $T$ [°C] is the mean daily air temperature, and $\rho$ [kg m$^{-3}$] is the fresh snow density.

According to Carturan et al. (2012), systematic errors in precipitation measurements may strongly affect areal precipitation estimation in high mountainous basins, particularly when the estimation method incorporates precipitation-altitude relationships to describe the effect of the orography, such as the PRISM method by Daly et al. (1994) and various techniques that use elevation as auxiliary data (e.g., Saghafian and Bondarabadi, 2008).

#### 1.2.a.2. Nivo-glacial dataset

Calculating the glacial mass balance requires collecting and processing a nivo-glacial dataset. This dataset is a representative set of points, which is usually represented by stakes in the ablation zone and surveys, snow pits and core samples in the accumulation area. The snow cover on different dates during the summer is an additional observation that is very useful to extrapolate the glacial mass balance during the ablation season.

#### 1.2.a.3. Topographic dataset

This research project uses two different techniques, namely, a Light Detection and Ranging (LiDAR) technique and photogrammetric technique, to create a topographic dataset of the snow and ice area.

According to the National Oceanic and Atmospheric Administration (NOAA), LiDAR is a remote-sensing method that uses light in the form of a pulsed laser to measure ranges (variable distances) to the Earth. These light pulses—combined with other data that are recorded by the airborne system— generate precise, three-dimensional information regarding the shape of the Earth and its surface characteristics. A LIDAR instrument principally consists of a laser, a scanner, and a specialized GNSS receiver. Airplanes and helicopters are the most commonly used platforms for acquiring LIDAR data over broad areas. Topographic LIDAR typically uses a near-infrared laser to map the land (NOAA). When an airborne laser is pointed at a targeted area on the ground, the beam of light is reflected by the surface that it encounters. A sensor records this reflected light to measure a range. When laser ranges are combined with position and orientation data from integrated GNSS and Inertial Measurement Unit systems, scan angles, and calibration data, the result is a dense, detail-rich group of elevation points, which is called a "point cloud." Each point in the point cloud has three-dimensional spatial coordinates (latitude, longitude, and height) that correspond to a particular point on the Earth's surface from which a laser pulse was reflected (NOAA). These point clouds are used to generate other geospatial products, such as digital elevation models, canopy models, building models, and contours (NOAA).

Recent technological improvements in the field of image analysis and computer vision have prompted the development of a low-cost digital photogrammetric approach, which is referred to as structure-from-motion (SfM) (Piermattei et al., 2015). Combined with dense image-matching algorithms, this method has become competitive for the production of high-quality 3D models. However, several issues from this approach should be considered for application in glacial environments. In particular, the surface morphology, the different substrata, the occurrence of sharp contrasts from solar shadows and the variable distance from the camera positions can negatively affect the image’s texture and reduce the possibility of obtaining a reliable point cloud from the images (Piermattei et al., 2015). Several tools and methods exist to obtain information regarding the 3D geometry of scenes from 2D views with techniques from the field of photogrammetry (Verhoeven et al., 2012). This technique has been extensively applied in geomorphology (Lane et al., 1993; Chandler, 1999) and multi-temporal analysis (Stojic et al., 1998; Lane et al., 2003; Lim et al., 2005). In the field of glaciology, photogrammetry has provided an efficient method to quantify changes in glacier surfaces and mass balance (Welch and Howarth, 1968; Kääb and Funk, 1999; Fox and Gooch, 2001; Baltsavias et al., 2001). However, the use of traditional photogrammetric techniques requires specialized training and equipment (Karpilo, 2009). An emerging low-cost and straightforward photogrammetric method that is based on SfM and dense-image-matching algorithms represent the latest development in which imagery has been employed for spatial measurements in earth science and specifically geomorphology (Piermattei et al., 2015). This method is based on overlapping digital images from different positions to ensure the convergence of camera orientations on the scene (James and Robson, 2012). This approach differs from conventional photogrammetry because the geometry of the scene and the camera positions and orientations are automatically solved by the SfM software. The application of close-range photobased reconstructions of glacial and periglacial environments is currently limited and principally involves the employment of Unmanned Aerial Vehicles (UAV) for image acquisition (Solbø and Storvold, 2013; Whitehead et al., 2013; Immerzeel et al., 2014, Tonkin et al., 2014)

rather than ground-based surveys (Gómez et al., 2014; Piermattei et al., 2015). Permanent camera stations can be arranged on site and used to accurately determine local deformation and the movement of glacier surfaces. Kääb et al. (2013) tested the time-lapse SfM approach to measure vertical and horizontal changes in periglacial circles.

### *1.2.b. Glacial mass-balance methods*

The mass balance at any point on a glacier is the mass variation over a given time interval, specifically, the algebraic sum of accumulation and ablation. Normally, the mass balance refers to an annual period between two successive moments of a minimum balance. These moments generally correspond to the end of the ablation season, when the so-called summer surface is formed. This surface is usually a layer that is rich in impurities, with a surface crust with clear differentiations in the density, shape and size of the crystals compared to the superimposed snowpack layers during the subsequent season of accumulation.

The maximum balance value during the year is called the winter balance ($b_w$). The time at which this maximum point is attained (i.e., the end of the accumulation period) divides the year of balance into a winter season and summer season. The variation in the mass that occurs during the summer is called the summer balance ($b_s$). The net balance ($b_n$) is the variation in mass during a year of balance and can be expressed as the sum of the winter balance and summer balance or as the sum of the total accumulation ($c_t$) and total ablation ($a_t$):

*Equation 5*

$$b_n = b_w + b_s = c_t + a_t$$

All of the values are normally expressed as heights of water-equivalent millimetres or metres (w.e. mm or w.e. m). The net balance can be positive or negative because of prevailing accumulation or ablation. The total accumulation and total ablation are not the same as the winter balance and summer balance because the processes of accumulation and ablation may occur during any season. The literature introduced the concept of winter balance and summer balance for practical reasons because the total accumulation and total ablation are virtually impossible to directly measure (Østrem and Brugman, 1991). The winter balance ($b_w$) and summer balance ($b_s$), which are measured at individual points, are subsequently integrated over the entire glacier surface. The terms that refer to the entire glacier are similar to those for the individual points but are presented with capital letters ($B_w, B_S, B_n$). These variables are normally expressed in volumetric terms, usually as millions of cubic metres of water. However, the size that is normally used to express annual (or seasonal) variations in glacial mass is the average balance ($b_w, b_S, b_n$), which is obtained from $B_n/\,S$ ($B_s/\,S,\ B_w/\,S$), where $S$ is the area of the glacier.

Currently, four methods exist to calculate the glacial mass balance: i) the direct glaciological method, ii) geodetic method, iii) hydrological method, and iv) reconnaissance methods.

#### 1.2.b.1. Direct glaciological method

This method is the only method that is based on in situ measurements. The balance is measured at a representative set of points, which are usually represented by stakes in the ablation zone and surveys, snow pits, and core samples in the accumulation area. The balance is measured to determine the level variations in the surface between two dates. The level variation, which is multiplied by the density of the material that is affected by the variation (snow, ice or firn), provides the balance at that point. The density of the ice is assumed to be constant and equal to 900 kg $m^{-3}$. The density of the snow and firn is measured by sampling snow pits or coring from the surface. The point measurements are then extended to the entire surface of the glacier. The relationship between the balance and altitude is useful to spatialize measurements. Alternatively, mapping the balance by hand or with GIS software is useful. The snow cover on different dates during the summer is an additional observation that is very useful to extrapolate the point balance. The direct glaciological method is the most accurate method, although challenging in terms of costs, logistics and the required time for the acquisition and processing of data (Østrem and Brugman, 1991; Kaser et al., 2003).

#### 1.2.b.2. Geodetic method

The geodetic method requires the detection of variations in the height by topographic surveys. The main limitation is that this method cannot establish the spatial distribution of the balance on the glacier, which occurs because the glacier is in motion and the moving vectors are not parallel to its surface. Consequently, fictitious subsidence occurs in the accumulation area and fictitious elevations occur in the ablation zone. Furthermore, the continuous compaction of layers of snow and firn occurs in the accumulation zone with an additional reduction that does not necessarily indicate a loss of mass. The estimation of the density of ice, snow and firn is another limit when obtaining the actual change in mass from the volumetric change. This method is commonly used in combination with other methods for validation or to determine variations in the mass of multi-annual intervals.

#### 1.2.b.3. Hydrological method

This method measures the terms of the water balance and calculates the balance with the following relationship:

*Equation 6*

$$B_n = P - R - E$$

where $P$ is the precipitation, $R$ is the runoff and $E$ is the evaporation. The main limitation of this method involves the difficult evaluation of the spatial distribution of precipitation, this method's inaccurate estimation of the evaporation, and the possible presence of temporary accumulations of water inside the glaciers.

#### 1.2.b.4. Reconnaissance methods

These methods are based on observations of Equilibrium Line Altitudes (ELA) at the end of the melting season on the surface of the glacier. While not an accurate result, the trend of the annual balance is estimated based on the ratio of the area of accumulation and the total area (AAR). A more accurate estimation can be conducted with a series of mass balances from the direct glaciological method because a clear correlation between the balance and share of the equilibrium line exists. Conversely, estimates of glaciers without balance measurements are much more inaccurate (Braithwaite, 1984).

The direct glaciological method, although requiring certain costs and a significant logistical and organizational commitment, is recognized as the most suitable method for long-term measurements of glacial mass balance. Currently, this method is the international reference standard. Every two years, the World Glacier Monitoring Service, which is organized by the International Association of Hydrological Sciences (IAHS), the United Nations Environment Programme (UNEP) and the United Nations Educational, Scientific and Cultural Organization (UNESCO), collects and publishes the measured mass balances from this method for a significant sample of glaciers worldwide (Haeberli et al., 2003). Other methods are used if direct measurements are impossible to obtain or to verify direct measurements. Indeed, combining two or more methods is useful to determine the reliability of long-term results.

### *1.2.c. Nivo-hydrological modelling*

The distributed modelling of the mass balance is very interesting from practical and scientific perspectives because this process improves the knowledge of the processes and predicts the evolution of the ice and snow resources in response to possible future climate scenarios. Distributed modelling is also an important component in the monitoring of glaciers because this method i) connects different types of observations (measurements of change fronts, mass-balance measurements, and cadastres of glaciers) and ii) extrapolates these measurements in time and space (Machguth et al., 2006b). Paul et al. (2007) recommended reconsidering the traditional techniques of extrapolating mass balance using mass-balance models alongside GIS software and techniques. The use of models to extrapolate point measurements from stakes and snow pits instead of simple regressions with altitude can produce more realistic profiles of the mass balance. Indeed, models are the only approach to consider the variability of the local topography and its influence on the distribution of accumulation and ablation (Arnold et al., 2006).

The complexity of modelling should be related to the aims of the modelling and the desired spatial and temporal resolution in the simulations (Hock and Jansson, 2005). However, the main limitation in the modelling of glacial and snow mass balance is the availability and quality of input meteorological variables. In addition, the availability and good quality of the input data can contrast with the extreme spatial and temporal variability of climatic conditions and accumulation and ablation processes. Therefore, an efficient model must i) produce satisfactory results when using only normally available input data (which usually include temperature, precipitation and digital terrain models - DTM) and ii) capture

the dominant processes that govern the exchanges of energy and mass within snow and glaciers. Accumulation can involve i) the horizontal and vertical gradients of precipitation and ii) the redistribution of wind and avalanche snow. On the other hand, ablation is mainly controlled by i) the vertical lapse rate, ii) the cooling effect of glaciers, iii) the albedo, iv) the cloud cover, and v) the variations in the relative importance of the energy-balance components at different altitudes. Much of the research carried out until now on the glaciers covered energy flows and the processes of ablation. However, accumulation processes have been less frequently studied, probably because of a lack of an adequate experimental basis. Accumulation is frequently simulated by using only the vertical gradients of precipitation without considering the redistribution of snow. The result is a linear increase in accumulation with altitude, which does not occur in reality. In this regard, Machguth et al. (2006a) showed that significant improvements in the modelling of glacial mass balance can be achieved by focusing on accumulation processes. Klok and Oerlemans (2002) reported similar conclusions

More complex models are based on physics. These models calculate accumulation and ablation by using a rigorous physics-based description of all the processes that are involved in the exchange of mass and energy between the atmosphere and the surface. The main advantage is the capacity to accurately calculate the energy and mass balances, thus improving the understanding of the individual processes. However, the use of this type of model involves knowledge of numerous meteorological variables. In addition, the need to simulate a large number of processes requires the use of many parameters, which must be adequately estimated to produce reliable simulations. These limits are a serious problem when applying the models on ungauged areas, outside their area of implementation (Blöschl, 1999). These areas are generally experimental basins with small size and a sufficient amount of sensors and instruments.

The simplest models are conceptual models, which use the most commonly available meteorological variables (for example, the air temperature) as indices of the processes that govern accumulation and ablation rather than input to the calculations of rigorous energy balances. The most widely used method is the so-called "degree-day method" (Martinec, 1975), which uses the air temperature as the only index for the melting calculation. These models are simple to apply and calibrate and produce good results, especially for concentrated simulations. However, these models are very empirical models, and their applicability to glacial systems is affected by the high complexity and heterogeneity of the variables and the physical processes that are involved, which generally requires distributed approaches. In addition, the degree-day method is too sensitive to the air temperature, whereas the radiative component of the energy balance is usually far from negligible within glacial systems.

Among the many modelling approaches that have been proposed in the literature (Hock, 2005), melting models that are based on the morpho-energy index are probably a good compromise between simplicity and parsimony compared to meteorological data being required as input, thus capturing the process variability of accumulation and fusion. These models aim to improve the degree-day method, adding a morpho-energy distributed index that is calculated from the measured or simulated solar radiation from DTMs to the air temperature (Cazorzi and Dalla Fontana, 1996; Hock, 1999; Pellicciotti et al., 2005).

The application of these models to glacial environments must consider the dominant processes that act on accumulation and ablation.

### 1.2.c.1. Energy-index snow-and-ice model (EISModel)

The EISModel is a good example of a melting model that is based on the morpho-energy index, which i) considers the dominant processes that act on accumulation and ablation and ii) requires only a few meteorological data as input and a few calibration parameters.
The next section reports a summary of EISModel from Carturan, Cazorzi et al. (2012).

The EISModel was derived from the grid-distributed model in Cazorzi and Dalla Fontana (1996). This model simulates accumulation and melt processes at hourly intervals and only requires a DTM of the watershed and precipitation and 2-m air-temperature data from at least one weather station as input (Carturan et al., 2012). For each pixel $X$ and for each hour $t$ at elevation $EL_x$ (m a.s.l.), the 2-m air temperature $T_{X,t}$ is computed by an hourly lapse rate $LR_t$ (°C m$^{-1}$):

*Equation 7*

$$T_{X,t} = T_{s1,t} + LR_t\,(EL_x - EL_{s1})$$

where $T_{s1,t}$ is the 2-m air temperature at the reference weather station (s1) with elevation $EL_{s1}$. $LR_t$ can be assigned as a constant value or calculated for each time step by the model from at least two weather stations at different altitudes. The precipitation data at the gauging stations $s$ (s1,s2...sn) are extrapolated at the pixel elevation by using a Precipitation Linear Increase Factor (PLIF; % km$^{-1}$) to consider the typical increase in precipitation with altitude. PLIF can be assigned as a constant value or calculated by the model from at least two weather stations at different altitudes.
When the temperature at the pixel elevation exceeds the snow/rain threshold $T_{snow}$, the rainfall increases the liquid content of the snowpack $LQW$ (mm); otherwise, the snowfall increases the water equivalent of snow $WEs$ (mm):

*Equation 8*

$$LQW_X = LQW_X + P_{X,t}$$

$if\ P_{X,t} > 0\ and\ T_{X,t} \geq T_{snow}$

*Equation 9*

$$WEs_X = WEs_X + P_{X,t} * SRF_X$$

$if\ P_{X,t} > 0\ and\ T_{X,t} < T_{snow}$

$SRF_x$ (the snow redistribution factor) considers the preferential deposition and redistribution of snow from wind drift and gravity. Snow and ice melt are assumed to occur when the air temperature exceeds the threshold temperature for melting $T_{melt}$ = 0 °C. The melt rate $MLT_{X,t}$ (mmh$^{-1}$) is calculated as a function of $T_{X,t}$ and the clear-sky shortwave radiation $CSR_{X,t}$ (Wm$^{-2}$). The model calculates $CSR_{X,t}$ based on the DTM according to the effects of

the surrounding relief, which determines the local sunrise and sunset times and shadowing (Oke, 1987; Dubayah et al., 1990; DeWalle and Rango, 2008). Following, we report three melt algorithms from the literature, which have been successfully applied to glaciers. The Cazorzi and Dalla Fontana (1996) algorithm is

*Equation 10*

$$MLT_{X,t} = RTMF * CSR_{X,t}(1 - \alpha_{X,t})T_{X,t}$$

The Hock (1999) algorithm is

*Equation 11*

$$MLT_{X,t} = (TMF * T_{X,t}) + [RTMF * CSR_{X,t}(1 - \alpha_{X,t})T_{X,t}]$$

The Pellicciotti et al. (2005) algorithm is

*Equation 12*

$$MLT_{X,t} = (TMF * T_{X,t}) + [RMF * CSR_{X,t}(1 - \alpha_{X,t})]$$

where $\alpha_{X,t}$ is the surface albedo and $RTMF$, $TMF$ and $RMF$ are empirical coefficients, namely, the radiation–temperature melt factor ($mmh^{-1}\ °C^{-1}\ W^{-1}\ m^2$), temperature melt factor ($mmh^{-1}\ °C^{-1}$) and radiation melt factor ($mmh^{-1}\ W^{-1}\ m^2$), respectively. These three coefficients are the calibration parameters of the model. Henceforth, we call the algorithms in Equation 10, Equation 11, and Equation 12 ‘multiplicative’, ‘extended’ and ‘additive’, respectively. The extended and multiplicative algorithms have been modified by incorporating the surface albedo, as suggested by Pellicciotti et al. (2005). The multiplicative algorithm was derived from a classical degree-day model with the melt factor corrected in space and time by the net fraction of CSR. Hock (1999) extended the multiplicative algorithm by adding a simple degree-day term. The additive algorithm, however, was derived from an extreme simplification of the energy equation to preserve some physical significance while using the air temperature as the unique meteorological input to calculate melt. These differences significantly affect melt calculation. In particular, a different sensitivity to air temperature has been reported in the literature (e.g., Pellicciotti et al., 2005), and possible compensation effects are expected to exist with respect to air-temperature extrapolations from weather stations. The albedo is related to the ‘thermal history’ of the surface layer of the snowpack (Brock et al., 2000), which can be represented by the positive temperature sum ($\sum T$, updated hourly) since the formation of the snow layer. The model calculates the snow albedo by using a stack algorithm at the pixel scale. At every snowfall ($P_{X,t}$ > 0.5 mm), a new snow layer is created and set active with a fresh-snow albedo. When the air temperature exceeds the melting point, the positive temperature sum that is assigned to the surface layer $\sigma$ is increased as follows:

*Equation 13*

$$\sum T_{X,\sigma(t)} = \sum T_{X,\sigma(t-1)} + T_{X,\sigma(t)}$$

The snow albedo is calculated as follows:

*Equation 14*

$$\alpha_{X,t} = \beta_1 - \beta_2 * log_{10}\left(\sum T_{X,\sigma(t),}\right)$$

where $\beta_1$ and $\beta_2$ are the parameters of the decay function, which are both given as inputs. The thermal sum and albedo values are stored when a new layer overlaps. The 'active' layer is the upper layer; when this layer completely melts, the thermal history and albedo calculations restart from the stored values of the underlying layer if its albedo is lower than the final albedo of the depleted layer. On the contrary, the albedo and thermal history of the depleted layer are assigned to the new active layer if the albedo is higher. The glacier ice albedo is assumed to be constant in time and can be input as a single uniform value or spatially variable map. At the beginning of the winter season (normally 1 October at mid-latitudes in the Northern Hemisphere), the residual snow is considered to be firn and converted to a single layer. During the night, $CSR_{X,t}$ is zero and Equation 11 and Equation 12 automatically calculate the melt as a function of only the air temperature, while Equation 10 always calculates a melt rate of zero. To overcome this problem, the nocturnal melt rate is calculated as follows:

*Equation 15*

$$MLT_{X,t} = TMF * T_{X,t}$$

which uses a $TMF$ with the same units and significance as described above.
When melt is generated by rainfall ($T_{X,t}$ > 0 °C and $P_{X,t}$ > 0.2 mm), the energy flux at the surface is dominated by longwave radiation and turbulent heat exchanges (Anderson, 1968). In this case, a temperature-index function, which was derived from an extreme simplification of the energy budget (Anderson, 1973), is used to calculate the melt rate:

*Equation 16*

$$MLT_{X,t} = \left(RF + 0.0125P_{X,t}\right) T_{X,t}$$

where 0.0125 $C^{-1}$ is the amount of melt (w.e. mm) per 1 mm of rainfall at 1 °C, and $RF$ is a rainfall melt factor (mm $°C^{-1}$ $h^{-1}$). The snowpack is assumed to be constantly at the melting point, and its 'cold content' is not modelled. However, the threshold temperature for melting, $T_{melt}$ = 0 °C, is used to refreeze a fraction of liquid water under low-temperature conditions:

*Equation 17*

$$LQW_{X,t+1} = LQW_{X,t} - FRZ\left(T_{melt} - T_{X,t}\right)$$

and

*Equation 18*

$$WES_{X,t+1} = WES_{X,t} + FRZ\left(T_{melt} - T_{X,t}\right)$$
$$if\ T_{X,t} < T_{melt}\ and\ WES_{X,t} > 0$$

where $FRZ$ is a freezing factor (mm °C$^{-1}$ h$^{-1}$) and $T_{X,t}$ is the air temperature. The final w.e. of the snowpack includes both ice and liquid water. The glacier ice temperature is also assumed to be constant at the melting point, but no refreezing of meltwater is calculated.

Observations of the snow-cover distribution during the ablation season reveal a typical pattern that repeats nearly unchanged from year to year. Numerous authors have recognized the persistence of topographic control on snow distribution (e.g., Elder et al., 1991; Luce et al., 1998; Grayson and Bloschl, 2001; Erickson et al., 2005; Sturm and Wagner, 2010). The topography influences snow accumulation by regulating the spatial distribution of precipitation (i.e., vertical and horizontal gradients) and the wind-driven processes of preferential snow deposition and redistribution (Blöschl et al., 1991; Machguth et al., 2006b; Lehning et al., 2008; Dadic et al., 2010). During precipitation events, enhanced deposition occurs on the lee side of mountain ridges, while reduced deposition occurs on the windward side. Post-event winds typically erode snow from wind-exposed sites (e.g., ridges and convex areas) and accumulate snow on wind-sheltered areas. In addition, snow is transferred by gravity from steep slopes to underlying flatter areas in avalanche runout zones. Carturan et al. (2012) proposed using topographic indices from DTMs to consider wind and avalanche redistribution and, indirectly, preferential deposition. A snow redistribution factor ($SRF$) is calculated offline from i) a relative elevation attribute ($REA_r$), which considers wind exposure (Carturan et al., 2009), and ii) a gravitative mass transport and deposition ($MTD$) algorithm that was proposed by Gruber (2007). The $REA_r$ is the difference between the DTM and a smoother DTMs, which is calculated as the average elevation of each pixel within an assigned radius $r$ (m). The indexed $REA_r$ ($REAindex$) can be >1 (dips), <1 (peaks or crests) or 1 (flat areas). In MTD, the mass transport is driven along flow paths that are derived from the DTM and is controlled by a slope limit, the available mass and the maximum deposition, which is a local variable.

Glacier mass-balance models rely on accurate spatial calculations of input data, particularly air temperature. Lower temperatures (the so-called glacier-cooling effect) and lower temperature variability (the so-called glacier-damping effect) generally occur over glaciers compared to ambient conditions. These effects depend on the geometric characteristics of glaciers and display high spatial and temporal variability (Carturan et al., 2015). According to Carturan et al. (2015), even small deviations in calculated on-glacier temperatures from observations can significantly affect the calibration of EISModel and its efficiency, thus confirming that accurate temperature estimations are an essential prerequisite for model development, calibration, and generalizability. Furthermore, Carturan et al. (2015) suggested the likely existence of important reinforcing mechanisms during glacier decay and fragmentation because of the magnitude of the cooling effect and the occurrence of a katabatic boundary layer (KBL). Katabatic winds are gravity winds that

originate from the cooling of near-surface air layers, resulting in density gradients that force a downward movement of the air under the effect of gravity. The two main processes that affect the temperature of the air during this downslope movement are cooling from the exchange of sensible heat and adiabatic heating. The interplay of these processes has a twofold effect, consisting of lower on-glacier temperatures (the so-called glacier-cooling effect) and lower temperature variability (the so-called glacier-damping effect, which is also referred to as reduced climate sensitivity) compared to ambient conditions (Braithwaite, 1980; Greuell and Böhm, 1998; Braithwaite et al., 2002; Gardner et al., 2009). Thus, on-glacier lapse rates generally differ from average environmental lapse rates (i.e., −0.0065 °C $m^{-1}$). Cooling and damping effects are not homogeneous over glacial surfaces and mainly depend on the size and geometric characteristics, particularly the slope, of single glaciers and the specific position along the glacier (Carturan et al., 2015). Generally, these effects are directly related to the size of the glaciers and the fetch distance along the flow line and inversely related to the slope of the glaciers. The last factor controls the prevalence of cooling from turbulent exchanges over the adiabatic heating of air that is forced to move downward by katabatic winds (Carturan et al., 2015).

Few methods have been proposed in the literature to model these processes. The first attempt to parameterize the mean summer cooling effect at the firn line altitude was conducted by Khodakov (1975), who proposed a relationship with the glacier length based on temperature data from mountain glaciers and ice sheets. Davidovich and Ananicheva (1996) analysed direct observations from glaciers in Caucasus, Pamir, Scandinavia, Tian Shan, and Altay and provided a simple relationship to calculate the mean summer temperature at the equilibrium line altitude (ELA) as a function of the mean off-glacier summer temperature at the same altitude. These authors suggested that the cooling effect peaks at the ELA and decreases towards both the terminus and up-glacier area. The first comprehensive glacial–meteorological experiment that provided distributed temperature measurements was conducted in the summer of 1994 on Austria's Pasterze Glacier and comprised five automatic weather stations along a flow line. Greuell and Böhm (1998) developed a thermodynamic model from this experiment to calculate the air temperature as a function of the slope and distance along the flow line according to sensible heat exchanges and adiabatic heating. Braithwaite et al. (2002) used an empirical approach and a formulation from data that were gathered in two Canadian Arctic glaciers (Sverdrup and White), similar to the approach by Davidovich and Ananicheva (1996) but applied to monthly temperatures. Shea and Moore (2010) suggested empirical relationships that were based on piecewise linear regressions of on-glacier vs ambient temperatures that were collected in British Columbia (Canada) between 2006 and 2008 to calculate (i) the threshold temperature that triggered KBL development and (ii) the glacier-damping effect as a function of the elevation and flow-path length (i.e., the "average flow distance to a given point starting from an upslope limit or ridge").

#### 1.2.c.2. AHM

AHM is a deterministic, conceptual and continuous hydrological model that can simulate all the processes of the hydrological cycle. AHM was derived from the Anderson version of the known Stanford Watershed model IV (Crawford and Linsley, 1966). Subsequently, the

Anderson version was improved at the Strathclyde University (Fleming MCKenzie 1982) and further modified by Cazorzi and Dalla Fontana at the University of Padova..

As in the physical reality, the Stanford model separately studies slope processes (LAND module) and hydraulic network processes (CHANNEL module). This schema is shown in Figure 2.

The catchment is the modelling unit in AHM and is subdivided into three elevation bands (segments). The different calculations begin from the upper segment. Subsequently, the calculations are replicated on the second segment according to the contribution from the previous calculations, and then the calculations are transferred to the third segment with all the contributions. Figure 1 shows the connections between the three segments.

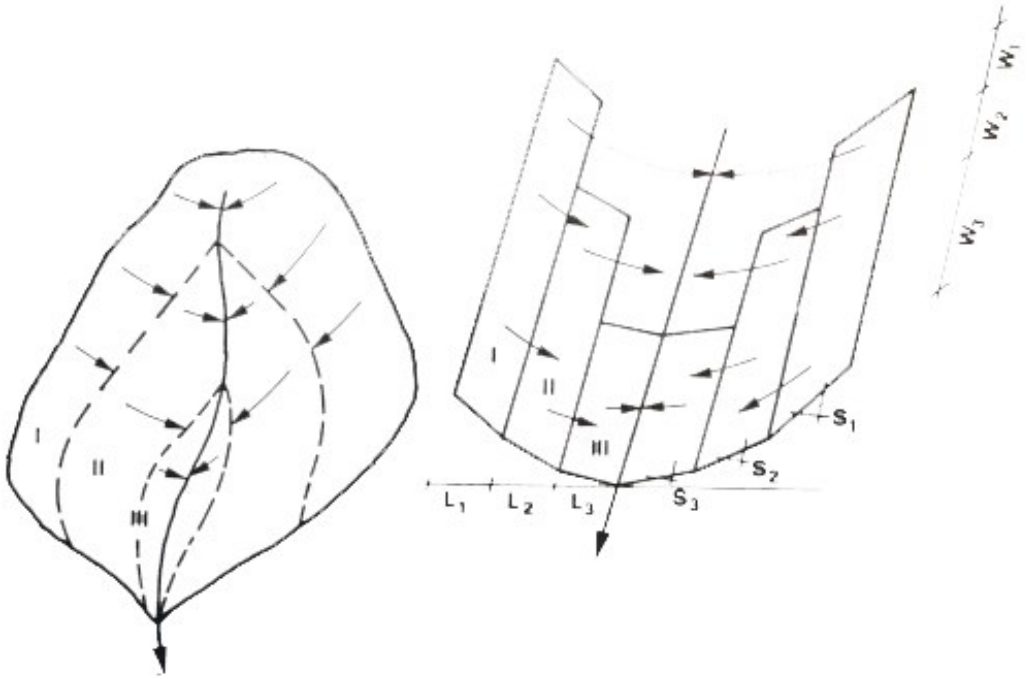


*Figure 1: Catchment-subdivision schema with elevation bands (from Cazorzi* et al.*, 1984. "Simulazione idrologica del bacino del Cordevole").*

Each segment is characterized by the following parameters: area (AREA), length (LL) and slope (SS). In addition, the model uses another parameter (RIVER) that represents the outflow percentage for each segment that directly contributes to the hydrographic network.

The RIVER parameter is calculated according to the percentage of each segment's hydrographic network compared to the total length of the hydrographic network. Evidently, the RIVER parameter always equals 1 in the lower segment because all the outflow reaches the hydrographic network.

This model requires some hydro-meteorological series: temperatures series, precipitation series and finally the discharge series (optional input) that can use for comparison in calibration and validation phase. This model elaborates the precipitation series, produces the hydrological cycle values for each segment, and calculates the total runoff for the CHANNEL module.

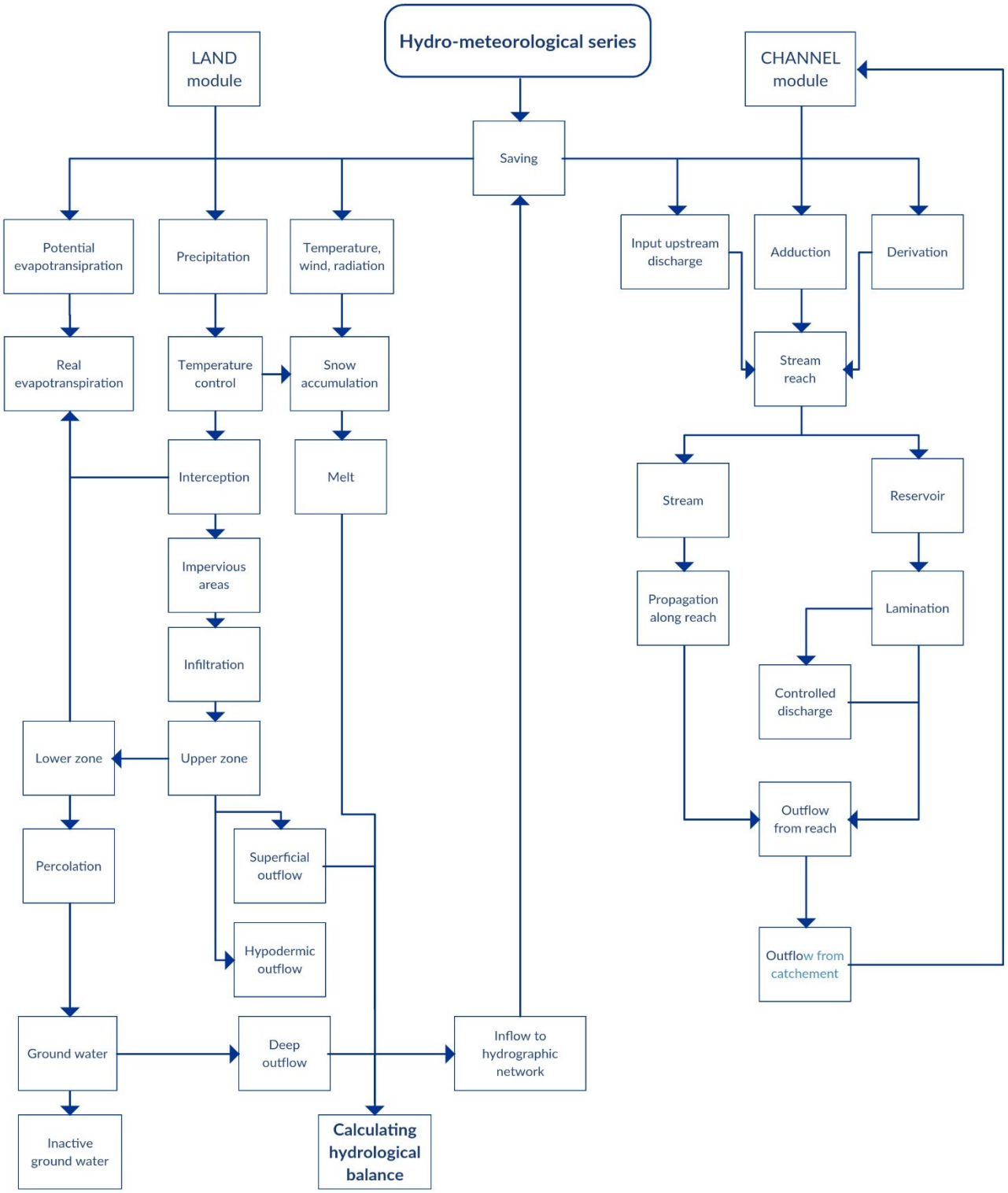


*Figure 2: Flowchart of the LAND and CHANNEL modules (edited from Cazorzi* et al.*, 1984. "Simulazione idrologica del bacino del Cordevole").*

#### 1.2.c.2.1. LAND module

The LAND subroutine considers the slope's hydrological processes for each segment inside the catchment (Figure 2).

The first step is to consider the precipitation series and the interception losses. The interception losses are simulated by fixing a maximum capacity EPXM (generally from 0 mm

to 5 mm) and assuming that the precipitation is storage until the maximum value. When this value is exceeded, the interception continues at a rate that equals that of the potential evapotranspiration.

The waterproof area IMPV (percentage of the segment's total area) directly provides a fraction of the outflow to the hydrographic network. Waterproof areas include rocks, urban areas and streamflow, river or water reservoirs.

Considering the important and complex infiltration processes that occur, AHM can retain variations in the infiltration on both the temporal and spatial scales. Variations on the temporal scale are determined by correlating the infiltration capacity with the soil moisture content. Indeed, the soil moisture content varies as a function of time. However, variations on the spatial scale are determined using a linear function of the spatial distribution of the infiltration capacity. Figure 3 shows the cumulative frequency of the infiltration capacity. For simplicity, the cumulative frequency is considered a linear function that begins from zero and ends at the maximum b value as a function of

*Equation 19*

$$b = \frac{CB}{(LZS/LZSN)^{POWER}}$$

where

$b$ = maximum value of the infiltration capacity at time t

$CB$ = parameter that represents the infiltration index; its unit of measurement is the same as that of the velocity and varies as a function of the catchment's physical characteristics

$LZS$ = instantaneous soil water content in the lower zone

$LZSN$ = nominal soil moisture in the lower zone, which corresponds to the field capacity

$POWER$ = constant that is larger than unity; its value usually equals 2.

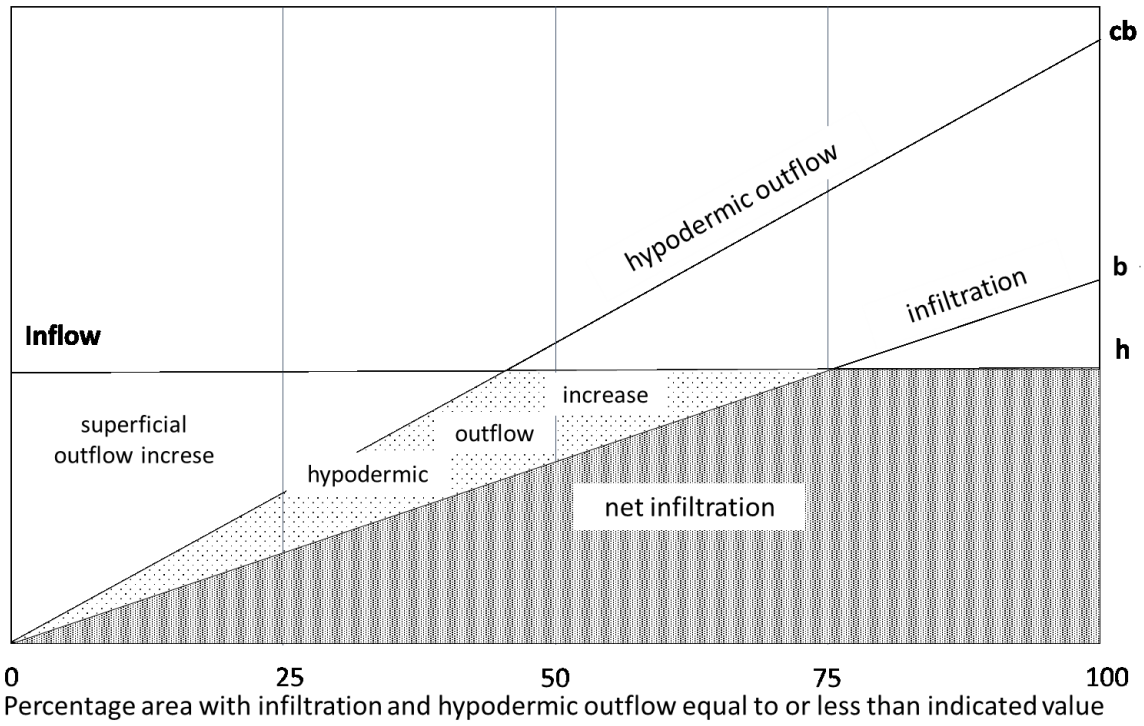


*Figure 3: Spatial-distribution schema of infiltration and subsurface outflow processes (edited from Cazorzi* et al.*, 1984. "Simulazione idrologica del bacino del Cordevole").*

A portion of the meteoric input that infiltrates the soil descends into the lower zone and the groundwater, while another portion contributes to subsurface outflow. The position of the upper line, which regulates subsurface outflow, depends on the index c value (Figure 3):

*Equation 20*

$$c = CC\ 2^{LZS/LZSN}$$

where CC is an a-dimensional parameter that regulates the volume of the subsurface outflow.

After fixing a specific inflow H (equal to the total rainfall minus the intercepted rainfall), the infiltration volume is represented by the dashed area in Figure 3, the subsurface outflow volume is represented by the dotted area, and the surface outflow volume is represented by the white area below the line H.

Even superficial layers of the soil can retain some water, which increases the soil water content. Generally, the upper section has specific characteristics: low thickness, lower storage capacity, good permeability and fast evapotranspiration and percolation speeds.

The water that does not remain in the upper zone, which contributes to the hypodermic and superficial outflow, can be calculated as a function of the UZS/UZSN ratio, where UZS is the instantaneous soil moisture in the upper zone, and UZSN is the maximum capacity in the same zone.

Figure 4 shows the trend of the percentage of the outflow in the upper zone.

Percolation involves the transfer of water from upper zones to lower zones and groundwater. Percolation occurs when the UZS/UZSN ratio is larger than the LZS/LZSN ratio.

The volume of the superficial detention, which is produced by the remnant water, can be simulated by a simple continuity equation:

*Equation 21*

$$D_2 = D_1 + \Delta D - q\Delta t$$

where $D_1$ and $D_2$ are the superficial detention volume at the start and end of the time interval $\Delta t$, respectively, for a strip with length l and unitary width. $\Delta D$ is the increase in detention and $q$ is the unitary runoff of the superficial outflow to the hydrographic network in the time interval. $q$ is calculated from

*Equation 22*

$$q = \frac{1}{n} S^{0.5} y^{1.667}$$

where
n = Manning's roughness coefficient
S = slope of the studied stretch of the stream
y = depth of the water flow

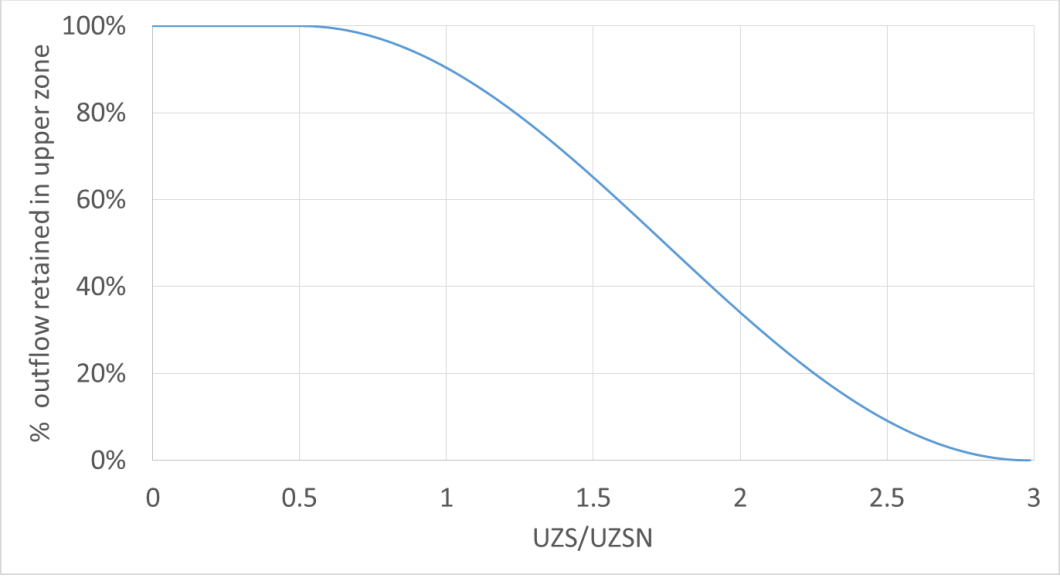


*Figure 4: Trend of the percentage of retained outflow in the upper zone (edited from Cazorzi* et al.*, 1984. "Simulazione idrologica del bacino del Cordevole").*

AHM uses the following empirical expression to correlate the water-flow depth with the detention volume:

*Equation 23*

$$y = \frac{D}{D_e}\left[1.0 + 0.6\left(\frac{D}{D_e}\right)^3\right]$$

where $D_e$ represents the superficial detention volume under equilibrium conditions.
The superficial outflow is characterized by parameters that are specific for each segment, including the mean length L, mean slope S, and Manning's roughness coefficient c.
At the end of each time interval, the portion of water that includes the superficial detention volume is available for infiltration during the subsequent period.
The following formula calculates the subsurface outflow, which is derived from the lateral movement of water through the upper soil layers:

*Equation 24*

$$INTF = 1 - (IRC)^{1/96}\, SRGX$$

where
$INTF$ = subsurface outflow volume that reaches the hydrographic network within a fixed time interval of 15 min
$IRC$ = daily depletion constant of the subsurface outflow
$SRGX$ = invaded volume of the subsurface outflow

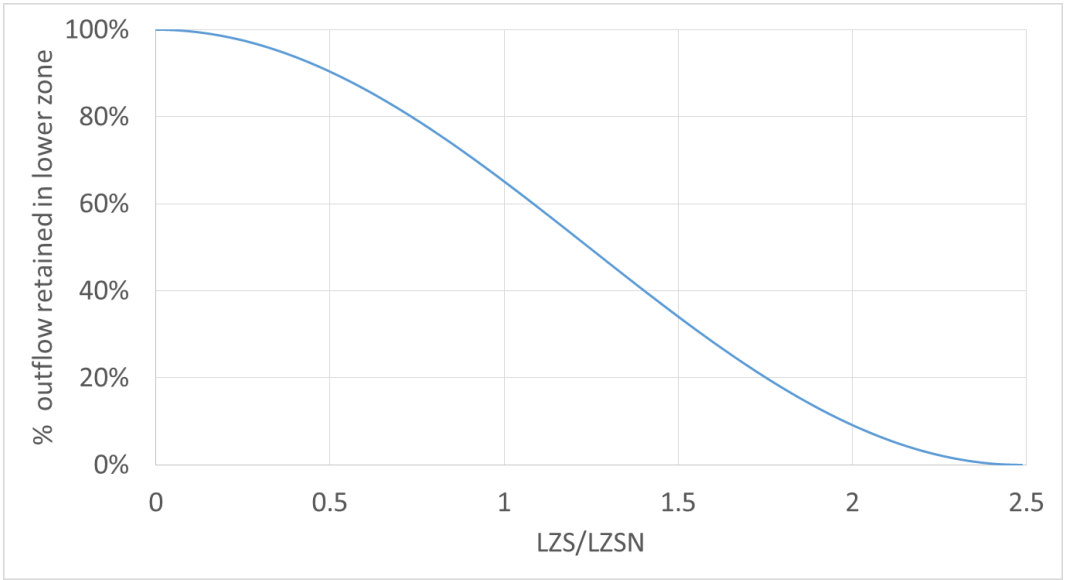


*Figure 5: Trend of the percentage of retained outflow in the lower zone (edited from Cazorzi* et al.*, 1984. "Simulazione idrologica del bacino del Cordevole").*

The water that leeches from the upper zone feeds the lower soil zone. Subsequently, some of this water is stored in the lower zone, and another portion feeds the groundwater.
The model calculates the percentage of the lower-zone water by using the $LZS/LZSN$ ratio as a function of the behaviour in Figure 5.
This figure shows that a greater portion of the water feeds the lower zone's water content when the $LZS/LZSN$ ratio is smaller than unity. In contrast, a greater amount of water reaches the groundwater when this ratio is larger than unity.

Some of the water that feeds the groundwater can be deflected into deep aquifers according to the $K24L$ parameter. At the same time, the remaining water can feed the active groundwater and subsequently reach the hydrographic network as a function of

*Equation 25*

$$GWF = 1.0 - (KK24)^{1/96} (1.0 + KV\ GWS)\ SGW$$

where

- $GWF$ = deep outflow volume that reaches the hydrographic network during the fixed time interval
- $KK24$ = depletion constant of the daily deep outflow
- $KV$ = parameter that allows the depletion constant to change
- $GWS$ = groundwater slope
- $SGW$ = groundwater volume

Evapotranspiration losses occur at different times of the hydrological cycle.
The model assumes that both the evaporation of the intercepted volume by the vegetation cover and the evaporation of the upper zone's volume occur with the same potential evapotranspiration rate. The model uses a similar schema to that of the infiltration and subsurface outflow for evapotranspiration in the lower zone. AHM considers the concept of "evapotranspiration possibility", which is the maximum amount of available water for evapotranspiration at a specific point in the catchment and within a specific time interval.
A linear function that varies from zero to a maximum value of $r$ expresses the spatial variation in the evapotranspiration possibility (Figure 6).
The $r$ value, which is the maximum value that evapotranspiration can assume, is derived from the following expression:

*Equation 26*

$$r = \frac{0.25}{1.0 - K3} \frac{LZS}{LZSN}$$

where $K3$ is a parameter that is connected to the forest cover's characteristics.

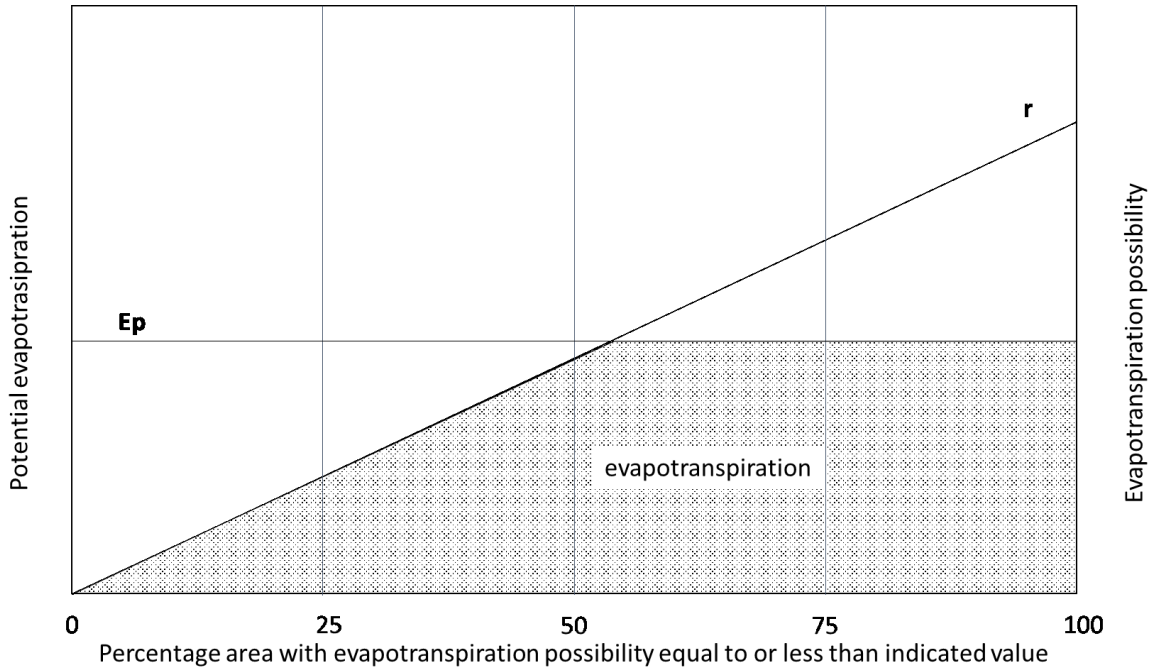


*Figure 6: Relationship between the potential and real evapotranspiration (edited from Cazorzi* et al.*, 1984. "Simulazione idrologica del bacino del Cordevole").*

When the potential evapotranspiration is larger than $r$, the evapotranspiration assumes the maximum value, which is

*Equation 27*

$$E = r/2$$

However, the value in the other cases is

*Equation 28*

$$E = EP - EP^2 /2r$$

where $EP$ represents the potential evapotranspiration value and $E$ represents the lower zone's evapotranspiration losses. For shallow groundwater, AHM considers the evaporation losses by using the $K24EL$ parameter.

### *1.2.d. Climatic variations and cryosphere*

The average global temperature increased by approximately 0.6 °C (IPCC, 2013) over the last century. The most tangible effects of this warming include decreasing snow and ice resources and increasing mean sea levels. General Circulation Models (GCMs) predict enhanced global warming in the coming decades because of anthropogenic greenhouse warming (IPCC,2013). In the past, this climatic variation was not linear: two phases of

temporary and modest cooling culminated at approximately 1915 and 1975, and two stages of significant rises in temperature occurred at approximately 1950 (maximum) and the present (still in progress). Additionally, heating was not uniform over either time or space (IPCC, 2013). Climate changes affect high-altitude areas in a complex manner. Instrumental evidence proved that heating in mountainous areas was greater than the global or hemispheric average (Auer et al., 2006). However, uncertainty persists in the quantification of the effects of global changes on these areas because of the scarcity of measurements and the difficulty of simulating the climatic conditions through mathematical models (Beniston et al., 1997). Auer et al. (2006) implemented the HISTALP database, which collects the main series of climate observations for the so-called "Greater Alpine Region", an area that includes the European Alps and surrounding regions. Their analysis of these climatic series showed that the Alps are affected by amplified climate change, which caused a warming of 1.2 °C over the last century, much higher than the global average. Rainfall showed less significant and variable seasonal and regional variations, with opposite variations between the northwest (+ 9%) and southeast (-9%).

#### 1.2.d.1. Nivo-glacial perspective

The global cryosphere is regarded as one of the most effective indicators of climatic and environmental changes. Fluctuations in glaciers and ice caps in cold mountain areas have been systematically observed for longer than a century in various areas of the world and are considered to be highly reliable indicators of worldwide warming trends (Haeberli, 2005). Thus, mountain glaciers and ice caps are key variables for early detection strategies in global climate-related observations. Long-term mass-balance measurements provide direct signals of climate change and constitute the basis for developing coupled energy-balance/flow models for sensitivity studies (Haeberli, 2005). These investigations explore complex feedback effects (albedo, surface altitude, and dynamic responses) and can be used in conjunction with coupled ocean-atmosphere general-circulation models (Beniston, 1997). These approaches combine direct glaciological and geodetic/photogrammetric methods to determinate changes in the volume/mass of entire glaciers (repeated mapping) with high spatio-temporal resolution (annual measurements at stakes and pits). Laser altimetry with a kinematic GNSS has been applied to monitor the thickness and volume changes of very large glaciers, which are the main meltwater contributors to ongoing sea-level rise (Arendt et al., 2002). Modern glacier inventories are compiled by using a combination of remote sensing and GIS techniques (Haeberli, 2005). Surveys occur at time intervals of several decades – the characteristic dynamic response time of medium-sized mountain glaciers. Length and area changes can be measured for a great number of ice bodies. Area changes mainly enter calculations of glacier contributions to sea-level rise and regional hydrological effects (Meier and Bahr, 1996).

Records of glacier mass balance and changes in glacier length, alongside a worldwide but rather preliminary glacier inventory, have been compiled by the World Glacier Monitoring Service (WGMS) in Zurich. This organization coordinates worldwide glacier monitoring, annually reports mass-balance data for approximately 50 glaciers and publishes comprehensive information regarding the length, area and volume changes of

approximately 500 glaciers every 5 years (Haeberli, 2005). The WGMS's mandate is to continuously upgrade, collect and periodically publish glacier-inventory and fluctuation data, including satellite observations of remote glaciers and assessments of ongoing changes (Haeberli, 2005). The WGMS maintains data exchanges with the International Council of Scientific Unions' (ICSU) World Data Center A (WDC-A) for Glaciology (Haeberli, 2005).

The global retreat of mountain glaciers during the XX Century is striking. The trends in long time series of cumulative glacier-length and volume changes present convincing evidence of fast climatic change at a global scale (Haeberli, 2005). The Earth's climate system is currently subject to unequivocal warming. Since 1990, the Intergovernmental Panel on Climate Change (IPCC) has documented such changes as evidence of the existence of global warming, independent of various surface-temperature datasets. This approach is considered valid because a worldwide retreat is unlikely to be related to a reduction in global mountain precipitation (Haeberli, 2005). Numerical modelling studies (Oerlemans et al., 1998) confirmed that many glaciers within the current worldwide mass-balance network could disappear within decades if warming trends continue or even accelerate. Analyses of repeated glacier-inventory data showed that the European Alps, for instance, have lost 30 to 40% of their glacierized surface area and approximately 50% of their ice volume between approximately 1850 and 1970 (Haeberli and Hölzle, 1995). A further 25% of the remaining volume is estimated to have been lost afterwards (Haeberli, 2005). The frequency and scale of glacier responses to climatic fluctuations depend on the glacier size (Oerlemans, 2001). Small cirque glaciers and glacierets provide annual signals, whereas the tonguing of medium and long valley glaciers undergoes decadal to secular smoothing. Varying and predominantly slope-dependent dynamic response times of individual glaciers must be considered during analyses of glacier retreat compared to instrumental proxy-temperature records.

#### 1.2.d.2. Hydrological perspective

Glaciers are characteristic features of mountain environments but often are not recognized for their strong influence on the catchment runoff quantity and distribution (Hock et al., 2005). Such modification occurs with the glacierization of only a few percent of the total catchment area and affects adjacent lowlands far beyond the limits of mountain ranges (Hock et al., 2005). The main effects occur because glaciers temporarily store water as snow and ice over many different time scales (Jansson et al., 2003), and any release from storage is controlled by both climate and internal mechanisms. Mountain glaciers have generally experienced worldwide retreating and thinning since the beginning of the XX Century in response to an ~0.6-°C increase in the mean global temperature (IPCC, 2013). This current situation will likely accelerate the decline of glaciers. Consequently, additional water is expected to be released from glacier storage, thus further modifying current streamflow regimes (Hock et al., 2005). Any change in the storage and release of water by glaciers is important for all aspects of watershed management, including the operation of hydroelectric facilities and flood forecasting; therefore, such changes have direct economic implications in many areas of the world.

Various studies have investigated the effects of climate warming on glacier discharge by analysing historic discharge data from glacierized and non-glacierized basins (Fountain and Tangborn, 1985; Chen and Ohmura, 1990) or runoff modelling (Singh and Kumar, 1997; Kuhn and Batlogg, 1998; Braun et al., 2000). The primary effect of climate warming on runoff is increased streamflow from larger glacier-melting rates (Hock et al., 2005), which are further accelerated by positive feedback mechanisms, such as the enlargement of bare ice areas, reducing the albedo compared to that of snow cover. The runoff distribution is also modified by changes in meltwater routing through the glacier, which are caused by a reduction in the thickness and extent of firn and snow cover (Hock et al., 2005). Water flow velocities through ice considerably exceed those through snow and firn (Fountain and Walder, 1998), so a reduced firn body and snow cover reduces the water retention capacity and thus speeds up the average transport of water on and through the glacier. Enhanced diurnal discharge peaks and amplitudes are a direct consequence (Hock et al., 2005) (Figure 7).

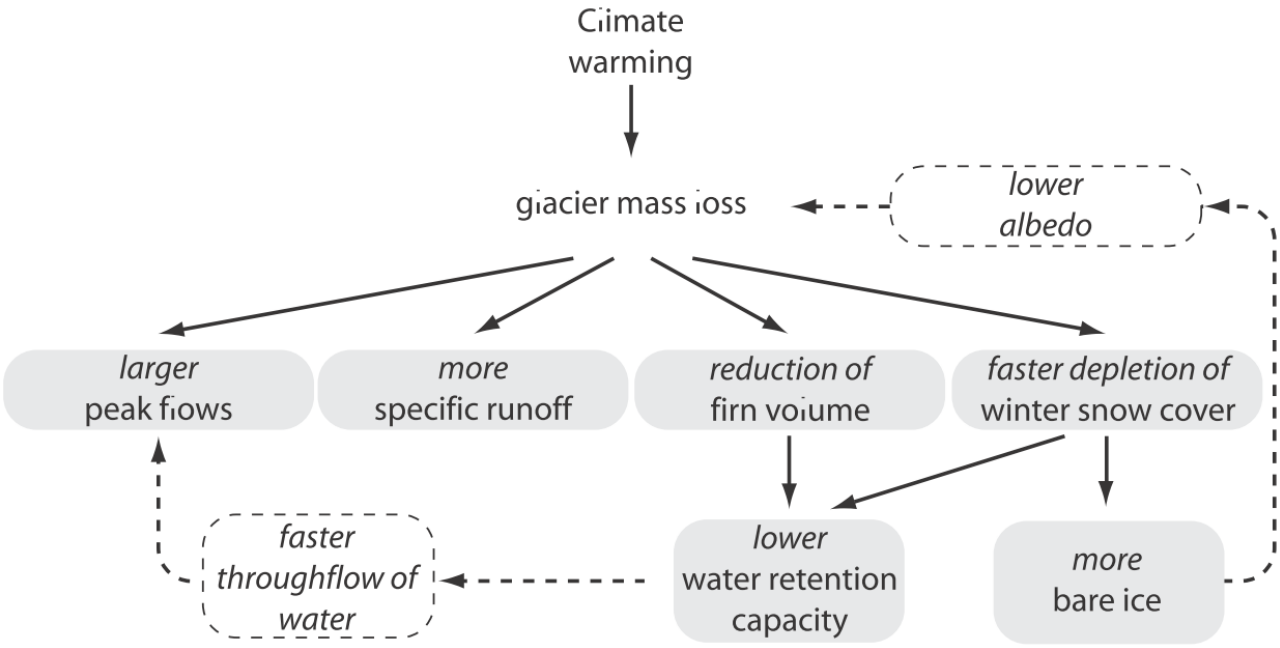


*Figure 7: Short-term effects of climate warming on glacier discharge, including feedback mechanisms (from Hock* et al.*, 2005 in U. M. Huber, H. K. M. Bugmann, and M. A. Reasoner (Eds.), 2005: Global Change and Mountain Regions (A State of Knowledge Overview), Springer, Dordrecht. page 246).*

Assuming unaltered precipitation conditions, the unit discharge initially increases because of the release of water from storage when mass balances are negative. However, prolonged long-term mass loss reduces the glacier volume, which decreases the water yields in turn (Braun et al., 2000; Jansson et al., 2003). Fountain and Tangborn (1985) found that the streamflow in basins in Washington State for a glacier mass balance of -1000 mm, a mean annual runoff of 2000 mm and a glacierization of 20% was enhanced by approximately 10% because of glacier mass loss. Climate warming is expected to prolong the melting season, thereby reducing the seasonal runoff concentration, i.e., the ratio of the maximum monthly to mean monthly discharge. In addition, diurnal discharge fluctuations initially will become

amplified by enhanced daily meltwater production and more efficient water transport through the glacier (Braun et al., 2000; Willis et al., 2002). The effect of climate warming on year-to-year runoff variability will depend on the initial glacierization, i.e., whether the glacierization is above or below the ~10 to 40% minimum variability (Hock et al., 2005). When glacierization falls below this threshold, the runoff variability tends to increase. In the long term, the runoff will be positively correlated with the precipitation instead of the air temperature because the percentage of temperature-dependent melt-derived glacier runoff decreases with decreasing glacierization. However, the correlation with the air temperature may initially increase because the meltwater yield is increased from rising temperatures (Hock et al., 2005).

While previous research focused on the effects of climate change on glacier mass balance (Braithwaite and Zhang, 1999) and glacier size variations (Oerlemans 1994), far less attention has been paid to the effects on glacier discharge. More than 280 glaciers have been subject to annual mass-balance measurements since 1946 (Dyurgerov, 2002), but only a few glaciers have been subject to simultaneous mass-balance and discharge monitoring programmes, partially because of the practical difficulties that are associated with measuring stream discharge in glacier environments, which is characterized by considerable turbulence, high sediment load and frequently changing channel geometry. Glaciers that have been involved in such programmes include Austria's Vernagtferner glacier (Escher-Vetter and Reinwarth, 1994) and the USA's South Cascade Glacier (Krimmel, 2001), where streamflow monitoring has been combined with annual mass-balance measurements since 1974 and 1958, respectively.

## **1.3.** Research questions and objectives

The topic of this PhD programme is to understand how different climatic and glacier cover conditions can modify the hydrological response of glacierized catchments with increasing area. The following research questions are formulated according to the topic and the state of knowledge on the four topic arguments (collection and management of nivo-meteorological and topographic datasets, glacial mass-balance methods, nivo-hydrological modelling and climatic variations and cryosphere):

- What is the behaviour of the alpine cryosphere in relation to different climatic conditions?
- How can the behaviour of the alpine cryosphere modify the runoff regimes of downstream rivers?

The overall objective of this research project is to recognize the scale dependence of hydrological effects on glacierized catchments under different climatic conditions.
The specific objectives are as follows:

- To understand how runoff regimes change in relation to different climatic and glacier-cover conditions.
- To understand how the effects of variations in the alpine cryosphere change in relation to the climate and different scales of investigation, moving downstream from head catchments with progressive upscaling.

## 2. Materials and methods

We implemented a glacio-hydrological modelling to the Noce Basin for three different glacier cover scenarios, three different periods with specific meteorological conditions, and four water basins with different areas.

The first glacier-cover scenario considered the maximum extent of the alpine glaciers over the last two centuries (Little Ice Age - LIA). The second scenario represented the current extent of the alpine glaciers (2000s), and the third scenario considered the complete absence of ice cover. We analysed the hydrological response of the catchments by combining different meteorological conditions for each glacier-cover scenario (Figure 8). For this study, we considered that the LIA extension was very close to the extension in the 1920s-1940s based on geomorphological landforms and previous research (e.g., Carturan et al., 2014). Table 1 shows the characteristics of each scenario.

*Table 1: Characteristics of the studied scenarios. We considered three different periods with measured data for each scenario.*

| *Scenario* | *Topographic input* | *Duration* | *Meteorological input* |
|---|---|---|---|
| 1st scenario | LIA glacial extension | Ten years | 1940s measured data<br>1970s measured data<br>2000s measured data |
| 2nd scenario | 2000s glacial extension | Ten years | 1940s measured data<br>1970s measured data<br>2000s measured data |
| 3rd scenario | No glacier coverage | Ten years | 1940s measured data<br>1970s measured data<br>2000s measured data |

We combined different periods (the characteristics of the climatic conditions are described in section 2.3.a) with the topographic ice surfaces of each scenario and modelled the runoff discharge of four water basins with increasing drained areas. Figure 8 shows the flowchart of glacio-hydrological modelling for each of the four catchments. We analysed the scale effect on the runoff from the catchments with a progressive decrease in the percentage of the glacierized area (and increase in the catchment area) under different glacier cover and meteorological conditions. Thus, we modelled the runoff from the smallest catchment (Val de La Mare, 8.4 $km^2$) to the largest catchment (Tassullo, 1046 $km^2$) by combining the different glacier cover and meteorological conditions. Subsequently, we compared the runoff (unit discharge) from the different topographic inputs and different glacier cover extensions for each catchment and period.

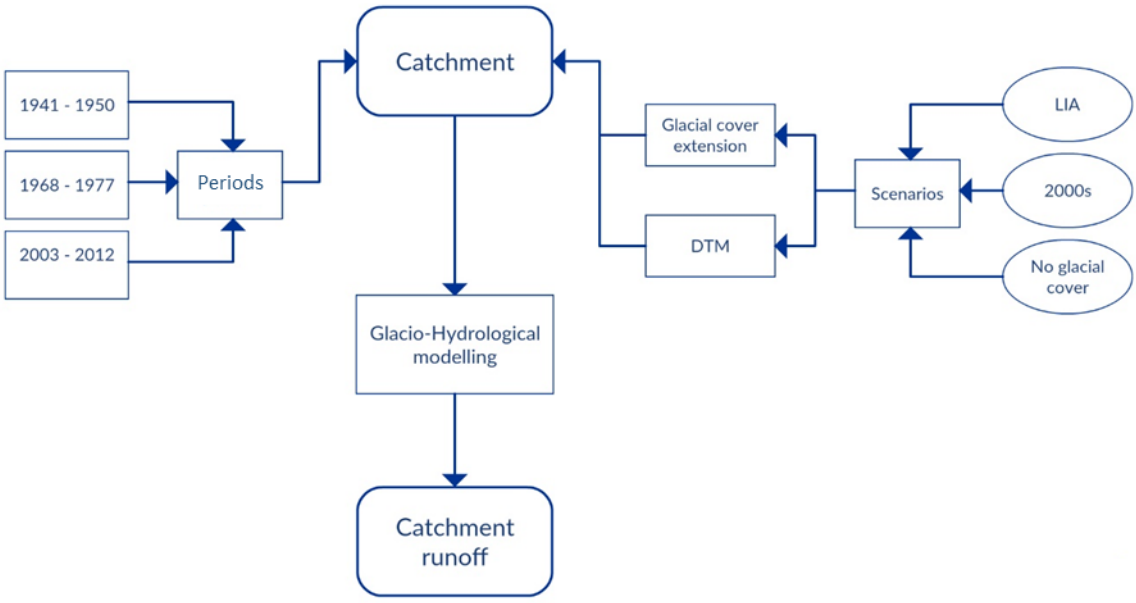


*Figure 8: Flowchart of the glacio-hydrological modelling for the four considered catchments.*

We used the daily data from five weather stations inside the Noce basin to recognize the climatic conditions of the three periods. We validated and processed the temperature and precipitation series of five weather stations from 1920 to 2015. We considered the glaciers inside the Noce basin, which were present in the Glacier Word Inventory (WGMS, 1989), in relation to each scenario. We considered forty-five glaciers (Zanoner et al., 2017) for the first scenario (45.0 $km^2$), fifty-six glaciers for the second scenario (considering the fragmentation of the total area of 16.3 $km^2$), and the bedrock of the fifty-six glaciers during the 2000s for the third scenario.

## **2.1.** Study area

This project took advantage of more than ten years of research activities which are in progress in the Val di Peio (Eastern Italian Alps, Provincia Autonoma di Trento), especially in its glacierized catchment head, Val De la Mare in the Ortles-Cevedale group. The La Mare glacier feeds the Noce Bianco stream, which is a tributary of the Noce River. This valley, in which the upper portion of the Noce River is located, is called Val di Sole. According to this area's research activities and the abovementioned progressive upscaling, the study area is a progressive extension of the catchment head (Val de La Mare). We considered the Noce river basin near the Tassullo station. Furthermore, we subdivided the basin into four sub-basins with increasing drained areas (Figure 9 and Figure 10).

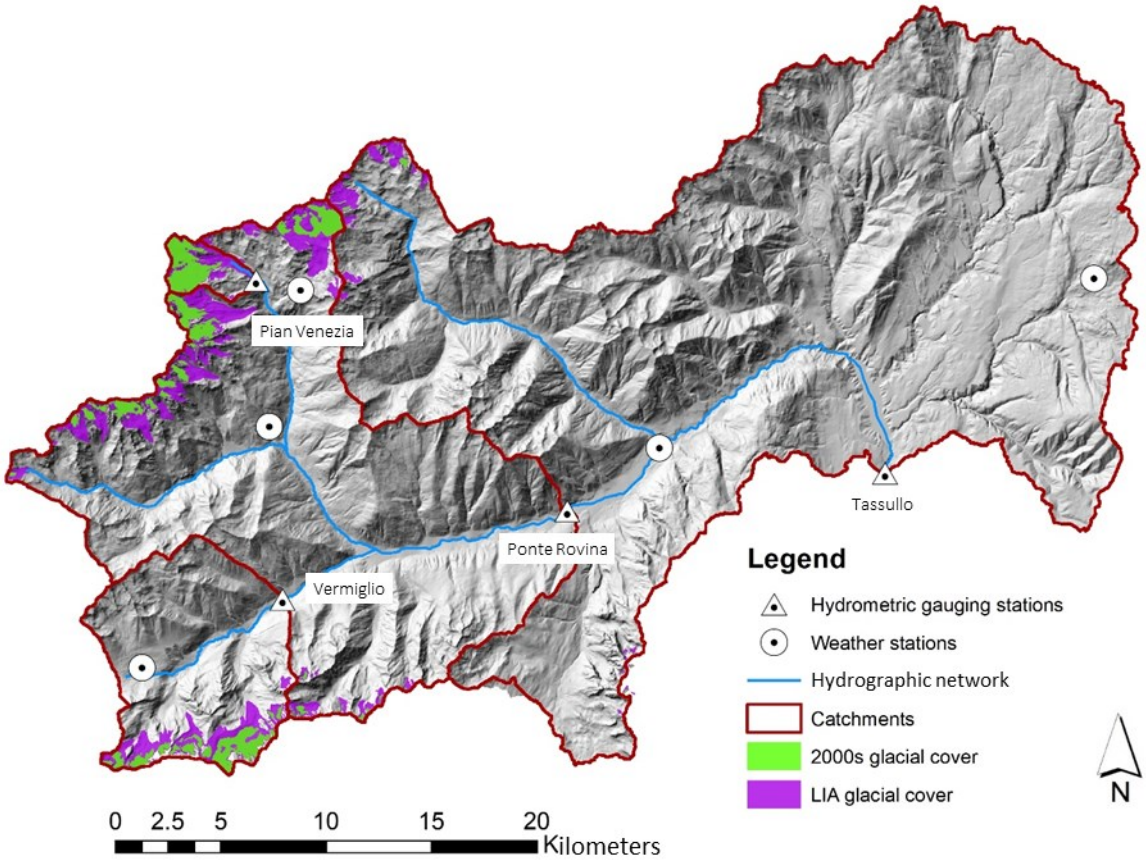


*Figure 9: Study area of the Tassullo catchment. The reported names are referred to the relative hydrometric gauging stations.*

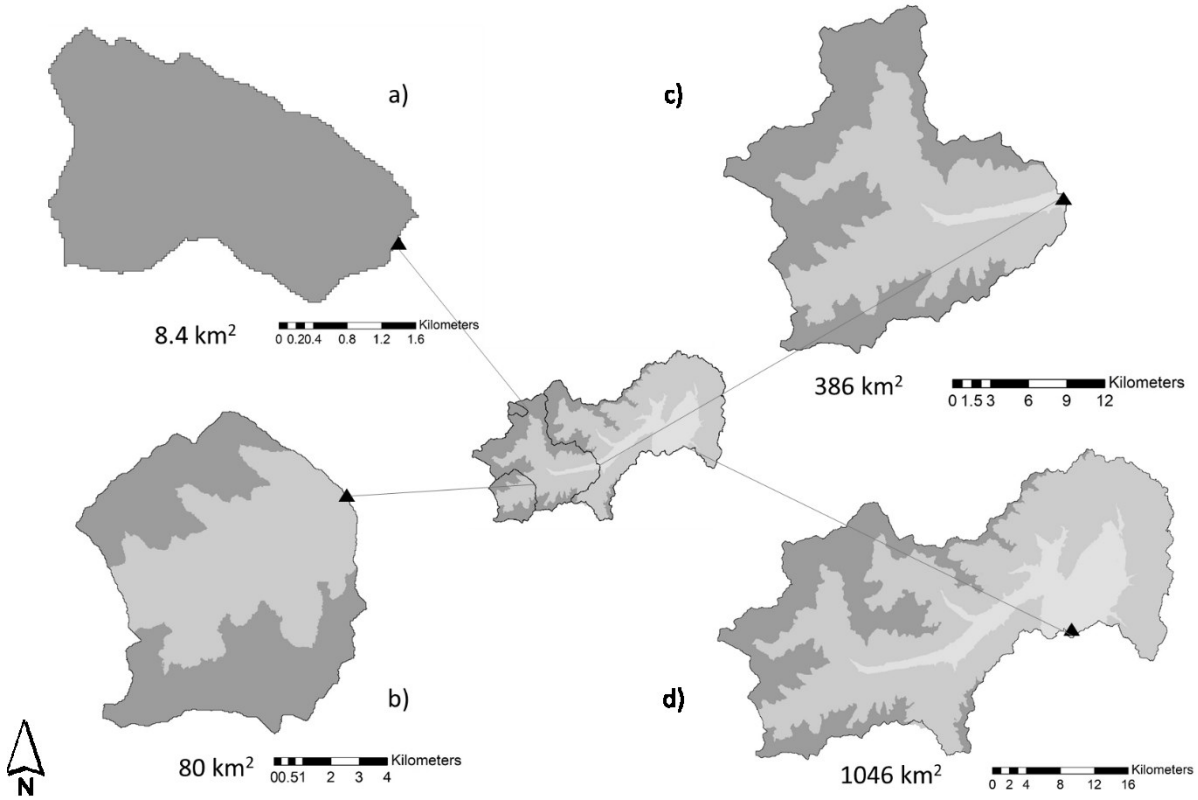


*Figure 10: Representation of the subdivision of the study area into four catchments with increasing area. a) Val de La Mare, b) Vermiglio, c) Ponte Rovina, d) Tassullo.*

We report a brief summary of the characteristics of the catchment head of the Noce basin and the research activities in this area.

Val de La Mare, which is one of the two catchments at the head of the Noce River, is a 68.3 $km^2$ experimental watershed where detailed studies of climate-change effects on the cryosphere and hydrology are conducted. The La Mare glacier (2650 – 3769 m, 3.50 $km^2$ in 2013) faces to the east (Figure 11). The glacier still has an accumulation area and shows "active" retreat towards higher altitudes (Zanon, 1982; Small, 1995; Carturan et al., 2009, 2014). The highest summit is Mt. Cevedale (3769 m), while the outlet's altitude is 1158 m a.s.l. The catchment lies in the southern portion of the Ortles-Cevedale massif. The Ortles-Cevedale group is the most extensively glaciated group of the Italian Alps. In this mountain group, glaciers are highly differentiated in terms of their morphological and topographical features. The study of glacial dynamics in the dolomite area is of particular interest because several areas exhibit a transition from cirque glaciers to debris-covered glacier and rock glaciers. The Ortles-Cevedale group is located in the Eastern Italian Alps and covers an area of 1638 $km^2$. The highest peaks of this mountain group, namely, Mt. Ortles (3905 m), Mt. Gran Zebrù (3851 m) and Mt. Cevedale (3769 m), are aligned in a NW–SE direction. Rather sharp ridges exist in the north-western area, which consists of sedimentary rocks (dolomites and limestones), whereas metamorphic rocks (mica schists, paragneiss and phyllites) prevail elsewhere forming more rounded reliefs (Carturan et al., 2013). These lithological differences influence the terrain morphology and significantly affect the distribution and morphology of the glaciers (Desio, 1967). The glaciers of the Ortles-Cevedale group constitute a major resource for the local population because they have a great touristic appeal and are precious water resources. This mountain group is one of the largest glacierized regions along the southern side of the European Alps (76.8 $km^2$, approximately 3.5% of the total alpine glacierized area) and hosts the largest Italian valley glacier (Forni, 11.3 $km^2$). Similar to most of the glaciers in the European Alps, the Ortles-Cevedale glaciers have been retreating since the end of the Little Ice Age (LIA), with phases of temporary re-advancement during the 1890s, 1910–1920s and 1970–1980s (Carturan et al., 2013). A new phase of strong retreat began during the second half of the 1980s and continues today (Citterio et al., 2007; CGI, 1978–2011, Zemp et al., 2008, Salvatore et al. 2015, Smiraglia et al. 2015). The Ortles-Cevedale group lies in a transition zone between the "inner dry alpine zone" to the north (Venosta Valley - Frei and Schär, 1998) and the wetter area under the influence of the Mediterranean Sea to the south-western Adamello and Orobie. Climatically, the Ortles-Cevedale massif is characterized by the lowest precipitation in the entire European Alps (500 mm $yr^{-1}$ at the floor of the Venosta Valley). Precipitation does increase southward, however, reaching 900 mm $yr^{-1}$ in the valleys at the southern edge of Ortles-Cevedale, while a total annual precipitation of 1300 – 1500 mm $yr^{-1}$ has been estimated at 3000 – 3200 m a.s.l. in the area of the Careser glacier (Carturan, 2010; Carturan et al., 2012). In the valleys, the annual precipitation ranges from ~900 mm at the southern edge of the group to ~500 mm at the northern edge. Precipitation increases with altitude, up to values of 1300 –1500 mm $yr^{-1}$ at 3000–3200 m within the glacierized areas of the group (Carturan, 2010; Carturan et al., 2012). The mean annual 0-°C isotherm is located at approximately 2500 m. The longest time series of direct mass-balance measurements in the Ortles Cevedale group is available for the Careser glacier (World Glacier Inventory code I4L00102519; WGMS, 1989), which began in 1967 (Zanon, 1992;

Carturan and Seppi, 2007; WGMS, 2011). Other much shorter mass-balance series in this group exist for the Fontana Bianca glacier (1984–1988, restarted in 1992) and Sforzellina glacier (since 1987) (CGI, 1978–2011; WGMS, 2008). Mass-balance investigations also began in 2003 on the La Mare glacier (Carturan et al., 2009) and in 2004 on the Vedretta Lunga glacier (WGMS, 2008). The proposed head catchment has a good availability of climatic and hydrometric data and glacier mass-balance measurements (Carturan, 2010). In particular, Luca Carturan (TESAF - University of Padua) installed a piezometer at the close section of the La Mare Basin (fuelled by the La Mare glacier) in 2007. The time series of the mass-balance measurements (more than ten years) and experimental hydrometric data (approximately ten years) enable us to recognize the variations in seasonal runoff with respect to variations in La Mare's extension. The La Mare basin has also previously been selected for studying the behaviour of meteorological variables at high altitude (Carturan et al., 2012) and developing an enhanced temperature-index glacier mass-balance model (Carturan et al., 2012).

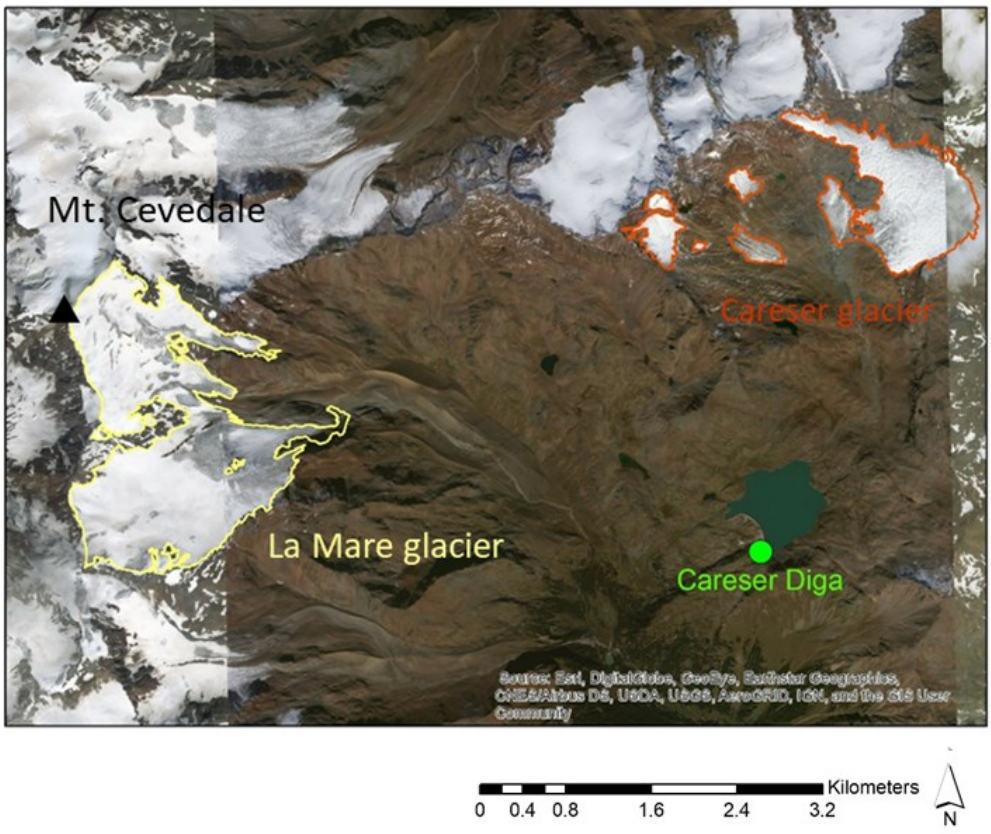


*Figure 11: Orthophotos of the upper Val di Peio and the locations of two glaciers, namely, the La Mare glacier (2650 m – 3769 m) within the yellow line and the Careser glacier (2865 m - 3280 m) within the red line, and the Careser weather station at Careser dam (2605 m). Sources of the orthophotos: Esri, DigitalGlobe, GeoEye, Earthstar Geographics, CNES/Airbus DS, USDA, USGS, AEX, Getmapping, Areogrid, IGN, IGP, swisstop and the GIS User Community.*

Two weather stations have operated since the 1930s in Val de la Mare, namely, Careser Diga (2605 m a.s.l.) and Cogolo (1200 m a.s.l.), which record the 2-m air temperature and precipitation. Since the 1990s, these stations have recorded hourly data. Daily observations of the snow depth and fresh-snow height are also available for Careser Diga. At this station, the mean 1979–2009 annual precipitation (corrected for gauge errors) is 1233 mm, and the

mean annual air temperature is –0.4 °C (Carturan et al., 2012). During the accumulation season, precipitation is mainly delivered by synoptic disturbances and southerly winds, while thermal convection and thunderstorms prevail during the summer. Post-event snow redistribution during the accumulation season typically occurs with strong north-westerly winds. The Careser Diga weather station has one of the longest available series of meteorological data in the Alps at such altitude. Since 2007, an automatic weather station that is owned by the University of Padua has operated on the surface of the La Mare glacier, whose mass-balance measurement series began in 2003.

We selected four additional basins (with increasing drained area) inside the Noce basin according to the progressive extension of Val de La Mare. Our selection of the basins was based on the availability of runoff data to calibrate and validate the glacio-hydrological model. Consequently, we searched for some hydrometric stations inside the Noce basin with specific characteristics. We required two essential characteristics: first, the hydrometric stations had to have recorded data since 1930, and second, the hydrometric stations had to be located in basins with no hydroelectric infrastructure. However, the Noce basin has provided very little data before the 1960s; furthermore, three dams have been built since the 1960s for hydroelectric uses. The Careser dam and Pian Palù dam were built in the upper region of the basin, while the Tassullo dam was built in the middle region of the basin. We selected four hydrometric stations inside the Noce basin according to our modelling needs and the limitations of the available data. Two of these stations represent the conditions until the 1960s with no hydroelectric infrastructure, while the other two stations represent the conditions after the 1960s with hydroelectric infrastructure. We selected the hydrometric stations at Pian Venezia and Vermiglio for the period after the 1960s and the stations at Ponte Rovina and Tassullo for the period before the 1960s (Table 3).

We used Pian Venezia for calibration and validation and Vermiglio for validation for the 2000s period. However, we used Tassullo for calibration and validation and Ponte Rovina for validation for the 1940s period. Table 2 shows the characteristics of the four hydrometric stations that we used during the modelling and calibration of the model.

*Table 2: Management and locations of the hydrometric stations. PAT = Provincia Autonoma di Trento.*

| *Hydrometric station* | *Reference* | *Longitude [°]* | *Latitude [°]* | *Elevation [m]* |
|---|---|---|---|---|
| Pian Venezia | TESAF department | 10.67 | 46.43 | 2295 |
| Vermiglio | PAT Hydro-network | 10.68 | 46.29 | 1173 |
| Ponte Rovina | PAT Hydro-network | 10.86 | 46.33 | 783 |
| Tassullo | PAT Hydro-network | 11.06 | 46.34 | 380 |

*Table 3: Validity and reference periods of the hydrometric stations.*

| *Hydrometric station* | *Validity period* | *Reference period* |
|---|---|---|
| Pian Venezia | After 1960s | 2000s |
| Vermiglio | After 1960s | 2000s |
| Ponte Rovina | Before 1960s | 1930s |
| Tassullo | Before 1960s | 1930s |

After we selected the hydrometric stations for the modelling, we extracted the four catchments drained at these stream-gauging stations (Figure 9). Even if it is a sub-catchment, the catchment drained at Pian Venezia is call Val de La Mare from here on. Table 4 and Figure 12 show the topographic characteristics of the four studied basins

*Table 4: Topographic characteristics of the four studied basins.*

| Catchment | Area [km$^2$] | $Z_{mean}$ [m] | $Z_{min}$ [m] | $Z_{max}$ [m] | LIA glacierized area | 2000s glacierized area |
|---|---|---|---|---|---|---|
| Tassullo | 1046.1 | 1705 | 380 | 3759 | 4% | 2% |
| Ponte Rovina | 385.6 | 2148 | 783 | 3759 | 11% | 4% |
| Vermiglio | 79.8 | 2210 | 1173 | 3556 | 14% | 6% |
| Val de La Mare | 8.4 | 3082 | 2295 | 3759 | 69% | 45% |

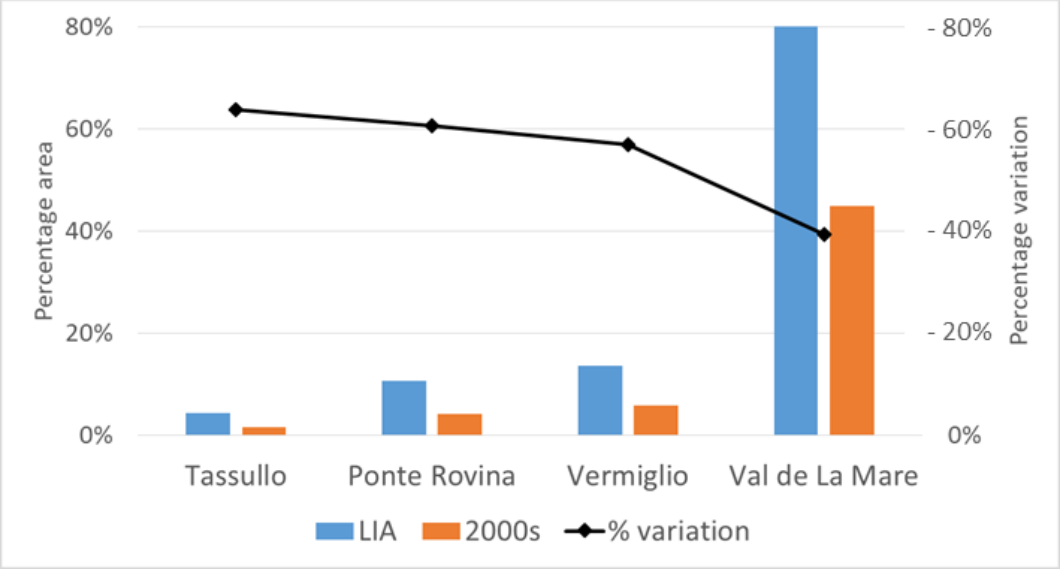


*Figure 12: Percentage of the glacierized area and the related percentage variation from the LIA to the 2000s.*

## **2.2.** Management of data input

In this section, we describe the collection of the primary data, the methodology to prepare the data input for the glacio-hydrological model, and, the methodology to apply the modelling. We considered two types of data input. The first was the meteorological input, and the second was the topographic input. In addition, we used the runoff datasets from the four hydrometric stations to calibrate and validate the model.

### *2.2.a. Meteorological input*

We used the weather stations at Careser Diga, Peio and Passo Mendola to reconstruct the temperature series. Furthermore, we used the weather stations at Careser Diga, Peio, Passo Mendola, Tonale and Malè to reconstruct the precipitation series (Figure 13 and Table 5). The three temperature series and the five precipitation series were homogenized

with homogeneous data from other stations in the Alps (Auer et al., 2006). After obtaining homogeneous data, we filled the gaps in the series and obtained complete temperature and precipitation series. We selected seven weather stations in the Noce basin (close to the Tassullo station) to reconstruct the temperature and precipitation series.

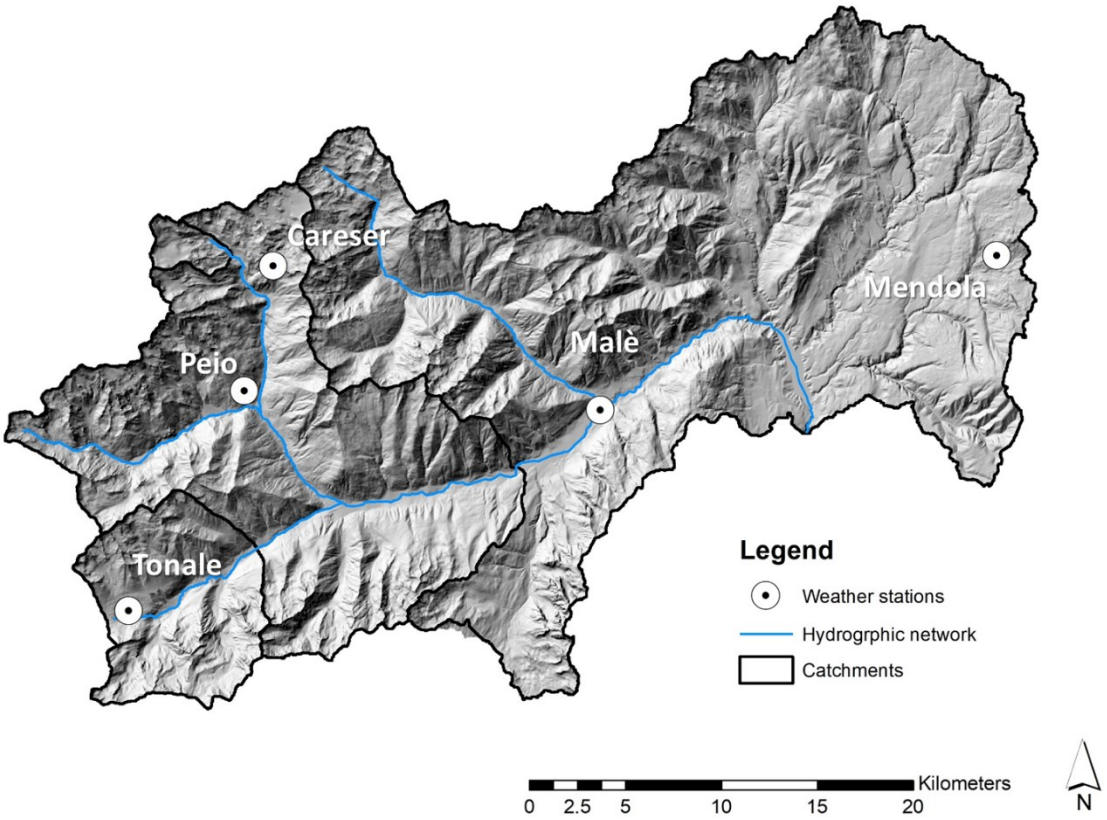


*Figure 13: Spatial distribution of the weather stations in this research.*

However, frequent problems were present in the time series. Despite the large number of stations, we could not definitively establish which periods were homogeneous for each station. Indeed, several problems were found, for example, a lack of continuity in the series, a lack of specific metadata for individual stations, and a lack of homogeneous reference series in the study area. Thus, we only selected the weather stations most representative of the study area with the least problems. We used the weather stations at Careser Diga, Peio and Passo Mendola; for the temperature series and the weather stations at Careser Diga, Peio, Passo Mendola, Tonale and Malè for the precipitation series.

*Table 5: Characteristics of the weather stations, including the altitude and following meteorological variables: T = temperature and P = precipitation.*

| *Weather station* | *Altitude [m] a.s.l.* | *Meteorological variable* |
|---|---|---|
| Careser Diga | 2607 | T, P |
| Peio | 1586 | T, P |
| Passo Mendola | 1316 | T, P |
| Tonale | 1735 | P |
| Malè | 730 | P |

According to the WMO (Aguilar et al., 2003), two important steps are required to process raw meteorological data: checking the homogeneity of the time series data and filling any gaps in the series. Homogenization is the procedure of making a time series homogeneous by using a technique to remove artificial bias (Aguilar et al., 2003). According to the WMO (Aguilar et al., 2003), homogeneity testing is performed to ensure that time fluctuations in the data are only caused by vagaries in the weather and climate. The temporal homogeneity of a climate record is essential in climatological research, particularly when data are used to validate climate models. The procedure for filling gaps in the time series after obtaining homogeneous data is crucial to obtain continuity in the time series.

In the next section, we describe the techniques that we used for the homogenization and gap-filling of the time series.

#### 2.2.a.1. Homogenization of the time series

We tested the homogeneity of the series using the Craddock test (Craddock, 1979), which is one of the most recognized and used tests for the homogenization of time series. The Craddock test is a statistical test that checks the homogeneity of a series of data (candidate series, $CS$) and the eventual homogenization through a comparison with measurements from neighbouring stations. This test requires the elaboration of a reference series ($\mathrm{RS}$) from the weighted average of data from meteorological stations that are close to the candidate series. The weight of each station is proportional to the square of the correlation coefficient with the same candidate series. The difference between the reference and candidate series is assumed to be constant during temperature and precipitation analysis. This assumption was made when the candidate series was perfectly homogeneous with reference series. Actually, the natural climate variability that exists between stations always produces a certain deviation. A reconstructed series ($Ric$) was created according to the following formula to better analyse trends:

*Equation 29*

$$Ric_i = ST - RS + RS_i$$

where $ST$ is the average value of the series that must be tested for all the period on which the test is conducted and $RS$ is the mean value of the reference series during the same period. At this point, the Craddock series ($C_i$) is calculated with the differences that accumulated each year between the candidate and reconstructed series according to the following formula:

*Equation 30*

$$C_i = C_{i-1} + Ric_i - CS_i$$

The accumulated differences for homogeneous series should form a horizontal line, specifically, s (t) = 0, when plotting the Craddock chart. However, the diversity of climate

regimes between the series to be homogenized and the reference series introduce a climatic noise in the Craddock function that causes a slight deviation from the above curve s (t) = 0.

If the curve is very different from zero, and at one point there was a net increase in its slope, at that point it is likely that there is a lack of homogeneity (Figure 14) of the time series; however, if the curve transitions from a steep slope to a lower or null slope, this lack of homogeneity disappears.

The calculation of corrections for temperature series involves the constant difference:

*Equation 31*

$$\Delta T = d_{hom} - d_{err}$$

where $d_{hom} = CS - RS$ for homogenous periods and $d_{err} = CS - RS$ for non-homogenous periods.

The homogenization of temperatures (Figure 14 and Figure 15) is conducted through the following relationship:

*Equation 32*

$$T_{hom} = T_{orig} + \Delta T$$

where $T_{orig}$ is the non-homogeneous real value and $T_{hom}$ is the homogenous temperature value.

This test includes a subjective margin, which is based on the experience of the climatologist in identifying inhomogeneous periods to correct.

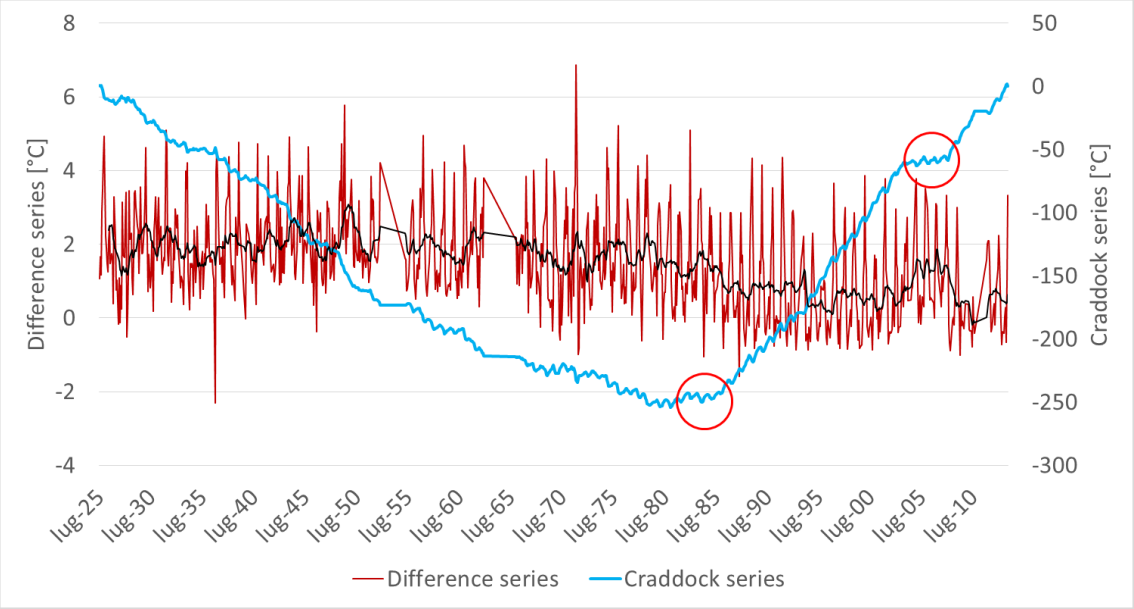


*Figure 14: Example of non-homogenized series (Peio weather station). The blue line marks the Craddock series, the red line marks the temperature-difference series, and the black line marks the 12-month moving average. The red circles represent inhomogeneities, which were identified as slope changes in the Craddock series.*

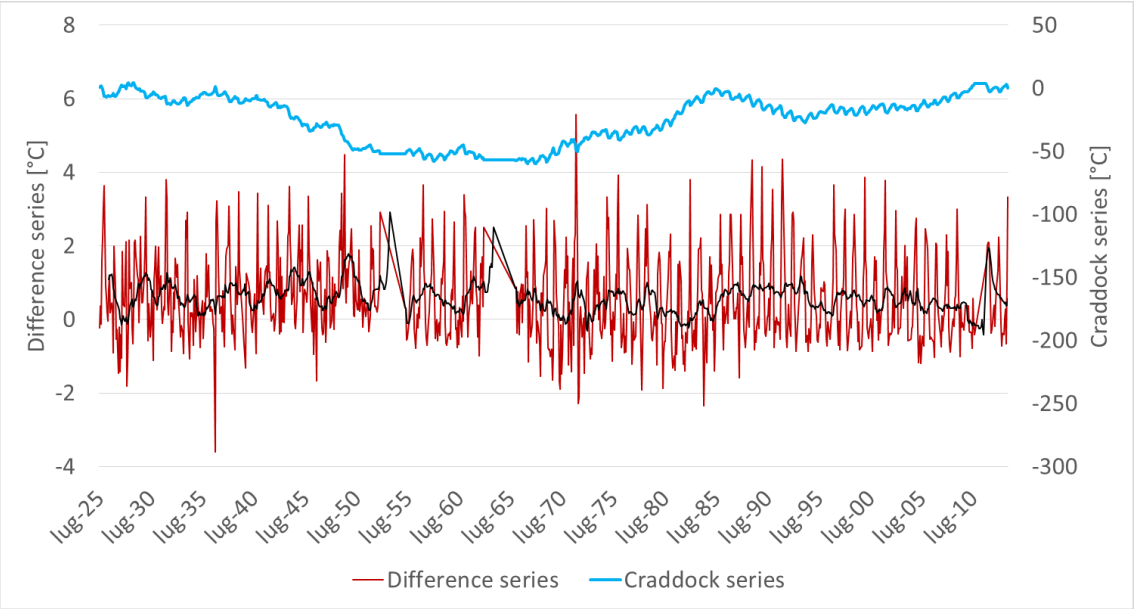


*Figure 15: Example of homogenized series (Peio weather station). The blue line marks the Craddock series, the red line marks the temperature-difference series, and the black line marks the 12-month moving average.*

### 2.2.a.2. Gap-filling of the time series

The second important step in the processing of raw meteorological data is filling gaps in the homogeneous series. We use the linear regression (or polynomial relationship) between two stations that are well-correlated for temperature series. We can analyse both the temperature-difference series and the scatterplot among the stations to search for the best correlation between stations. The average difference must remain constant in time for difference series. After identifying the best weather station to fill the gaps in the candidate station, we must validate the determined relationship model. One of the best efficiency indices for the management of meteorological and hydrological data is the Nash and Sutcliffe index (Nash and Sutcliffe, 1970).

The Nash and Sutcliffe index has the following equation:

*Equation 33*

$$N = \frac{F_o^2 - F^2}{F_o^2}$$

where $F^2$ is defined as

*Equation 34*

$$F^2 = \sum_{i=1}^{n} [q_o(t) - q_s(t)]_t^2$$

and $F_o^2$ is defined as

*Equation 35*

$$F_o^2 = \sum_{i=1}^{n} [q_o(t) - \bar{q}]_t^2$$

$q_o$ is the observed value, $\bar{q}$ is the average observed value and $q_s$ is the calculated value.

We used the ratio between the cumulated precipitation during the same period between two stations that are well-correlated to fill any gaps in the precipitation series. Furthermore, we must consider separately the ratio between the accumulated solid precipitation and the accumulated liquid precipitation. This distinction (solid precipitation vs liquid precipitation) can be considered through two methods. The first method is based on a daily temperature threshold (equal to 2 °C), and the second method is based on the monthly sums of precipitation. Consequently, the ratio between the sums of precipitation considers only two periods (one ratio between the sum of the solid precipitation and the sum of the liquid precipitation) or twelve periods (one period for each monthly ratio). We can analyse both a simple scatterplot among the stations and a scatterplot of the accumulated precipitation (by diversifying the solid and liquid precipitation) to search for the best correlation among the stations. The slope of the scatterplot must not change during the analysis of the scatterplot of the progressive sum. In contrast, an inhomogeneity in one of the two analysed stations may occur. In this case, we must adopt the Craddock method for the homogenization of the precipitation series. Furthermore, we can use the Nash and Sutcliffe index to validate the determined relationship model.

#### 2.2.a.3. Temperature series

We used daily data from the PAT website to reconstruct the temperature series of the stations at Peio and Passo Mendola. We used three different series that had historical metadata for the temperature series at Careser. The first series was a dataset of printed daily data that were stored in the annual hydrological archive at the Careser dam (available from 1959 to 1993). The second series was the daily dataset from the PAT website (from 1930 to 2015). Finally, the third series was that from an Onset Hobo temperature data-logger that was installed in 2002 by Luca Carturan (TESAF - University of Padua) inside the Stevenson screen, which was used by manual observers until the installation of automatic instruments in 1991. Initially, we wanted to consider the maximum and minimum daily temperature series to test the homogeneity and fill any gaps in the series before calculating the mean daily temperature. However, we had to calculate the mean daily temperature before the homogeneity tests because the minimum and maximum daily temperatures were not homogenous during the same periods. In contrast, we considered the maximum and minimum daily temperatures for the period around 2002 for the weather station at the Careser dam. Indeed, the PAT weather station did not correctly work from 2002 to 2015, so we had to use the Hobo temperature sensor. We also had to test the homogeneity between

two temperature sensors, namely, the PAT and Hobo temperature sensors, because of the sensor exchanges in the time series. After using the Craddock test, the Hobo minimum daily temperature was over 0.3 °C warmer than the PAT minimum daily temperature, while the Hobo maximum daily temperature was 0.7 °C colder than the PAT maximum daily temperature. However, these temperature differences compensated each other (ΔT of 0.2 °C), thus remaining below the threshold of 0.5 °C, which can be assumed as a minimum threshold for inhomogeneities because of the different sensors and radiation shield that were used. We tested the homogeneity of the data after calculating the mean daily temperature for the three weather stations (Careser Diga, Peio and Passo Mendola) from 1920 to 2015.

First, we used the Craddock test across the three weather stations (Careser, Peio and Passo Mendola) to test the homogeneity. However, we could not recognize the homogeneous and inhomogeneous periods for each station. Consequently, we had to find some homogeneous weather stations in the Alps that were useful for the analysis. We used monthly homogeneous data from weather stations at Bolzano (IT), Davos (CH), Säntis (CH) and Segl-Maria (CH) for the period from 1920 to 2015 (Table 6). These four stations were homogenized by the HISTALP database (Bolzano - Auer et al., 2006) and the Swiss meteorological service (Davos, Säntis and Segl-Maria RIF).

*Table 6: Characteristics of the weather stations that were used to homogenize the temperature series: T = temperature, P = precipitation.*

| *Weather station* | *Altitude [m] a.s.l.* | *Coordinate [lat, long]* | *Meteorological variable* |
|---|---|---|---|
| Bolzano (IT) | 272 | 46°50’, 11°33’ | T, P |
| Davos (CH) | 1594 | 46° 49’, 9° 51’ | T, P |
| Säntis (CH) | 2502 | 47° 15', 9° 21’ | T, P |
| Segl-Maria (CH) | 1804 | 46° 26, 9° 46’ | T, P |

We used two weighted distance reference series to apply the Craddock test because of the distance between the weather stations at Careser Diga and Peio and the weather station at Passo Mendola (Figure 13). The first series referred to the distance from the area near Careser Diga and Peio and the weather stations at Bolzano, Davos, Säntis and Segl-Maria. The second series referred to the distance between Passo Mendola and the weather stations at Bolzano, Davos, Säntis and Segl-Maria. Finally, we tested the homogeneity of the weather stations at Careser, Peio and Passo Mendola with the relative reference series. We found two inhomogeneous periods for Careser, two inhomogeneous periods for Peio and two inhomogeneous periods for Passo Mendola (Table 7) according to a sensitivity threshold of 0.5 °C. After calculating $\Delta T$(Equation 31), we corrected the temperature series by using Equation 32.

*Table 7: Inhomogeneous periods and corrections applied to the temperature series.*

| *Weather station* | *Inhomogeneous period from - to* | ΔT [°C] |
|---|---|---|
| Careser | 1949 -1957 | -0.8 |
| | 1958 – 1967 | + 0.7 |
| Peio | 1925 - 1985 | -1.3 |
| | 2004 – 2008 | -1.03 |
| Passo Mendola | 1925 – 1982 | + 0.58 |
| | 1990 – 2007 | + 0.96 |

We filled in any gaps after obtaining the three homogeneous series. In Appendix we report the table with the gaps in the raw series (Table 45). We used a linear regression for each constant period (homogenized period and non-homogenized period) between the two considered weather stations to fill in these gaps (e.g., we used seven linear regressions between Careser and Peio because each station had two homogenized periods and two non-homogenized periods). We calculated the linear regression for each constant period by only considering the periods with no gaps at both stations. We used seven linear regressions between Careser and Peio to fill in gaps in Careser's temperature series and vice versa for the Peio temperature series. Furthermore, some gaps existed in Peio's temperature series before 1930. Neither Careser nor Passo Mendola had data before 1930; therefore, we had to identify another homogeneous weather station to fill in any gaps before 1930. We processed data from three weather stations that recorded daily data before 1930: Innsbruck (A), Säntis (CH) and Sonnblick (A). The weather station at Sonnblick had the best correlation ($R^2$ = 0.81) with Peio for the period before 1930. Thus, we used the linear regression between Peio and Sonnblick to fill the gaps in the Peio series before 1930. Finally, we used seven linear regressions between Passo Mendola and Careser and between Passo Mendola and Peio to fill in any gaps in the Passo Mendola temperature series. We had to use two stations (Careser and Peio) to fill in gaps in the temperature series at Passo Mendola because neither Peio nor Careser could fill all the gaps in the Mendola series. Some gaps could be solved with Careser, while other gaps could be solved with Peio (Table 8).

*Table 8: Stations that were used for the gap-filling of the temperature series.*

| *Selected station* | *Station for gap-filling* |
|---|---|
| Careser | Peio |
| Peio | Careser |
| | Sonnblick |
| Passo Mendola | Careser |
| | Peio |

#### 2.2.a.4. Precipitation series

We used daily data from the PAT website to reconstruct the precipitation series of the stations at Peio, Passo Mendola, Tonale and Malè (Table 5). As for the temperature series, we used different series with historical metadata for the precipitation series at Careser. The first series was a dataset of printed daily data in the annual hydrological archive at the Careser dam (available from 1959 to 1993). The second and third series were daily datasets from the website of the PAT; the second series was recorded by a manual rain gauge from 1930 to 1993, and the third series was recorded by an automatic, tipping-bucket rain gauge from 1993 to 2015.

Further analysis was required before testing the homogeneity in the precipitation series. Indeed, we found some overestimated rainfall, underestimated rainfall and aggregations of several days of rainfall in the PAT series. We recognized these cases by observing the five precipitation series side by side. For every day and every station, we calculated the standard deviation between the considered station and the average of the data from the other four stations by using a threshold of 5 mm to spot irregularities. Subsequently, we crossed these results with a specific test to find the days when the considered station was the only station that recorded no precipitation. Finally, we individually analysed the days that were highlighted by the test; if we recognized them as anomalies, we considered the data as a gap in the precipitation series.

Unlike the temperature series, we could unequivocally recognize homogeneous and inhomogeneous periods crossing five weather stations (Careser, Peio, Passo Mendola, Tonale and Malè) by using the Craddock test. Indeed, three stations out of these five (Careser, Peio and Malè) were homogeneous with each other. We considered two reference series to calculate the corrections to homogenize the Tonale series ($\Delta P_{Ton}$) and Passo Mendola series ($\Delta P_{PM}$). The first reference series, which was used to calculate $\Delta P_{Ton}$, was weighted on the correlation (R) between the Tonale station and the Careser, Cogolo, Peio and Malè stations. The second reference series, which was used to calculate $\Delta P_{PM}$, was weighted on the correlation (R) between the Malè station and the Careser, Cogolo, Peio and Malè stations. Finally, we tested the homogeneity of the weather stations at Tonale and Passo Mendola with the relative reference series.

We found one inhomogeneous period for Tonale and one inhomogeneous period for Passo Mendola according to a sensitivity threshold of 15% (percentage correction compared to the measured data - Table 9).

*Table 9: Inhomogeneous periods and corrections that were applied to the precipitation series.*

| *Weather station* | *Inhomogeneous period from - to* | *ΔP [%]* |
|---|---|---|
| Tonale | 1923 - 1968 | +17 |
| Passo Mendola | 1930 - 1936 | -36 |

We filled in any gaps after obtaining five homogeneous series with no anomalies. In Appendix we report the table with the gaps in the raw series (Table 45). We used the ratio between the monthly sums of precipitation between stations with the highest correlation (R2)

to fill in these gaps. We only considered periods with no gaps at both stations to calculate the ratio between the monthly sums of precipitation. We calculated the twelve monthly ratios for each constant period (homogenized period and non-homogenized period) at the two homogenized stations (Tonale and Passo Mendola). In some cases, we had to use two or more stations to fill in gaps in a series because of gaps in the selected series: some gaps could be solved with one series, while other gaps could be solved with another series. Table 10 shows the stations that were used for the gap-filling in the precipitation series.

*Table 10: Stations that were used for the gap-filling of the precipitation series.*

| *Weather station* | *Stations for gap-filling* |
|---|---|
| Careser | Peio<br>Cogolo |
| Peio | Careser<br>Cogolo<br>Malè |
| Malè | Careser<br>Cogolo<br>Peio |
| Tonale | Careser<br>Cogolo<br>Malè |
| Passo Mendola | Careser<br>Cogolo<br>Malè |

Finally, we had to correct the data precipitation input because of precipitation underestimations from instrumental under-catching (Carturan et al., 2012), and we corrected the precipitation data with the snow correction function (SCF) and precipitation correction function (RCF). We used the method by Carturan et al. (2012), which considers the solid and liquid fraction of the precipitation. Table 11 shows SCF and RCF values that we used for each station.

*Table 11: RCF and SCF values in this work*

| Weather stations | Careser | Peio | Malè | Tonale | Mendola |
|---|---|---|---|---|---|
| Elevation [m] | 2067 | 1586 | 730 | 1735 | 1316 |
| RCF | 1.1 | 1 | 1 | 1 | 1 |
| SCF | 1.8 | 1.1 | 1.1 | 1.3 | 1.1 |

### *2.2.b. Topographic input*

We prepared the topographic dataset as input for the glacio-hydrological model after obtaining the continuous temperature and precipitation series. We required one DTM and one topographic ice surface for each glacier cover scenario based on the above three scenarios (Table 1). Consequently, we required both the DTM and the topographic ice surface relative to the glaciers' extension during the 1920s and 2000s. Furthermore, we required the bedrock surface for each glacier for the third scenario (hypothetical absence of glaciers). However, only the DTM of the study area in 1980 (extracted from the Carta Tecnica Provinciale) and the LiDAR DTM in 2006 (PAT survey) represented our raw topographic dataset. According to Table 1, we only had the DTM from the 2000s glacial extension as data input. We lacked the bedrock surfaces and the topographic surface of the LIA; therefore, we calculated them using the topographic surface in 2000s and LIA glacier boundaries (Zanoner et al., 2017).

#### 2.2.b.1. HFB model

We reconstructed two topographic surfaces in this study. The first was the LIA ice surface of forty-five glaciers in the study area (1$^{st}$ scenario, Table 1). The second surface was the bedrock of fifty-six glaciers in the study area (2$^{nd}$ scenario, Table 1). We implemented a model that was based on Huss and Farinotti (2012) and a model by Benn and Hulton (2010) to reconstruct both the ice surface relative to any period and the bedrock surface.

The HFB model calculated each type of surface. HFB calculated the bedrock surface by using a known ice surface as input. In addition, HFB calculated the 2D ice surface of one or more specific flowlines (Ice Surface Flowline - "$I_{ce}S_{urf}$-FL") inside the glacier by using the bedrock surface.

HFB followed three steps. During the first phase, HFB calculated the bedrock surface by using the known ice surface (in this work, we used the 1980 DTM). During the second phase, HFB used the calculated bedrock to simulate the $I_{ce}S_{urf}$-FL. During the third step, we use the calculated $I_{ce}S_{urf}$-FL as constraints to hand-draw the glacier contours inside the known glacier boundary. To calculate the $I_{ce}S_{urf}$-FL, HFB used the flowlines inside the glacial extension, which were drawn from the glacier tongue to the upper glacier point and watershed according to the topographical evidence.

We calibrated the model by using two different types of data. For the first phase (the calculation of bedrock with the model by Huss and Farinotti, 2012), we calibrated HFB by using three different datasets of geo-radar measurements. We used geo-radar measurements from the La Mare glacier (2011 and 2015 surveys), the Careser glacier (2007 survey) and the Agola glacier (2005 survey). For the second phase (the simulation of $I_{ce}S_{urf}$-FL), we calibrated HFB based on the geomorphological evidence (e.g., trimlines and moraines) for each glacier. Finally, we validated the HFB model considering separately the bedrock calculations and the ice surface calculations. We validated the bedrock calculations using the 2007 geo-radar survey (in the glaciated area) and the 2014 LiDAR survey (in the

deglacierized area) in the area of Careser glacier. Subsequently, we validated the ice surface calculations using the topographic ice surface of Careser glacier surveyed in August 1933 by terrestrial photogrammetry (Desio, 1967). After the calibration and validation, we applied the HFB model to every glacier in the study area by using a threshold area of 50 ha. For glaciers with an area below this threshold, we drew contours of the topographic ice surface by using only the known boundary extension with no constraints.

HFB was developed from the models by Huss and Farinotti (2012) and Benn and Hulton (2010). Huss and Farinotti (2012) proposed a simple dynamic model to obtain the spatially distributed thickness of individual glaciers. This model is a physically based approach to calculate the distribution and volume of the glacier-ice thickness (Huss and Farinotti 2012). We considered a steady state condition for the glaciers inside the study area. This steady state was represented by the extension relative to the 1980s. Thus, we did not use the apparent mass-balance gradient, as explained by Huss and Farinotti (2012). On the other hand, we used the actual mass-balance gradient based on available mass-balance measurements from the study area (Carturan and Seppi, 2009, Carturan et al., 2013, Carturan 2016). Huss and Farinotti (2012) proposed the use of the apparent mass balance for glaciers that are not in a steady state. This steady state condition is often violated in today's climate, with many glaciers out of equilibrium. However, glaciers were closer to equilibrium during the 1980s, so we could use the actual mass balance and the available surface topography for that period. In our study, we divided the set of glaciers into two typologies. Glaciers with an annual mass-balance gradient that was driven by direct alimentation characterized the first type. These types of glaciers had a specific annual mass-balance gradient of 0.0006 m/m in the ablation area and 0.0003 m/m in the accumulation area. These values were the empirical values that were calculated on the La Mare and Careser glaciers (Carturan and Seppi, 2009, Carturan et al., 2013, Carturan 2016). We considered these two glaciers to be sufficiently representative for direct accumulation. Conversely, glaciers with an annual mass-balance gradient that was driven by avalanche alimentation characterized the second type. These types of glaciers had the same annual mass-balance gradient values for the accumulation and ablation areas. We considered this value to equal 0.012 m/m according to the calculated value for the Agola glacier (Carturan and Seppi, 2009, Carturan et al., 2013, Carturan 2016). We divided the glacial surface into elevation bands of 1 m, rather than 10 m as performed by Huss and Farinotti (2012), because this interval facilitated the calculation of the Equilibrium Line Altitude (ELA). In HFB, we applied a weight to the distance of each DTM cell from the glacier boundary and the local slope of each DTM cell. Table 12 shows the values of the calibrated parameters from the calibration of HFB for the geo-radar surveys on the La Mare, Careser and Agola glaciers.

*Table 12: Calibration of the parameters for HFB and a comparison with the values from Huss and Farinotti (2012).*

| *Parameter* | *Description* | *HFB value* | *Huss and Farinotti (2012) value* |
|---|---|---|---|
| $A_f(T)$ | Rate factor of the flow law | 0.15 (bar$^{-3}$ yr$^{-1}$) | 0.075 (bar$^{-3}$ yr$^{-1}$) |
| *e_b* | Elevation band | 1 (m) | 10 (m) |
| *s_l* | Slope limit | 9 (°) | 6 (°) |
| *P_dist* | Parameter for nonlinear distance weighting | 0.005 (-) | Not reported |
| *P_slo* | Parameter for nonlinear slope weighting | 1.5 (-) | Not reported |

HFB calculated the ice thickness ($h_i$) for each DTM cell (Equation 36) and then the elevation of the bedrock from the difference between the ice surface and thickness.

*Equation 36*

$$h_i = \sqrt[n+2]{\frac{(1 - f_{sl})\, q_i}{2\, A_f(T)} \frac{n+2}{\left(F_{s,i}\, \rho g \sin \bar{\alpha}_i\right)^n}}$$

where $q_i$ is the ice flux that is normalized by the glacier width, $f_{sl}$ is a factor that considers basal sliding (Equation 37), $n$ = 3 is the exponent of the flow law, $\rho$ is the ice density, $g$ is the acceleration of gravity, $\alpha$ is the local slope, and $F_{s,i}$ is the valley shape factor (Nye, 1965).

*Equation 37*

$$f_{sl} = c_1 + c_2\,(S - 10) + c_3\,(C - 1)$$

where $c_1$ = 0.2, $c_2$ = 0.1, $c_3$ = 4, $S$ is the glacier area (km$^2$), and $C$ is the continentality. The area-dependent term $c_2\,(S - 10)$ is restricted to the range [-0.1, 0.1], and the continentality term $c_3\,(C - 1)$ is restricted to [-0.25, 0.25].

*Equation 38*

$$C = \left(\frac{ELA_{lat} - ELA_g}{f_{cont}} + 1\right)$$

where $C$ is a continentality index and $f_{cont}$ = 2400 m is a constant parameter that is calibrated to the observed differences in mass-balance gradients between continental and maritime

glaciers (WGMS, 2008). The observed range of $ELA_{lat} - ELA_g$ is from –880 m to +1580 m (2.5% and 97.5% quantiles). $ELA_g$ is the median altitude of a specific glacier, and $ELA_{lat}$ is the latitude-dependent reference ELA.

We attempted to improve Huss and Farinotti's (2012) procedure, particularly over steeper glaciers (such as the La Mare glacier). The first question was related to the spatial distribution of the bedrock surface. We obtained a discontinuous bedrock surface by applying Huss and Farinotti's (2012) model. Although we used an elevation band of 1 m, we obtained an overly discretized surface. HFB proposed progressive smoothing inside the glacier boundary to obtain a more continuous bedrock surface. After obtaining the original bedrock surface from Huss and Farinotti (2012), HFB applied circular smoothing with a constant radius within an area inside the glacier boundary with an internal buffer (negative buffer). The value of this radius could be parameterized (we calibrated this value to be 50 m) and was the same as the absolute value of the negative buffer. HFB applied progressive circular smoothing within the area of the negative buffer from the glacier boundary to the boundary of the negative buffer. The use of a buffer was useful for another issue that we found. The area that was closest to the glacier boundary exhibited a very steep local slope, using the Huss and Farinotti model (2012). Initially, we could calibrate the P_dist and P_slo parameters (Table 12) to obtain a simulated bedrock surface that more closely coincided with the measured bedrock (geo-radar surveys). However, we calibrated the model by using glaciers with different areas, slopes and alimentation types (direct vs avalanche alimentation); therefore, we could not reduce the local slope close to the glacier boundary without worsening the coincidence between the simulated and measured bedrock. Thus, HFB proposed progressive circular smoothing in two directions. The first direction was inside the glacier boundary, and the second direction was outside the boundary. Furthermore, we could parameterize the value of the external buffer (positive buffer) of the boundary. We found a calibrated buffer value of 20 m.

After applying the proposed modifications proposed, HFB could produce a more continuous bedrock surface and reduce the interval between the measured bedrock outside the glacier and the simulated bedrock inside the glacier.

During the second step, HFB used the model by Benn and Hulton (2010). We used the Excel™ spreadsheet from Benn and Hulton (2010) to reconstruct the surface profile of the glaciers in the study area, starting from the bedrock morphology. This Excel™ spreadsheet enabled us to reconstruct the $I_{ce}S_{urf}$-FL. This approach did not use a spatial distribution on the $I_{ce}S_{urf}$-FL (to reconstruct the entire ice surface of the glaciers) but did enable us to more precisely draw the contours of the glacier by using the constraints from the $I_{ce}S_{urf}$-FL. The model by Benn and Hulton (2010) can calculate the surface profiles of former glaciers by using an exact solution of a 'perfectly plastic' glacier model. This model was built on the assumption that ice deforms in response to the driving stress ($\tau_D$) (resulting from the weight and surface gradient of the ice) only when a specified yield stress ($\tau_Y$) is reached. If the driving stress is less than the yield stress, no ice movement occurs and the glacier thickens and/or steepens in response to surface-snow accumulation and melting, increasing $\tau_D$. However, the driving stress can never exceed the yield stress because the ice-surface profile is assumed to continuously adjust to maintain the condition that $\tau_D = \tau_Y$. This equality can be expressed as

*Equation 39*

$$\tau_Y = \tau_D = \rho g H \frac{dh}{dx}$$

where $\rho$ is the glacier's density (~900 kg m$^{-3}$), $g$ is the gravitational acceleration (9.81 m s$^{-2}$), $H$ is the glacier's thickness, $h$ is the ice-surface elevation and $x$ is the horizontal coordinate, with the x-axis parallel to the glacier flow and positive up-glacier:

*Equation 40*

$$\frac{dh}{dx} = \tan \alpha$$

where $\alpha$ is the ice surface's slope. The assumption that the shear stress on the bed equals the driving stress (Equation 39) might be a good approximation for more slowly flowing areas of ice sheets but is unrealistic for ice streams, outlet glaciers, valley glaciers and other topographically controlled ice masses. In these cases, significant resistance to flow can also be produced by side-drag and differential 'pushes and pulls' in the direction of flow (longitudinal stress gradients). The latter are not considered in the 'perfect plasticity' model, but the effects of side-drag can be readily incorporated using a 'shape factor' (Nye, 1952). The shape factor $f$ represents the proportion of the driving stress that is supported by the bed such that

*Equation 41*

$$\tau_B = \tau_Y = f \tau_D$$

where $\tau_B$ is the basal shear stress. The remainder of the driving stress is assumed to be supported by the side drag, which is a function of the shape of the confining valley or channel. If we assume that $\tau_B = \tau_D$ at the centerline, $f$ can be defined as

*Equation 42*

$$f = \frac{A}{Hp}$$

where $A$ is the area of the glacier cross-section, $H$ is the maximum ice thickness in the cross-section and $p$ is the 'glacierized perimeter' of the cross-section (Paterson, 1994). Shape factors are incorporated into the model by replacing $\tau_Y$ with $\tau_Y / f$, so

*Equation 43*

$$\tau_D = \frac{\tau_B}{f}$$

During the application of Benn and Hulton's (2010) model, we applied some modifications to the original procedure that were required to obtain reliable results in our case studies. After drawing one or more flowlines for the glacier and extracting the bedrock elevation, we drew some cross-sections for each flowline and calculated $f$ for each cross-section. We suggest some precautions when applying HFB. First, we suggest drawing the flowline to be perpendicular to the bedrock contours according to geomorphological evidence (e.g., medial moraines or flute moraines) beginning from the lower portion of the tongue and finishing at the upper portion of the glacier. Furthermore, we suggest equally distributing the cross-sections along the flowline, starting and ending the cross-sections along the glacier boundaries at the same elevation. After calculating $f$ for each cross-section, HFB considered the distance of each cross-section from the glacier tongue along the flowline and interpolated the $f$ value by using a second-order polynomial function. Thus, we obtained a continuous variation of $f$ along the flowline. HFB calculated the ice thickness at each vertex of the flowline by using the reduction in the basal shear stress as proposed by Benn and Hulton (2010) with a continuous variation of $f$ along the flowline. HFB used a succession of discrete steps (numbered 1, 2, 3. $i$, $i$ +1, $i$ + 2) to calculate the ice thickness. We calibrated HFB for each glacier. Indeed, we used the target elevation to calibrate the basal shear stress. The target elevations were specific for each glacier and were based on geomorphological evidence (e.g., glacier boundaries, trimlines, and moraines). The target elevations were known elevations of the ice surface that were recognized from the DTM according to geomorphological evidence. We suggest positioning the target elevation near the lower portion of the glacier. Indeed, we could more simply recognize the ice elevation along the glacier tongue. Compared to the model by Benn and Hulton (2010), HFB proposed a possible improvement for the calculation of target elevations that considers concavities and convexities in glacier surface along ice cross-sections.

We studied eighteen alpine valley glaciers, whose surface topographies were available in the form of old maps and/or DTMs. We divided each glacier tongue into three zones, namely, an upper zone, central zone and lower zone, to study the concavity. We calculated the concavity of cross-sections through each zone by using the distance from two subsequent contours. We started the cross-section at the same elevation of the end of the cross-section. After calculating the concavity, we normalized the result with respect to the width of the ice cross-section. The convexities could be greater than + 20% with respect to the width of the ice cross-section. We extracted an average value for each zone of the glacier tongue and calculated an average standard error of 4.41 m (Table 13).

*Table 13: Results of our study on eighteen alpine valley glaciers to estimate the concavity of the tongue as a function of the width of the cross-section.*

| *Glacier-tongue zone* | *Normalized concavity [%]* | *Standard error [m]* |
|---|---|---|
| Lower zone | -7.6 | 3.19 |
| Central zone | -5.9 | 4.9 |
| Upper zone | 7 | 5.13 |
| | | |
| Average | | 4.41 |

HFB fixed the target elevation along the flowline by using the elevation of the cross-section according to the normalized concavity. We could calibrate HFB for each glacier and extract the $I_{ce}S_{urf}$-FL from the target elevation.

During the third step of glacier-surface reconstruction, we used the $I_{ce}S_{urf}$-FL as a constraint to hand-draw the glacier contours inside the glacier boundary. We linked contours outside the glacier that had the same elevation by using the elevation from the $I_{ce}S_{urf}$-FL. The $I_{ce}S_{urf}$-FL provided essential objective information to draw these contours. Indeed, drawing without the $I_{ce}S_{urf}$-FL is highly subjective and is affected by the experience and sensitivity of the user in identifying the topographic ice surface.

#### 2.2.b.1.1. Case study: Taviela glacier

We report a case study to explain the HFB model in detail. We present a summary of the application of the HFB model on the Taviela glacier, which is located in the upper region of the Noce basin close to Peio (Figure 16). The Taviela glacier is one of the glaciers that we consider in this study.

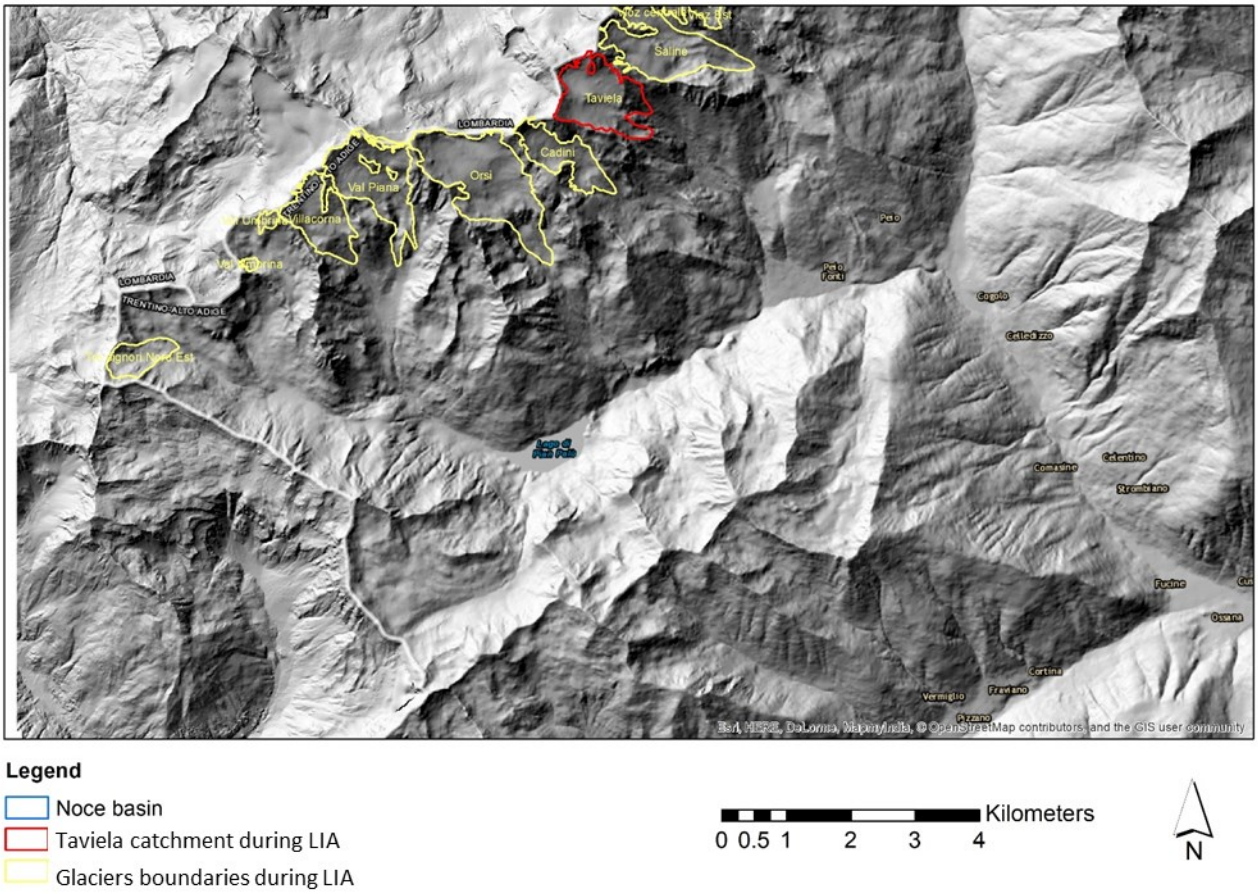


*Figure 16: Location of the Taviela glacier in the Peio valley (inside the Noce basin).*

This case study summarizes the reconstruction of the topographic ice surface of the LIA Taviela glacier (Figure 17). We used the following input for the first step of HFB ($HFB_{bed}$): the Taviela glacier boundary in 1980 (extracted from the Carta Tecnica Provinciale, which also provided elevation data for the 1980 DTM), the 1980 DTM and the 2006 DTM of the area outside the Taviela glacier boundary. We calculated the local slope from the 1980 DTM layer using the ArcGIS software and the topographic parameter for $HFB_{bed}$ (glacier area, median altitude of the glacier and basal sliding factor).

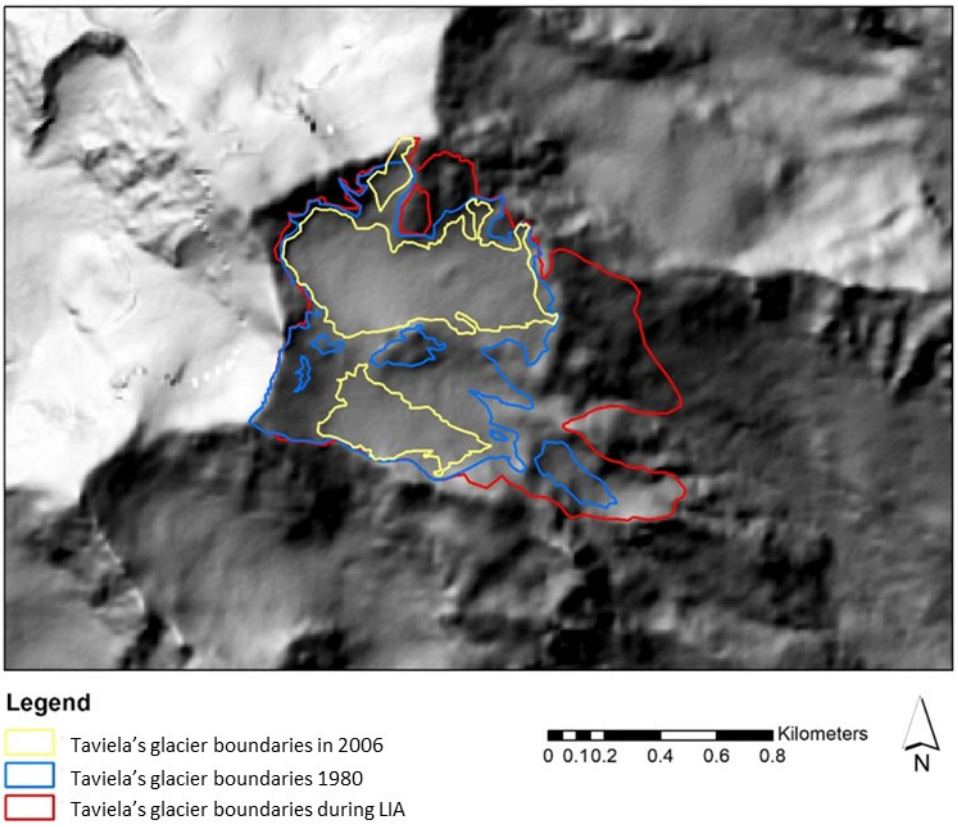


*Figure 17: Extension of the Taviela glacier in three different periods: 2006, 1980 and the LIA.*

Before calculating the 1980 bedrock surface, we calibrated the ELA in $HFB_{bed}$ to obtain a minimum positive *balance ice flux* at the glacier tongue. We applied an annual mass balance gradient that is driven by direct feeding according to the geomorphology of the Taviela glacier (annual_MB_grad, Table 14).

*Table 14: Input parameters for $HFB_{bed}$.*

| *Value* | *Description* | *Units* |
|---|---|---|
| Taviela_dtm_80 | DTM raster FLT | Input |
| Taviela_1980 | Boundary raster FLT | Input |
| | | |
| 0.006 | annual_MB_grad db/dz ablation | $yr^{-1}$ |
| 0.003 | annual_MB_grad db/dz accumulation | $yr^{-1}$ |
| 0.007373052 | $F_{sl}$ Basal sliding factor | dimless |
| 0.15 | $A_f(T)$ Rate factor of the flow law | $bar^{-3}\ yr^{-1}$ |
| 900 | **ρ** ice density | $kg/m^3$ |
| 9.822 | g gravity | $m/s^2$ |
| 3 | enne exponent | (-) |
| 3244 | ELA | m |
| 1 | band_interval | m |
| 0.024 | H initial value | km |
| 10 | number of iterations | (-) |
| 19 | mobile τ moving average amplitude | (-) |
| 9 | slope limit | deg |
| 0.005 | POWER_DST; used for nonlinear distance weighting | (-) |
| 1.5 | POWER_SLO; used for nonlinear slope weighting | (-) |
| 50 | max smoothing radius | m |
| 20 | external smoothing fringe | m |
| | | |
| Taviela_80_deepness | Deepness raster FLT | Output |
| Taviela_83_bedrock | Bedrock raster FLT | Output |

Consequently, $HFB_{bed}$ calculated the Taviela glacier ice depth in 1980 (Figure 18) according to the abovementioned progressive smoothing and the bedrock surface according to the extension of the Taviela glacier in 1980. We used the 2006 DTM, which reported the measured bedrock in the de-glaciated area, for the area between the 1980 boundary and the LIA boundary. We considered a buffer of 50 m from the 1980 Taviela glacier boundaries to merge the $HFB_{bed}$ and 2006 bedrock (Figure 19, Figure 20, and Figure 21).

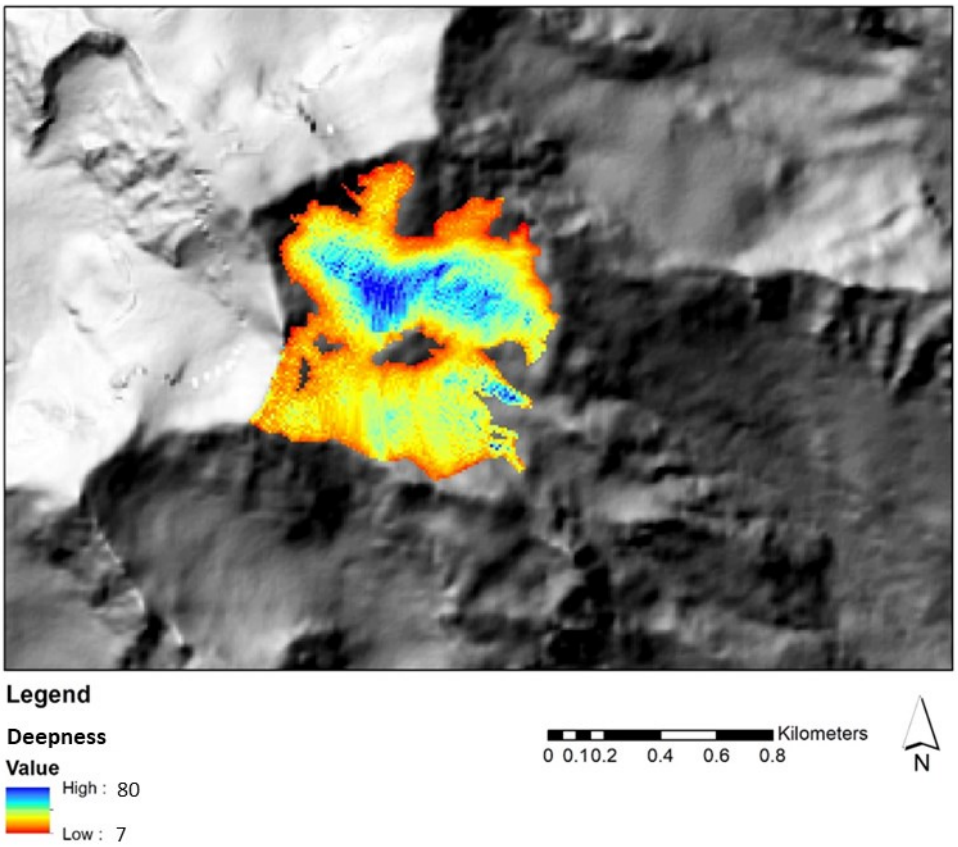


*Figure 18: Raster of the deepness of the Taviela glacier in 1980 that was calculated by $HFB_{bed}$.*

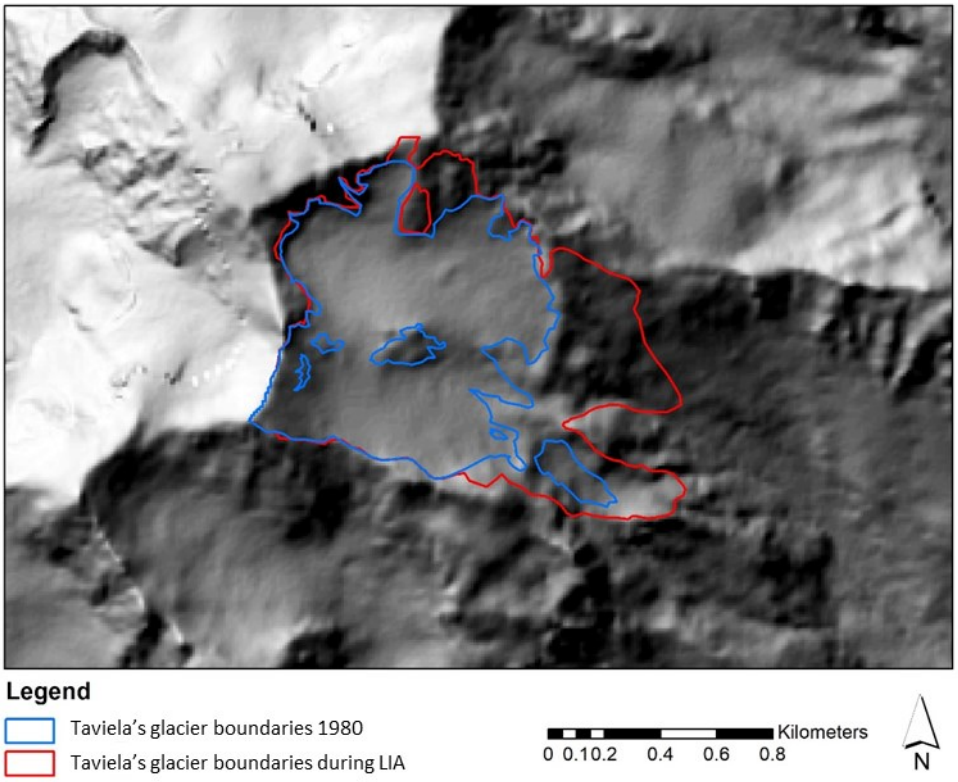


*Figure 19: Surface that was measured in 1980.*

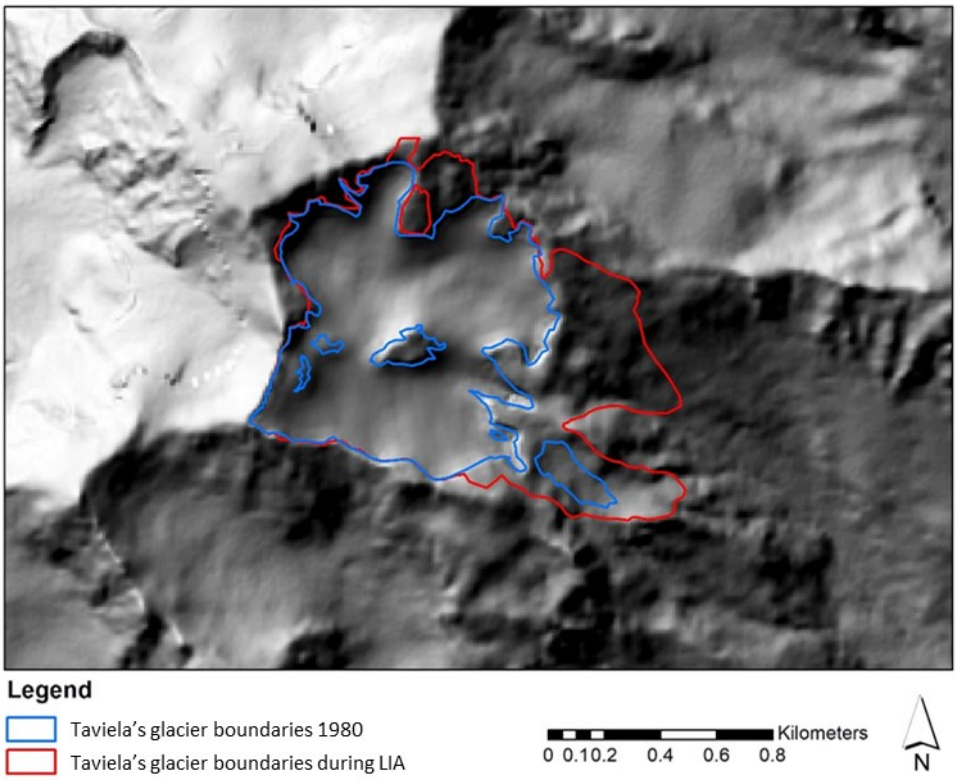


*Figure 20: Bedrock surface that was calculated by $HFB_{bed}$.*

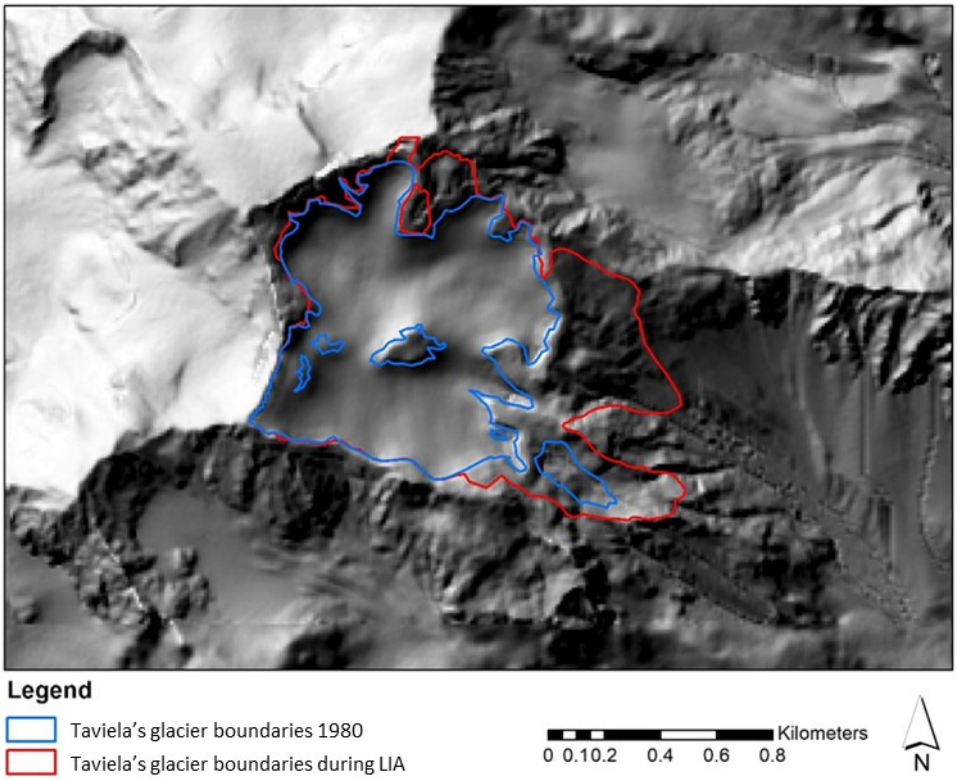


*Figure 21: Merged bedrock that was calculated by $HFB_{bed}$ between the calculated bedrock surface (inside the glacier) and measured 2006 DTM (outside the glacier).*

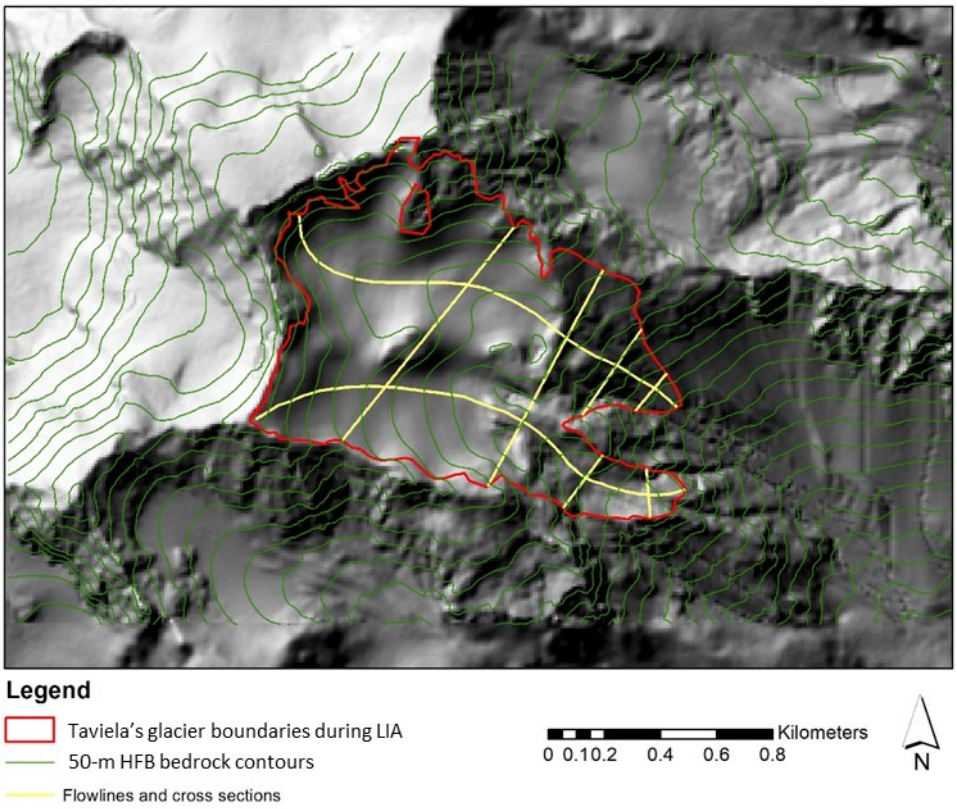


*Figure 22: Merged bedrock with the flowlines and cross-sections.*

After obtaining the merged bedrock, we drew two flowlines (ESRI shapefile) and three cross-sections for each flowline following the above procedure. We drew one flowline for each sub-basin, with each basin feeding its tongue (Figure 22).

Consequently, we extracted the bedrock value for each flowline and cross-section. The bedrock flowlines and cross-sections were the input for the second step of HFB (HFBice). At this point, we considered each flowline and its cross-sections. We applied the same procedure for each flowline. We calculated three $f$ values (one for each cross-section, Figure 23) to obtain a continuous value of $f$ along the flowline (interpolating the $f$ values with the distance of each cross-section from the glacier tongue along the flowline using a second-order polynomial function).

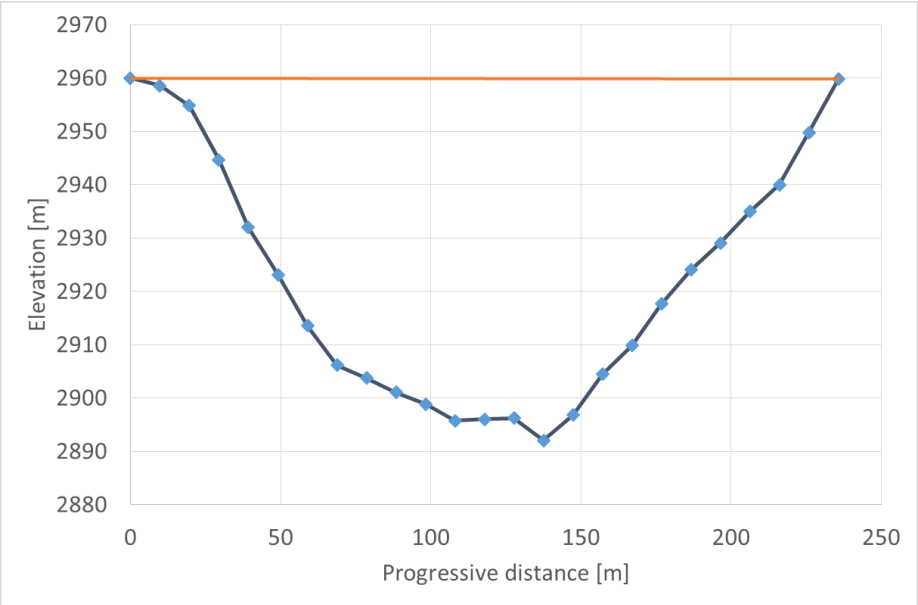


*Figure 23: Example of a cross-section for the calculation of the shape factor.*

HFB$_{ice}$ calculated the ice surface after calculating the $f$ value for every vertex of the flowline (I$_{ce}$S$_{urf}$-FL, Figure 24). Subsequently, we calibrated the ice surface that was calculated with HFB$_{ice}$ by using five target elevations in the three zones of the tongue (upper zone, central zone and lower zone). We applied a correction for each target elevation as a function of the width of the cross-section (Table 13). We calculated a Root Mean Square Error (RMSE) of 15 m for the target elevations (as an average between the two flowlines).

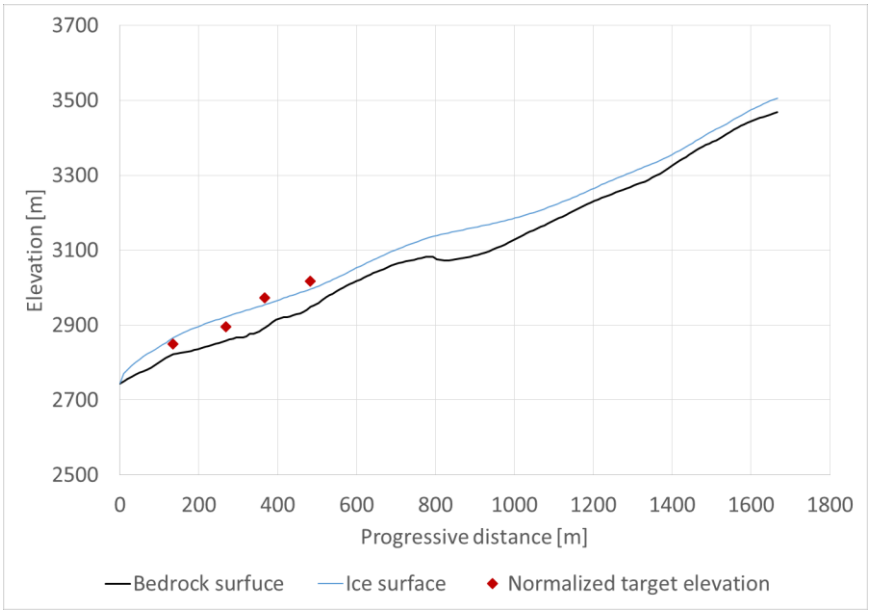


*Figure 24: Ice surface of the flowline that was calculated by HFBi$_{ce}$.*

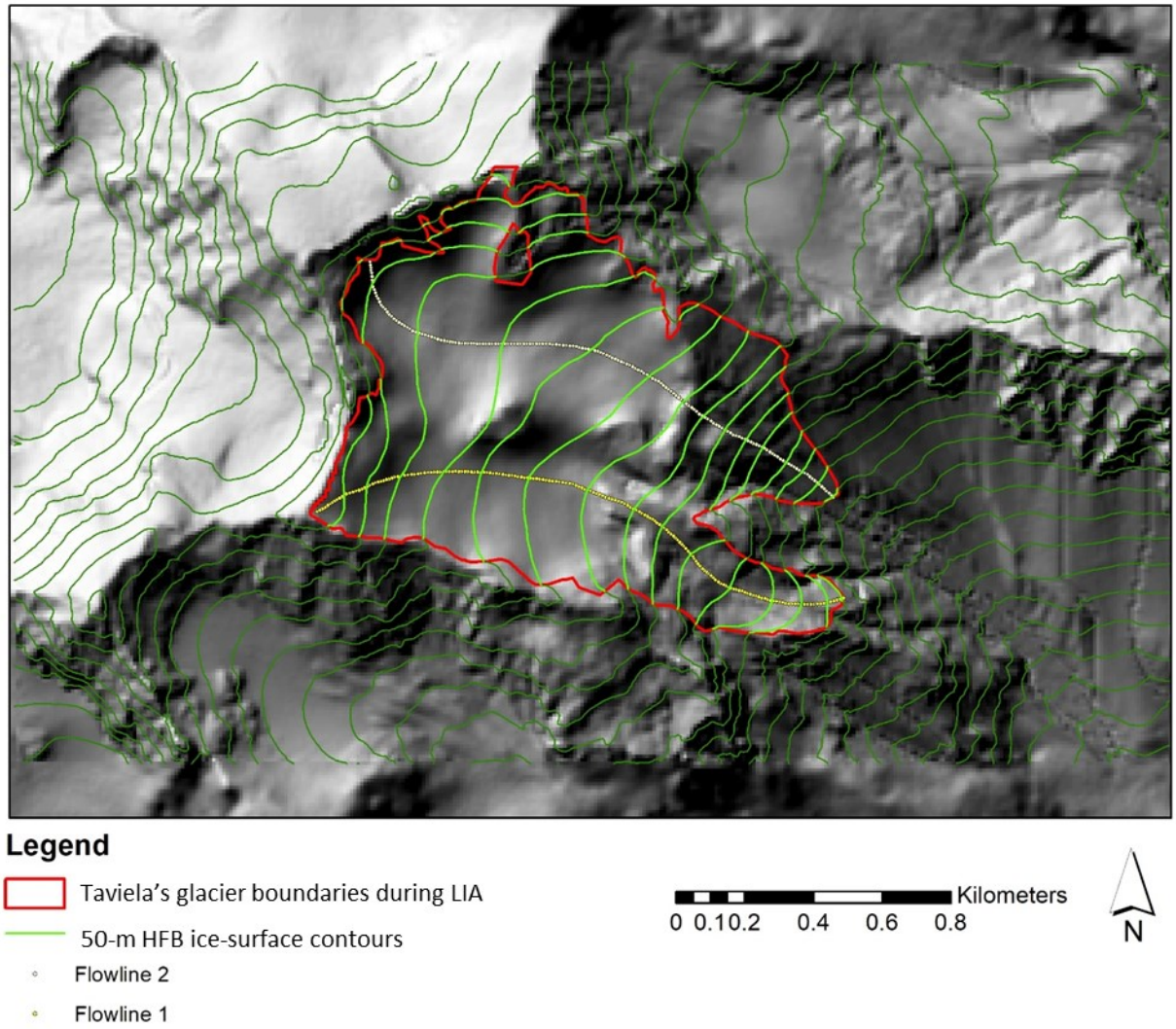


*Figure 25: Reconstruction of the topographic ice surface of the LIA Taviela glacier. The light-green lines mark the contours for the 2D ice surface (Flowlines 1 and 2) that were calculated by $HFB_{ice}$.*

During the third and last step of HFB, we hand-drew the contours (every 50-m elevation) of the Taviela ice surface during the LIA (Figure 25). We used the elevations of the $I_{ce}S_{urf}$-FL (as constraints inside the glacier boundaries), the extension of the LIA Taviela glacier, and the contours of the bedrock and de-glaciated area outside the glacier boundaries to draw these contours. We linked contours outside the glacier boundaries that had the same elevation by using the fixed elevation of the vertices of the $I_{ce}S_{urf}$-FL. Finally, we interpolated the 50-m ice contours by using the *Topo to Raster* ArcGIS tool.

## **2.3.** Glacio-hydrological modelling

We used the glacio-hydrological model to recognize the contribution from the cryosphere to the runoff under different i) glacier extent, ii) meteorological conditions, and iii) spatial scales (of the drained area).

We simulated the streamflow across the four basins under three glacier cover scenarios after obtaining the meteorological and topographic input (Table 1). We considered ten years of daily data for each scenario to simulate the glacier mass balance and the runoff at the daily scale. We collected the hydrometric data for calibration and validation. After submitting a request to the PAT service, we collected hydrometric data from the PAT hydrological archive for the Vermiglio, Ponte Rovina, and Tassullo catchments. However, we used experimental data from a hydrometric station that has operated since 2007 for the basin at Pian Venezia (Figure 9).

Glacio-hydrological modelling was conducted by combining the snow-and-ice component with the hydrological component. First, we performed fully distributed modelling by using a new version of EISModel (EISModel 041d), which exhibits some interesting improvements. In addition, we applied semi-distributed modelling with AHM for the hydrological component. We described EISModel and AHM in detail in the first section of this work (Nivo-hydrological modelling). We used the output of EISModel (rain and meltwater) as the input for AHM. EISModel produced base-flow runoff by considering precipitation and melting from snow- and ice-cover areas. Subsequently, AHM propagated this runoff by considering hydrological processes (e.g., infiltration). Figure 26 shows the glacio-hydrological flowchart.

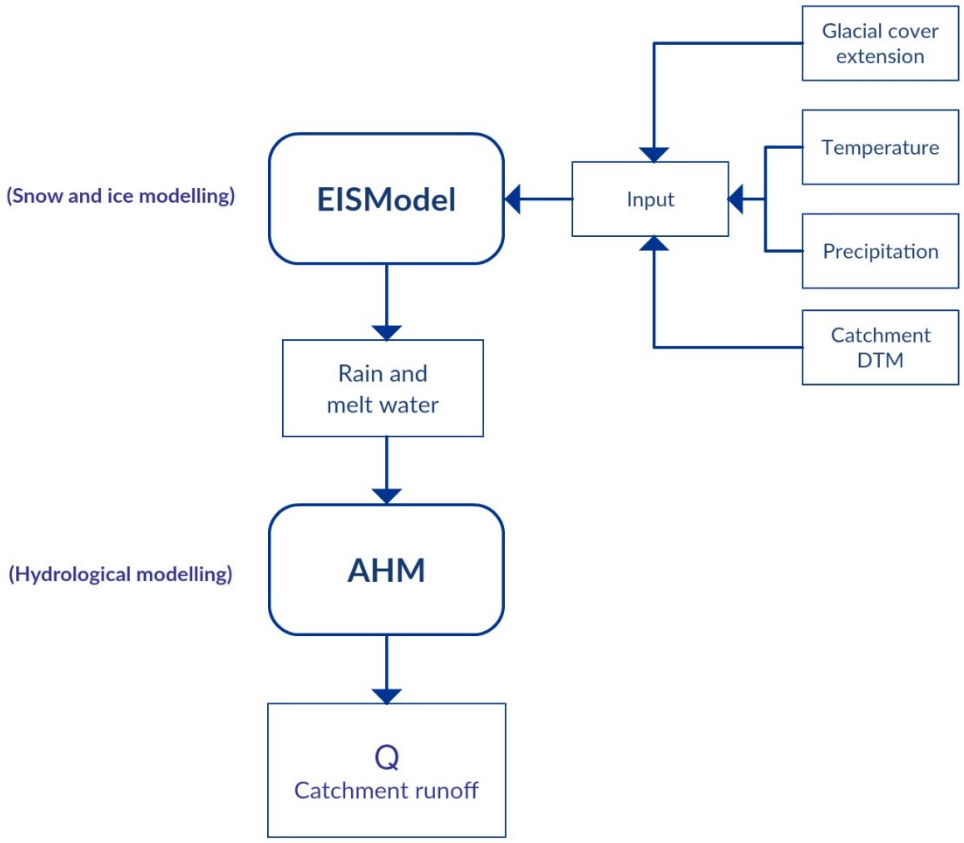


*Figure 26: Glacio-hydrological modelling flowchart.*

### 2.3.a. Meteorological periods

We considered three ten-year periods, which were combined with three glacier cover scenarios, for the glacio-hydrological modelling of each catchment.
We considered both the climatic and glacial components when choosing the modelling length. Indeed, a ten-year period is sufficiently long to recognize the influence of meteorological conditions on runoff. However, we considered the glacial dynamics to be static during this ten-year period. Thus, we did not introduce bias from the volumetric evolution of the glaciers.
We considered the climatic conditions when choosing the three ten-year periods. We researched specific periods that represented certain climatic phases that characterized the XX Century (IPCC, 2013).
We recognized three different periods by analysing the temperature and precipitation series (Figure 27 and Figure 28 and Table 15). The first period represents the end of the first half of 1900, with hot and dry years (low winter precipitation and high summer temperatures). The second period represents the beginning of the second half of 1900, with particularly snowy and cold years. Finally, the third period at the end of 1900 and the beginning of the 2000s was characterized by very hot summers (2003) and winters with high precipitation (2009).

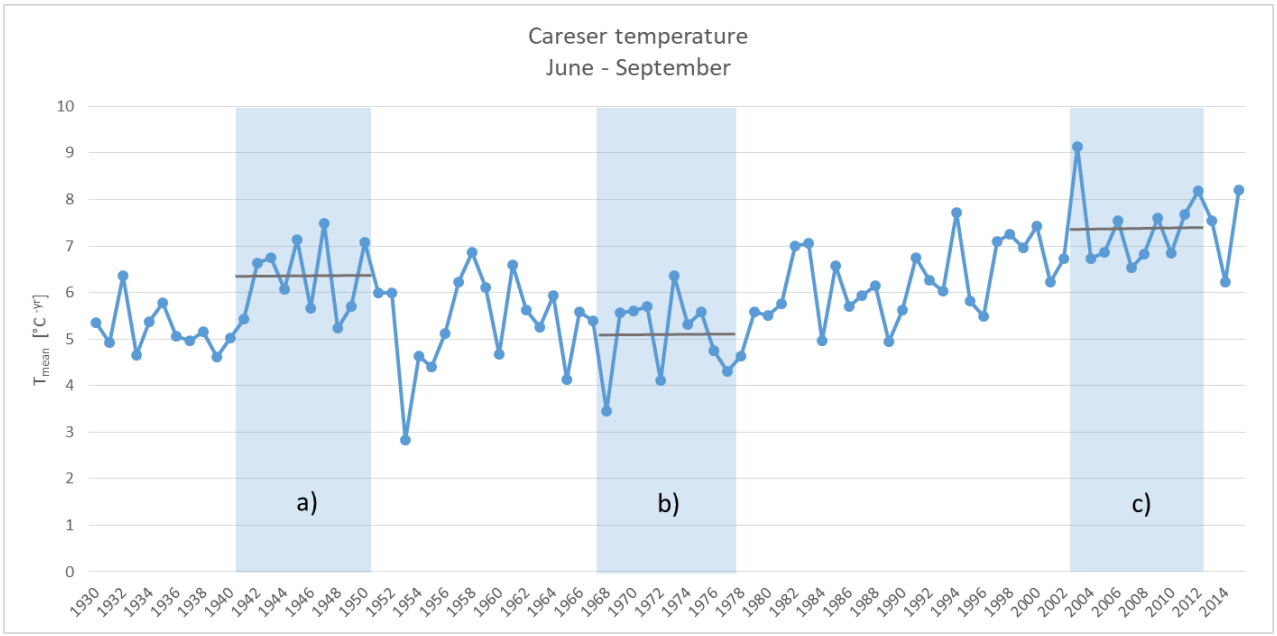


*Figure 27: Average temperature at the Careser dam (2607 m a.s.l.) during the summer periods from 1930 to 2015. The blue windows mark the following three periods: a) from 1941 to 1950 (average T = 6.3), b) from 1968 to 1977 (average T = 5.1), and c) from 2003 to 2012 (average T = 7.4).*

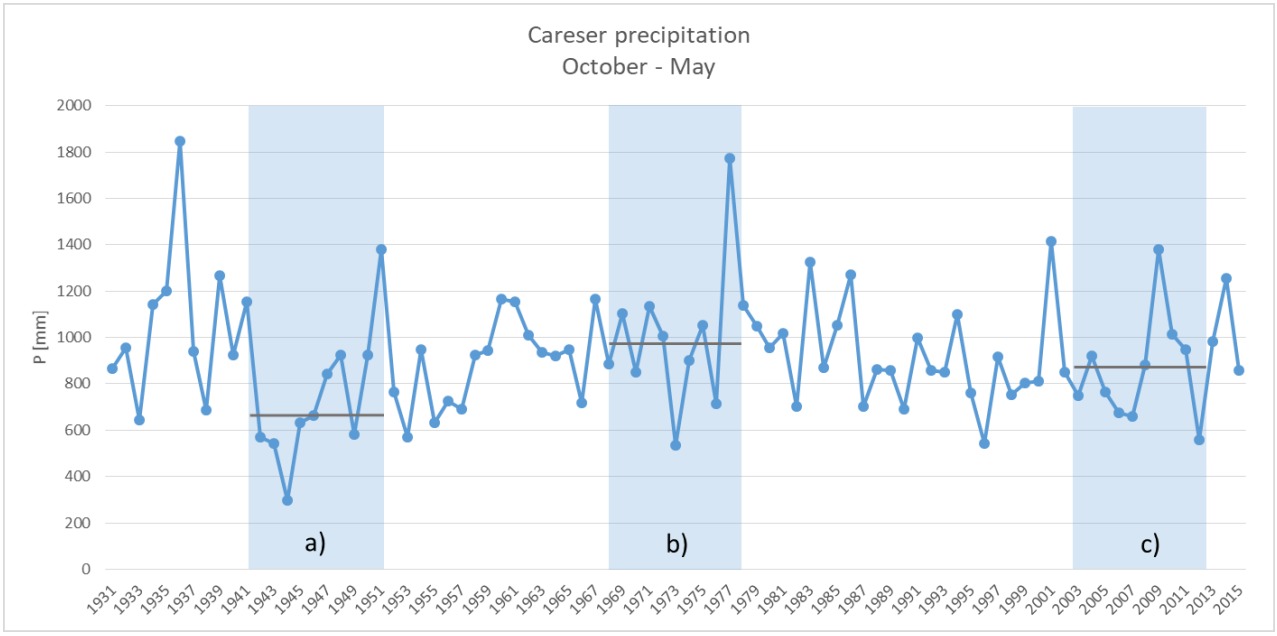


*Figure 28: Precipitation at the Careser dam (2607 m a.s.l.) during the winter periods from 1930 to 2015. The blue windows mark the following three periods: a) from 1941 to 1950 (average P = 713.5), b) from 1968 to 1977 (average P = 995.0), and c) from 2003 to 2012 (average P = 855.2).*

After choosing these three periods, we modelled the runoff of each catchment by combining the different glacier cover scenarios (Table 16).

*Table 15: Features of the studied periods.*

| *Period* | *Features* |
|---|---|
| a) 1941 – 1950 | • Low winter precipitation<br>• High summer temperatures |
| b) 1968 – 1977 | • High winter precipitation<br>• Low summer temperatures |
| c) 2003 – 2012 | • High winter precipitation (2009)<br>• High summer temperatures |

*Table 16: Studied periods and glacier cover scenarios in the glacio-hydrological modelling of each catchment.*

| *Period* | *Glacier cover scenario* |
|---|---|
| a) 1941 – 1950 | LIA<br>2006<br>No glacier cover |
| b) 1968 – 1977 | LIA<br>2006<br>No glacier cover |
| c) 2003 – 2012 | LIA<br>2006<br>No glacier cover |

### 2.3.b. EISModel 041d

We introduced some improvements to the fully distributed modelling process with EISModel to improve snow and ice modelling and optimize the simulation of the dominant processes during the accumulation and ablation seasons.
The first of these modifications involved the modelling of daily data. Indeed, previous versions could only model at the hourly scale. However, the daily scale is necessary to manage historical data series from old analogical weather stations (e.g., from 1930 to 2015, as in our work).
In the next section, we report the main improvements to the new version of EISModel 041d.

#### 2.3.b.1. Double temperature lapse rate

EISModel 041d has a new algorithm to calculate the temperature of a pixel. We considered a double monthly temperature lapse rate to consider the thermal inversion of downstream areas. We fixed a temperature reference station at the monthly scale and calculated the pixel temperature by using two different linear lapse rates. We used a monthly linear lapse rate for pixels below the elevation of the reference station and a different monthly linear lapse rate for pixels above the referent station. We used seven weather stations from 700 m to 3300 m a.s.l. to calculate the two monthly lapse rates for this research. We calculated the average monthly temperature for the period from 2003 to 2014 for each station (Table 17).

*Table 17: Average monthly temperature of the seven weather stations from 2003 to 2014.*

| | Average temperature [°C] | | | | | | |
|---|---|---|---|---|---|---|---|
| Elevation [m] | 724 | 1316 | 1586 | 1877 | 2607 | 3055 | 3328 |
| Month | Malè | Mendola | Peio | Tonale | Careser | Hobo Careser | Beltovo |
| Jan | 0.8 | -0.3 | -1.2 | -3.6 | -7.3 | -9.8 | -12.6 |
| Feb | 1.8 | 0.3 | -1.2 | -3.7 | -8.1 | -10.8 | -13.5 |
| Mar | 5.6 | 3.4 | 1.7 | -0.9 | -5.6 | -8.6 | -10.8 |
| Apr | 10.3 | 7.5 | 5.6 | 3.2 | -1.8 | -5.1 | -6.8 |
| May | 14.1 | 11.3 | 9.4 | 7.3 | 1.8 | -1.7 | -3.7 |
| Jun | 18.2 | 15.5 | 13.7 | 11.4 | 6.6 | 2.6 | 0.4 |
| Jul | 19.8 | 17.5 | 15.4 | 13.1 | 8.9 | 4.9 | 2.3 |
| Aug | 19.4 | 17.1 | 15.2 | 12.7 | 8.6 | 4.9 | 2.5 |
| Sep | 15.5 | 13.4 | 11.7 | 9.6 | 5.5 | 2.1 | -0.5 |
| Oct | 10.7 | 8.7 | 7.2 | 5.4 | 1.6 | -0.9 | -3.5 |
| Nov | 5.2 | 4.0 | 2.9 | 0.8 | -2.8 | -5.3 | -8.0 |
| Dec | 0.7 | 0.2 | -0.4 | -3.0 | -6.8 | -9.2 | -12.0 |
| *Average* | 10.2 | 8.2 | 6.7 | 4.4 | 0.0 | -3.1 | -5.5 |

Compared to the standard temperature lapse rate, which uses a reference elevation, a double linear lapse rate can correct errors during the estimation of temperatures in

downstream areas and at high elevations (e.g., above 3000 m that is the typical glacial elevation band). Table 18 shows a comparison between the observed and calculated annual values from these two methods.

*Table 18: Comparison between the observed and calculated annual values: Double LR = calculated value when using a double linear lapse rate, and Linear LR = calculated value when using a standard linear lapse rate.*

| | Temperature [°C yr $^{-1}$] | | |
|---|---|---|---|
| | Observed | Double LR | Linear LR |
| Malè | 10.2 | 10.3 | 12.3 |
| Mendola | 8.2 | 7.8 | 8.4 |
| Tonale | 4.4 | 4.7 | 4.8 |
| Careser | 0.0 | -0.3 | 0.0 |
| Hobo Careser | -3.1 | -3.3 | -2.9 |
| Beltovo | -5.5 | -5.2 | -4.7 |
| *Average* | 2.4 | 2.3 | 3.0 |
| N&S | | 0.9987 | 0.9933 |
| $R^2$ | | 0.9974 | 0.9867 |
| ME % | | -1% | 27% |

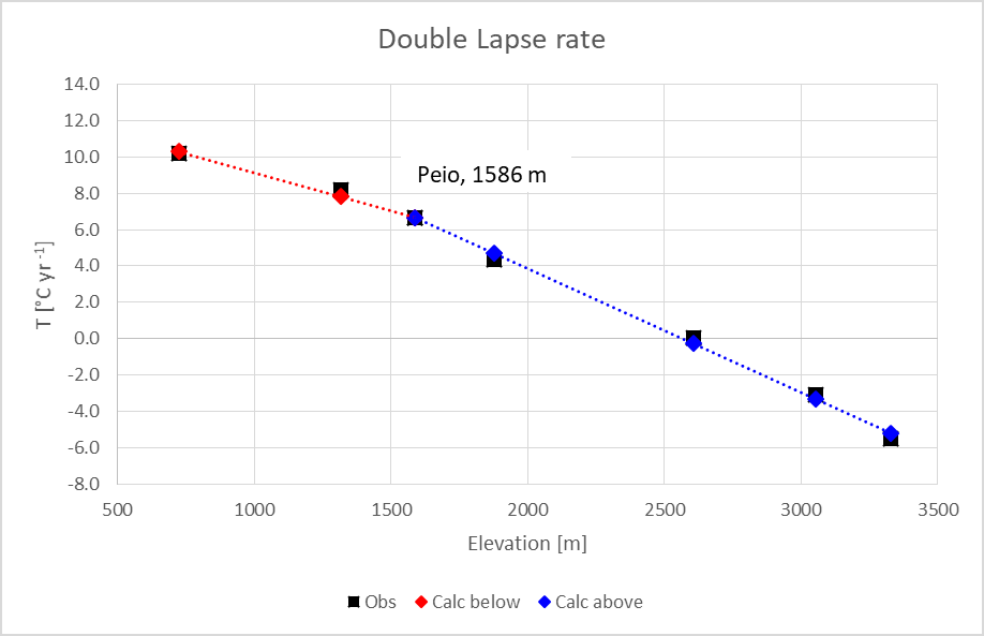


*Figure 29: Observed vs calculated annual values when using a double linear lapse rate and a reference elevation of 1586 m a.s.l.*

Figure 29 and Figure 30 show the differences from the two methods (observed vs calculated values), particularly the errors in the downstream areas and at high elevations when using a standard linear lapse rate.

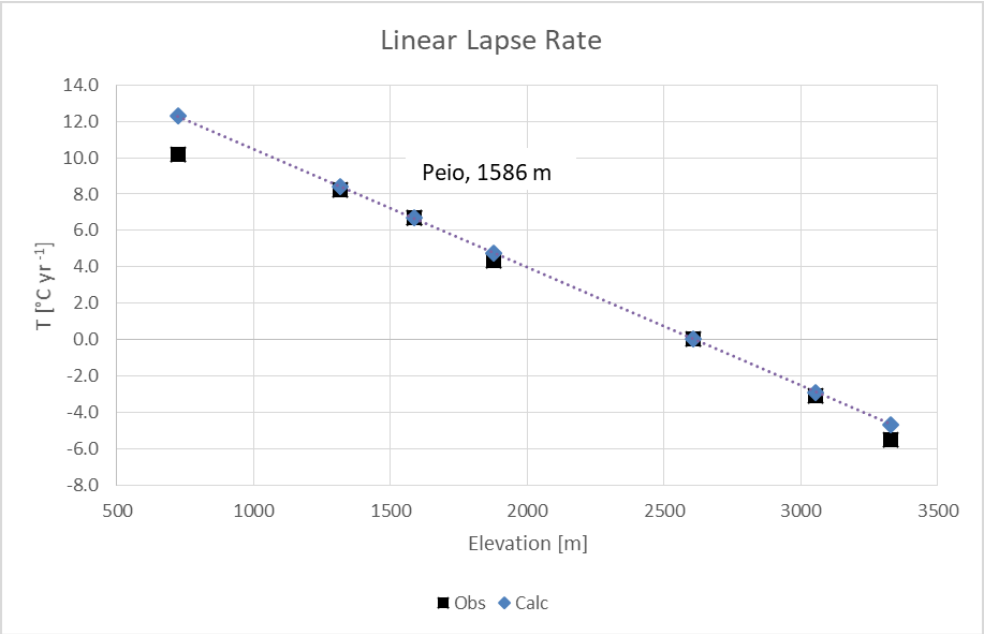


*Figure 30: Observed vs calculated annual values when using a linear lapse rate and a reference elevation of 1586 m a.s.l.*

*Table 19: Calculated temperature lapse rate from two different methods: Ab RE = temperature lapse rate above the reference elevation (1586 m), and Bl RE = temperature lapse rate below the reference elevation (1586 m).*

| | Double LR [°C / km] | | Linear LR [°C / km] |
|---|---|---|---|
| | Ab RE | Bl RE | |
| Jan | -6.2 | -2.4 | -5.8 |
| Feb | -6.9 | -3.6 | -6.5 |
| Mar | -7.2 | -4.7 | -6.9 |
| Apr | -7.2 | -5.6 | -7.1 |
| May | -7.5 | -5.6 | -7.3 |
| Jun | -7.5 | -5.4 | -7.2 |
| Jul | -7.2 | -5.3 | -7.0 |
| Aug | -7.1 | -5.0 | -6.8 |
| Sep | -6.7 | -4.6 | -6.5 |
| Oct | -5.8 | -4.1 | -5.6 |
| Nov | -6.0 | -2.7 | -5.6 |
| Dec | -6.4 | -1.3 | -5.8 |

Table 19 and Figure 31 show the monthly trends of the temperature lapse rate when using a double temperature lapse rate and a standard linear lapse rate.

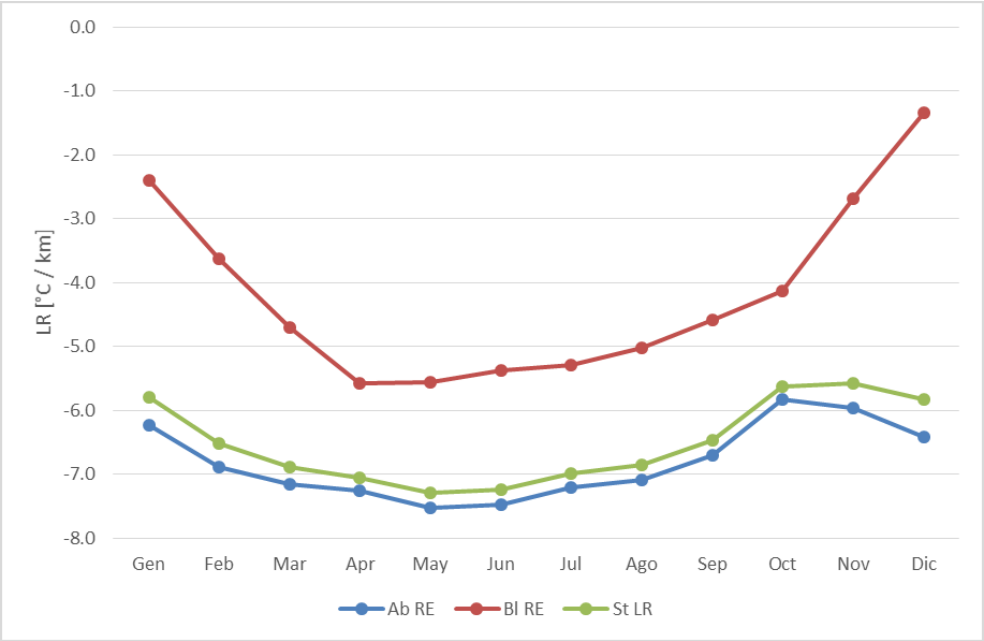


*Figure 31: Temperature lapse rate that was calculated with two different methods. Ab RE = temperature lapse rate above the reference elevation (1586 m), Bl RE = temperature lapse rate below the reference elevation (1586 m), and St LR = standard linear lapse rate.*

### 2.3.b.2. Percentage precipitation lapse rate: vertical and horizontal components

Another improvement in EISModel 041d is the ability to calculate a pixel's daily precipitation by using both the vertical and horizontal spatial distributions.
This approach normalizes the input precipitations at the reference elevation (with a specific percentage precipitation lapse rate for each weather station), spatializes the normalized precipitations with IDW, and calculates the pixel's precipitation by using a specific percentage lapse rate for each pixel.

We calculated a monthly precipitation lapse rate (mm/km) by using two weather stations with no difference in planimetric distances to determine the vertical spatial distribution. We used daily data from weather stations at Malga Mare (1950 m a.s.l.) and the Careser dam (2607 m a.s.l.) for the period from 1940 to 1984. Subsequently, we calculated the ratio between the monthly precipitation lapse rate (mm/km) and the average monthly precipitation of each weather station (%/km, Equation 44) to obtain five percentage lapse rates, one for each station:

*Equation 44*

$$\%\, LR_{\,st} = \frac{LR_{MC}}{P_{st}}$$

where
$\%\, LR_{\,st}$ = percentage precipitation lapse rate for the specific weather station [%/km]
$P_{st}$ = weather station's precipitation value

$LR_{MC}$ = precipitation lapse rate from the Malga Mare and Careser weather stations [mm/km]

*Equation 45*

$$LR_{MC} = \frac{\Delta \mathrm{P}}{\Delta z}$$

where

$\Delta P$ = variation in precipitation from Careser to Malga Mare

$\Delta z$ = variation in elevation from Careser to Malga Mare

We normalized the monthly $P_{st}$ to a reference elevation (we used the mean elevation of the Tassullo catchment, 1705 m a.s.l.) by using the above percentage lapse rates $\%\, LR_{st}$ to obtain five normalized monthly precipitation data ($P_{st,norm}$).

This model can spatialize each $P_{st,norm}$ by using the IDW algorithm as a function of the coordinates of each pixel ($P_{IDW}$) to determine the horizontal variation.
This model can calculate the monthly percentage precipitation lapse rate ($\%\, LR_{px}$) by comparing $LR_{MC}$ with $P_{IDW}$ to determine the monthly precipitation according to the pixel elevation.
Finally, this model can apply the monthly percentage precipitation lapse rate $\%\, LR_{px}$ to the daily $P_{IDW}$ after normalizing the input daily data with the monthly percentage lapse rate $\%\, LR_{st}$ to determine the pixel daily precipitation.

#### 2.3.b.3. Percentage division of rain/snow

In previous versions of EISModel, the classification of precipitation into a solid fraction (snowfall) and liquid fraction (rainfall) only depended on a fixed temperature threshold ($T_{tr}$). Consequently, all precipitation was considered solid (100% snowfall) for a temperature $T_x$ less than $T_{tr}$, while all precipitation was considered liquid (100% rainfall) for a temperature $T_x$ greater than $T_{tr}$.
We introduced a threshold temperature range ($\pm T_r$) in the new version of EISModel. When $T_x$ is less than $T_{tr} - T_r$, the model considers all precipitation as solid (100% snowfall). When $T_x$ is greater than $T_{tr} + T_r$, the model considers all precipitation as liquid (100% rainfall).

$$\text{with } T_x < (T_{tr} - T_r) \Rightarrow 100\% \text{ snowfall}$$
$$\text{with } T_x > (T_{tr} + T_r) \Rightarrow 100\% \text{ rainfall}$$

However, when $T_x$ is greater than $T_{tr} - T_r$ and when $T_x$ is less than $T_{tr} + T_r$, the model calculates a percentage of solid precipitation and a percentage of liquid precipitation as a function of the temperature by using a linear regression:

with $(T_{tr} - T_r) < T_x < (T_{tr} + T_r) \Rightarrow$

- $X\%$ snowfall $F(T_x)$
- $X\%$ rainfall $F(T_x)$

We calculated an experimental $T_{tr}$ value of 2.2, and an experimental $T_r$ value of 1 for this research. Figure 32 shows the percentage division of precipitation as a function of the temperature when using these experimental values.

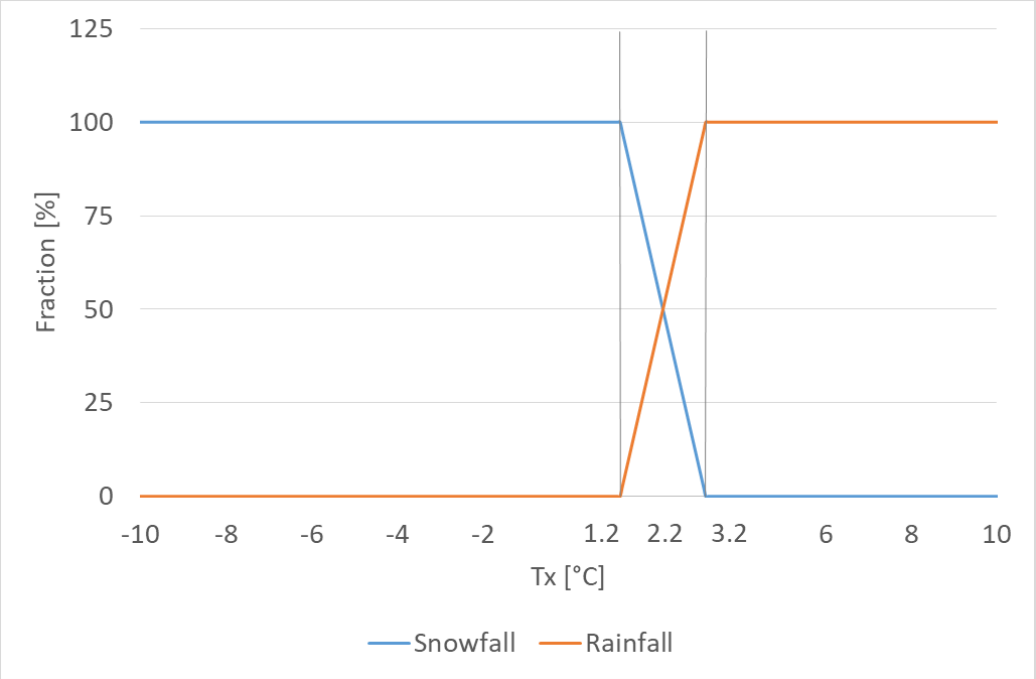


*Figure 32: Percentage of precipitation (% snowfall vs % rainfall) as a function of the temperature: $T_{tr}$ = 2.2, $T_{tr}$ = 1.*

### 2.3.b.4. Transition from snow to ice

EISModel 041d has the transition from snow to ice as a new implementation into its modelling procedures. EISModel 041d records the formation date of a snow layer and converts the snow layer into an ice layer after a fixed period (input parameter $Yr_{SI}$ [years]). This procedure takes advantage of snow-layer modelling already implemented in previous versions of EISmodel for the simulation of the surface albedo (Cazorzi, F. et al., 2009). Evidently, this transition from snow to ice is only possible if the layer does not completely melt during $Yr_{SI}$.

In a previous version of EISModel, snow layers which survived to melt (at high elevation) were added one after another with no limit. The result was an unrealistic increase in snow over ice at the higher elevations. In addition, we must consider the effects on the albedo and the capacity of the snowpack to retain liquid water. The albedo plays a crucial role during melt processes. The albedo is 0.9 for fresh snow and 0.2 for ice; therefore, ablation would be unrealistically low in case of exposure of old layers of firn in the upper part of glaciers

(old firn is rather dark, compared to old snow, and its albedo is more similar to that of ice). The effect on the capacity of the snowpack to retain liquid water is even more important for hydrological modelling, because thicker snowpack produces more inertia during the release of bottom water, and thus reduces the peak discharge. Simulating unlimited snow accumulation leads to excessive meltwater retention. Converting the old snow to ice at the end of the hydrological year leads at the contrary to excessive release of meltwater the next summer. Based on literature and on observed discharge, we used a time period of 5 years for $Yr_{SI}$. Figure 33 shows an example of a 15 year simulation of snow accumulation and transformation to ice at a site located on La Mare glacier (3570 m a.s.l.) when using $Yr_{SI}$ = 5.

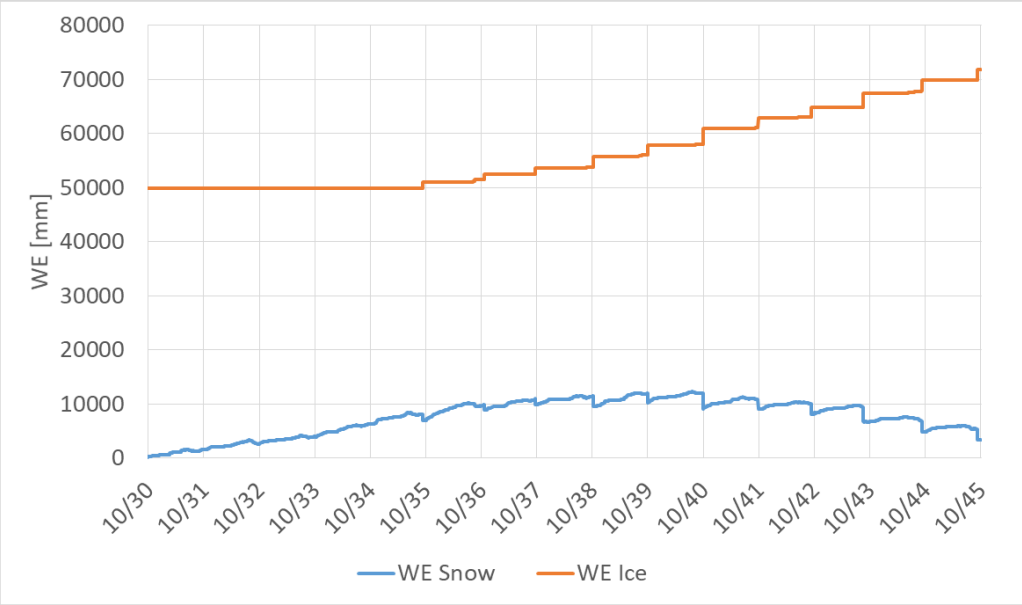


*Figure 33: Simulation of snow accumulation and its transition to ice at one point inside the La Mare glacier (3570 m a.s.l.): $Yr_{SI}$ = 5.*

### *2.3.c. AHM*

As reported before, we have used AHM model to propagate the runoff considering land hydrological processes. We have considered the hydraulic propagation (propagation in hydrographic network) as negligible due to the adoption of a daily interval, that is a far longer time than the routing time in the larger of the four basins. For this reason, in contrast to original Stanford model (Crawford and Linsley, 1966), we did not active the CHANNEL module but only the LAND module.

As mentioned above, catchments are the modelling unit in AHM and can be subdivided into three elevation bands (segments). Consequently, we divided each of the four catchments into three segments. The first segment ($S1$) included high-altitude environments beyond the forest limit (elevation > 2200 m a.s.l.). The second segment ($S2$) included the forest band (from 1000 to 2200 m a.s.l.). The third segment ($S3$) included the basal band (elevation < 1000 m a.s.l.). Table 20 shows the elevation ranges of each segment.

*Table 20: Elevation range of each segment.*

| *Segment* | *Elevation range from - to [m]* |
|---|---|
| *S1* | 2200 - $Z_{max}$ |
| *S2* | 1000 - 2200 |
| *S3* | $Z_{min}$ - 1000 |

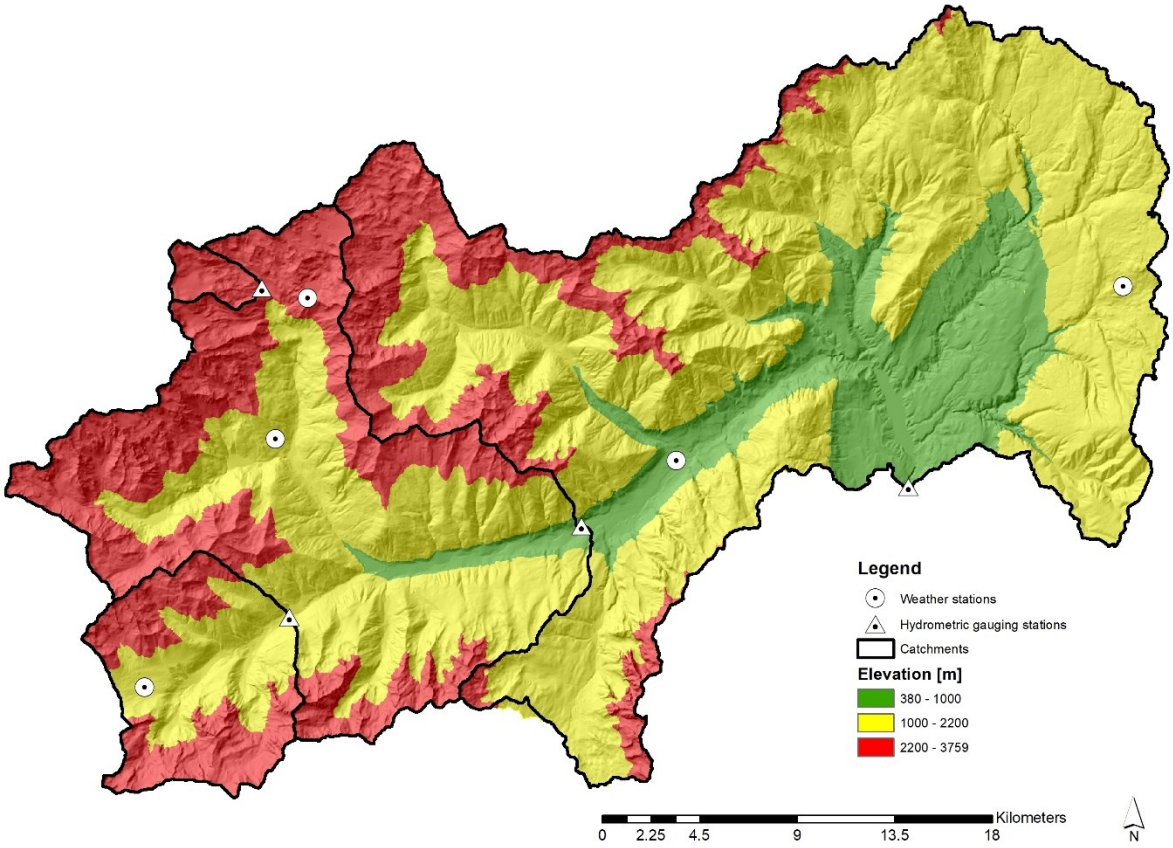


*Figure 34: Subdivision of each catchment into three segments.*

Figure 34 and Table 21 show the subdivision of the catchments into segments and the percentage area of each segment.

*Table 21: Percentage area of each segment in each catchment.*

| *Catchment* | *Area [km²]* | *S1* | *S2* | *S3* |
|---|---|---|---|---|
| Val de La Mare | 8 | 100% | 0% | 0% |
| Vermiglio | 80 | 51% | 49% | 0% |
| Ponte Rovina | 386 | 47% | 50% | 3% |
| Tassullo | 1046 | 27% | 59% | 14% |

AHM requires some features (parameters) that characterize each catchment segment (Table 22). We used GIS techniques to calculate these parameters reported. We considered the features from ID = 1 to ID = 5 to be morphometric characteristics. We used Equation 46 and Equation 47 to calculate the RIVER parameter (ID = 3) and RL parameter (ID = 5), respectively.

*Equation 46*

$$RIVER = \frac{2\,L}{2\,L + L_{cont\ inf}}$$

where

$L$ = length of the segment's hydrographic network

$L_{cont\ inf}$ = length of the segment's lower contour

*Equation 47*

$$RL = 1000\,\frac{AREA}{2\,L}$$

*Table 22: AHM parameters for the characterization of each catchment.*

| *ID* | *Name* | *Description* |
|---|---|---|
| 1 | AREA | Segment area [km$^2$] |
| 2 | ELEV | Segment average height [m] |
| 3 | RIVER | Direct channel runoff |
| 4 | SS | Segment slope |
| 5 | RL | Run length [m] |
| 6 | EPXM | Interception storage |
| 7 | RK3 | Areal deep-root vegetation |
| 8 | FDEN | Canopy density |
| 9 | FCOVER | Forest cover index |
| 10 | RNN | Manning overland flow |

The parameters from ID = 5 to ID = 10 were calculated from a land-use map (available from the PAT website, Figure 35) by using the weighted average area.

In addition, AHM requires some calibration parameters (Table 23). See the LAND module for a detailed description of the parameters in Table 23 and the algorithms for the calculations.

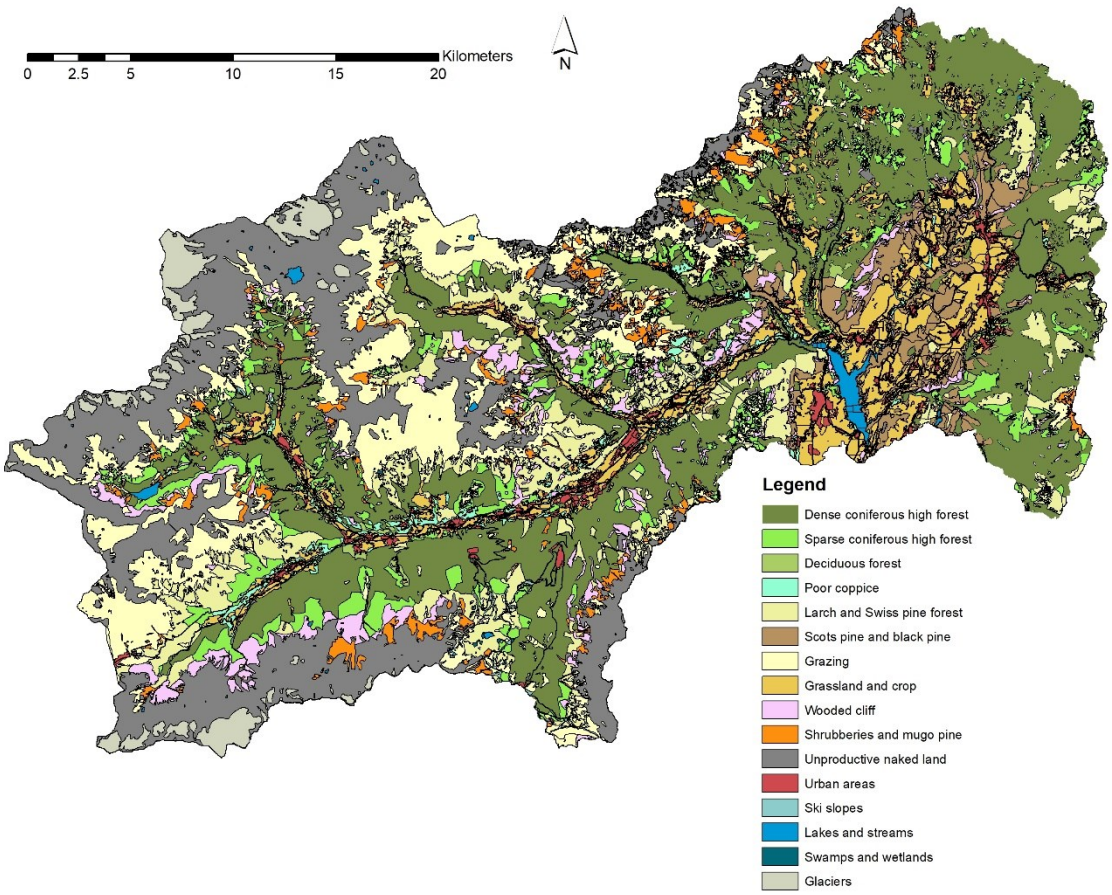


*Figure 35: Land-use map*

The ETPFRC parameter is particularly important. This model uses Hamon's formula (Hamon, 1961) to calculate the potential evapotranspiration. However, Hamon's formula is specific to agriculture lowland areas; therefore, we must adjust the potential evapotranspiration according to the elevation range of the catchments and the soil use (high percentage of forest and a considerable percentage of areas with no vegetation cover, Figure 35).

*Table 23: AHM calibration parameters.*

| *ID* | *Name* | *Description* |
|---|---|---|
| 11 | UZSN | Nominal soil moisture in the upper zone |
| 12 | RLZSN | Nominal soil moisture in the lower zone |
| 13 | CB | Infiltration index |
| 14 | CC | Parameter that regulates the volume of the subsurface outflow |
| 15 | ETPFRC | Reduction factor of the potential evapotranspiration |

### *2.3.d. Calibration*

Thanks to the distinction of processes (snow and ice and hydrological), and the producing of specific modelling output for each step of the water balance (from snow accumulation to

runoff and considering total precipitation, glacier storage change and evapotranspiration), we can have a complete control in the single phases of the modelling. This step by step control allows a crucial added value to our research. Indeed, in this way, we can distinctly calibrate and validate the two main processes. The importance of the internal validation is a crucial aspect that should be taken into account in glacio-hydrological modelling. Indeed, validating the modelling only on measured discharge data, it is not possible to control the snow and ice processes. Without internal validation and considering only a hydrological validation, we can obtain a good simulation but we do not have evidence that the results are positive only for the mediation between snow and ice processes and runoff propagation (e.g. overestimation of melt and overestimation of infiltration and runoff delayed).

We calibrated and validated the two models (EISModel 041d and AHM) with specific separated calibrations and validation, after collecting and elaborating the data input and improving the models for glacio-hydrological modelling. We calibrated EISModel 041d with both the measured glacial mass balances and the available snow-cover maps. Conversely, we calibrated AHM with the available discharge data at different hydrometric stations.

#### 2.3.d.1. EISModel 041d

We have used the multiplicative algorithm in function of Equation 10 according to the results of previous applications of EISModel (Carturan et al., 2012).

We performed progressive calibration from a single point to wider areas. During the first step, we considered the mass balance that was measured at a single ablation stake (2900 m a.s.l.). During the second step, we considered 8 stakes that were distributed across the La Mare glacier (elevation range from 2600 to 3350 m a.s.l.). Then, we extended the calibration from points to surfaces. Initially, we used measured snow-cover maps over a restricted area (36 $km^2$ - third step), and then we considered the snow-cover maps over a wider area (1046 $km^2$ - fourth step). We calibrated the temperature melt factor ($TMF$) and radiation melt factor ($RMF$) according to the multiplicative algorithm.

We considered two types of calibration for the measured mass balances: temporal calibration and spatial calibration.

First, we modelled the glacial mass balance at one ablation stake on the La Mare glacier during four summer periods (2010, 2011, 2012 and 2013). We performed one simulation run for each summer period by considering four dates for each ablation period to determine the variation in the mass balance during the ablation period (temporal calibration). Therefore, we calibrated the model by using sixteen measured values, specifically, four values each over four years.

Second, we considered eight ablation stakes on the La Mare glacier during the period from 2003 to 2006. Unlike for the temporal calibration, we performed continuous modelling from 28/09/2003 to 13/09/2006 and calibrated the model on the cumulative measured mass balance at the end of the simulation run (13/09/2006) to determine the spatial distribution of the glacial mass balance (spatial calibration). Figure 36 shows the positions of the ablation stakes on the La Mare glacier, which we used for the two types of calibration.

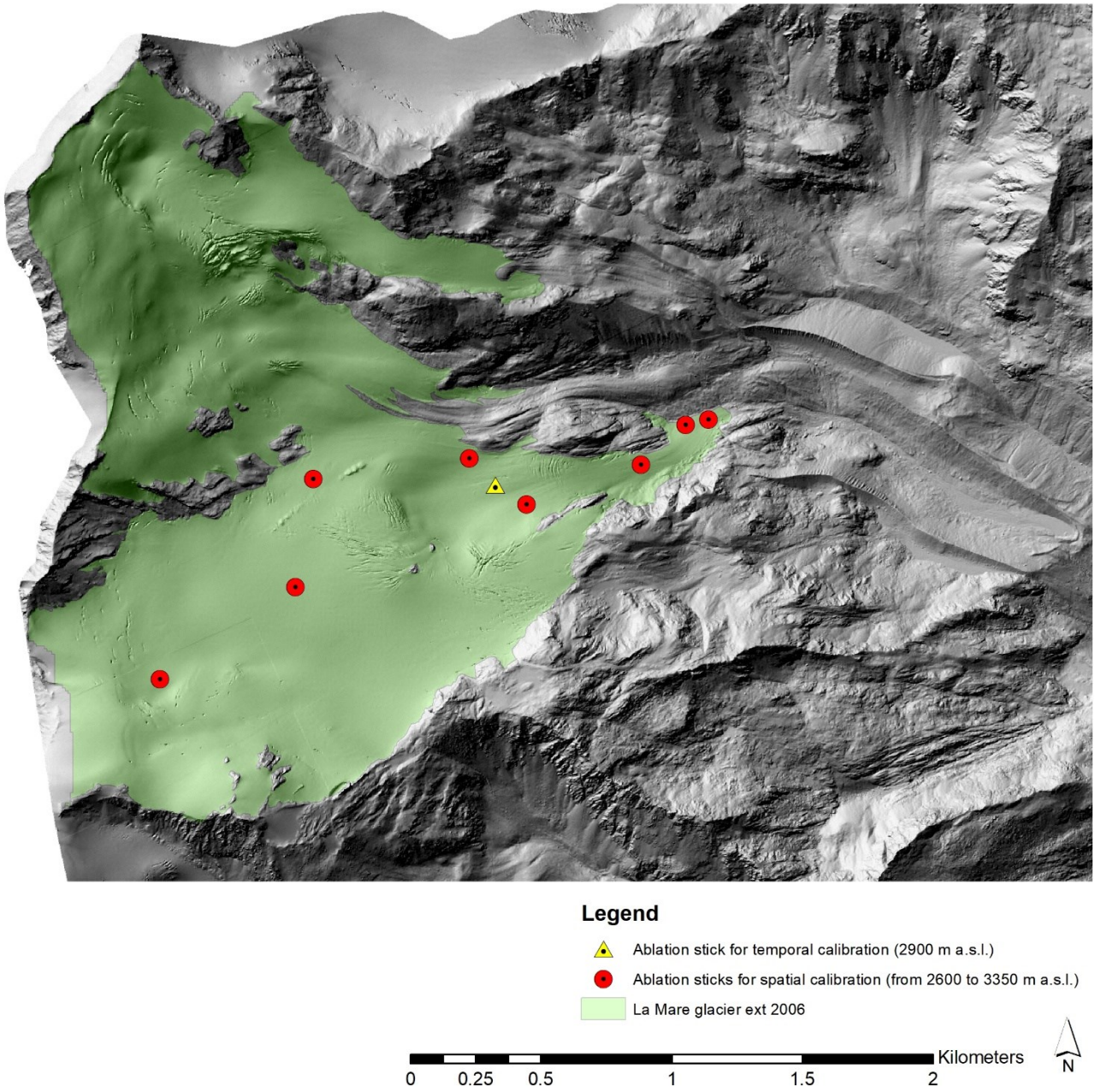


*Figure 36: La Mare glacier. The positions of the ablation stakes that were used to calibrate EISModel are shown in yellow (temporal calibration) and red (spatial calibration).*

We obtained six combinations of $TMF$ and $RMF$ values with very good statistical indices (N&S and ME), by the two types of calibration. Table 24 shows the best combinations of $TMF$ and $RMF$ values that maximize the N&S and ME indices. These statistical indices refer to the best pixel within a 3 X 3 kernel.

*Table 24: Best combination of the calculated $TMF$ and $RMF$ values from the calibration of the measured mass balance.*

| ID | RMF [(mm/t)/(kwm$^{-2}$)] | TMF [(mm/t)/°C] | N&S | ME [mm] |
|---|---|---|---|---|
| C_55-05 | 55 | 0.5 | 0.9866 | -44.63 |
| C_40-25 | 40 | 2.5 | 0.9860 | 110.19 |
| C_35-35 | 35 | 3.5 | 0.9868 | -25.19 |
| C_30-45 | 30 | 4.5 | 0.9866 | 57.29 |
| C_25-55 | 25 | 5.5 | 0.9877 | -1.47 |
| C_20-65 | 20 | 6.5 | 0.9870 | -52.49 |

After obtaining the above six combinations of $TMF$ and $RMF$, we improved the calibration by comparing the modelled snow cover from each combination of parameters to the detected snow cover.

We extended the calibration to measured snow-cover maps according to Hanzer et al. (2016). We considered two different catchments: an area near the Val de La Mare catchment and the Tassullo catchment. We focused on the period from May 2003 to August 2004 for Val de La Mare. For this period, we used five out of seven available detailed snow-cover maps (leaving the other two for validation) that were derived from tracking the snow line of the catchment with several photo images of the snow cover. We used three out of four available snow-cover maps for the period from October 2013 to July 2014 for the Tassullo catchment (leaving the remaining for validation). We used satellite images from MODIS (Moderate Resolution Imaging Spectroradiometer) and reclassified images from Eurac Research for two different areas with and without snow cover to identify the snow cover from 2013 to 2014.

We modelled the snow cover for each catchment and each detected snow-cover map by using the combinations of melt parameters in Table 24. We used a confusion matrix as a function of the snow-cover area to quantify the effects of each combination of melt parameters. Table 25 shows this confusion matrix. We considered four cases: a) correct snow-cover area, b) correct no-snow-cover area, c) early melting area and d) late melting area. Then, we calculated the percentage area of each case as a function of the catchment area. We excluded the forest area in the Tassullo catchment when calculating the percentage area of each confusion-matrix case. Indeed, we recognized a constant reduction in the snow cover inside the forest area when comparing the Eurac images with Sentinel 2 images (greater resolution than Eurac: 20 X 20 m vs 250 X 250 m).

*Table 25: Confusion matrix: a) correct snow-cover area, b) correct no-snow-cover area, c) early melting area, and d) late melting area.*

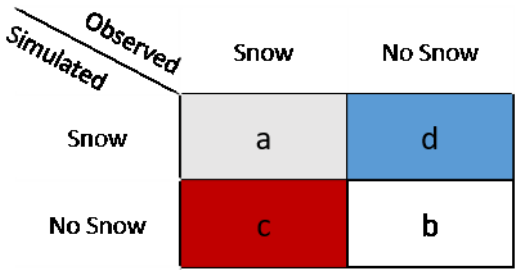

Figure 37 compares the simulated vs observed snow-cover maps in the two areas when using the confusion matrix.
We obtained the best combination of melt parameters that maximized the correct area (a + b) and minimized the incorrect area (c and d), namely, $TMF = 35$ and $RMF = 3.5$, by a comparison of simulated vs observed snow cover maps using the confusion matrix

Table 26 and Table 27 and Figure 38 and Figure 39 show the percentage area of each confusion matrix case (for each considered area) when using the above melt parameters.

Our application of the melt parameters (Table 24) constantly overestimated the melt along the southwest-oriented slopes. Thus, we introduced the Cloud Correction Factor ($CCF$) to improve the calibration of EISModel 041d. $CCF$ is a weighing factor that modulates the effect of the cloud index ($CI$) on the clear-sky radiation ($CSR$), which is reduced to $RCSR$ and then used as a melt index in lieu of $CSR$:

*Equation 48*

$$RCSR_{X,t} = CSR_{X,t}\left(1 - CCF\ CI_{X,J}\right)$$

$CCF$ significantly improved the comparison of the simulated vs observed snow-cover maps. It is useful to note that the use of $CCF$ did not change the melt processes on the slopes that faced from west to south, only those on the slopes that faced southwest. Therefore, the comparison of the simulated vs observed snow-cover maps remained constant on the slopes that faced from west to south and improved the comparison on the slopes that faced southwest. Figure 40 shows a comparison of the modelling both without and with $CCF$ (0.9). Figure 40 shows the modelling for June 21, 2003, which was the date with the worst comparison of the simulated vs observed snow-cover maps (Table 26).

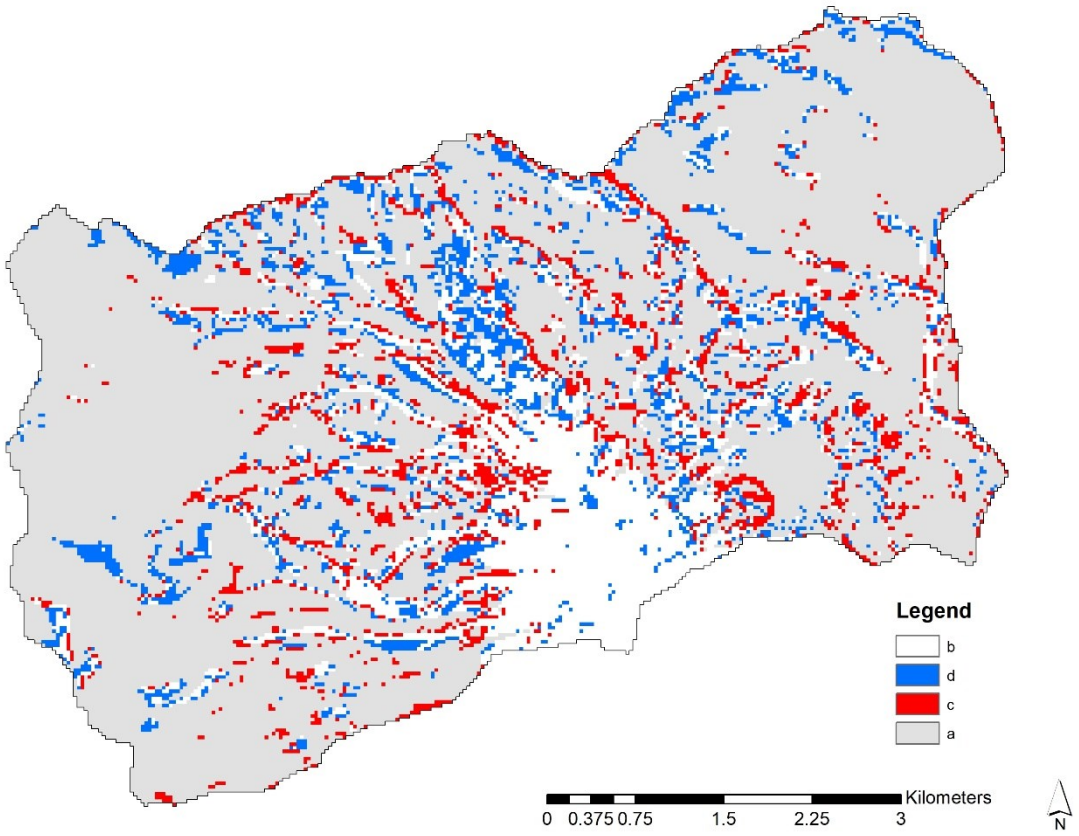


*Figure 37: Example of a comparison between simulated vs observed snow-cover maps for May 18, 2003 in the upper part of Val de La Mare. This figure reports the following four confusion matrices: a) correct snow-cover area, b) correct no-snow-cover area, c) early melting area, and d) late melting area.*

*Table 26: Percentage area near the Val de La Mare catchment (from 2003 to 2004) for each combination of confusion matrices.*

| *Date* | *Area [km²]* | *a* | *b* | *d* | *c* | *a + b* |
|---|---|---|---|---|---|---|
| 20030621 | 35.6 | 21% | 60% | 7% | 12% | 81% |
| 20030813 | 35.6 | 0% | 97% | 2% | 1% | 97% |
| 20040724 | 35.6 | 24% | 57% | 12% | 7% | 81% |
| 20040911 | 35.6 | 2% | 91% | 4% | 2% | 93% |
| Average | | 12% | 76% | 6% | 6% | 88% |

*Table 27: Percentage area near the Tassullo catchment (from 2013 to 2014) for each combination of confusion matrices.*

| *Date* | *Area [km²]* | *a* | *b* | *d* | *c* | *a + b* |
|---|---|---|---|---|---|---|
| 20131016 | 651 | 41% | 39% | 1% | 19% | 80% |
| 20140112 | 645 | 68% | 7% | 14% | 11% | 76% |
| 20140718 | 643 | 7% | 83% | 1% | 8% | 91% |
| Average | | 39% | 43% | 5% | 12% | 82% |

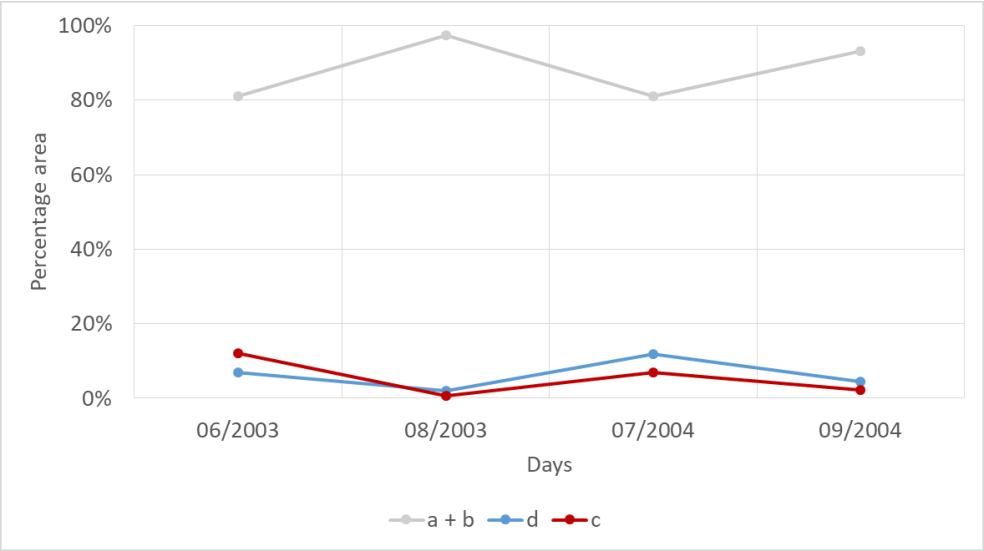


*Figure 38: Average percentage area near the Val de La Mare catchment (from 2003 to 2004) from combinations of the confusion matrices.*

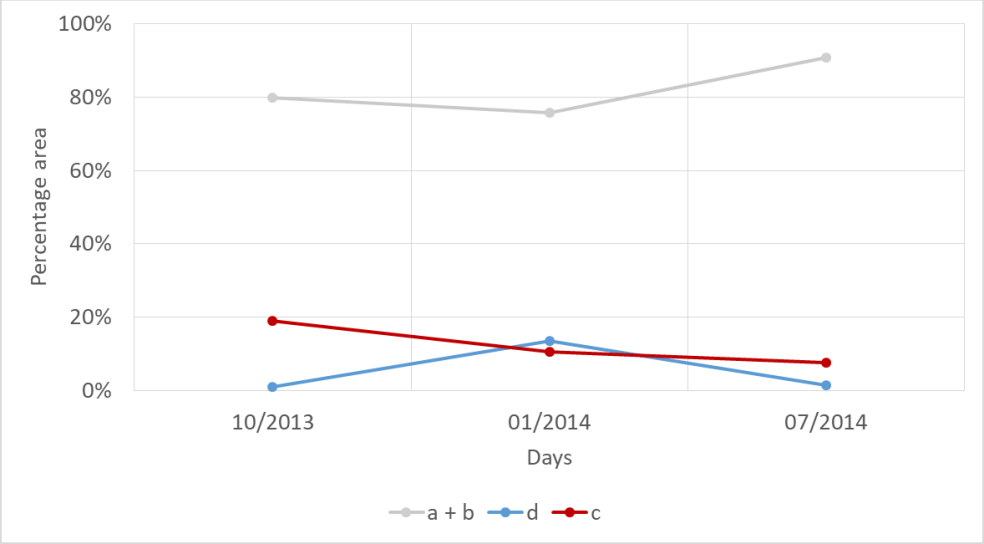


*Figure 39: Average percentage area of the Tassullo catchment (from 2013 to 2014) from combinations of the confusion matrices.*

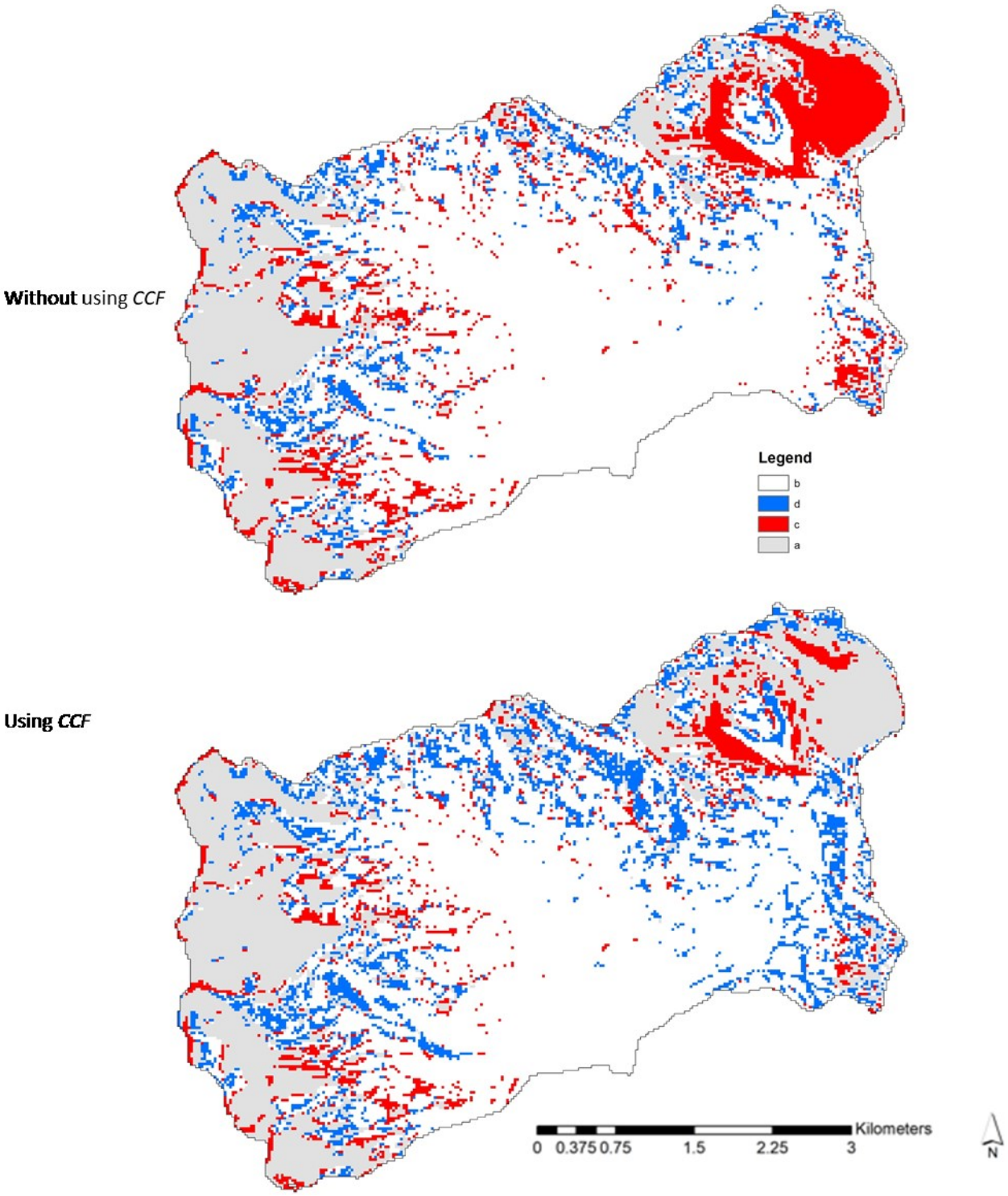


*Figure 40: Comparison of the areas in the upper part of Val de La Mare catchment (21 June 2003) when modelling without and with CCF.*

### 2.3.d.2. AHM

After the EISModel calibration, we focused on the calibration of AHM. We performed single calibrations for each segment of the catchment (Table 21) by using the available measured

discharges at different hydrometric stations to optimize the calibration parameters of AHM (Table 23).

Calibrating the hydrological model required simulating the runoff in catchments that were not influenced by hydroelectric infrastructures. Thus, we used the available discharge data at Tassullo station for the period from 1935 to 1939 (before the Careser, Pian Palù and Santa Giustina dams were constructed for hydroelectric use), and we used the measured discharge data at the Pian Venezia station for the period from 2008 to 2014. Pian Venezia is an experimental hydrometric station (owned by the TESAF department) that is located at 2295 m a.s.l. and is not influenced by human activity.

We focused on the relationship between $UZSN/RLZSN$ and $CB/RLZSN$ to calibrate the parameters (Table 23). First, we considered the guidelines of the Stanford model (Crawford and Linsley, 1966) to fix the relationship between the parameters as a function of the catchment topography and cover. An estimate of $UZSN$ relative to $RLZSN$ could be found from Table 28. Additionally, Table 28 could be used to estimate the relationships between parameters. The parameter $CC$ is an index of the ratio between the increment that is added to interflow detention and the increment that is added to surface-runoff detention.

The effects of variations in this parameter are shown in Figure 41 (Crawford and Linsley, 1966). Hydrograph (a) was simulated with a fixed $CC$ value. Increasing $CC$ produced hydrograph (b), and decreasing $CC$ produced hydrograph (c). We based our calibration of the ETPFRC parameter on evapotranspiration values from the literature according to the elevation range and cover of each catchment.

*Table 28: Relationship between $UZSN$ and $RLZSN$ according to the catchment topography and cover.*

| *Catchment* | $UZSN$ |
|---|---|
| Steep slopes, limited vegetation, low depression storage | 0.06 $RLZSN$ |
| Moderate slopes, moderate vegetation, moderate depression storage | 0.08 $RLZSN$ |
| Heavy vegetal or forest cover, soils subject to cracking, high depression storage, very mild slopes | 0.14 $RLZSN$ |

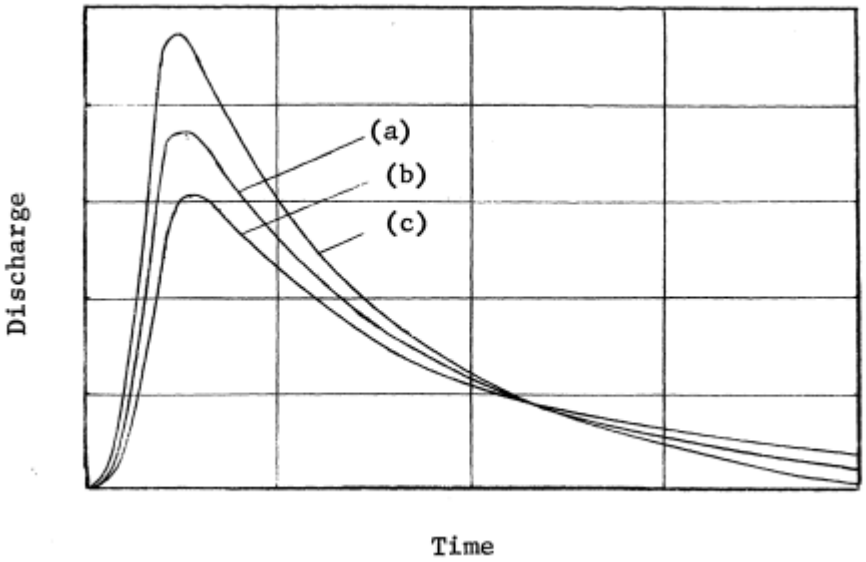


*Figure 41: Effects of variations in the CC parameter on the hydrograph (Crawford and Linsley, 1966).*

We calibrated the *S1* parameters for the Val de La Mare catchment by using the measured discharge at Pian Venezia from 2008 to 2014. Similarly, we calibrated the *S2* and *S3* parameters for the Tassullo catchment using the measured discharge at Tassullo from 1935 to 1939 (Table 29).

*Table 29: Calibration of the segment parameters and the periods and catchments that were used for calibration.*

| *ID calibration run* | *Segment* | *Period (from – to)* | *Hydrometric station* |
|---|---|---|---|
| C_1 | *S1* | 2008 – 2014 | Pian Venezia |
| C_2_3 | *S2, S3* | 1935 – 1939 | Tassullo |

We prepared the input for AHM by using EISModel 041d and the calibrated parameters above. EISModel calculated the average base flow for each segment of the catchment. We simulated the runoff using the topographic input that corresponded to the period of the measured discharge to calibrate the AHM parameters with the available discharge data. Table 30 shows the characteristics (meteorological and topographic inputs) of the calibration runs.

*Table 30: Characteristics of the calibration runs: meteorological input (T °C and P mm) and topographic input (glacial extension and DTM).*

| *ID calibration run* | *Segment* | *Catchment* | *Meteorological input T - P (from – to)* | *Glacial extension* | *DTM* |
|---|---|---|---|---|---|
| C_1 | *S1* | Val de La Mare | 2008 – 2014 | 2000s | 2000s |
| C_2_3 | *S2, S3* | Tassullo | 1935 – 1939 | LIA | LIA |

We began the modelling five years before the beginning of the calibration period to calibrate AHM. Indeed, we exploited the improvements of EISModel 041d (2.3.b.4) to consider the transition period between the remaining snow layers and new ice layers.
After we fixed the calibration parameters for the first segment (calibration C_1), we applied these parameters to calibration C_2_3 and then calibrated the parameters for the second and third segments (Table 31 and Table 32).

*Table 31: Calibration C_1.*

| *ID* | *Name* | $S1$ *Value* |
|---|---|---|
| 11 | UZSN | 3 |
| 12 | RLZSN | 50 |
| 13 | CB | 0.5 |
| 14 | CC | 10 |
| 15 | ETPFRC | 0.6 |

*Table 32: Calibration C_2_3.*

| *ID* | *Name* | $S1$ *Value* | $S2$ *Value* | $S3$ *Value* |
|---|---|---|---|---|
| 11 | UZSN | 3 | 10 | 15 |
| 12 | RLZSN | 50 | 80 | 100 |
| 13 | CB | 0.5 | 5 | 10 |
| 14 | CC | 10 | 10 | 10 |
| 15 | ETPFRC | 0.6 | 0.6 | 0.6 |

Table 33 shows some of the statistical indices that were related to the C_1 and C_2_3 calibrations. We considered the $KGE$ index (Equation 49) in addition to the N&S and ME indices. According to Gupta et al. (2009), the mean error and its related N&S criterion consist of three components, which represent the correlation, the bias and a variability measurement. Gupta et al.'s (2009) decomposition showed that the variability must be underestimated to maximize the N&S index. Furthermore, the bias is scaled by the standard deviation of the observed values, which complicates comparisons between basins. Gupta et al. (2009) proposed an alternative model performance criterion KGE because the error consists of three components. $KGE$ is formulated by computing the Euclidian Distance ($ED$) of the three components from the ideal point, which is equivalent to selecting a point from the three-dimensional Pareto front:

*Equation 49*

$$KGE = 1 - ED$$

*Equation 50*

$$ED = \sqrt{(r-1)^2 + (\alpha-1)^2 + (\beta-1)^2}$$

where
$r$ = correlation coefficient
$\alpha = STdev_{sim}/STdev_{oss}$
$\beta = Mean_{sim}/Mean_{oss}$

Such an alternative criterion avoids the problems that are associated with the N&S index. Indeed, $KGE$ facilitates an analysis of the relative importance of its different components in the context of hydrological modelling and shows how model-calibration problems can arise from interactions among these components (Gupta et al., 2009).

*Table 33: Statistical indices for the calibration of AHM.*

| *Index* | *C_1* | *C_2_3* |
|---|---|---|
| N&S | 0.7853 | 0.8154 |
| ME % | 0.2% | -2.3% |
| KGE | 0.8891 | 0.8840 |

Figure 42 and Figure 43 show a comparison of the observed vs simulated daily discharge data.

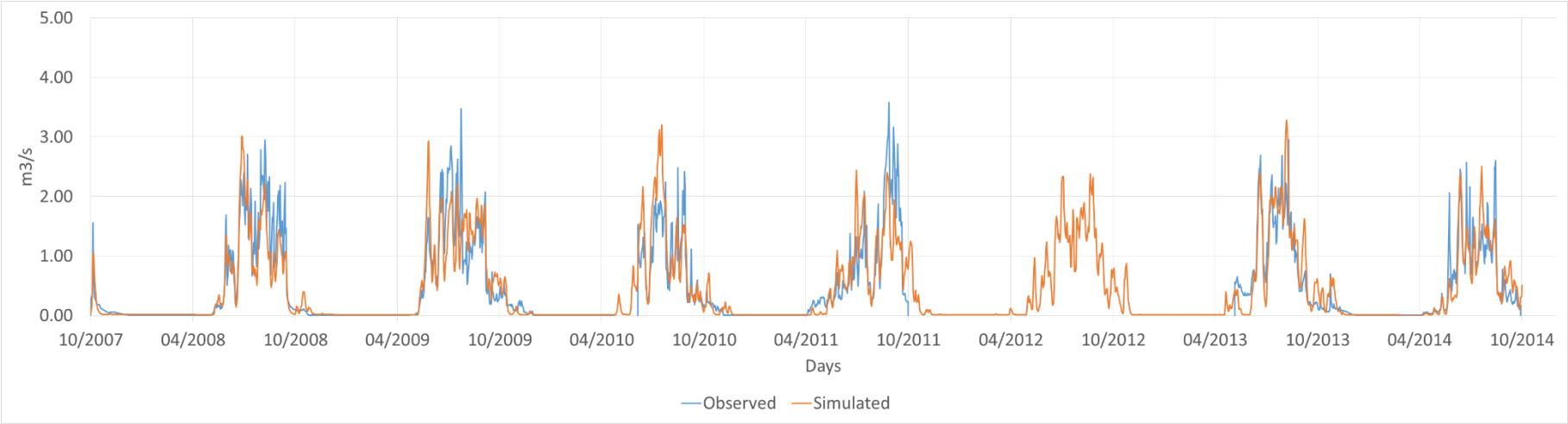


*Figure 42: Calibration C_1 – comparison of observed* vs *simulated daily discharge data from the Val de la Mare catchment from 1 Oct 2007 to 30 Sept 2014: N&S 0.7853, ME 0.2%, and KGE 0.8891.*

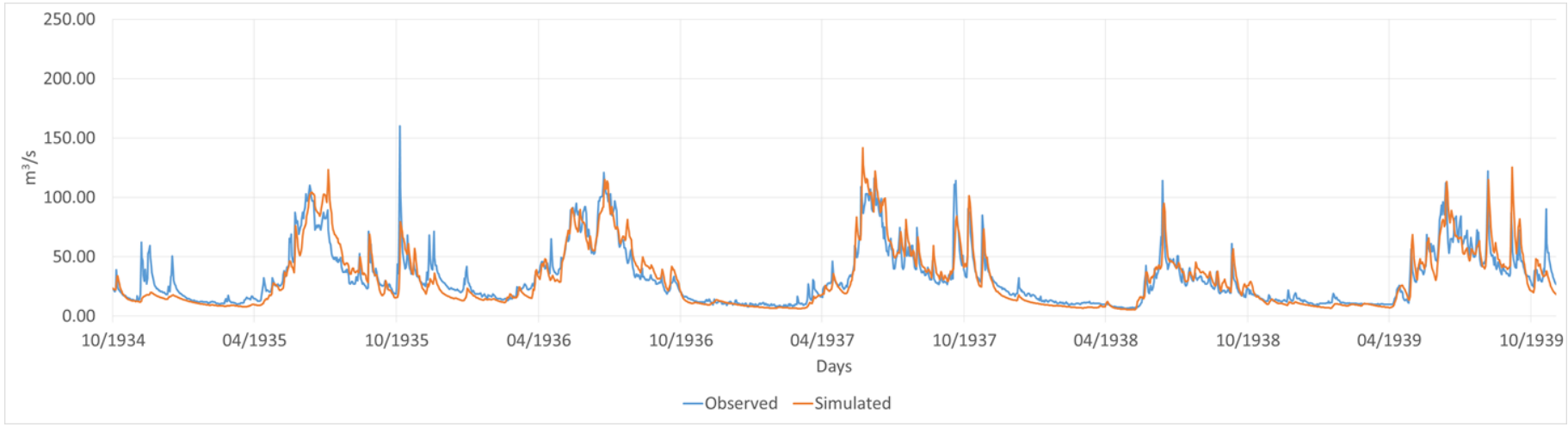


*Figure 43: Calibration C_2_3 – comparison of observed* vs *simulated daily discharge data from the Tassullo catchment from 1 Oct 1934 to 30 Sept 1939: N&S 0.8154, ME -2.3%, and KGE 0.8840.*

### 2.3.e. *Validation*

Similarly, to the calibration, we validated the nivo-glacial model and hydrological model. We validated EISModel 041d for both the measured glacial mass balances and the snow-cover maps. On the other hand, we validated AHM for the available discharge data at different hydrometric stations. The spatial and temporal distributions of the validation did not overlap with the calibration; therefore, we considered different areas and periods. Table 39 and Table 40 show synthetic schema of the spatial and temporal distributions of the calibration and validation.

#### 2.3.e.1. EISModel 041d

We considered two types of validation for EISModel, namely, validation of the measured glacial mass balance and the snow-cover maps

We modelled the glacial mass balance at fourteen ablation stakes on the La Mare glacier (elevation range from 2600 to 3350 m a.s.l.) for the period from September 2006 to September 2009. We performed continuous modelling from 13/09/2003 to 13/09/2009 and validated the model for the cumulative measured mass balance at the end of the simulation run (13/09/2009) to determine the spatial distribution of the glacial mass balance. Figure 44 shows a scatterplot of the simulated vs observed glacial mass balances at the ablation stakes. We obtained very good statistical indices (Table 34): the N&S index was 0.9643 and the ME percentage was 4.3%. We reported the statistical indices in relation to the best pixel within 1 X 1 and 3 X 3 kernels.

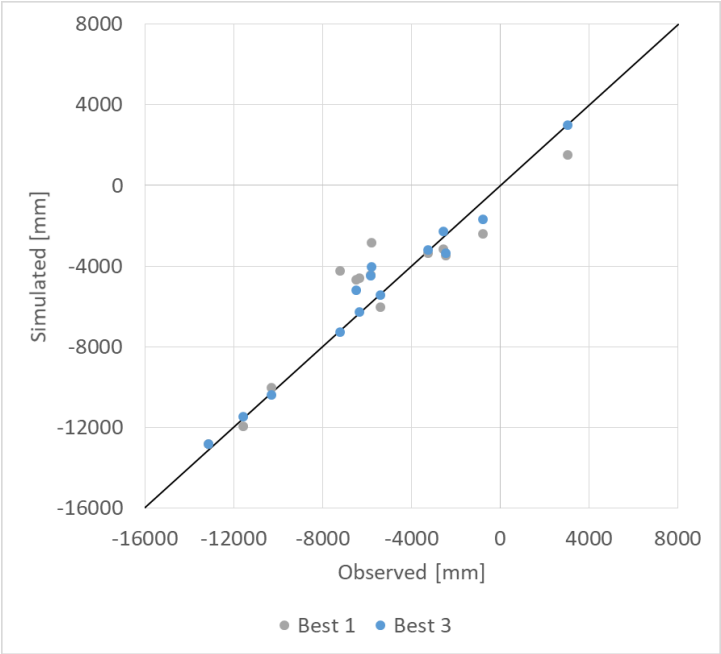


*Figure 44: Comparison of the observed* vs *simulated glacial mass balance at the fourteen ablation stakes (Best 1 and Best 3) on the La Mare glacier (elevation from 2600 to 3350 m a.s.l.). The black line represents the 1:1 relationship.*

*Table 34: Statistical indices for the validation of EISModel 041d of the simulated glacial mass balance at the fourteen ablation stakes.*

| Index | Best 1 | Best 3 |
|---|---|---|
| N&S | 0.86156 | 0.96429 |
| ME | 411.61 | 240.95 |
| $R^2$ | 0.87198 | 0.9678 |
| RMSE | 1544.06 | 784.21 |

Next, we considered the snow cover maps, calculating the confusion matrix in the same way as for calibration.

Table 35 and Table 36 show the percentage area of each confusion matrix case obtained when using the calibrated melt parameters. The results are good and the percentages of correct snow cover estimations match very well those obtained in calibration.

*Table 35: Statistical indices for the validation of EISModel 041d using confusion matrices. Percentage area near the Val de La Mare catchment (from 2003 to 2004) for each combination of confusion matrices: a) correct snow-cover area, b) correct no-snow-cover area, c) early melting area, and d) late melting area.*

| *Date* | *Area [km²]* | *a* | *b* | *d* | *c* | *a + b* |
|---|---|---|---|---|---|---|
| 20030518 | 35.6 | 69% | 15% | 9% | 8% | 84% |
| 20040520 | 35.6 | 82% | 6% | 9% | 3% | 88% |
| Average | | 76% | 10% | 9% | 5% | 86% |

*Table 36: Statistical indices for the validation of EISModel 041d using confusion matrices. Percentage area near the Tassullo catchment for each combination of confusion matrices: a) correct snow-cover area, b) correct no-snow-cover area, c) early melting area, and d) late melting area.*

| *Date* | *Area [km²]* | *a* | *b* | *d* | *c* | *a + b* |
|---|---|---|---|---|---|---|
| 20140504 | 645 | 39% | 36% | 0% | 24% | 76% |

Finally, we performed a visual comparison by comparing the observed vs simulated snow-cover maps for the Vermiglio catchment using LANDSAT 7 satellite images (Figure 45). These images have the same spatial resolution as the DTM used in input for EISModel 041d, and can be seen as a good compromise between spatial coverage and raster resolution, compared to available data for the Val de La Mare (high resolution but low spatial coverage) and for the Tassullo catchment (high spatial coverage but low resolution).. In addition, with LANDSAT 7 images we could validate the high-resolution snow and ice processes implemented in the model. We only did a visual comparison of modelled snowcover vs. LANDSAT false-colour composites, avoiding implementing automatic classification procedures because they were outside the aims of this work.

We conducted an analysis on four dates during the summer of 2009 (from May to September). We researched some satellite images without cloud cover to compare the observed vs simulated results. The good quality of the satellite images enabled us to recognize the snow line on the LANDSAT 7 layer. Additionally, overlapping the snow-cover

maps (modelled by EISModel 041c with the calibrated parameters above) with the satellite images enabled us to recognize acceptable matching between the two rasters for the four data.

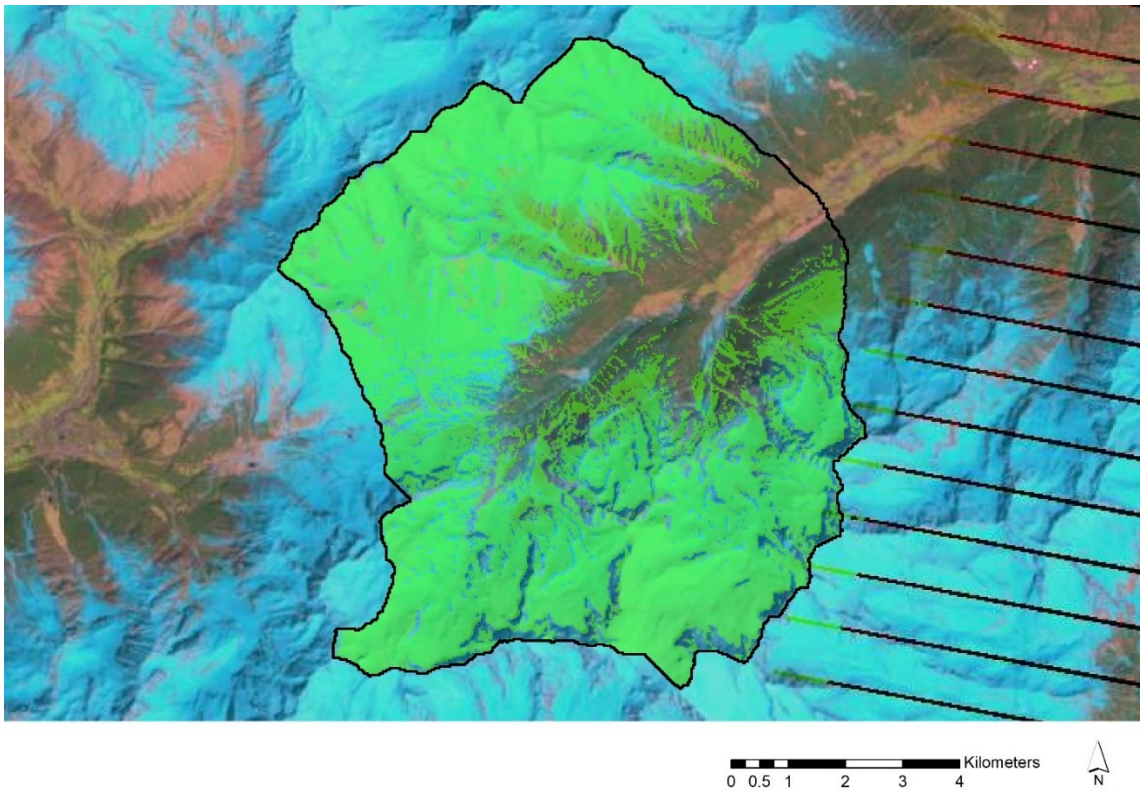


*Figure 45: Example of a comparison between simulated* vs *observed snow-cover maps from May 3, 2009 for the Vermiglio catchment. The light-blue area represents the measured snow-cover area (LANDSAT 7), and the green area represents the modelled snow-cover area (EISModel 041d).*

### 2.3.e.2. AHM

We validated the model under different conditions for this research. We considered catchments with different extensions during different meteorological periods (Table 37).

As with the calibration, we simulated the runoff in catchments that were not influenced by hydroelectric infrastructures. Thus, we used available discharge data from the Tassullo station for the period from 1940 to 1944, data from the Ponte Rovina station for the period from 1935 to 1940, and data from the Vermiglio station for the period from 2002 to 2008. We simulated the runoff by using the topographic input that corresponded to the period of the measured discharge to validate AHM with the available discharge data. Table 37 shows the characteristics (meteorological and topographic inputs) of the validation runs.

*Table 37: Characteristics of the validation runs: meteorological input (T °C and P mm) and topographic input (glacial extension and DTM).*

| *ID validation run* | *Segment* | *Catchment* | *Area [km$^2$]* | *Meteorological input T - P (from – to)* | *Glacial extension* | *DTM* |
|---|---|---|---|---|---|---|
| V_1 | *S1,2,3* | Tassullo | 1046 | 1940 - 1944 | LIA | LIA |

| | | | | | | |
|---|---|---|---|---|---|---|
| V_2 | *S1,2,3* | Ponte Rovina | 386 | 1935 – 1940 | LIA | LIA |
| V_3 | *S1,2,3* | Vermiglio | 80 | 2002 - 2008 | 2000s | 2000s |

Similarly, to the calibration, we began the modelling five years before the beginning of the validation period to consider the transition period between the remaining snow layers and new ice layers.

We obtained very good statistics from the validation. Table 38 shows some statistical indices that were related to the V_1, V_2, and V_3 validations. Figure 47 and Figure 48 show a comparison of the observed vs simulated discharge data.

We obtained a suitable model that could reproduce the runoff at different spatial distributions and during different periods according to the application of this research to determinate the sensitivity of the cryosphere to the runoff within different catchments and under different meteorological conditions. Indeed, we considered different periods and spatial scales during the validation of the model.

*Table 38: Statistical indices for the validation of AHM.*

| *Index* | *V_1* | *V_2* | *V_3* |
|---|---|---|---|
| N&S | 0.5451 | 0.7351 | 0.7144 |
| ME | -12% | 12% | 9% |
| KGE | 0.7493 | 0.7274 | 0.7736 |

Table 39 and Table 40 summarize the relationships between the calibration and validation of the hydrological model.

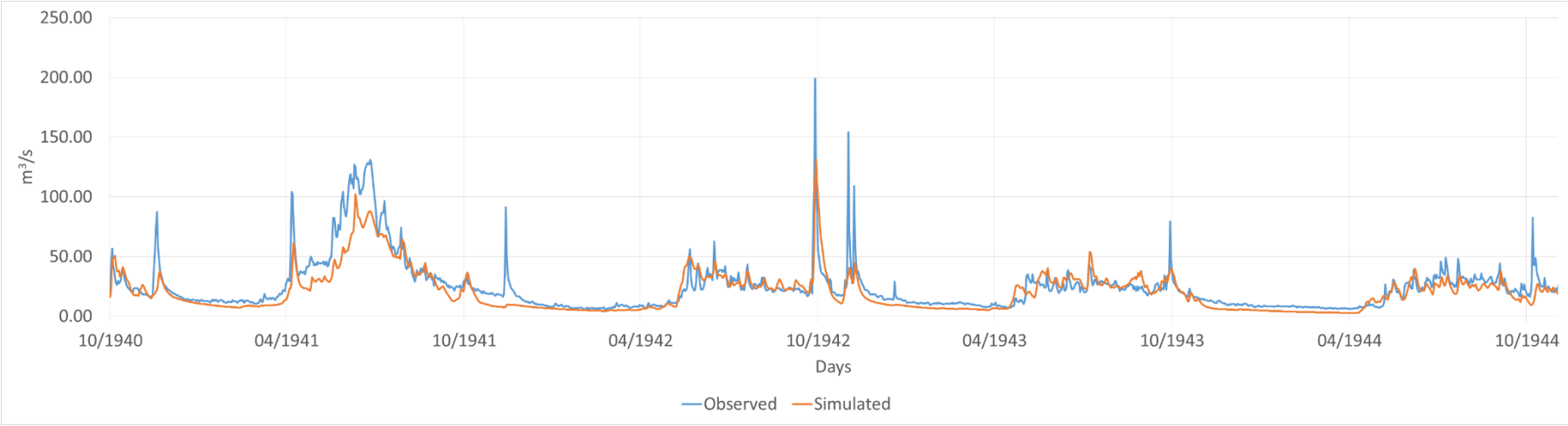


*Figure 46: Validation V_1 - comparison of observed* vs *simulated daily discharge data from the Ponte Rovina catchment from 1 Oct 1940 to 31 Dec 1944: N&S 0.5451, ME -12%, and KGE 0.7493.*

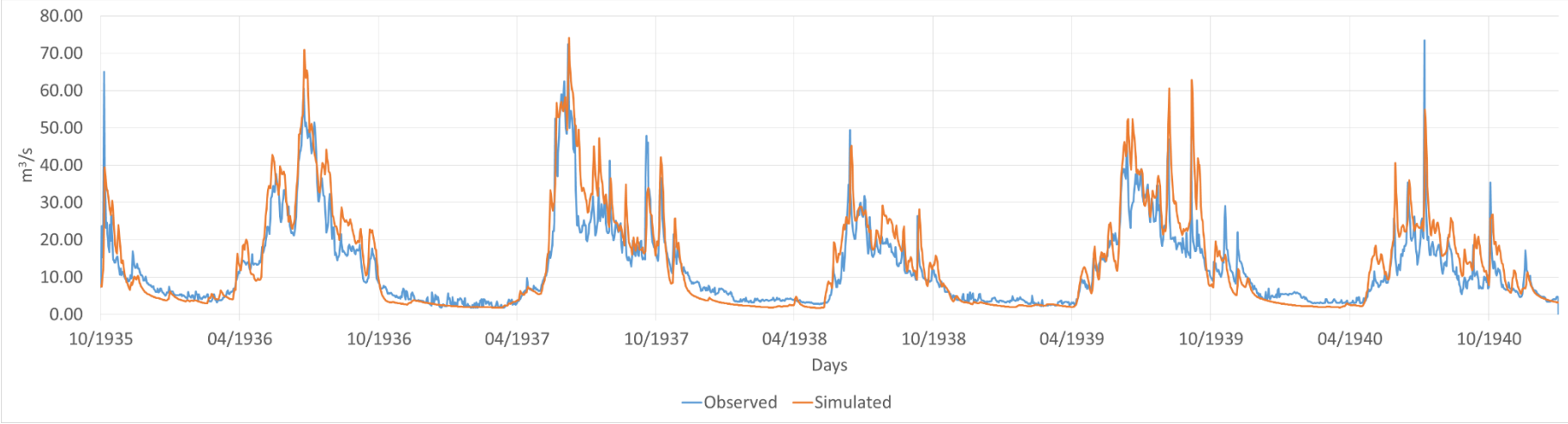


*Figure 47: Validation V_2 – comparison of observed* vs *simulated discharge data from the Ponte Rovina catchment from 1 Oct 1935 to 31 Dec 1940: N&S 0.7351, ME 12%, and KGE 0.7274.*

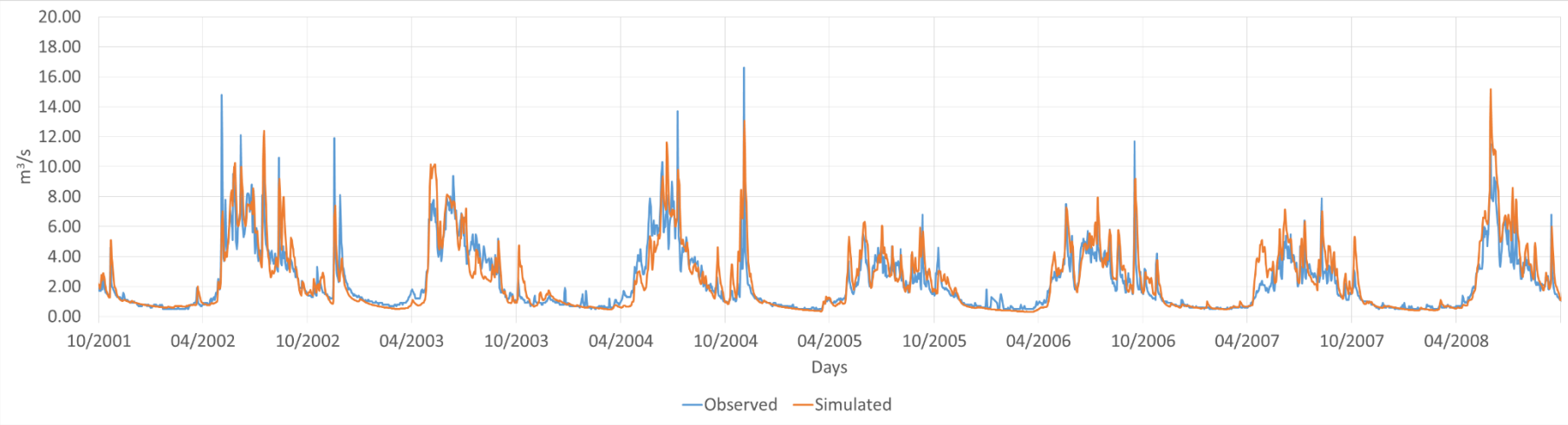


*Figure 48: Validation V_3 - comparison of observed* vs *simulated discharge data from the Vermiglio catchment from 1 Oct 2001 to 30 Sept 2008: N&S 0.7144, ME 9%, and KGE 0.7736.*

*Table 39: EISModel 041d calibration and validation: VdM = Val de La Mare catchment, $VdM_s$ = area in the upper part of Val de La Mare, Tassullo = Tassullo catchment.*

| | *Calibration* | | *Validation* | | |
|---|---|---|---|---|---|
| Year | *Snow stick* | *Snow-cover maps* | *Snow stick* | *Snow-cover maps* | Year |
| 2003 | | $VdM_s$ | | | 2003 |
| 2004 | VdM | $VdM_s$ | | | 2004 |
| 2005 | VdM | | | | 2005 |
| 2006 | VdM | | | | 2006 |
| 2007 | | | VdM | | 2007 |
| 2008 | | | VdM | | 2008 |
| 2009 | | | VdM | Vermiglio | 2009 |
| 2010 | VdM | | | | 2010 |
| 2011 | VdM | | | | 2011 |
| 2012 | VdM | | | | 2012 |
| 2013 | VdM | Tassullo | | | 2013 |
| 2014 | | Tassullo | | | 2014 |
| 2015 | | | | | 2015 |

*Table 40: AHM calibration and validation:* S1 *= segment 1,* S2 *= segment 2,* S3 *= segment 3.*

| | *Calibration* | | *Validation* | | | |
|---|---|---|---|---|---|---|
| Year | Val de La Mare | Tassullo | Vermiglio | Ponte Rovina | Tassullo | Year |
| 1934 | | *S2, S3* | | | | 1934 |
| 1935 | | *S2, S3* | | *S1, S2, S3* | | 1935 |
| 1936 | | *S2, S3* | | *S1, S2, S3* | | 1936 |
| 1937 | | *S2, S3* | | *S1, S2, S3* | | 1937 |
| 1938 | | *S2, S3* | | *S1, S2, S3* | | 1938 |
| 1939 | | *S2, S3* | | *S1, S2, S3* | | 1939 |
| 1940 | | | | *S1, S2, S3* | *S1, S2, S3* | 1940 |
| 1941 | | | | | *S1, S2, S3* | 1941 |
| 1942 | | | | | *S1, S2, S3* | 1942 |
| 1943 | | | | | *S1, S2, S3* | 1943 |
| 1944 | | | | | *S1, S2, S3* | 1944 |
| 2000 | | | | | | 2000 |
| 2001 | | | *S1, S2, S3* | | | 2001 |
| 2002 | | | *S1, S2, S3* | | | 2002 |
| 2003 | | | *S1, S2, S3* | | | 2003 |
| 2004 | | | *S1, S2, S3* | | | 2004 |
| 2005 | | | *S1, S2, S3* | | | 2005 |
| 2006 | | | *S1, S2, S3* | | | 2006 |
| 2007 | | | *S1, S2, S3* | | | 2007 |
| 2008 | *S1* | | *S1, S2, S3* | | | 2008 |
| 2009 | *S1* | | | | | 2009 |
| 2010 | *S1* | | | | | 2010 |
| 2011 | *S1* | | | | | 2011 |
| 2012 | *S1* | | | | | 2012 |
| 2013 | *S1* | | | | | 2013 |
| 2014 | *S1* | | | | | 2014 |
| 2015 | | | | | | 2015 |

# 3. Results

The calibrated glacio-hydrological model has been applied to 9 combinations of glacier cover and meteorological conditions, for 4 different catchments of increasing size (from 8 to 1050 km$^2$). Table 41 reports the combinations for each catchment.

*Table 41: Combinations of glacier cover and meteorological conditions for each catchment: Q = runoff, a = LIA, b = 2000s, c = no glacier cover.*

| Meteorological conditions \ Glacier cover conditions | ***a*** | ***b*** | ***c*** |
|---|---|---|---|
| ***1940*** | $Q_{1940,a}$ | $Q_{1940,b}$ | $Q_{1940,c}$ |
| ***1970*** | $Q_{1970,a}$ | $Q_{1970,b}$ | $Q_{1970,c}$ |
| ***2000*** | $Q_{2000,a}$ | $Q_{2000,b}$ | $Q_{2000,c}$ |

We recall here the main modelling steps. The average baseflow for each segment of the catchment was modelled using EISModel 041d, which manages the meteorological and topographic inputs and simulate the snow and ice accumulation and ablation processes. Subsequently, we have used the output of EISModel (average baseflow) as input for AHM, in order to propagate the runoff and to obtain the hydrographs (Figure 26). We have started the modelling five years before the beginning of each period, in order to take into account the formation of the firn layer and its transition to ice. To compare discharge from catchments with different extension, we have calculated the unit discharge (m$^3$/s km$^2$).

We have arranged the results in three different analyses: 1) analysis of climatic effects under unchanged glacier cover, 2) glacier cover effects under different climatic periods, and 3) scale effects. The same analyses were carried out considering two particular years with opposite extreme meteorological conditions (1968 and 2003).

## 3.1. Climatic effects under unchanged glacier cover

This analysis is aimed to highlight the runoff differences stemming from different climatic conditions, and how these differences change among different catchments. To analyze the influence of meteorological conditions, we have organized the daily unit discharge on three graphs, one for each glacier cover condition (Figure 49). We have compared the runoff in

the period from April to November, assuming that the glacier contribution from December to March is negligible.

The results are significantly different among Val de La Mare and the other 3 catchments.
In Val de La Mare we recognize a different behaviour between the 1940 and 2000 climatic conditions. There is an earlier and higher peak for 2000s compared to the 1940s, and for the no glacier scenario there is a peak for 2000s and a flat in 1940s. Generally, the difference between 2000 and 1940 increases from the LIA to the current to absence of glaciers conditions. This means that differences in hydrological behaviour induced by different climatic conditions are magnified by the absence of glaciers.
In contrast, the three larger catchments show smaller difference between the 1940 and 2000 climatic conditions, even if also in this case the climatic conditions of 2000s bring somewhat higher runoff in mid-summer.
Similar considerations can be done for the climatic conditions of the 1970s, with Val de La Mare and the other three basins responding rather differently. The Val de La Mare has a peculiar response, with a decreased and delayed runoff in late spring/early summer, similar mid-summer peak, and earlier runoff decrease at the end of summer, compared to the 2000s and 1940s climatic conditions, when glaciers are present in the catchment. Considering an absence of glaciers (Figure 49 c), we can recognize the same behaviour in spring, but in late summer there are no differences among the three glacier cover conditions.

In the other three catchments, the 1970 climatic conditions lead to very similar response, with significantly higher runoff in mid-summer compared to the 2000 and 1940 climatic conditions, and differences which increase from LIA to current to absence of glaciers.
It is interesting to note that the relative differences between periods remain constant from the smaller catchment to the larger catchment (e.g. Figure 49 a, d, g, l). This means that we can not recognize a scale effect caused by different meteorological conditions.

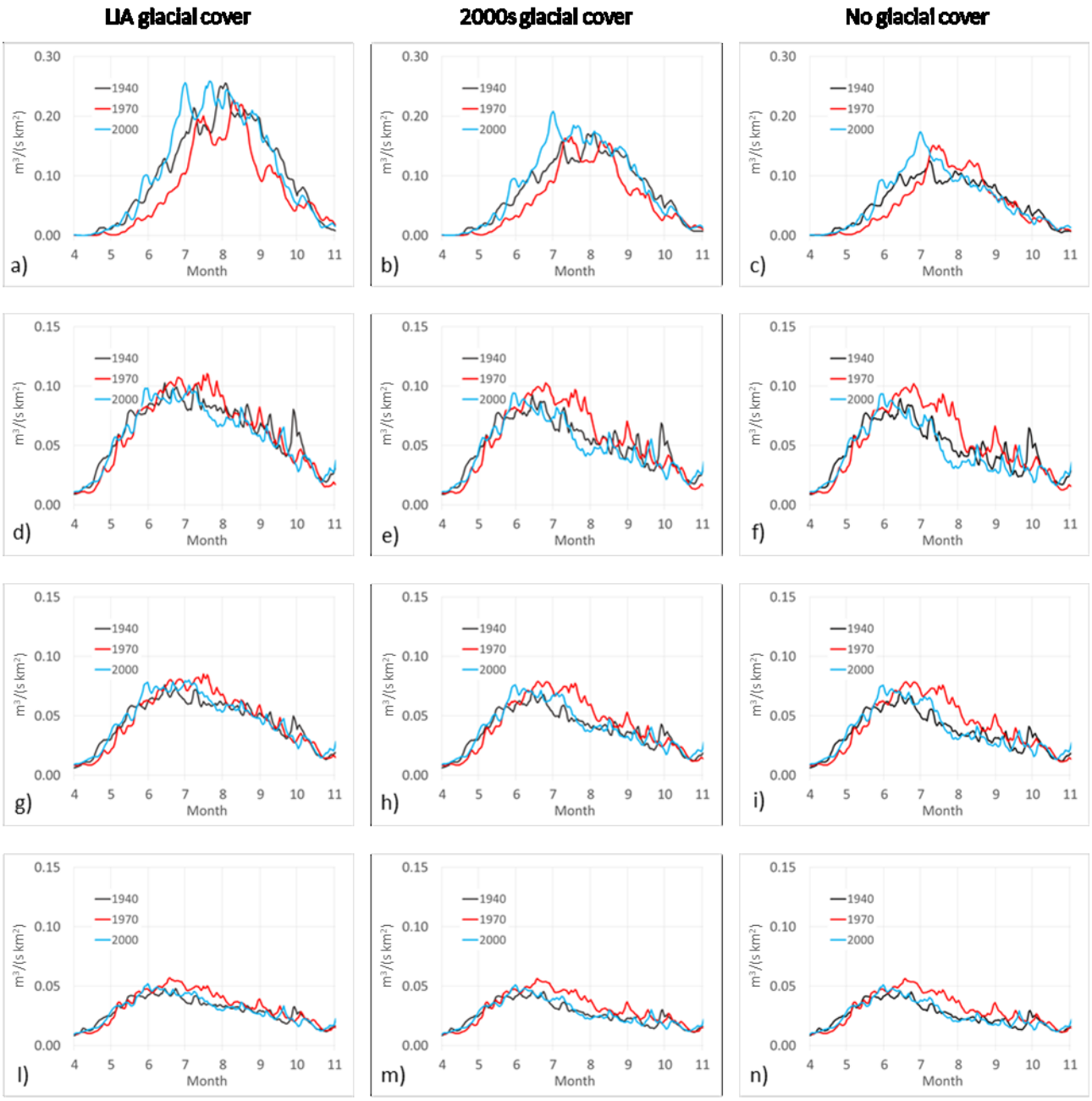


*Figure 49: Daily average unit discharge for each glacier cover extension (from April to November) for different periods: a) to c) Val de La Mare, d) to f) Vermiglio, g) to i) Ponte Rovina and l) to n) Tassullo. We used a different scale for Val de La Mare to adjust the unit discharge range.*

## 3.2. Glacier cover effects under different climatic periods

This analysis is aimed at highlighting the runoff differences coming from the interaction of different climatic conditions and different glacier cover scenarios.

To characterize the different modelled response, we have calculated the median monthly unit runoff, median difference in unit runoff and the 10$^{th}$ percentile of unit runoff difference in the period from April to November, reporting the results in Figure 50 to Figure 53.

We have used the median to characterize the unit discharge under average conditions, and the $10^{th}$ percentile to characterize the unit discharges under conditions of low runoff. We have used a monthly scale in order to reduce the noise, especially in the calculation of percentage differences. In calculation of percentage difference, we have used a threshold of unit discharge equal to $10^{-3}$ $m^3/s$ $km^2$. For the cases lower than this threshold, we have not calculated the difference and consequently, we have not plotted the values in the graphs. As in point 3.1, we have considered the glacier contribution as negligible in the period from December to March.

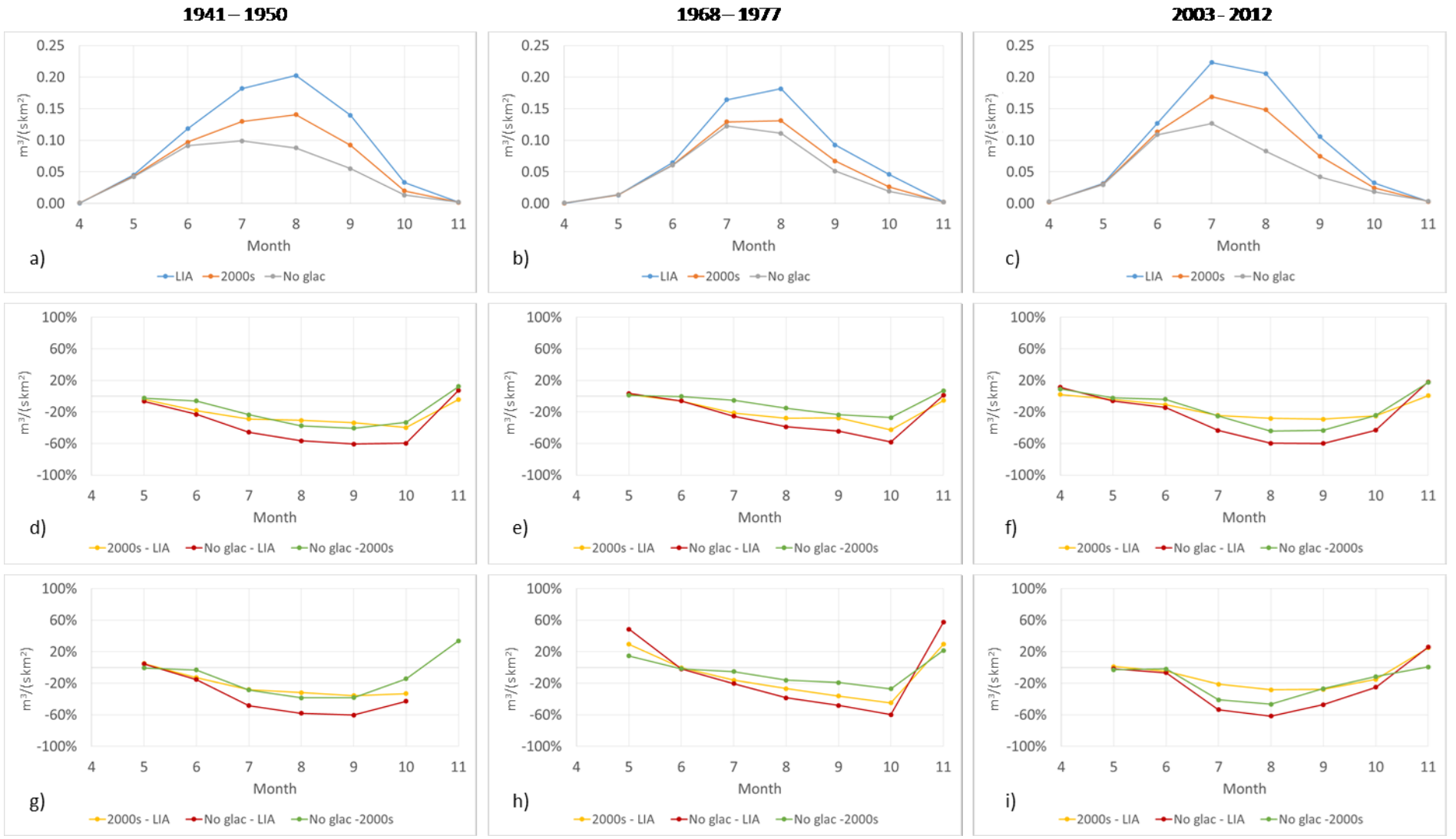


*Figure 50: a) to c) Median monthly unit discharge from April to November in the Val de La Mare catchment during three different climatic periods and under three different glacier-cover conditions, d) to e) percent difference in the median unit discharge, and g) to i) percent difference in the 10$^{th}$ percentile of the unit discharge.*

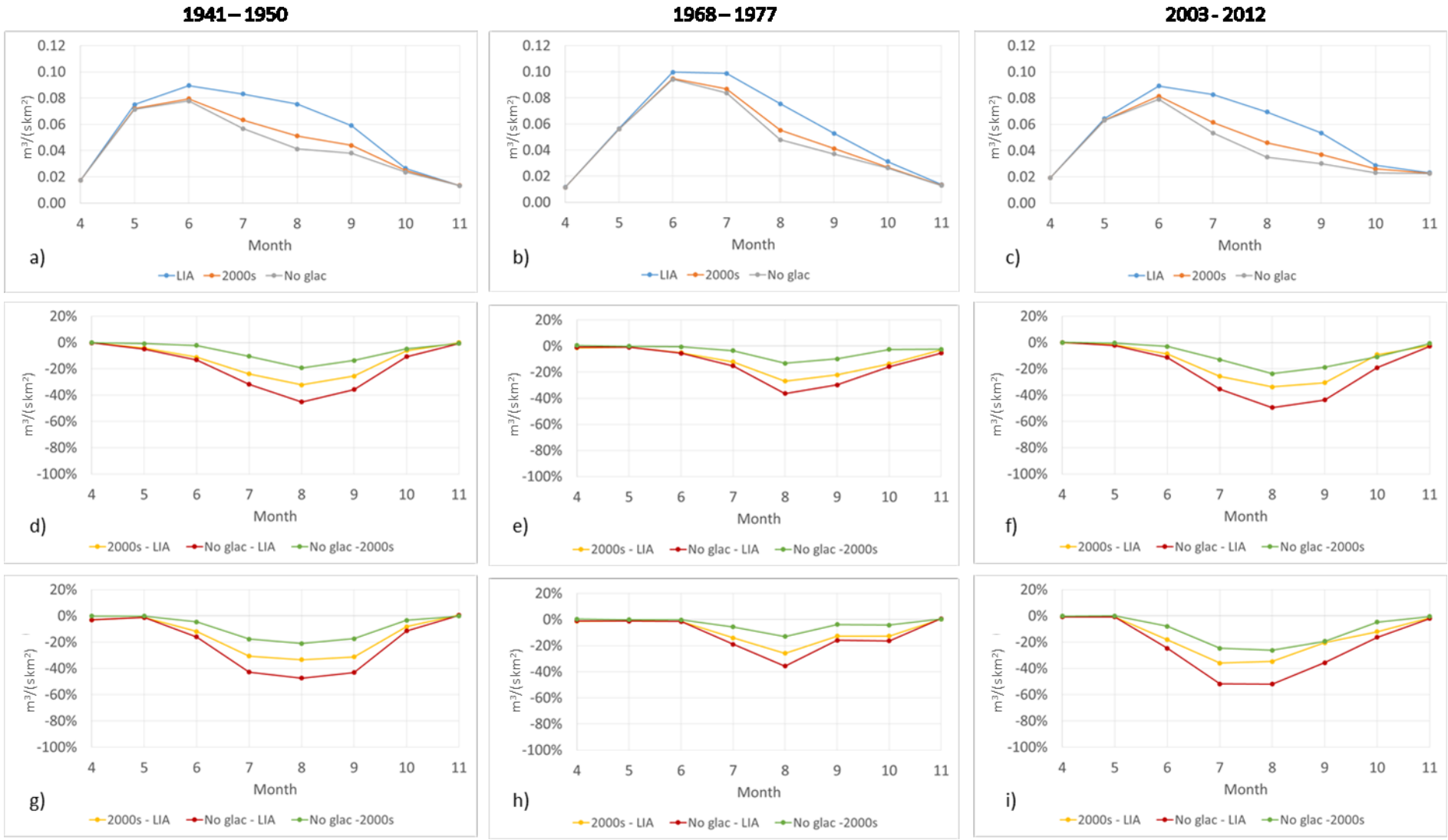


*Figure 51: a) to c) Median monthly unit discharge from April to November in the Vermiglio catchment during three different climatic periods and under three different glacier-cover conditions, d) to e) percent difference in the median unit discharge, and g) to i) percent difference in the 10th percentile of the unit discharge.*

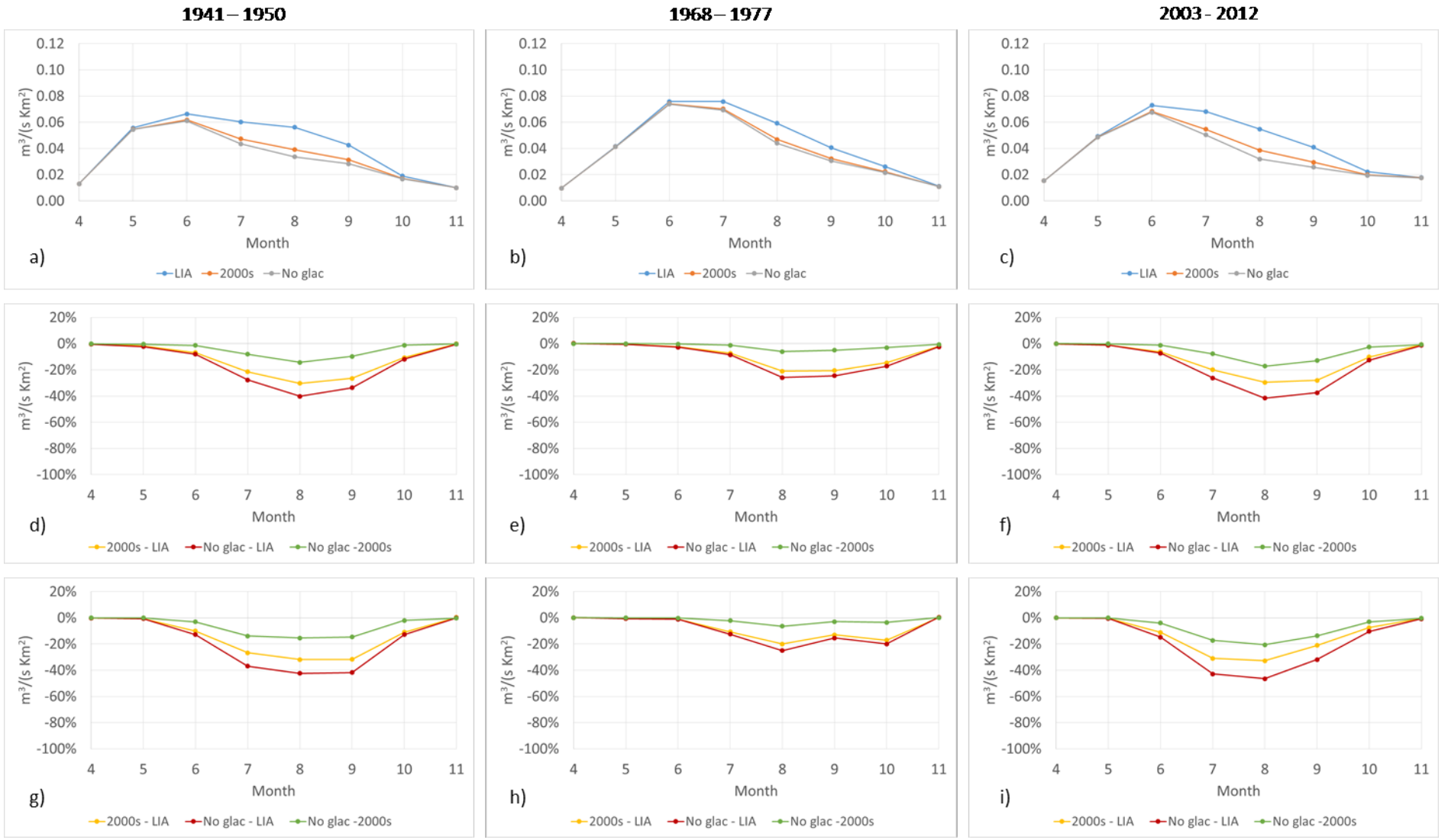


*Figure 52: a) to c) Median monthly unit discharge from April to November in the Ponte Rovina catchment during three different climatic periods and under three different glacier-cover conditions, d) to e) percent difference in the median unit discharge, and g) to i) percent difference in the 10th percentile of the unit discharge.*

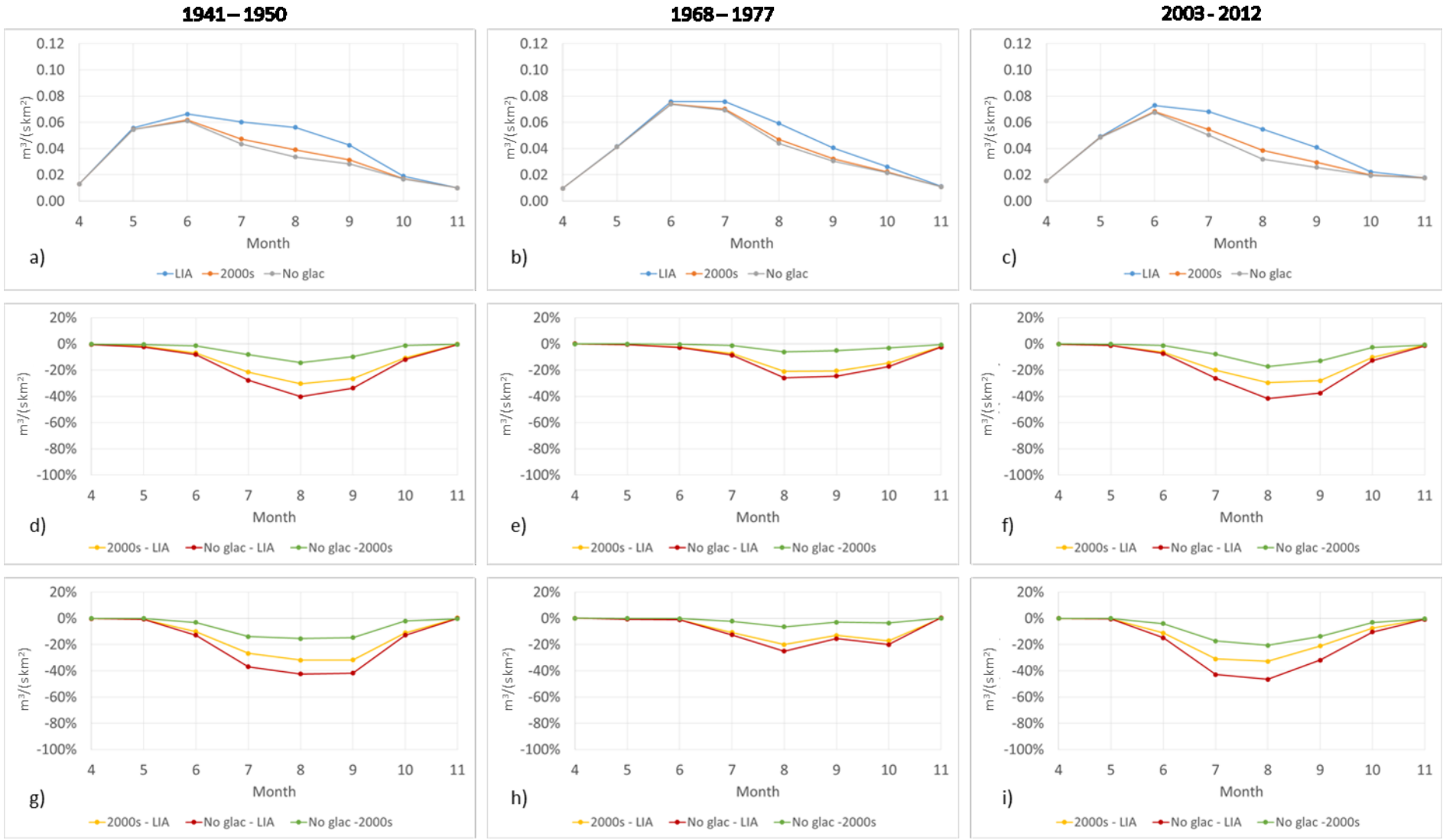


*Figure 53: a) to c) Median monthly unit discharge from April to November in the Tassullo catchment during three different climatic periods and under three different glacier-cover conditions, d) to e) percent difference in the median unit discharge, and g) to i) percent difference in the 10th percentile of the unit discharge.*

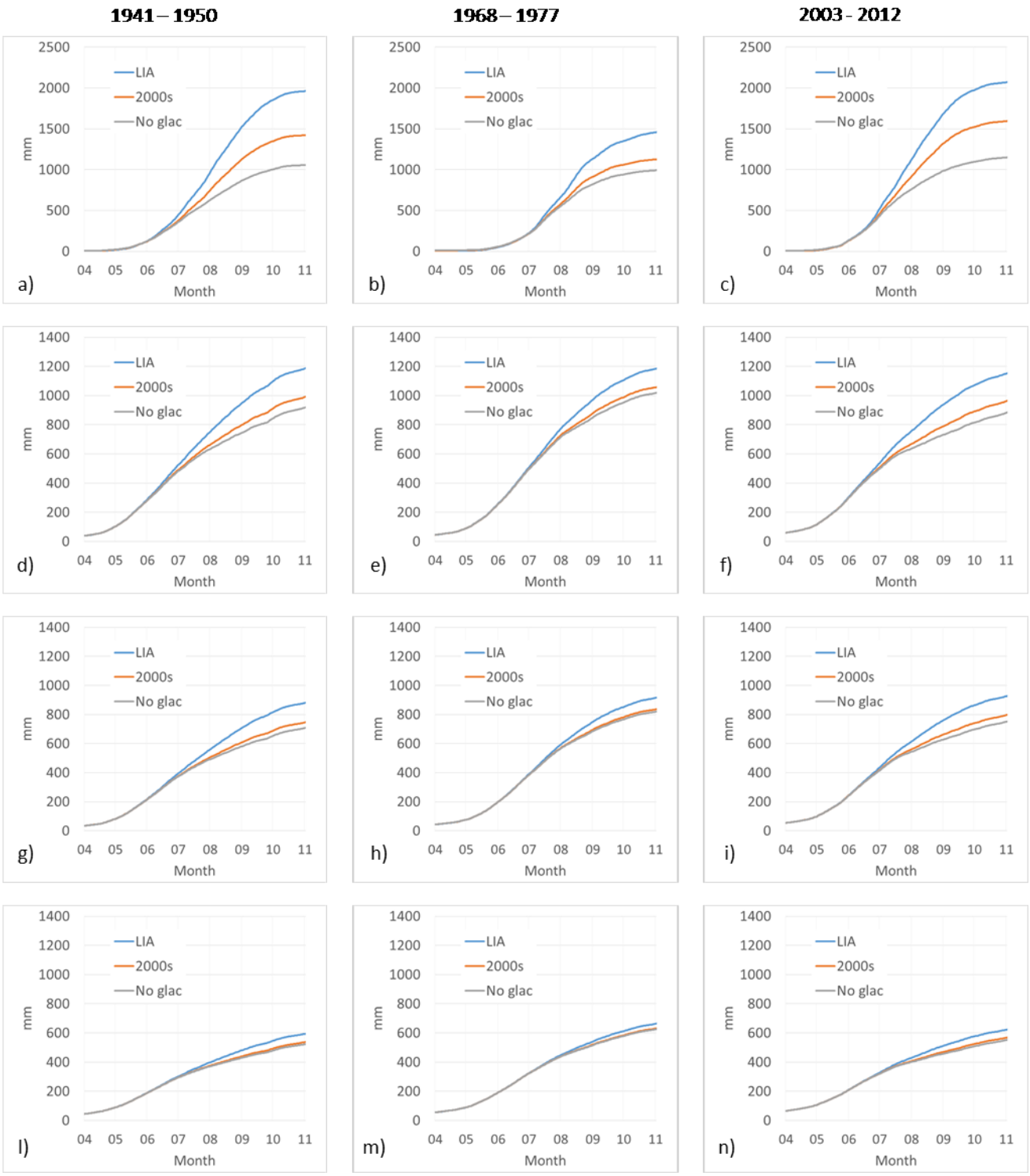


*Figure 54: Sum of the runoff for each period (from April to November) for each glacier cover extension: a) to c) Val de La Mare, d) to f) Vermiglio, g) to i) Ponte Rovina and l) to n) Tassullo. We used a different scale for Val de La Mare to adjust the runoff range.*

We have also analyzed the different hydrological response using the flow duration curve and the frequency distribution of unit discharge for each combination of climatic/glacier cover conditions (from Figure 55 to Figure 58).

In the Val de La Mare catchment, the runoff peaks in July and August. With the climatic conditions of the 1940s and 1970s, the peak shifts from August to July moving from the LIA

and current glacier cover to the no-glacier condition. In the 2000s the peaks is always in July. The highest difference among glacier cover conditions occurs in late summer/early autumn during the 1940s and 2000s, andin particular comparing the LIA and the no-glacier conditions, suggesting that in these periods the runoff is mainly fed by glacier wasting. In addition, these percentage differences do not show a unique peak but show a rather long period with high percent differences in median and 10th percentile runoff (about -50% for median value and -60% for minimum values). Comparing current glacier cover and no-glacier conditions provides very similar results.

With the climatic conditions of the 1970s, the differences among glacier cover scenarios are much smaller, and it is nearly zero if we consider late spring and first part of summer comparing current vs. no-glacier conditions. This suggests that runoff is mainly fed by seasonal snow cover, because current glaciers would remain mostly covered by snow with the climatic conditions of the 1970s. The highest peak in % differences is calculated for October, with sudden switches in November and May, which however are of low relevance because they are due to lower runoff (close to the $10^{-3}$ $m^3/s$ $km^2$ threshold).

Larger catchments show a peak in discharge during the first half of the ablation season, and it tends to occur earlier (may or June) increasing the size of the catchment. Larger catchments show much lower intra-seasonal variability of unit discharge with increasing catchment area. The graphs from Figure 55 to Figure 58 confirm that the unit discharge is clearly spread over a wider range in the Val de La Mare catchment, compared to the other three (please note that the runoff range in Figure 55 is larger than in Figure 56 to Figure 59).

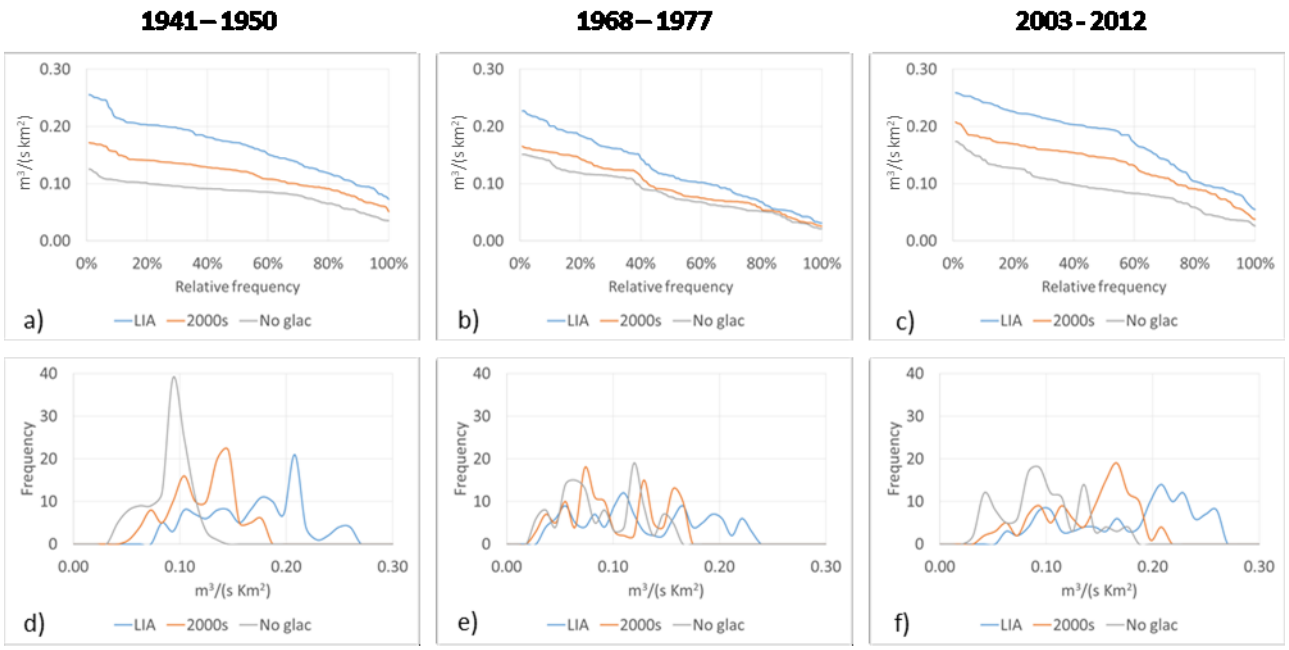


*Figure 55: a) to c) Flow-duration curve of the daily mean unit discharge from April to November in the Val de La Mare catchment under different glacier-cover conditions averaged over ten years. d) to f) Frequency distribution of the 10-year daily mean unit discharge.*

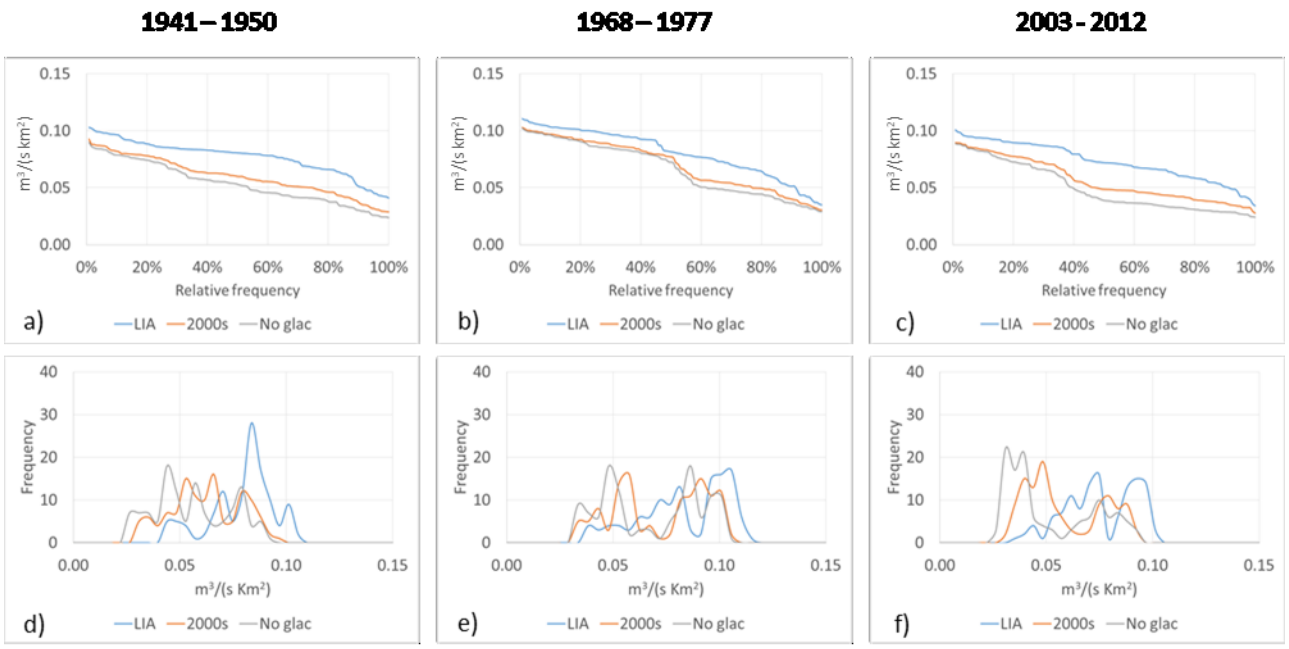


*Figure 56: a) to c) Flow-duration curve of the daily mean unit discharge from April to November in the Vermiglio catchment under different glacier-cover conditions averaged over ten years. d) to f) Frequency distribution of the 10-year daily mean unit discharge.*

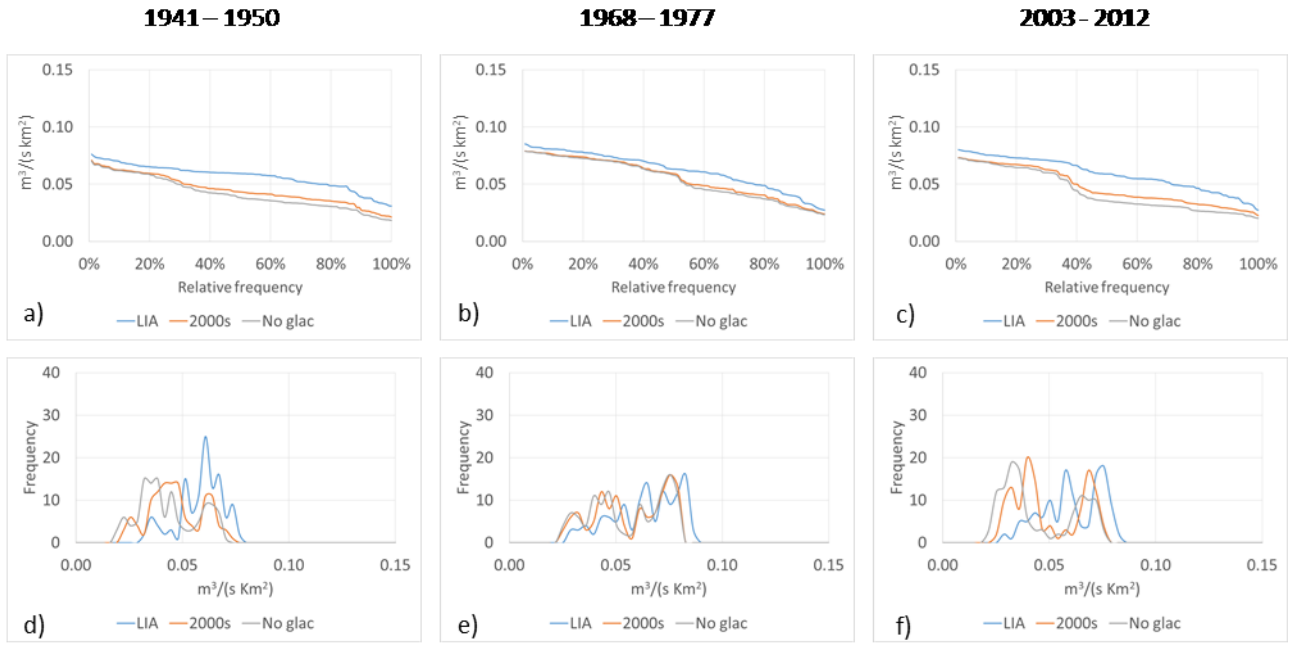


*Figure 57: a) to c) Flow-duration curve of the daily mean unit discharge from April to November in the Ponte Rovina catchment under different glacier-cover conditions averaged over ten years. d) to f) Frequency distribution of the 10-year daily mean unit discharge.*

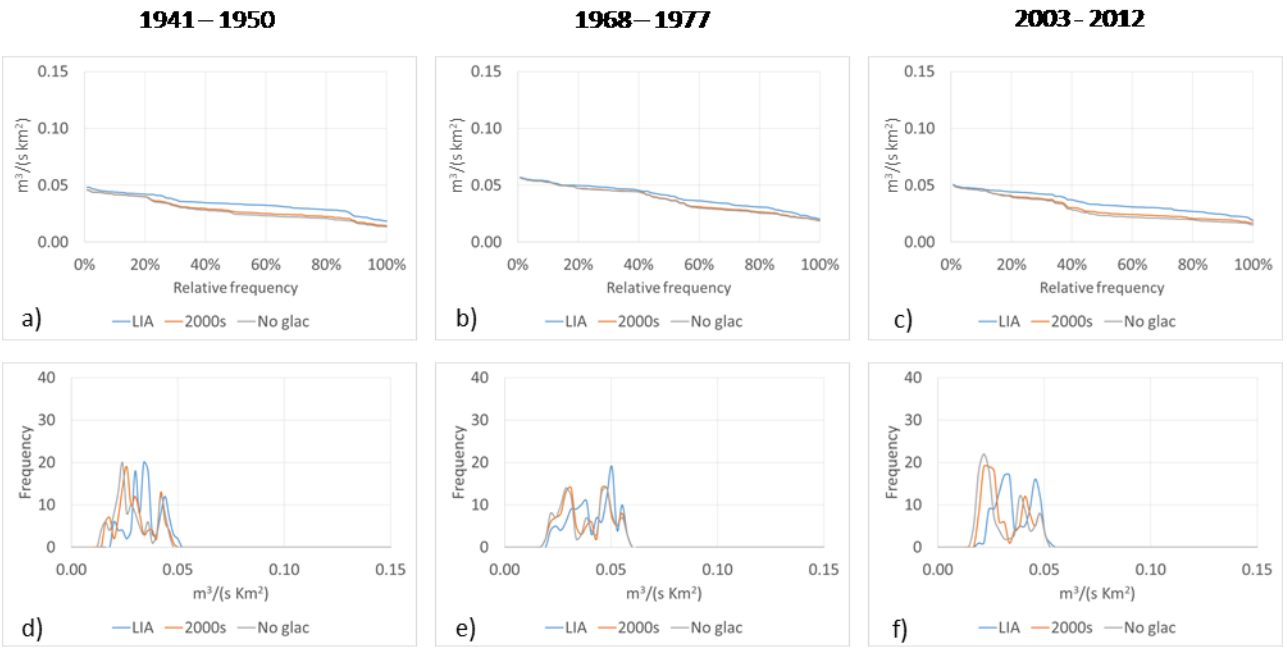


*Figure 58: a) to c) Flow-duration curve of the daily mean unit discharge from April to November in the Tassullo catchment under different glacier-cover conditions averaged over ten years. d) to f) Frequency distribution of the 10-year daily mean unit discharge.*

Different glacier cover scenarios lead to a change in the seasonal regime of runoff. These differences among glacier cover scenarios become progressively smaller, increasing the size of the catchment (Figure 50 to Figure 53). In addition, differences tend to show a clear peak in August. However, for the 10$^{th}$ percentile, for the 1940s and secondarily for the 2000s, there is an extended period of highly decreased runoff (from July to September). Overall, different glacier cover scenarios do not lead to a shift in the highest peak of unit discharge (with the exception of the Val de La Mare in the 1940s and 1970s). The most relevant change brought by the absence of glacier is a more rapid recession after the late spring peak, and for the most glacierized catchments a decrease of this peak as well. A clear shift in the frequency distribution of daily unit discharge, averaged over 10 years, is observable in Figure 55 to Figure 58 for different glacier cover scenarios, for all the analysed catchments. Indeed, analyzing the three periods, we calculated a decreased range of runoff and higher frequency of low runoff for the conditions with smaller or absent glaciers. This shift is more evident in the 1940 and 2000 periods, and less in the 1970 period.

It is interesting to observe that the difference between the 2000s and LIA glacier cover tends to converge with the difference between no-glacier and LIA glacier cover, towards larger catchments (Figure 53), whereas for Val de La Mare there is correspondence between the 2000 vs. LIA and the no glacier vs. 2000 glacier cover (Figure 50). In addition, for the larger catchment, the no glacier vs. 2000 curve hardly detaches from the zero difference line. Frequency distributions shown in Figure 55 to Figure 58 provide further confirmation to these observations. In particular, in Figure 58 d it can be seen that the LIA glaciers affect the low-to-mid discharge frequency even in a wide basin with a relatively small glacierized area. Whereas the current glaciers show little difference compared to the absence of glaciers. This suggests that for the larger catchment the damping effect of glaciers is already nearly disappeared, whereas for the smaller catchment this buffering still exists but is approximately halfway from the LIA to the no glacier scenario.

### **3.3.** Scale effects on the hydrological sensitivity to different climatic conditions and glacier cover scenarios

We have analyzed the variations of the unit discharge in August, which is the month with highest sensitivity, based on the results from sections 3.1 and 3.2, and the variations of the annual runoff and annual runoff volume under different climatic conditions and with different glacier cover scenarios. Results are compared in order to highlight the different sensitivity of catchments with different area and different percent glacierization (Figure 59 to Figure 70).

Climatic conditions during the 1940s and 2000s show similar results (Figure 59 b, Figure 67 b). Median unit discharge in August decreases by 30-60% from the LIA to the no-glacier cover scenarios, with percent decrease directly proportional to initial glacierization and inversely proportional to the catchment area. Current glacier cover leads to 10-40% larger unit discharge compared to no glacier conditions, with same proportionality to initial glacierization and catchment area. On the other hand, current versus LIA glacier cover show a more uniform decrease in unit runoff, averaging 30% in all catchments. These percent reductions from LIA to 2000 to no glacier conditions are only slightly higher considering the $10^{th}$ percentile of August unit discharge. The smaller catchment, Val de La Mare, is the only one where the current glacier cover, if compared with the no glacier conditions, ensures a unit runoff larger than its reduction modelled from the LIA. In other words, the reduction in runoff from the LIA to the current glacier conditions is smaller than the expected reduction after complete glacier disappearance. Current glaciers still ensure higher runoff in all climatic conditions, compared to the no glacier conditions. However, this ‘damping’ effect is largely decreased if compared to the LIA conditions, and this decrease is directly related to catchment area.

Differences among glacier cover conditions are significantly smaller in the 1970s (Figure 63), due to decreased runoff from glacier melt, which is more effective over the larger LIA glaciers, compared to the 2000 glaciers, and increased runoff from higher precipitation over bare ground in the no glacier scenario.

Similar results are obtained analysing the annual runoff, which obviously shows much smaller differences among glacier cover scenarios, with the exception of Val de La Mare. In this catchment, the decrease from LIA to the 2000s glacier cover is of the same magnitude of the expected reduction with complete glacier meltout. For the larger catchments most of the glacier damping effect is already vanished, and there is very little difference between runoff obtained with current glaciers or without them (Figure 59 to Figure 70 section b).

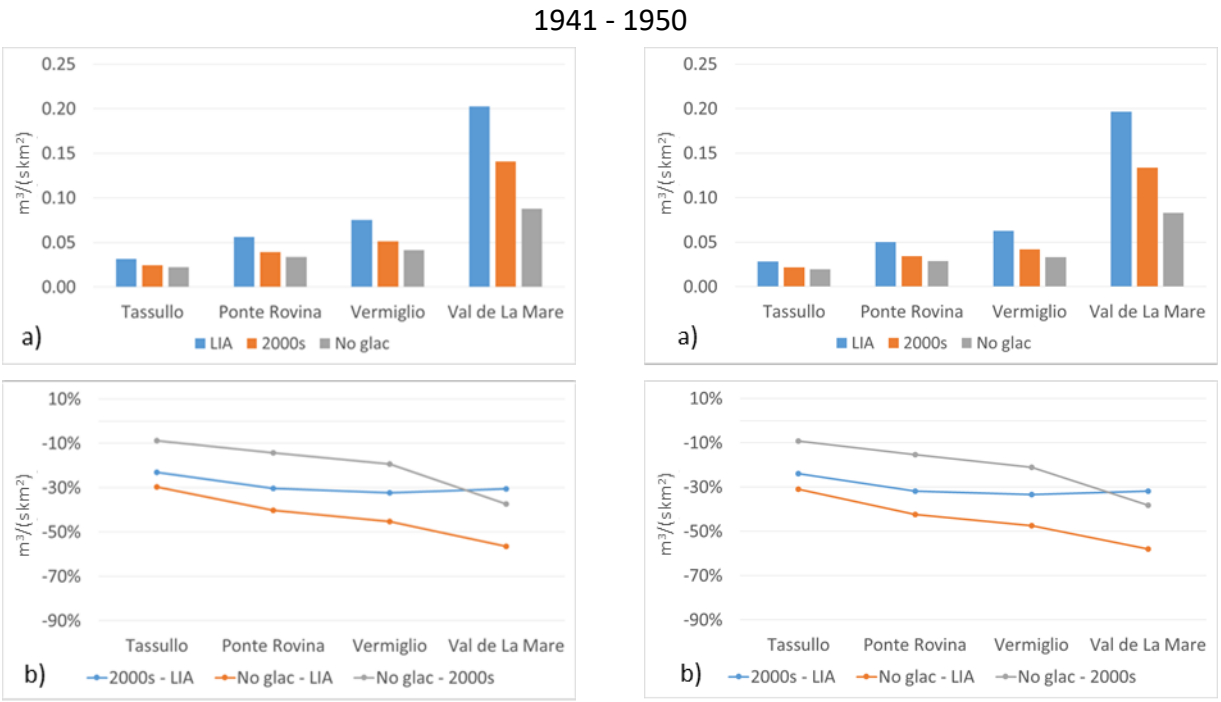


*Figure 59: Scale effect on the median monthly unit discharge in August from 1940 to 1951 ($m^3\ s^{-1}\ km^{-2}$). The second panel represents the percentage difference.*

*Figure 60: Scale effect on the 10$^{th}$-percentile monthly unit discharge in August from 1940 to 1951 ($m^3\ s^{-1}\ km^{-2}$). The second panel represents the percentage difference.*

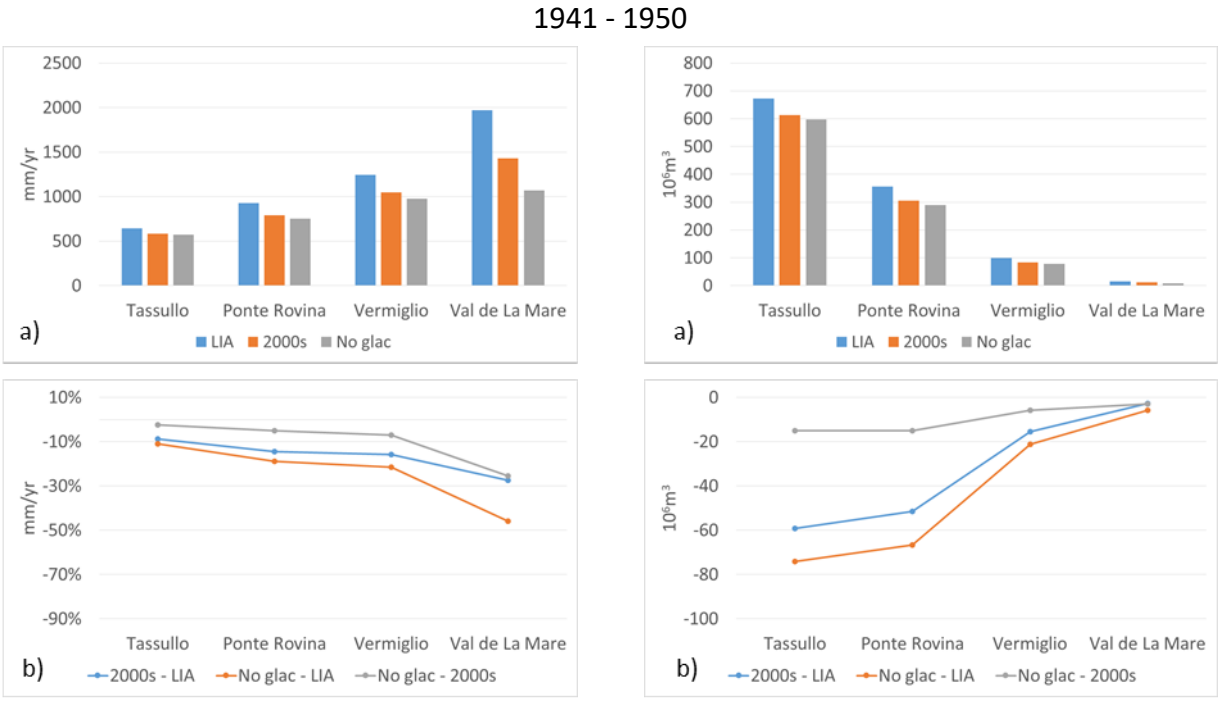


*Figure 61: Scale effect on the annual unit discharge from 1940 to 1951 (mm $yr^{-1}$). The second panel represents the percentage difference.*




*Figure 62: Scale effect on the annual runoff from 1940 to 1951 ($10^6\ m^3$). The second panel represents the difference.*

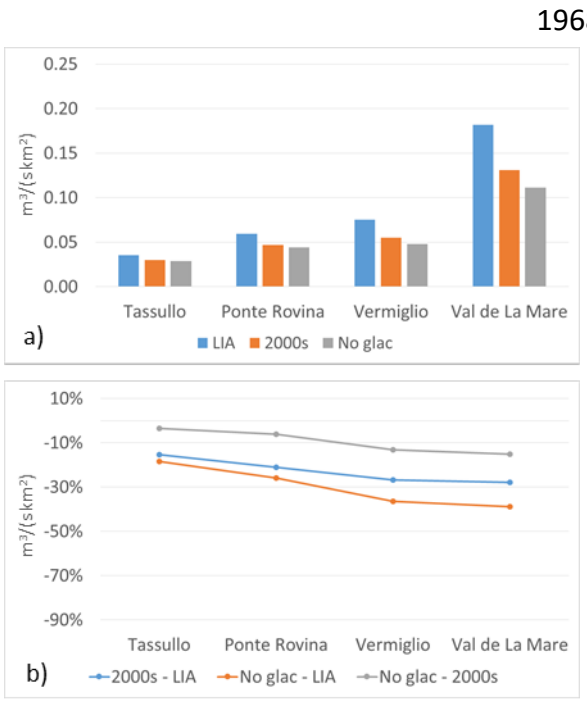


*Figure 63: Scale effect on the median monthly unit discharge in August from 1968 to 1977 ($m^3$ $s^{-1}$ $km^{-2}$). The second panel represents the percentage difference.*

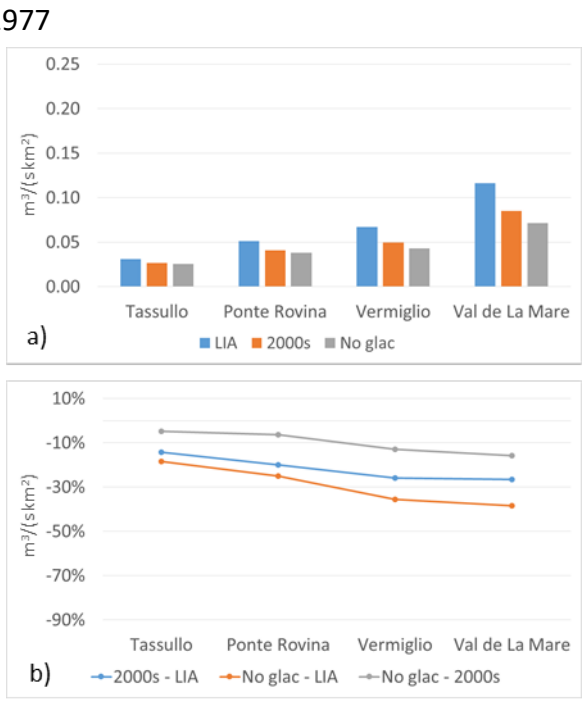


*Figure 64: Scale effect on the 10$^{th}$-percentile monthly unit discharge in August from 1968 to 1977 ($m^3$ $s^{-1}$ $km^{-2}$). The second panel represents the percentage difference.*


*Figure 65: Scale effect on the annual unit discharge from 1968 to 1977 (mm $yr^{-1}$). The second panel represents the percentage difference.*

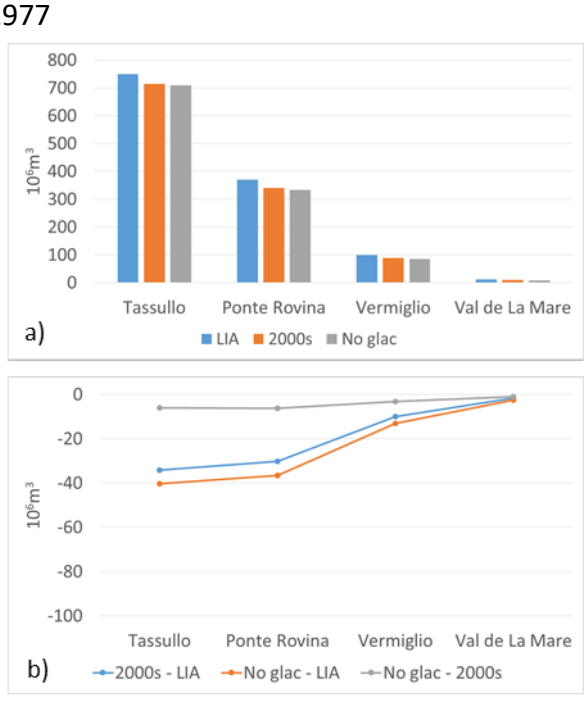


*Figure 66: Scale effect on the annual runoff from 1968 to 1977 ($10^6$ $m^3$). The second panel represents the difference.*

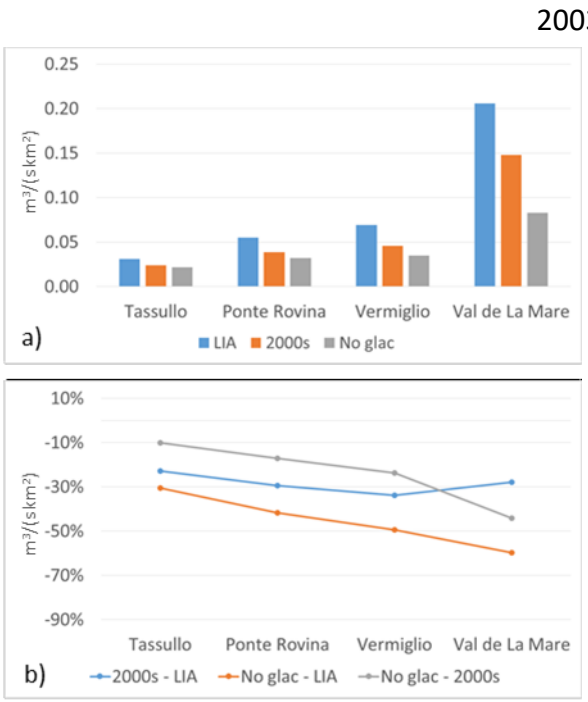


*Figure 67: Scale effect on the median monthly unit discharge in August from 2003 to 2012 ($m^3$ $s^{-1}$ $km^{-2}$). The second panel represents the percentage difference.*

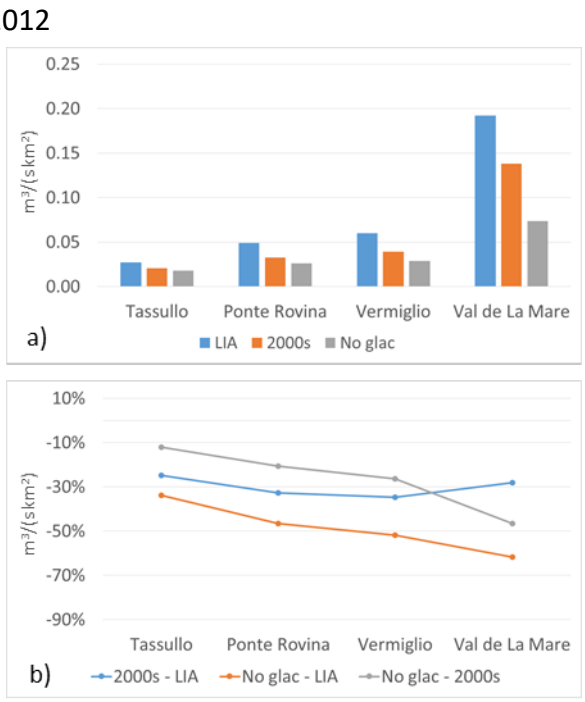


*Figure 68: Scale effect on the 10$^{th}$-percentile monthly unit discharge in August from 2003 to 2012 ($m^3$ $s^{-1}$ $km^{-2}$). The second panel represents the percentage difference.*


*Figure 69: Scale effect on the annual unit discharge from 2003 to 2012 (mm $yr^{-1}$). The second panel represents the percentage difference.*

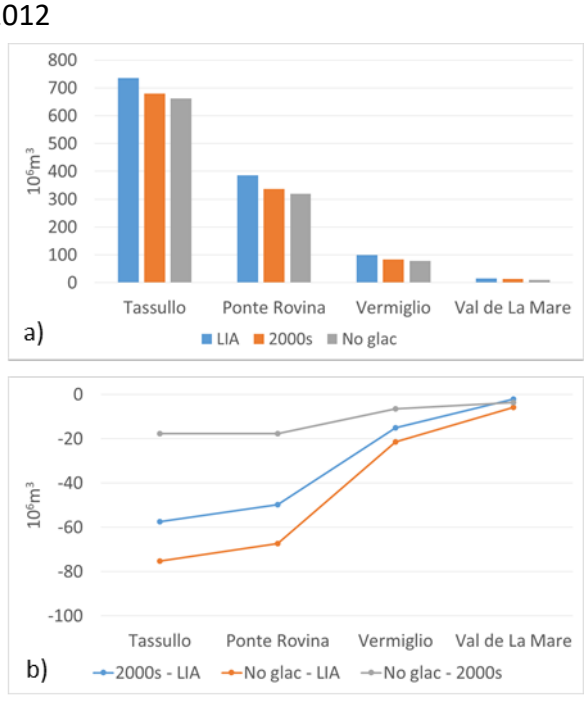


*Figure 70: Scale effect on the annual runoff from 2003 to 2012 ($10^6$ $m^3$). The second panel represents the difference.*

## 3.4. Specific case studies under extreme climatic conditions

We have analysed the two extreme hydrological years 2003 and 1968, in order to emphasize differences in the hydrological regime and response under different climatic conditions and glacier cover, and to understand possible impacts of future climatic drifts or extreme years. We took into account 2003 as an extreme year for high temperatures in summer and low winter precipitation, and 1968 as an extreme year especially for low temperature in summer. In Table 42 and Table 43, and from Figure 71 to Figure 73, we report the meteorological characteristics of the two extremely years and the comparison with the entire period from 1961 to 2010.

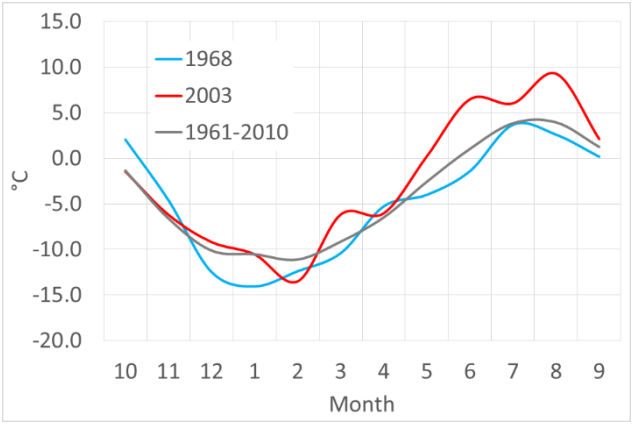


*Figure 71: Comparison of the average monthly temperature at the mean elevation of Val de La Mare catchment (2800 m a.s.l.) in the 1968 and 2003 hydrological years, and in the period from 1961 to 2010.*

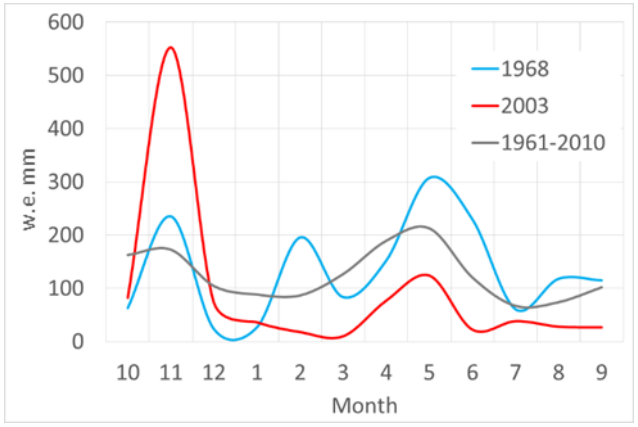


*Figure 72: Comparison of the sum of the monthly snowfall at the mean elevation of the Val de La Mare catchment (2800 m a.s.l.) in the 1968 and 2003 hydrological years, and in the period from 1961 to 2010.*

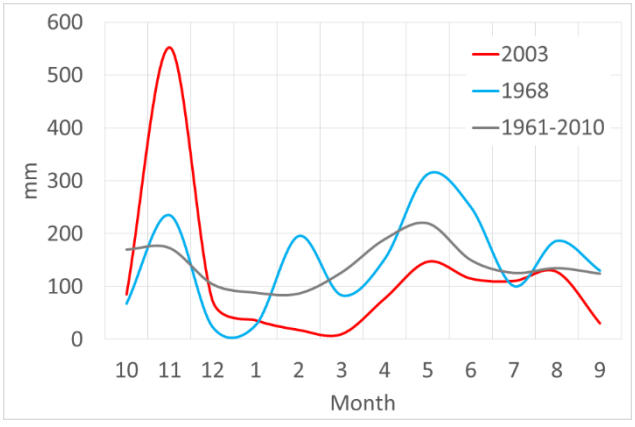


*Figure 73: Comparison of the sum of the monthly total precipitation at the mean elevation of the Val de La Mare catchment (2800 m a.s.l.) in the 1968 and 2003 hydrological years, and in the period from 1961 to 2010.*

*Table 42: Average temperature in 1968 and 2003 hydrological years and anomalies respect to the period from 1961 to 2010.*

| *Month* | *Temperature [°C]* | |
|---|---|---|
| (from - to) | 1968 | 2003 |
| 10 - 04 | -8.1 (- 0.3) | -7.5 (+ 0.4) |
| 05 - 09 | 0.2 (- 1.3) | 4.8 (+ 3.3) |

*Table 43: Cumulated snowfall, rainfall and total precipitation in 1968 and 2003 hydrological years and anomalies respect to the period from 1961 to 2010.*

| *Month* | *Snowfall [we mm]* | | *Rainfall [mm]* | | *Total precipitation [mm]* | |
|---|---|---|---|---|---|---|
| (from - to) | 1968 | 2003 | 1968 | 2003 | 1968 | 2003 |
| 10 - 04 | 711 (-18 %) | 780 (-9 %) | 5 (-42 %) | 3 (-62 %) | 715 (-18 %) | 783 (-10 %) |
| 05 - 09 | 781 (+48 %) | 190 (-64 %) | 151 (-16 %) | 291 (+63 %) | 932 (+32 )% | 481 (-32 %) |

In these years the mass balance measurements available for the Careser glacier confirm very unusual and opposite behaviour. 1968 was a positive mass balance year (+247 mm w.e.), characterized by a very low summer ablation (summer balance = -541 mm w.e.) and uncommon positive summer balance above 3200 mm. In contrast, 2003 was a very negative mass balance year (-3317 mm w.e.), led by an unusually warm summer (summer balance = -4338 mm w.e., Carturan et al., 2013).

### *3.4.a. The 2003 hydrological year*

The LIA glacier cover would have ensured high runoff in the warmest part of the 2003 summer season. In August, the runoff would have been comparable to early summer for the three larger catchments, and nearly double in Val de La Mare, due to enhanced glacier melt. A secondary peak is evident in the Ponte Rovina catchment in August (Figure 74 and Figure 75). Interesting, analyzing the daily runoff of Vermiglio in August, we can recognize an opposite behaviour from the scenarios (Figure 74), due to glacier melt. Interestingly, the daily runoff on the Vermiglio catchment under the LIA glacier cover shows an increase in the first half of August, whereas the 2000s and the no glacier scenarios show a continuous decrease in runoff, started in July. We can recognize this behaviour also in the other two larger catchments, even if reduced.
The difference between LIA and absent glacier cover is astonishing, as well as the difference between LIA and current glacier cover. Differences among the glacier cover scenarios are largest between July and August, but the period with significant water shortage with current glaciers and no glaciers spans across five months, from May to September (Figure 74 and Figure 75). LIA glaciers but also current glaciers lead to much higher runoff in mid- to late-summer, and this is observable in all catchments, also in the larger ones.

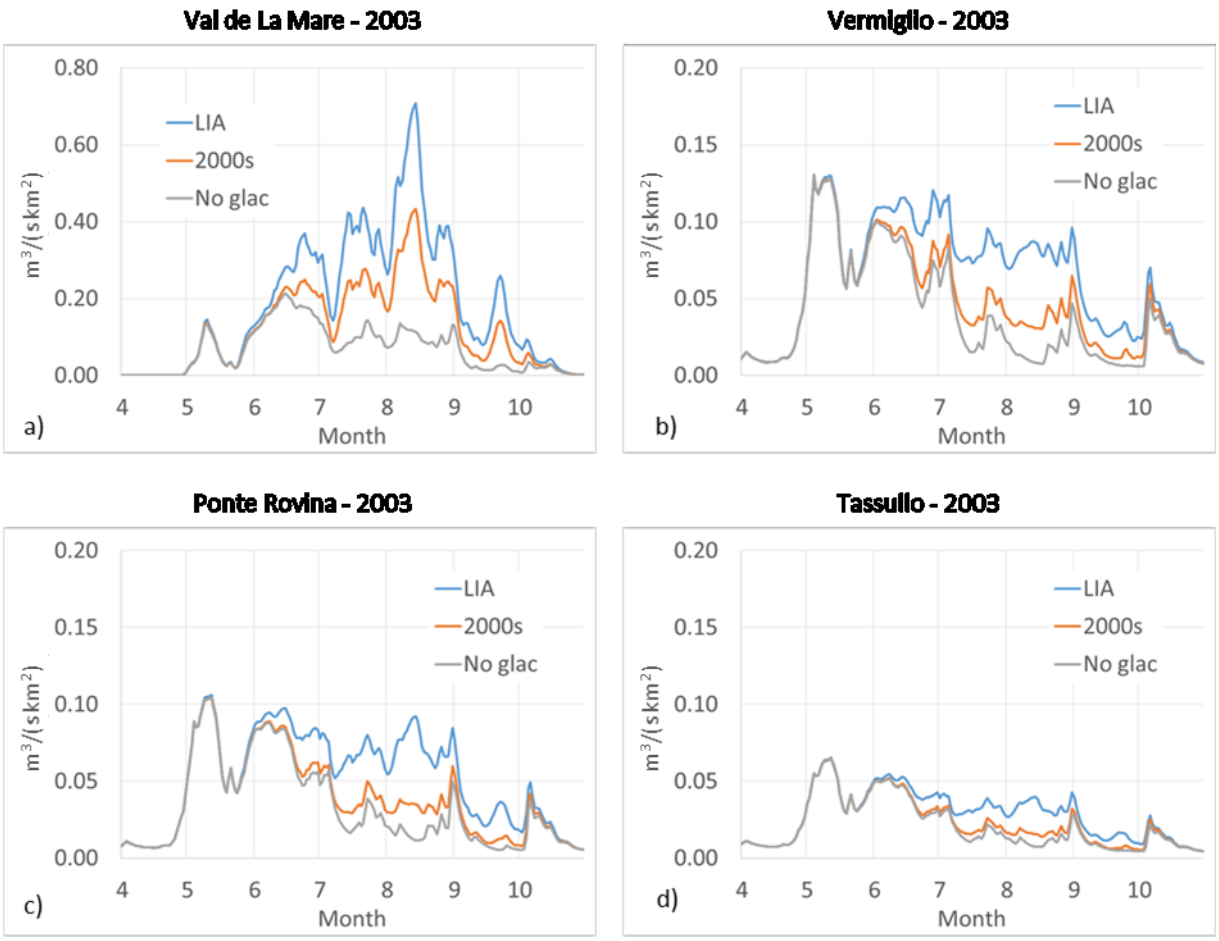


*Figure 74: Daily average unit discharge (from April to October) for different glacier cover extensions and related topography in 2003. Please, note that for the Val de La Mare we have used a different vertical scale.*

It is very interesting to note that in 2003, and in particular in the month of August, the current glaciers ensure much higher runoff compared to the no glacier scenario, and this difference is up to 3 times larger if compared to the 2003-2012 average conditions (Figure 50 to Figure 53). This increase is higher for the larger basins, while it is only 50% in the smaller basin. (Figure 75 e and h). This highlights the importance of current glaciers, which even though they have small residual impacts (compared to the LIA glaciers) on late summer runoff under 'normal' conditions, they still play a significant role under excessive warm and dry conditions. In conditions similar to August 2003 they ensure 30-60% higher mean runoff, and 50-80% higher minimum runoff, compared to deglacierized catchments. The upper values are referred to the smaller catchments, with higher percent glacier cover. The lower values are obtained on the larger catchments, but they are not negligible, in particular for minimum runoff (Figure 76 and Figure 77).

Interestingly, considering the impact on the management of water resources, we have calculated that in August the LIA glaciers ensured 60 $10^6$ $m^3$ higher runoff respect to an absence of ice cover. On the other hand, current glaciers still ensure 15 $10^6$ $m^3$ higher runoff respect to no glacier scenario (Figure 76 e).

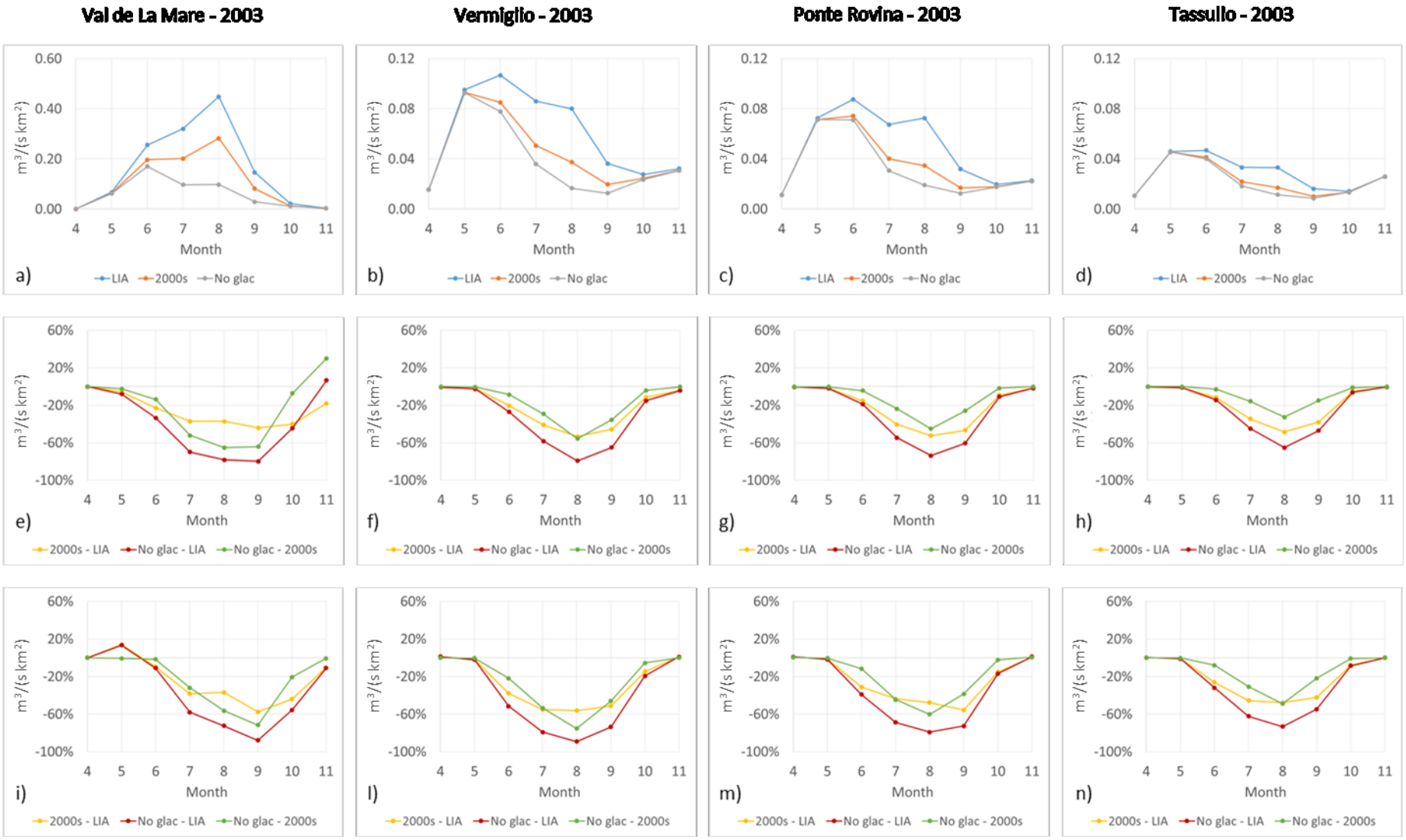


*Figure 75: Monthly unit discharge (from April to November) for different glacier cover extensions and related topography in 2003: a) to d) average monthly unit discharge, e) to h) percent difference in the average unit discharge and i) to n) percent difference in the minimum unit discharge. Please, note that for the Val de La Mare (a) we have used a different vertical scale.*

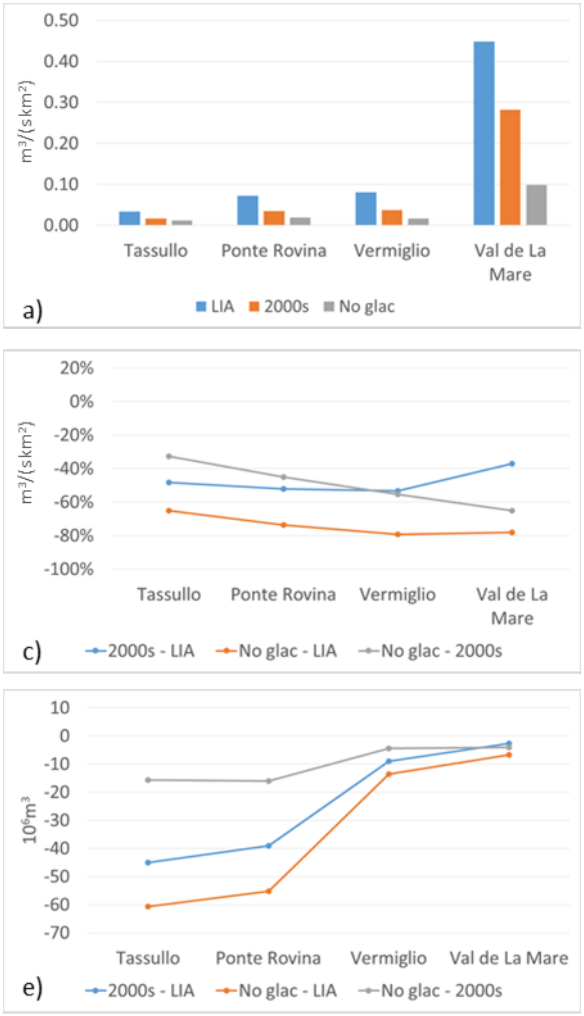


*Figure 76: a) Scale effect on the average monthly unit discharge in August 2003 ($m^3\ s^{-1}\ km^{-2}$), c) percent difference in the average unit discharge, and e) volumetric difference.*

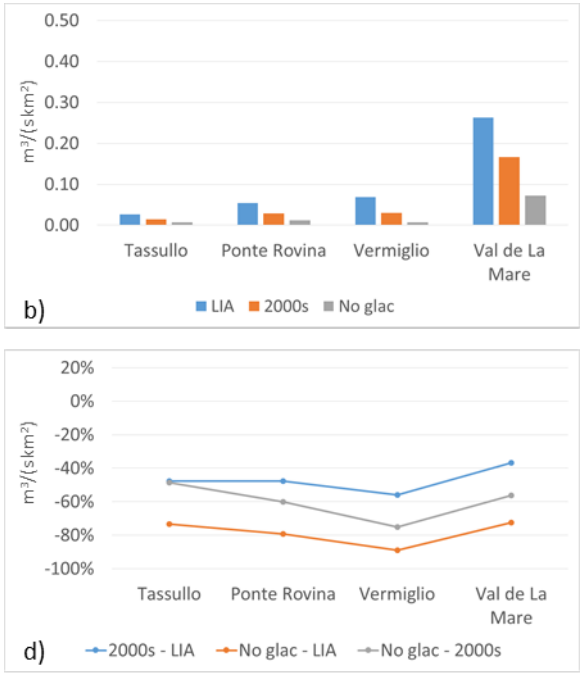


*Figure 77: b) Scale effect on the minimum monthly unit discharge in August 2003 ($m^3\ s^{-1}\ km^{-2}$), d) percent difference in the average unit discharge.*

### 3.4.b. The 1968 hydrological year

Under cool and wet summer conditions, like in 1968, there is little if no difference between the runoff from 2000s glacier cover and from deglacierized catchments (Figure 79 to Figure 81). This difference, in the Vermiglio and Val de La Mare catchments hardly reaches 10% for average and 20% for minimum August runoff (Figure 80 and Figure 81). As in 2003 hydrological year, we have calculated the higher differences in runoff comparing the LIA scenario with no glaciers scenario. These difference decrease from smaller to larger catchments, and reach 15-35% for mean August runoff and 20-45% for minimum August runoff (Figure 80 c and Figure 81 d).

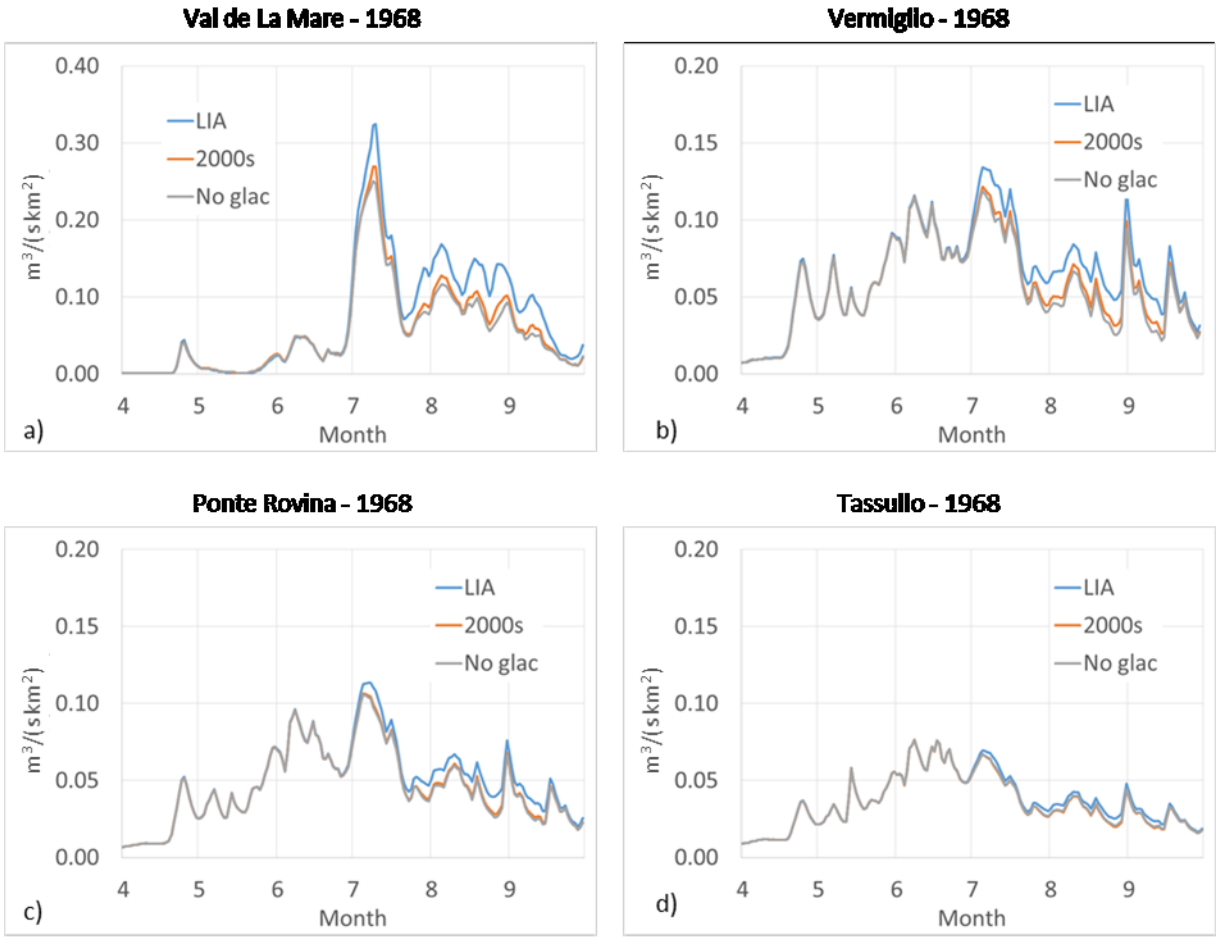


*Figure 78: Daily average unit discharge (from April to September) for different glacier cover extensions and related topography in 1968. Please, note that for the Val de La Mare we have used a different vertical scale.*

Differently from 2003, considering the monthly scale, we do not recognize a unique month where the differences among the scenarios get the maximum absolute value. Except for Val de La Mare, the behaviour of the average difference is on average constant, with two minimum values at August and October (Figure 79 f, g and h). About the minimum monthly difference, the relationship among the scenarios is similar to the average monthly differences. On the other hand, analyzing Val de La Mare catchment, the differences on average and minimum value increase until October with a maximum negative value. In October, current glaciers ensure 25% higher average runoff and 40% higher minimum runoff respect to an absence of glacier cover (Figure 79 e and i).

These results can be explained by the persistent snow cover under 1968 climatic conditions, with limited or null additional runoff from 2000s glaciers, which would have been covered by snow for most part of the ablation season and in most of their area. Only the larger and lower-reaching LIA glaciers would have lost the snow cover in their ablation area, this contributing with additional runoff during summer, and in particular in the second half of it.

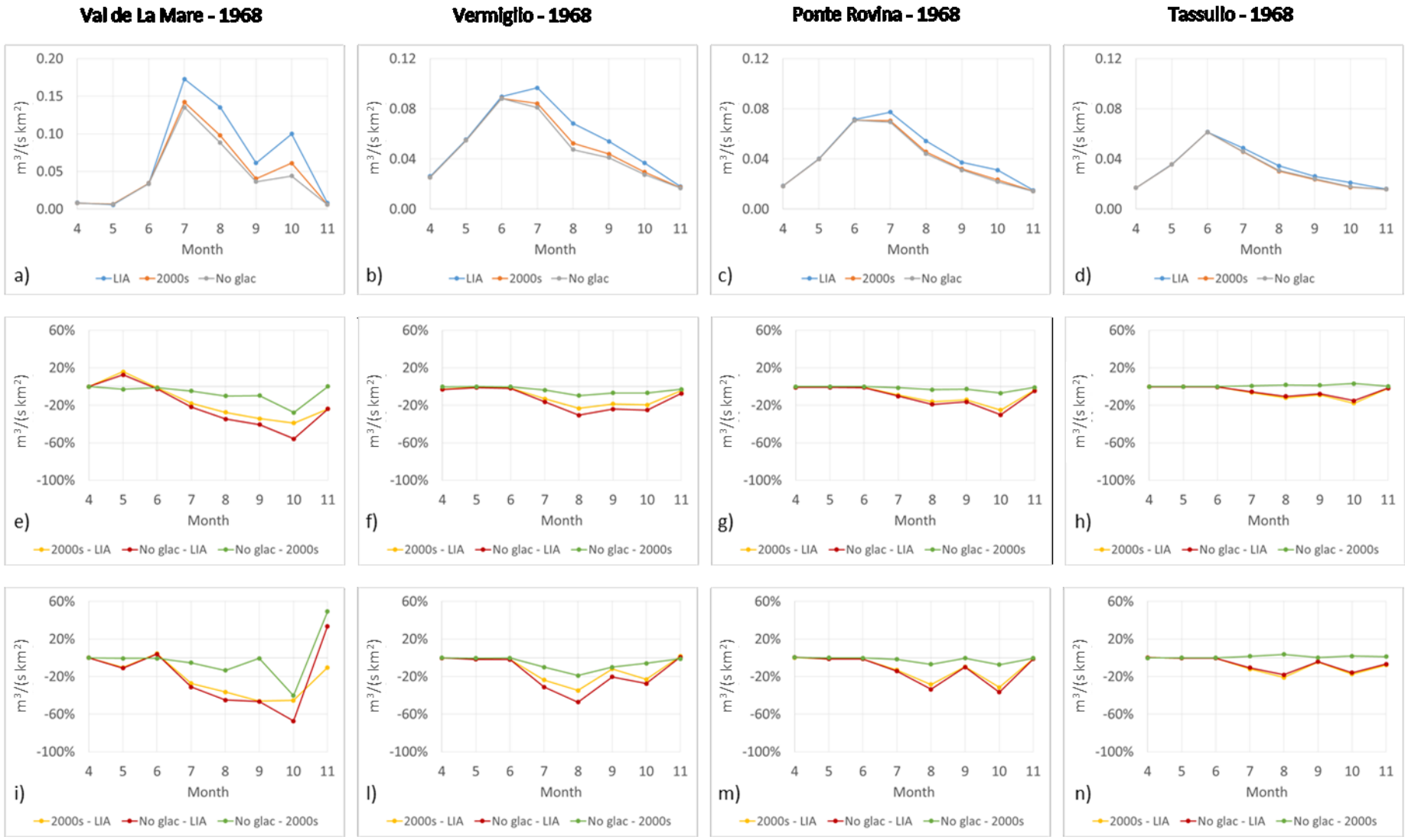


*Figure 79: Monthly unit discharge (from April to November) for different glacier cover extensions and related topography in 1968: a) to d) average monthly unit discharge, e) to h) percent difference in the average unit discharge and i) to n) percent difference in the minimum unit discharge. Please, note that for the Val de La Mare (a) we have used a different vertical scale.*

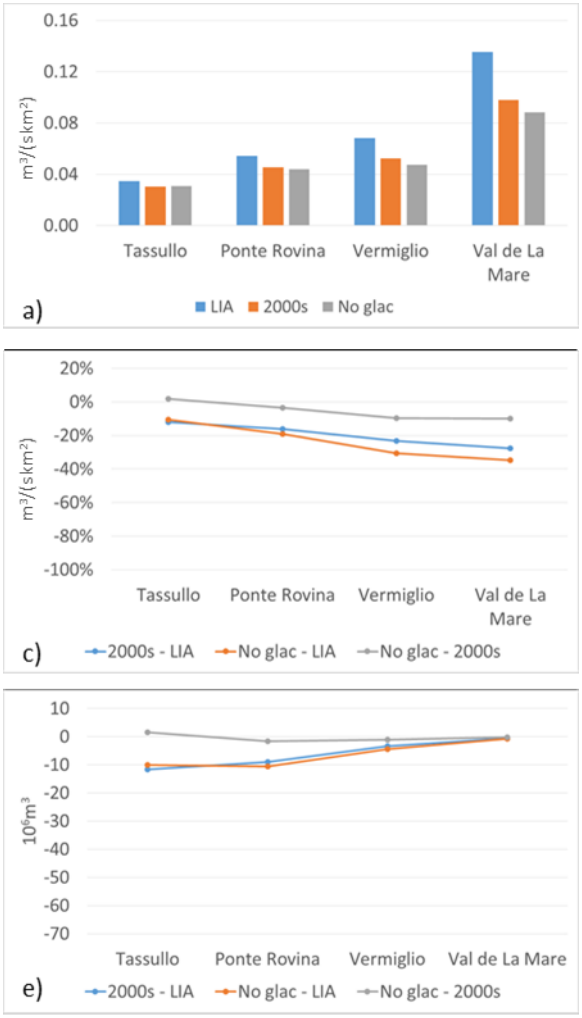


*Figure 80: a) Scale effect on the average monthly unit discharge in August 1968 ($m^3\ s^{-1}\ km^{-2}$), c) percent difference in the average unit discharge, and e) volumetric difference.*

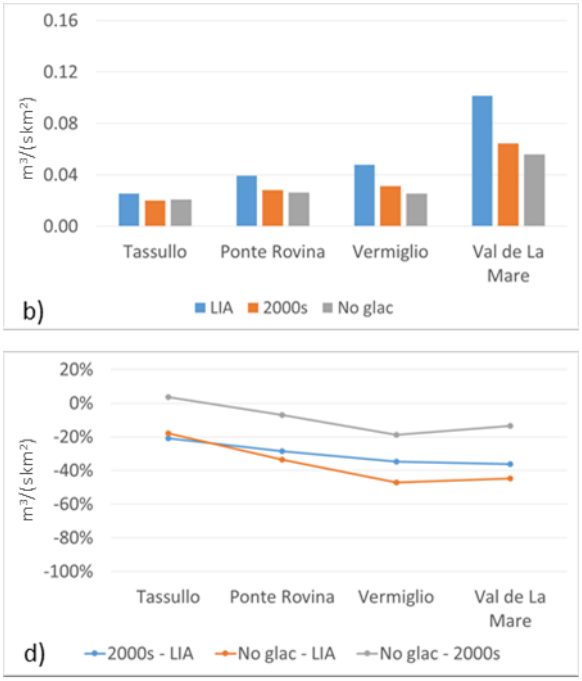


*Figure 81: b) Scale effect on the minimum monthly unit discharge in August 1968 ($m^3\ s^{-1}\ km^{-2}$), d) percent difference in the average unit discharge.*

# 4. Discussion

In this chapter we provide a discussion on both the methodological aspects and the results of this work.

The methodology was intended to fully exploit the rare dataset of historical hydro-meteorological data, glacier mass balance observations, and reconstruction of past glacier extent available in the study area. This information represents a solid base that has been essential for reliable glacio-hydrological modelling. However, there are several points in the methodology that require a discussion.

The results are based on observations in the past, rather than future projections. This is a strong and characterizing point of this work, which is different from approaches based on modelled future scenarios of climate and glacierization (e.g. Huss, 2011; Farinotti et al., 2012; Majone et al., 2016; Farinotti et al., 2016 ). This choice was dictated by the availability of historical data and by considerations on the large uncertainties affecting future runoff projections from glacierized catchments (Machguth et al., 2008; Huss, 2011; Huss et al., 2014). It is therefore interesting to discuss the results in view of other studies based on different methodologies, and in particular the possible implications for future water availability.

## 4.1. Methodological considerations

The use of past available observations provided the opportunity of analyzing the sensitivity of the glacio-hydrological system of the Val di Sole, under rather different climatic and glacier conditions. Assessing the sensitivity based on past observations, instead of future projections, is likely to reduce the main source of error of modelling approaches based on future climatic scenarios, whose prediction still show a considerable uncertainty (e.g. Kjellström et al., 2011). Past climatic observations, however, are not free from problems. In particular, they are subject to inhomogeneities in the observation procedures and instrumentation, and measurement errors.

We focused on implementation of a solid experimental basis for glacio-hydrological modelling, given the importance of the input data and the central role of the measured meteorological conditions in our research. The homogenization technique adopted in this work was primarily intended to preserve as much as possible the original data available for the weather stations of the Val di sole. For this reason, we avoided using precipitation data from outside the study area to homogenize the raw series, taking in consideration the high spatial variability of precipitation fields in mountain areas. In addition, we avoided correcting smaller inhomogeneities in temperature and precipitation, because such corrections would have deeply affected some inputs data used in the glacio-hydrological model. We refer in particular to the effects that a constant shift in temperature could have in the solid vs. liquid partitioning of precipitation (and amplification effects from successive application of snow correction factors). Inhomogeneities in temperature measurements are indeed expected to be larger under stable weather conditions (high radiation, low wind speed), instead of during

precipitation events. Therefore, applying a fixed correction to inhomogeneous periods in temperature series is expected to have a higher impact (excessive correction) during precipitation events, which in our opinion deserves further investigations and the possible implementation of a correction procedure that accounts for these effects.

As demonstrated by various studies, the precipitation data require a correction factor to account for gauge undercatch errors (Sevruk and Zahlavova, 1994; Carturan et al., 2012) which are significant in case of solid precipitation and high wind speed. We used direct observation of snow depth and fresh snow, and a classification of gauge site exposure to wind, for calculating snow- and rain correction factors to be applied at the weather stations of the Val di Sole. This procedure is described in Carturan et al., (2012), where the authors tested the results against glacier winter balance measurements. They found that the correction procedure is reliable, and that precipitation correction is mandatory before model implementation and calibration.

Various assumptions have been made concerning the meteorological data used in this study, and how they were pre-processed before applying the glacio-hydrological model. These assumptions mainly regard the constancy in time of precipitation correction factors and of vertical gradients of temperature and precipitation. Precipitation correction factors are likely different for different instruments and prevailing meteorological conditions during precipitation events. These differences should be higher at high altitude, were the fraction of solid precipitation and the wind speed are larger. Carturan (2010) and Carturan et al. (2012) investigated this problem at the high-altitude weather station of the Careser diga (2605 m), finding negligible difference in precipitation correction factors between the old manual rain gauge, used until 1991, and the new tipping-bucket automatic heated rain gauge, in use since then. No information exist for other rain gauges of the Val di Sole, but given the smaller undercatch of precipitation at lower altitude, we think that the assumption of unchanged correction factors between the old manual instruments and the new automatic ones is reasonable.

Precipitation and temperature vertical gradients exhibit a significant variability in space and time (Basist et al., 1994). In our work, the horizontal gradients of precipitation are accounted for using a spatial interpolation procedure that we have optimized in the glacio-hydrological model, whereas the horizontal variability of temperature has been neglected. The second mainly derives from complex processes like, for example, the valley winds, warm and cold advection, local adiabatic heating, warming or cooling of different surfaces, which are highly complex and difficult to model. The glacier cooling effect is a dominant factor of temperature variability, with relevant implications for glacier sensitivity to climatic changes over a long period of time (Greuell and Böhm 1998; Carturan et al., 2015). However, its implementation in EISModel is still in development and would have required further testing. For this reason, and because we have decided to focus on time windows with unchanged glacier extent, the glacier cooling effect has been excluded from processes modelled in EISModel.

Monthly vertical gradients in temperature and precipitation were calculated in periods with overlapping data from available weather stations located at different elevation: from 1940 to 1984 for precipitation, and from 2003 to 2014 for temperature. In absence of data from the same stations outside these periods, we have calculated a mean annual regime for

temperature and precipitation vertical gradients, applying it unchanged in all the modelled time windows. This simplification, that does not consider the inter-annual variability of vertical gradients, was imposed by the availability of meteorological data.

Gap filling procedure for precipitation data was based on the correlation among different weather stations. The choice of using the ratio between cumulated precipitation, instead of applying interpolation techniques such as the commonly-used IDW, was dictated by practical and logical reasons. In particular, the technique used in this thesis enables to account for vertical precipitation gradients, and at the same time it avoids circular reasoning and calculation, because the IDW algorithm is already applied by the glacio-hydrological model for the spatialisation of input precipitation data.

Considerations similar to those related to future climatic conditions can be done also for the future extent of glaciers. As their behaviour will be determined by the future evolution of climate, which is uncertain, and because there are several regulating processes and feedbacks that still require improved understanding, the modelling of glaciers in the next decades is prone to large errors. Available reconstructions of glacier extent and topography for the glaciers in Val di Sole in the last century, encompassing periods with different climatic conditions, enabled to investigate the hydrological response using constraints from actual measurements of glacier change, meteorological variables and runoff at different spatial scales.

While the current extent and surface topography of glaciers are very well documented by recent LiDAR surveys, there are uncertainties in the reconstruction of glacier bedrock topographies (i.e., the no-glacier scenario) and of surface topographies for the Little Ice Age glacier extent. We have implemented a calculation procedure that exploits recent developments in glacier bedrock and surface topography semi-automatic reconstructions (Huss and Farinotti, 2012; Benn and Hulton, 2010), with specific adaptations that have been required for the glaciers of our study area. The adaptations were necessary because our glaciers are significantly different from the prevailing larger valley glacier where the original methods have been developed. This procedure provided satisfactory results and has to be considered a relevant ‘secondary’ outcome of this work. The error in our bedrock and ice surface calculations averages respectively 20% and 34% and is in line with results from Huss and Farinotti (2012). It still requires refinements, but in our opinion, it is a valuable tool that can be used for calculating past glacier surface topographies, whose reconstruction is useful for paleo-climatic and paleo-ELA determinations (e.g. Bate, 2008; Cossart, 2011) but is often carried out manually with large degrees of subjectivity.

One of the main issues of this work was finding information on glacier geometry as close as possible to the oldest meteorological and hydrometric data available in the study area (i.e. for the 1920s-1940s). We used the maximum Little Ice Age extent of glaciers, whose reconstruction by Zanoner et al., (2017) is based on the high-resolution mapping of geomorphological landforms (moraines, trimlines, etc.) and on the survey of documentary data for the Trentino. Other reconstructions for time periods closer to the 1920s-1940s exist only for two glaciers in the Val di Sole (Carturan et al., 2013; Carturan et al., 2014), due to the scarcity of documentation and of landforms associated with this period. In general, the reconstruction of glacier extent is much more reliable for the LIA maximum, compared to

more recent fluctuations in the late XIX Century or in the first half of the XX Century, due to the well preserved and widespread landforms left by the glaciers in that period.

However, assuming that in the 1920s-1940s the glacier extent was close to that of the LIA is allowable, if the objective is to inspect the hydrological behaviour of catchments in the study area. Indeed, based on available reconstructions (Carturan et al., 2013; Carturan et al., 2014), the La Mare and Careser glaciers were only 9-10% smaller in the 1920s-1930s compared to the maximum LIA extent. The choice of focusing on single decades, keeping unchanged the glacier extent during these periods, was done because continuous modelling of glacier dynamics and geometric adjustment was outside the aims of this work. Nevertheless, it would be interesting to make use of the full dataset of the Val di Sole for a continuous modelling of glaciers in the last century. This application would provide a closer insight into the behaviour of glaciers and their response to climatic changes, but in that case, we will have to implement modelling tools able to reproduce their dynamic adjustment.

The glacio-hydrological model that has been used in this work is a combination of a fully distributed model, for the simulation of snow and ice accumulation and ablation processes (EISModel - Cazorzi, 2009), coupled to a semi-distributed model for runoff routing (AHM). The choice of the modelling tools, and of the spatial domain to which they have been applied, was dictated by various factors. First, these models were available and in development at the Cryosphere and Hydrology Group of the University of Padova (Carturan et al., 2012). Thanks to Prof. Federico Cazorzi (University of Udine), these models were also available with a graphical user interface and complemented by other tools (some of them developed by Federico during this PhD) that made easier their use and the analysis of outputs, e.g. for calibration and validation. The spatial domain of applications was primarily dictated by the modelled processes. Because glacial processes typically show a high spatial variability, at the scale of tens of meters, they require sufficiently high spatial resolution to be taken into account with enough accuracy (Martin and Church, 2004; Hebeler and Purves, 2008; Michlmayr et al., 2008). This is even more true if investigations aim at capturing the high sensitivity of snow and ice to climatic fluctuations, as in this case. Hydrological processes also show high spatial variability, but commonly used approaches for modelling snow and ice hydrology in mountain catchments are conceptual and semi-distributed (e.g. Bergström, 1992; Norbiato et al., 2009; Konz and Seibert, 2010; Bellin et al., 2016 ). This is justifiable in this work with the fairly lower climatic sensitivity of the processes controlling runoff routing, compared to cryospheric processes, and in our case also by the availability of measurements to be used for constraining model parameters. In this work, the internal consistency of EISModel could be ensured by numerous measurements of snow and ice mass balance, at various spatial scales, but only outlet streamflow was available for constraining runoff routing. Further development of the modelling tools will be devoted to the implementation of some feedbacks in glacier response, as for example the glacier cooling effect (Greuell and Böhm 1998; Carturan et al., 2015), and the role of increasing debris cover.

## 4.2. Considerations on the results

Analysing the hydrological response of four catchments with different area and % glacierization, across different climatic periods and with three glacier cover conditions, enabled to obtain results that are mostly in line with previous studies, but also present interesting peculiarities.

The climatic conditions in the 1940s were similar to those in the 2000s. The analysed decades were similarly warm in summer, but winters were colder in the 1940s (Figure 82). The precipitation were also similarly distributed, with a pronounced minimum in winter and a maximum in spring, but the 2000s also display a sharp maximum in November and December, caused by the heavy precipitation of November 2002, November and December 2008 and November 2010. Considering the mass balance of glaciers, in the 2000s there have been compensating effects from higher precipitation in the accumulation season and higher temperature in the ablation season when compared to the 1940s.

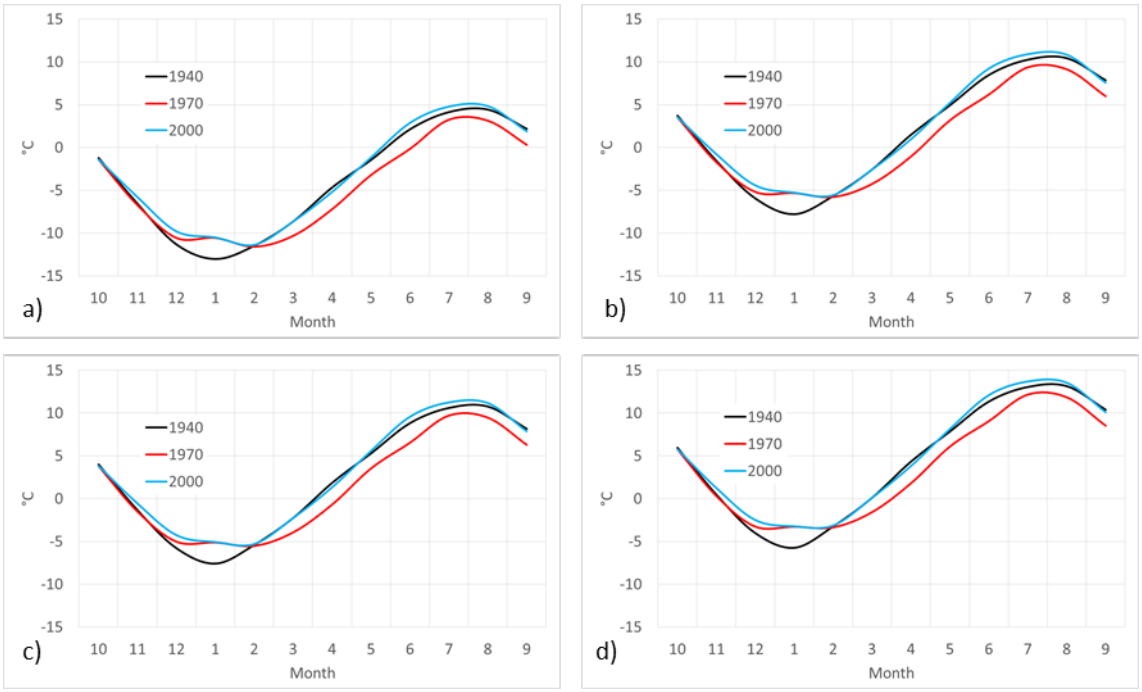


*Figure 82: Average monthly temperature at the mean catchment altitude in the 1940s, 1970s and 2000s for: a) Val de La Mare, b) Vermiglio, c) Ponte Rovina, d) Tassullo*

The climatic conditions of the 1970s were significantly different, and more favourable for glaciers (leading to their observed expansion between the 1970s and 1980s, Zanon, 1991). Temperature was ~2°C lower than in the 1940s and 2000s between March and September and similar to the 2000s in the other months. Precipitation was higher, in particular during winter and spring (Figure 85), and the solid fraction was also larger thanks to the lower temperature (Figure 83 and Figure 84). This is mostly visible for the ablation season, with important effects on the summer balance of glaciers, which greatly benefits from summer snowfall (Escher-Vetter and Siebers, 2007; Carturan et al., 2013).

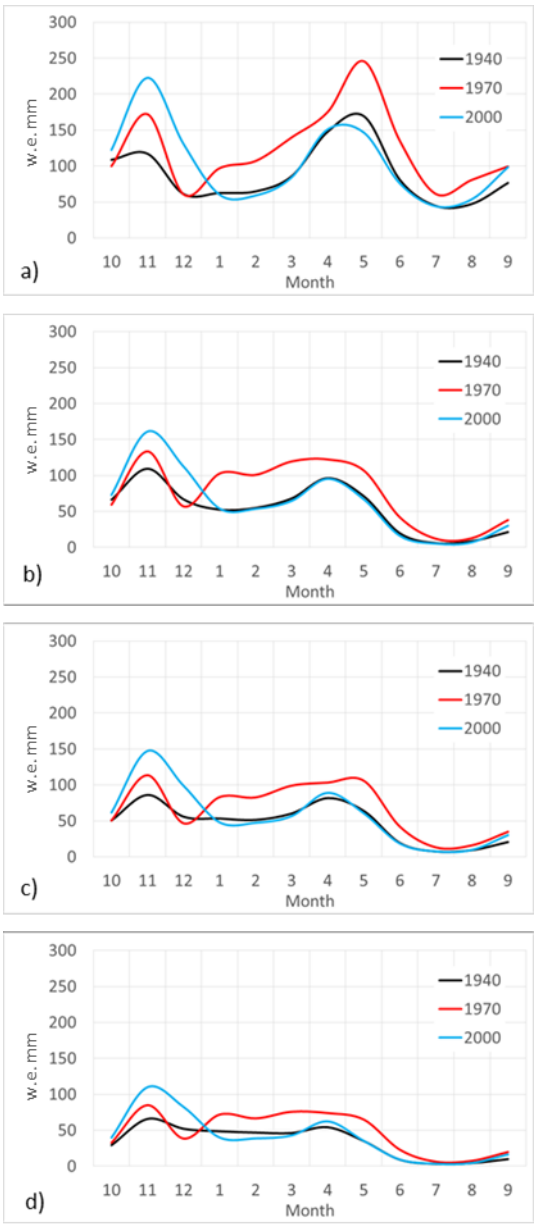


Figure 83: Monthly average precipitation at the mean catchment altitude for: a) Val de La Mare, b) Vermiglio, c) Ponte Rovina, d) Tassullo.

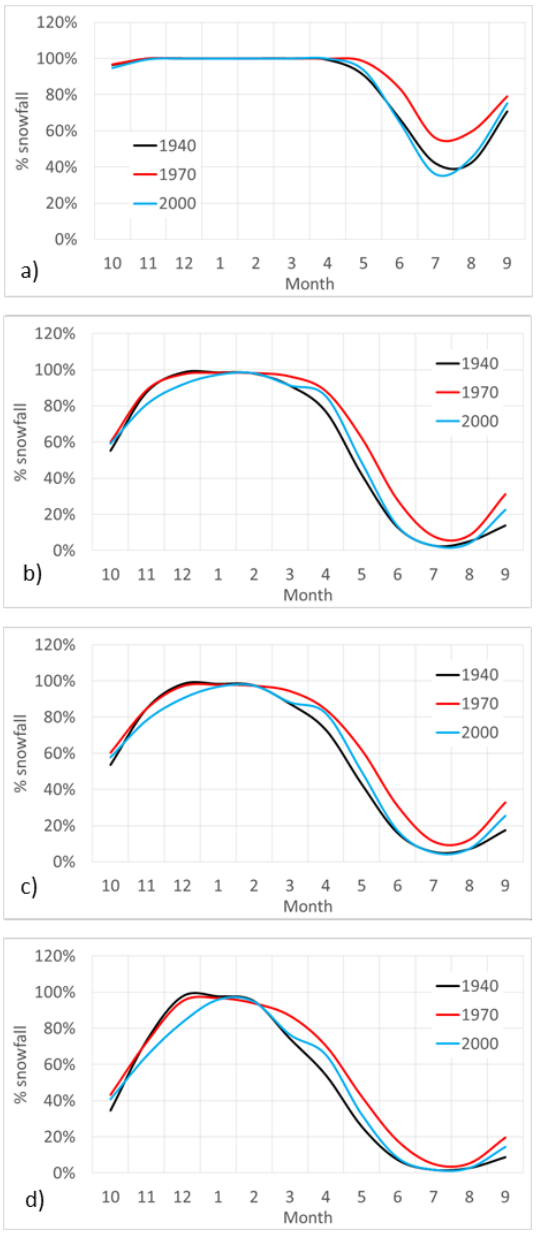


Figure 84: Monthly average solid fraction of precipitation at the mean catchment altitude for: a) Val de La Mare, b) Vermiglio, c) Ponte Rovina, d) Tassullo

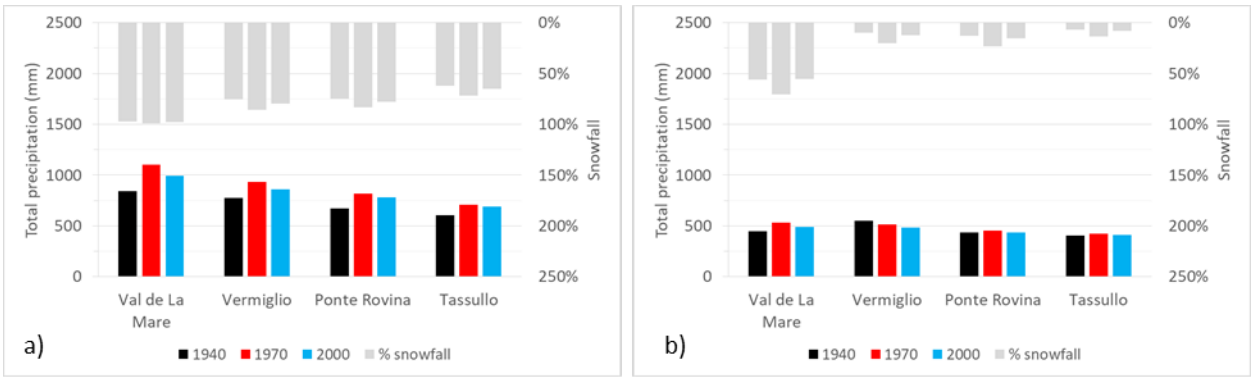


Figure 85: Seasonal average precipitation and solid fraction of precipitation. a) winter season (from October to May), b) summer season (from June to September).

The similarity between the 1940s and the 2000s is remarkable, as well as the particular conditions measured in the 1970s. This behaviour is likely affected by multi-decadal patterns of oceanic thermal anomalies, like the Atlantic Multidecadal Oscillation (AMO) and the Pacific Decadal Oscillation (PDO), further modulated by continental-scale circulation patterns such as the North Atlantic Oscillation (NAO) and the East Atlantic pattern (EA), which influence the temperature and precipitation distribution in winter and summer across Europe (Quadrelli et al, 2001; D'Aleo et al., 2010; Olafsdottir et al., 2013). Most of these patterns favoured positive glacier mass balance (i.e. positive storage) in the 1970s, and negative mass balance (i.e. negative storage) in the 1940s and 2000s.

These analogies/differences among the three periods are clearly visible in the hydrological response of the four analyzed catchments, under unchanged glacier cover (Figure 49). The 2000s and 1940s behave very similarly, and with distinct differences when compared to the 1970s. Smaller catchments with higher glacierized area fraction (%) are comparatively more affected by changes in glacier storage, while larger catchments are more affected by changes in the precipitation regime and seasonal snow accumulation/ablation (Huss, 2011). Climatic conditions during the 1970s are emblematic. There is significantly higher runoff in mid-summer during the 1970s, and differences increase from LIA to current to the absence of glaciers (Figure 49). Therefore these differences are not attributable to enhanced glacier runoff under 1970 climatic conditions (absence of glaciers would bring a higher decrease of runoff for 1970 climate, which is the contrary of observations), but to specific climatic characteristics of the 1970s. In particular, the larger snow accumulation from October to May (Figure 85) ensures sustained runoff from seasonal snow during summer, also in case of absence of glaciers.

Inspecting results obtained crossing three glacier cover scenarios and three different climatic periods reveals that there is a considerable change in the hydrological regime in the months from June to October, in response to decreasing glacier cover. This change consists mainly in a strong decrease of unit discharge after the seasonal snow is melt, in the second half of summer, with a maximum decrease in the month of August (from Figure 50 to Figure 53). There is also the tendency to an anticipation of the runoff peak from August to July in the smallest and most glacierized basin (Figure 50). In the 2000s the peak is in July also for the LIA glacier cover, due to the warmer spring temperature compared to the 1940s and 1970s, in combination to higher snow accumulation outside the glaciers in autumn and early winter (Figure 85). Variations in summer runoff among glacier cover conditions are much more evident for the 1940 and 2000 warm climatic periods, compared to the cooler 1970s.

These results confirm findings from previous works (e.g. Junghans et al., 2011) and suggest impacts of glacier retreat and climatic change for downstream catchments, not only for high mountain catchments but also for large basins with very small glacierization. According to the literature, also macroscale transboundary catchments, as for example the Po valley, benefit from glacier runoff during the second half of summer in a significant way. Even if they are far from glaciers, the runoff from glacier melt is relevant because in the plains the summer is much warmer and drier, with strong evapotranspiration. Huss, (2011), for example, demonstrated that glacier contribution to August, runoff at Pontelagoscuro and Piacenza reaches 15-20% on average, with peaks of 30% during warm and dry summers

like 2003. Our calculated glacier contribution in August (calculated as negative glaciers storage change from the water balance equation) ranges from 39% to 84% with the LIA glacier cover, and from 26% to 79% with the current glacier cover for the catchments of the Val di Sole (Figure 86), with % contributions that are inversely proportional to catchment area. For catchments with similar glacierization, Huss (2011) calculated glacier contributions in August ranging from 10% to 60%, but on catchment larger by 1-2 orders of magnitude.

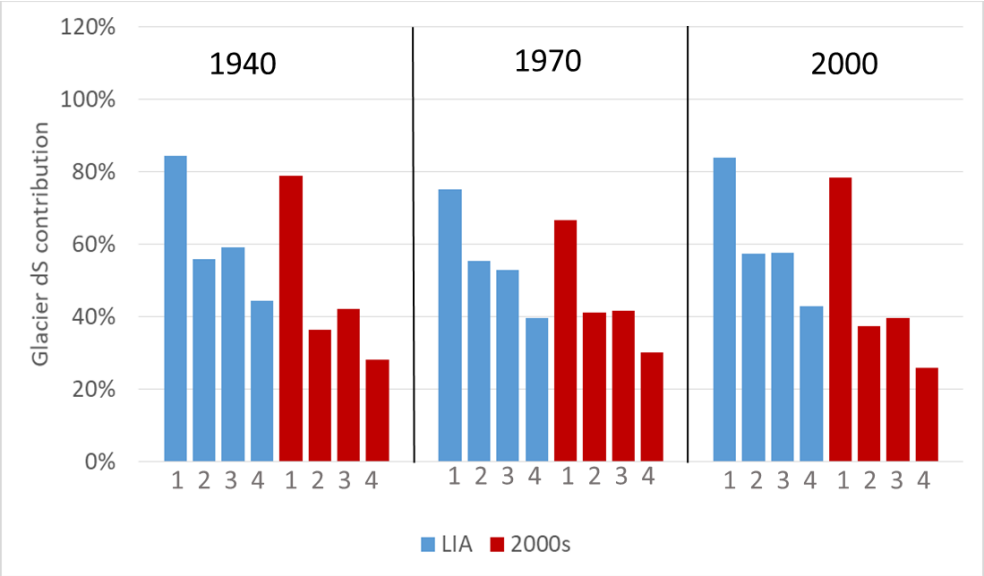


*Figure 86: Average glacier storage change contribution to August runoff in three meteorological periods. 1= Val de La Mare, 2= Vermiglio, 3 = Ponte Rovina, 4 = Tassullo.*

As can be seen, the decrease in glacier contribution with increasing catchment area is not linear. The largest decrease is observed between the smaller catchments, in our case between the Val de La Mare and Vermiglio basins, and becomes much slower for larger catchments. According to Huss, (2011), the importance of glacierization for streamflow runoff in August actually increases with drainage basin size, and in particular for macroscale drainage basins with the largest part consisting of low-lying plains, where precipitation is low and largely exceeded by evapotranspiration. Such effect is not visible in our larger catchment (Tassullo), because it is rather small and because the climatic conditions are comparable to those of smaller catchments in Val di Sole.

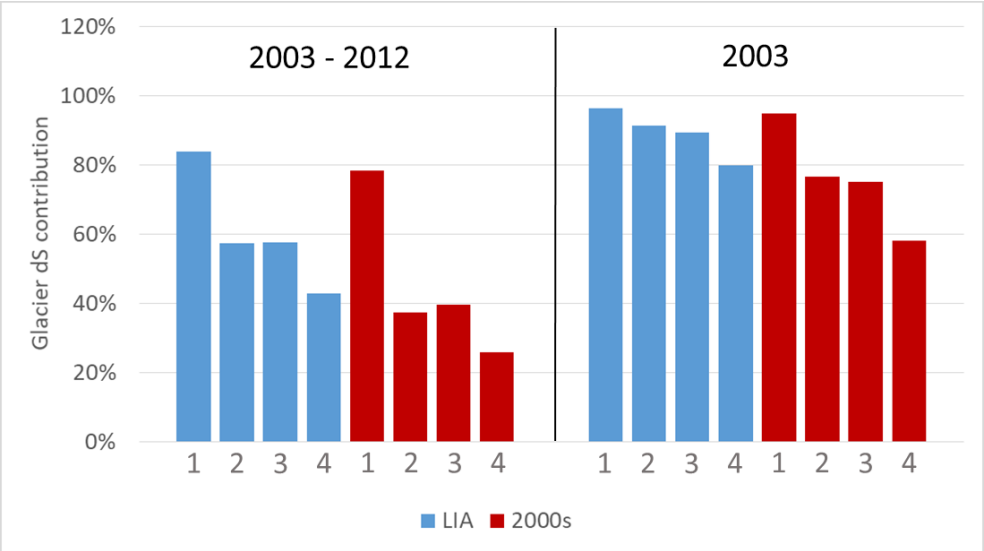


*Figure 87: Comparison of glacier storage change contribution to August runoff in average conditions for the 2000s and in the extreme August 2003. 1= Val de La Mare, 2= Vermiglio, 3 = Ponte Rovina, 4 = Tassullo.*

However, glacier contribution can strikingly increase during extreme conditions, like in summer 2003. Figure 87 shows that in August 2003 the % glacier contribution is nearly twofold for the three larger catchments analyzed, compared to average meteorological conditions in the 2000s, reaching 58% at Tassullo. The increase in the headwater catchment is of only 15% because it is already dominant in normal meteorological conditions. Based on these calculations, the impacts of glacier vanishing are expected to be important for the Val di Sole and Val di Non, in particular during warm/dry years like 2003, 2006, 2012 and 2015 (Figure 27 and Figure 28).

These results, and former glacio-hydrological experiments that use future modelled atmospheric warming scenarios (IPCC, 2007; van der Linden and Mitchell, 2009), indicate a strong decrease in the capability of glacierized catchments in damping the runoff fluctuations caused by precipitation variability. This decrease is related to the progressive melt out of residual ice masses but is preceded by a period of increased runoff derived from negative glacier storage change, with a peak expected between 2020-2040 (Jansson et al., 2003; Huss et al., 2008; Farinotti et al., 2012; ). It is therefore interesting to assess 'at which point is' our study area in this transition. To do that, we have quantified the residual damping effect (RDE) of current glacier coverage, compared to that of the LIA glacier coverage:

*Equation 51*

$$RDE = \frac{LIA\ DE}{2000s\ DE}$$

where $DE$ is the damping effect, calculated as:

*Equation 52*

$$DE = q_{gc} - q_{ga}$$

where, $q_{gc}$ is the unit discharge of August with the LIA or 2000s glacier cover, and $q_{ga}$ is the unit discharge of August in absence of glacier cover. Results are displayed in Figure 88 and show that in the smaller and most glacierized catchment the RDE is around 50%, whereas in the larger catchments it decreases with increasing area, from about 30% to about 25%. This means that three/quarter of the original damping effect during the LIA are already vanished from the study area, and only in headwater catchments it still reaches half of the original value.

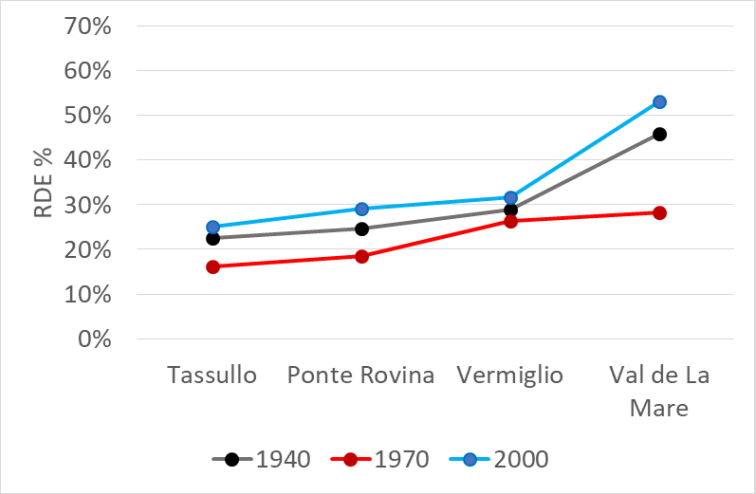


*Figure 88: Residual damping effect of current glaciers, compared to LIA glaciers, in three different meteorological periods and in four different catchments.*

The summer 2003 has been frequently referred to as a possible example of future climatic conditions during summer in the Alps, under sustained $CO_2$ emissions scenarios (Beniston and Stephenson, 2004; Schär et al., 2004). Therefore it is interesting to compare the runoff in August with the meteorological conditions of 2003 with the runoff under 'normal' conditions during the 2000s, with different glacier cover. This analysis should reveal if the peak in runoff due to glacier wastage still has to come or has already passed in the study area.

*Table 44: Comparison of mean unit discharge in August between the average conditions of the 2003-2012 decade and the extreme conditions in 2003. The cases where the 2003 unit discharge is higher than average 2003-2012 conditions are highlighted in red.*

| | LIA glacier cover | | 2000s glacier cover | | No glacier cover | |
|---|---|---|---|---|---|---|
| *Catchments* | *2003-2012* | *2003* | *2003-2012* | *2003* | *2003-2012* | *2003* |
| Val de La Mare | 0.206 | 0.448 | 0.148 | 0.282 | 0.083 | 0.098 |
| Vermiglio | 0.069 | 0.080 | 0.046 | 0.037 | 0.035 | 0.017 |
| Ponte Rovina | 0.055 | 0.073 | 0.039 | 0.035 | 0.032 | 0.019 |
| Tassullo | 0.031 | 0.033 | 0.024 | 0.017 | 0.021 | 0.012 |

The LIA glaciers would have ensured higher unit runoff on all four analysed basins in August 2003, compared to average 2000s meteorological conditions (Table 44). In contrast, the current glacier cover enables increased unit runoff only in Val de La Mare. These results are not conclusive because a complete assessment would have required continuous modelling of climate, glacier mass balance, glacier dynamics and geometric adjustments, and runoff,

for a sufficiently long time period, spanning the latest decades and the next two or three decades. However, the values displayed in Table 44 strongly suggest that the peak in late-summer runoff due to glacier wastage has already passed in Val di Sole, with the exception of few glacierized headwater catchments. Koboltschnig and Schöner, (2011), came to similar results, finding that only Austrian catchments with glacierization larger than 10% were able to provide larger runoff in August 2003, compared to mean long-term August runoff.
This result is a consequence of the prevailing characteristics of the glaciers in Val di Sole, which are generally small, and with low residual thickness and volume, and much less low elevation reaching compared to the LIA (Figure 89 and Figure 90). Several works in the recent literature agree with our observations and indicate that the peak in runoff under warming scenarios are expected earlier for catchments with lower initial glacierization and smaller/thinner glaciers (e.g. Collins, 2008; Huss et al., 2008; Farinotti et al., 2012). Therefore, additional runoff from melting ice surfaces during warm and dry summers is already smaller than the runoff decrease from lowering precipitation, earlier melt of the seasonal snow, and enhanced evapotranspiration. It is interesting to note that, also without glaciers, there is a small increase in unit runoff during August 2003 in Val de La Mare. This increase is brought by the melt of snow accumulated at high altitude in previous years (impending formation of small glaciers with model initialization in 1997). However, this marginal increase in unit runoff and the formation of small glaciers is observed when 2003 represents an exceptionally warm summer, and are unlikely to occur in a climatic scenario with average conditions similar to 2003.

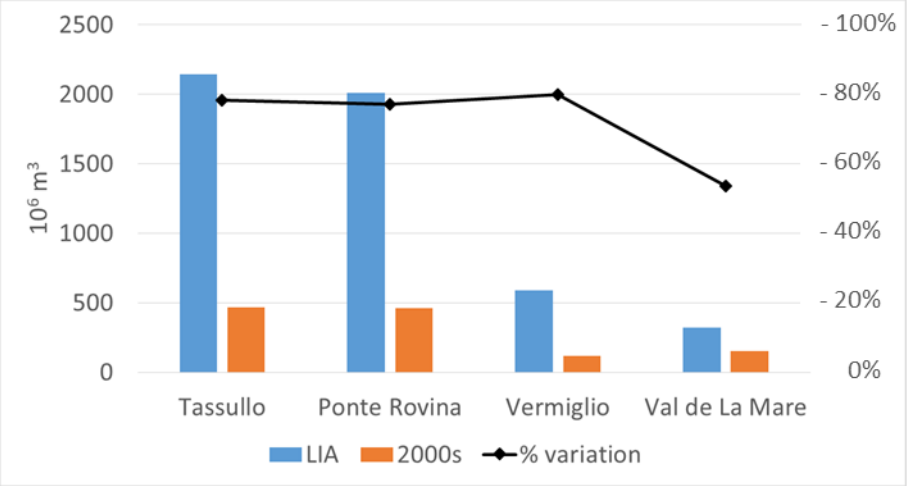


*Figure 89: Glacier volume and percent variation from LIA to 2000s.*

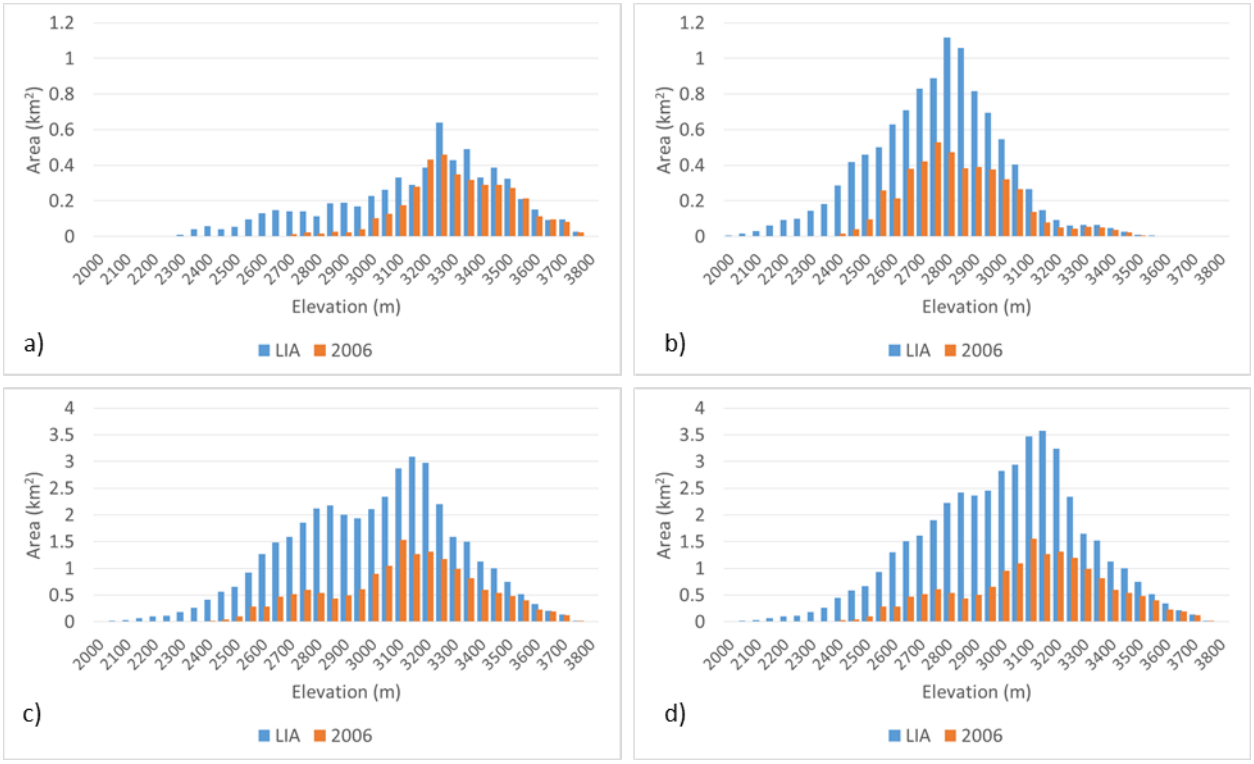


*Figure 90: The frequency distribution of glacierized area elevation bands. a) Val de La Mare, b) Vermiglio, c) Ponte Rovina, d) Tassullo. Please, note that for the Val de La Mare and Vermiglio we have used a different vertical scale.*

# 5. Conclusion

In this study we have analysed the hydrological sensitivity of four glacierized catchments located in the north-western Trentino (Eastern Italian Alps), with different area and percent glacierization, under different climatic conditions and with three glacier cover scenarios. Investigations were carried out using a glacio-hydrological model that combines the EISModel, a fully-distributed model that simulates the mass balance of snow and glaciers, and the AHM, a conceptual semi-distributed hydrological model that is used for runoff routing. The analyses were carried out on the basis of past glacier cover and meteorological observations, rather than using future projections of climate and glacier dynamics. This has the advantage of reducing the errors stemming from future predictions of climatic conditions and glacier response, but has the drawback of neglecting possible extreme future conditions, outside the range of variability given by observations in the XX and XXI centuries. To partly compensate for this, we investigated the hydrological response of the catchments with a complete absence of glaciers (calculating the shape of the bedrock underneath current glaciers), and in recent extreme years, like 2003.

The study reveals that a progressive transition from a glacial regime to a nival regime is under way in the analyzed catchments, caused by the shrinking of glaciers in response to warming climate. With smaller glaciers (as mapped in 2006) and warmer meteorological conditions (average conditions from 2003 to 2012), the runoff is strongly decreased after the seasonal snow has melted, in the second half of summer, compared to results obtained using the LIA glacier scenario. The runoff peak tends to shift from mid- to early summer, and this tendency is more evident in the headwater catchments.

Different glacier cover scenarios (LIA, current and absence of glaciers) present the highest difference in hydrological response in the month of August runoff, and effects are more evident during periods of glacier wastage as in the 1940s and in the 2000s, and in the smaller catchments with high percent glacierization. The meteorological conditions in the 1940s and the 2000s look rather similar, with lower precipitation and higher temperature compared to the 1970s. Besides secular trends in climatic variables, and in particular in temperature, the similarity of the 1940s and 2000s that have been both extremely unfavourable for glacier preservations suggest interconnection with multi-decadal modes of atmosphere circulation and oceanic temperature anomalies (AMO, PDO, AO, EA, NAO).

Compared to the absence of glaciers, current glaciers still ensure higher runoff during summer, in all climatic conditions and basins considered, with significant contribution to late summer runoff also in the larger catchments. However, this glacier damping effect, i.e. the difference between late summer runoff with or without glacier cover, is largely decreased if compared to the LIA conditions. This decrease is larger for wider basins. If smaller and highly glacierized catchment still preserves ~50% of the initial damping effect in August, the larger catchments keep only 25-30% of it. In other words, the damping effect is already nearly vanished for catchments similar to the larger one analysed in this study, at least if meteorological conditions averaged over periods of ten years are considered. However, this effect is expected to be still relevant in extremely warm and dry conditions (like in 2003, 2015 and 2017), and according to Huss (2011), it does not decrease downstream. Actually,

for macroscale catchments extended at low altitude (e.g. the Po catchment), glacier percent contribution to runoff increases because of lower summer precipitation and higher evapotranspiration.

This behaviour is confirmed in our study area. The glacier contribution to late summer runoff decreases from headwater to lower and larger catchments. However, the decreasing rate tends to flatten for catchment area larger than 80-100 $km^2$, and for the larger analyzed catchment it still reaches 26%. It was interesting to observe, however, that the glacier contribution of current glaciers to late summer runoff reaches ~60% in the larger catchment, during the extremely warm and dry summer of 2003. This is a result of combined effects from enhanced glacier melt, lowered precipitation and increased evapotranspiration.

Future conditions of nearly complete deglacierization, combined with summer season conditions similar to 2003, would have strong impacts in the runoff of the study area. In our calculations, increased runoff due to glacier wastage in 2003 (compared to 2003-2012 average meteorological conditions) occurred only in the headwater and most glacierized catchment, whereas the LIA glacier cover would have ensured increased runoff in all analyzed catchments. This suggest that the expected peak in runoff under warming climate, attributable to glacier melt, has already passed in the largest part of the study area.

Without glacier cover we obtained a small increase in runoff only in the smallest catchment. This increase is brought by the melt of snow accumulated at high altitude in previous years, but is only possible when 2003 represents an exceptionally warm summer, whereas it is unlikely to occur if 2003 will represent ‘normal’ future climatic conditions.

The dataset implemented in this work would enable additional analyses, which were not carried out because outside the aim of this PhD. In particular, it would be interesting to do a continuous simulation of the glacio-hydrological system throughout the last century. This work has the potential of highlighting peculiar aspects in glacier response to climatic changes, and related hydrological effects. However, it will require the setup of routines for the simulation of glacier dynamics and year to year geometric adjustments. Moreover, there are some processes whose importance has been stressed by several works in literature, such as the glacier cooling effect and the debris cover dynamics, which significantly influence the behaviour of glaciers and consequent hydrological effects. Future work is required to parameterize these processes, understand their role in the glacio-hydrological response to climatic changes, and possibly incorporate them in a glacio-hydrological model.

# 6. References


- Adam J.C. and Lettenmaier D.P. (2003). Adjustment of global gridded precipitation for systematic bias. Journal of Geophysical gap
- Alexandersson H. (1986). A homogeneity test applied to precipitation data', J. Climate, 6, 661–675.
- Alexandersson H. and Moberg A. (1997). Homogenization of Swedish temperature data. Part I: A homogeneity test for linear trends', Int. J. Climatol., 17, 25–34.
- Anderson E.A. (1968). Development and testing of snow pack energy balance equations. Water Resour. Res., 4(1), 19–37
- Anderson E.A. (1973). National Weather Service River Forecast System – snow accumulation and ablation model. NOAA Tech. Mem. NWS HYDRO-17
- Arck M. And Escher-vetter H. (1997). Topoclimatological analysis of the reduction of the glaciers in the Zugspitz region, Bavaria. Zeitschrift für Gletscherkdunde und Glazialgeologie, 33, 57-71.
- Arendt A., Echelmeyer K., Harrison W. D., Lingle G., and Valentine V. (2002). Rapid wastage of Alaska Glaciers and their contribution to rising sea level. Science 297, 382–386
- Arnold N. S., Rees W. G., Hodson A. J. and Kohler J. (2006). Topographic controls on the surface energy balance of a high Arctic valley glacier. J. Geophys. Res., 111, F02011.
- Auer I. and 31 others. (2006). HISTALP – historical instrumental climatological surface time series of the Greater Alpine Region. Int. J. Climatol., 27(1), 17–46.
- Baltsavias E.P., Favey E., Bauder A., Bosch H., Pateraki M. (2001). Digital surface modelling by airborne laser scanning and digital photogrammetry for glacier monitoring. The Photogrammetric Record 17: 243 – 273.
- Barnett T.P., Aadam J.C. and Lettenmaier D.P. (2005). Potential impacts of a warming climate on water availability in snow-dominated regions. Nature,438(7066), 303-309.
- Barry R.G., (2006). The status of research on glaciers and global glacier recession: a review. Prog. Phys. Geog., 30, 3, 285-306.
- Basist, A., Bell G.D., and Meentemeyer V. (1994). Statistical relationships between topography and precipitation patterns. Journal of climate, 7(9), pp.1305-1315.
- Bate S. (2008). A reconstruction of equilibrium line altitudes of the little ice age glaciers in Linnédalen, Western Spitsbergen, Svalbard . Term project report, University Centre in Svalbard, 19 pp
- Bellin A., Majone B., Cainelli O., Alberici D. and Vill, F. (2016). A continuous coupled hydrological and water resources management model. Environmental Modelling & Software, 75, pp.176-192.
- Beniston M., and Stephenson D. B. (2004). Extreme climatic events and their evolution under changing climatic conditions, Global Planet. Change, 44, 1–9, doi:10.1016/j.gloplacha.2004.06.001.
- Beniston M., Diaz H.F. and Bradley R.S. (1997). Climatic change at high elevation sites: an overview. Clim. Change, 36, 233-251.
- Beniston M., Haeberli W., Hölzle M., and Taylor A. (1997). On the potential use of glacier and permafrost observations for verification of climate models. Annals of Glaciology 25, 400–406.
- Beniston M. (2010). Impacts of climatic change on water and associated economic activities in the Swiss Alps. Journal of Hydrology,
- Benn D.I. and Hulton N.R.J., (2010). An Excel TM spreadsheet program for reconstructing the surface profile of former mountain glaciers and ice caps. Computers and Geosciences, 36(5), pp.605–610. Available at: http://dx.doi.org/10.1016/j.cageo.2009.09.016.
- Bergström S. (1986). Recent developments in snowmelt-runoff simulation. Proceedings of the Symposium: Cold Regions Hydrology. University of Alaska-Fairbanks, Fairbanks, Alaska. American Water Resources Association, Bethesda Maryland, 461-468.
- Bergström S. (1992). The HBV model—its structure and applications. SMHI Reports RH, No. 4, Norrköping, Sweden.
- Blöschl G., Kirnbauer R. and Gutknecht D. (1991). Distributed snowmelt simulations in an Alpine catchment. I. Model evaluation on the basis of snow cover patterns. Water Resour. Res.,27(12), 3171–3179
- Blöschl G. (1999). Scaling issues in snow hydrology. Hydrol. Proc., 13, 2149-2175.
- Braithwaite R. J. (1980). Regional modelling of ablation in West Greenland, Grønlands geologiske undersøgelse, 98, 20 pp.
- Braithwaite R.J. (1984). Can the mass balance of a glacier be estimated from its equilibrium-line altitude? J. Glaciol., 30, 364–368.
- Braithwaite R. J. and Olesen O. B. (1988). Effect of glaciers on annual run-off, Johan Dahl Land, south Greenland. Journal of Glaciology34, 200–207.
- Braithwaite R. J. and Zhang Y. (1999). Modelling changes in glacier mass balance that may occur as a result of climate changes.Geografiska Annaler 81A, 489–496.
- Braithwaite R. J., Zhang Y. and Raper S. C. B. (2002). Temperature sensitivity of the mass balance of mountain glaciers and icecaps as a climatological characteristic, Zeitschrift fur Gletscherkunde und Glazialgeologie, 38, 35–61.
- Braun L. N., Weber M., and Schulz M. (2000). Consequences of climate change for runoff from Alpine regions. Annals of Glaciology 31, 19–25
- Brock B.W., Willis I.C. and Sharp M.J. (2000). Measurement and parameterization of albedo variations at Haut Glacier d'Arolla,Switzerland. J. Glaciol., 46(155), 675–688.
- Cannone N. (1999). Vegetazione e dinamica dei rock glaciers durante l'Olocene in Alta Valtellina (Italia). In: Orombelli G. (Ed.): Studi geografici e geologici in onore di Severino Belloni, 145-160.
- Carturan L. and Seppi R. (2007). Recent mass balance results and morphological evolution of Careser Glacier (Central Alps). Geografia Fisica e Dinamica Quaternaria, 30 (1), 33-42.
- Carturan L., Cazorzi F. and Dalla Fontana G. (2009). Enhanced estimation of glacier mass balance in unsampled areas by means of topographic data. Ann. Glaciol., 50(50), 37–46.
- Carturan L., (2010). Climate change effects on the cryosphere and hydrology of a high-altitude watershed. PhD diss., TeSAF - University of Padova, Italy
- Carturan L., Cazorzi F. and Dalla Fontana G. (2012). Distributed mass-balance modelling on two neighbouring glaciers in Ortles-Cevedale, Italy, from 2004 to 2009. Journal of Glaciology, 58(209), pp.467–486.

- Carturan L., Dalla Fontana G. and Borga M. (2012b). Estimation of winter precipitation in a high-altitude catchment of the Eastern Italian Alps: Validation by means of glacier mass balance observations. Geografia Fisica e Dinamica Quaternaria, 35(1), pp.37–48.
- Carturan L., Filippi R., Seppi R., Gabrielli P., Notarnicola C., Bertoldi L., Paul F., Rastener P., Cazorzi F., Dinale R., and Dalla Fontana G. (2013). Area and volume loss of the glaciers in the Ortles-Cevedale group (Eastern Italian Alps): Controls and imbalance of the remaining glaciers. Cryosphere, 7(5), pp.1339–1359.
- Carturan L., Baroni C., Carton A., Cazorzi F., Dalla Fontana G., Delpero C., Salvatore M. C., Seppi R., and Zanoner T. (2014): Reconstructing fluctuations of La Mare Glacier (Eastern Italian Alps) in the Late Holocene: new evidences for a Little Ice Age maximum around 1600 AD, Geogr. Ann. A, 96, 287–306.
- Carturan L., Cazorzi F., De Blasi F., Dalla Fontana G. (2015). Air temperature variability over three glaciers in the Ortles – Cevedale (Italian Alps): effects of glacier fragmentation , comparison of calculation methods , and impacts on mass balance modeling. The Cryosphere, 9(i), pp.1129–1146.
- Carturan, Luca. (2016). “Replacing Monitored Glaciers Undergoing Extinction: A New Measurement Series on La Mare Glacier (Ortles-Cevedale, Italy).” Journal of Glaciology, in press, doi:10.1017/jog.2016.107.
- Caussinus H. and Mestre O. (1996). New mathematical tools and methodologies for relative homogeneity testing’, Proceedings of the Seminar for Homogenization of Surface Climatological Data, Budapest, 6–12 October, pp. 63–82.
- Caussinus H. and Lyazrhi F. (1997). Choosing a linear model with a random number of change-points and outliers’, Ann. Inst. Stat. Math., 49, 761–775.
- Cazorzi F. and Dalla Fontana G. (1996). Snowmelt modeling by combining air temperature and a distributed radiation index. J. Hydrol., No 181, 169-187.
- Cazorzi F., Dalla Fontana G. and Carturan L. (2009). EISMODEL - Energy Index Snow Model. Manuale, 41 pp.
- CGI (Comitato Glaciologico Italiano) (1978–2011). Reports of the glaciological surveys, Geogr. Fis. Din. Quat., 1–34.
- Chandler J. (1999). Technical communication: effective application of automated digital photogrammetry. Earth Surface Processes and Landforms 24(1): 51 – 63.
- Chen J., and Ohmura A. (1990). On the influence of Alpine glaciers on runoff. In “Hydrology of mountainous regions I.” (H. Lang, and A. Musy, Eds.), Proceedings of two Lausanne Symposia, 1990: IAHS Publ. 193, 117–126.
- Chueca J., Julian A. and Lopez-Moreno J.I. (2007). Recent evolution (1981-2005) of the Maladeta glaciers, Pyrenees, Spain: extent and volume losses and their relation with climatic and topographic factors. Journal of Glaciology, 53 (183), 547-557.
- Citterio M., Diolaiuti G., Smiraglia C., D’Agata C., Carnielli T., Stella G., and Siletto G.B. (2007). The fluctuations of Italian glaciers during the last century: a contribution to knowledge about Alpine glacier changes, Geogr. Ann., 89, 164–182.
- Collins D.N., and Taylor, D.P. (1990). Variability of runoff from partially-glacierised Alpine basins. In “Hydrology of mountainous regions I.” (H. Lang, and A. Musy, Eds.), Proceedings of two Lausanne Symposia, 1990: IAHS Publ. 193, 365–372.
- Collins D. N. (2008). Climatic warming, glacier recession and runoff from Alpine basins after the Little Ice Age maximum, Ann. Glaciol., 48, 119–124.
- Cossart É. (2011). Mapping glacier variations at regional scale through equilibrium line altitude interpolation: GIS and statistical application in Massif des Écrins (French Alps). Journal of Geographic Information System, 3(3), p.224.
- Craddock J.M. (1979). Methods of comparing annual rainfall records for climatic purposes. Weather, 34(9), pp.332–346.
- Crawford N.H., and Linsley R.K. (1966). Digital Simulation in Hydrology: Stanford Watershed Model IV. Technical Report No. 39, Department of Civil Engineering, Stanford University, p. 210
- D'aleo J. and Easterbrook D. (2010). Multidecadal tendencies in ENSO and global temperatures related to multidecadal oscillations. Energy & Environment, 21(5), pp.437-460.
- Dadic R., Mott R., Lehning M. and Burlando P. (2010). Wind influence on snow depth distribution and accumulation over glaciers. J. Geophys. Res., 115(F1), F01012.
- Daly C., Neilson R.P. and Phillips D.L. (1994). A statistical-topographic model for mapping climatological precipitation over mountainous terrain. Journal of Applied Meteorology, 33, 140-158.
- Davidovich N. V. and Ananicheva M. D. (1996). Prediction of possible changes in glacio-hydrological characteristics under global warming: Southeastern Alaska, USA, J. Glaciol., 42, 407–412.
- Degli Esposti S., Norbiato D., Dinale R., Borga M. (2005). Valutazione di alcune componenti del bilancio idrologico in bacini di tipo alpino. In D’AgostinoV. and Carraio V. (eds.), Conoscere il sistema fiume in ambiente alpino, Pubblicazione del Corso di Cultura in Ecologia, Atti del 41.mo corso, Università di Padova: 64-74
- Desio A. (1967). I ghiacciai del Gruppo Ortles-Cevedale, Consiglio Nazionale delle Ricerche, Comitato Glaciologico Italiano, Milano, 875 pp.
- De Walle D.R. and Rango A. (2008). Principles of snow hydrology, Cambridge University Press, Cambridge
- Dubayah R., Dozier J. and Davis F. (1990). Topographic distribution of clear-sky radiation over the Konza Prairie, Kansas. Water Resour. Res., 26(4), 679–691
- Dyurgerov M. (2002). Glacier mass balance and regime: Data of measurements and analysis. Institute of Arctic and Alpine Research, University of Colorado. Occasional Paper No. 55.
- Easterling D.R. and Peterson T.C. (1995a). A new method for detecting and adjusting for undocumented discontinuities in climatological time series, Int. J. Climatol., 15, 369–377.
- Easterling D.R. and Peterson T.C. (1995b). The effect of artificial discontinuities on recent trends in minimum and maximum temperatures, Atmos. Res., 37, 19–26.
- Elder K., Dozier J. and Michaelsen J. (1991). Snow accumulation and distribution in an alpine watershed. Water Resour. Res., 27(7),1541–1552
- Erickson T.A., Williams M.W. and Winstral A. (2005). Persistence of topographic controls on the spatial distribution of snow in rugged mountain terrain, Colorado, United States. Water Resour. Res., 41(W4), W04014.
- Escher-Vetter H., and Reinwarth O. (1994). Two decades of runoff measurements (1974 to 1993) at the Pegelstation Vernagtbach/Oetztal Alps. Zeitschrift für Gletscherkunde und Glazialgeologie 30, 53–98.

- Escher-Vetter H. and Siebers M. (2007). Sensitivity of glacier runoff to summer snowfall events. Annals of Glaciology, 46(1), pp.309-315.
- Etzelmüller B., Hagen J.O. , Vatne G. , Ødegård R.S. and Sollid J.L. (1996). Glacier debris accumulation and sediment deformation influenced by permafrost, examples from Svalbard. Ann. Glaciol., 22, 53-62.
- European enviroment agency. (2009). Regional climate change and adaptation. The Alps facing the challenge of changing water resources. Report n 8,143 pp. ISSN 1725-9177.
- Eybergen F.A. (1986). Glacier snout dynamics and contempory push moraine formation at the Turtmannglacier, Switzerland. Proceedings. INQUA Symposium on Genesis and Lithology of Glacial Deposits, Amsterdam, p. 217-231.
- Farinotti D., Huss M., Bauder A. and Funk M. (2009). An estimate of the glacier ice volume in the Swiss Alps. Global and Planetary Change, 68, 225-231.
- Farinotti D., Usselmann S., Huss., Bauder A., and Funk M. (2012). Runoff evolution in the Swiss Alps: Projections for selected high-alpine catchments based on ENSEMBLES scenarios. Hydrological Processes, 26(13), pp.1909–1924.
- Farinotti, D., Pistocchi, A. and Huss, M. (2016). From dwindling ice to headwater lakes: could dams replace glaciers in the European Alps? Environmental Research Letters, 11(5), p.54022
- Fountain A., and Tangborn W. (1985). The effect of glaciers on streamflow variations. Water Resources Research 21, 579–586.
- Fountain A. G., and Walder J. S. (1998). Water flow through temperate glaciers. Reviews of Geophysics 36, 299–328.
- Fox A.J., Gooch M.J. (2001). Automatic DEM generation for Antarctic terrain. The Photogrammetric Record 17: 275 – 290.
- Frei C. and Schär C. (1998). A precipitation climatology of the Alps from high-resolution rain-gauge observations, Int. J. Climatol., 18, 873–900.
- Gardner A. S. and Sharp M. J. (2009). Sensitivity of net mass-balance estimates to near-surface temperature lapse rates when employing the degree-day method to estimate glacier melt, Ann. Glaciol.,50, 80–86.
- Gómez-Gutiérrez Á., de Sanjosé-Blasco J. J., de Matías-Bejarano J. and Berenguer-Sempere F. (2014): Comparing Two Photo-Reconstruction Methods to Produce High Density Point Clouds and DEMs in the Corral del Veleta Rock Glacier (Sierra Nevada, Spain). Remote Sensing, 6(6), 5407-5427.
- Goodison B., Louie P. and Yang D. (1998). WMO Solid Precipitation Measurement Intercomparison, Final Report. WMO/TD-No. 872, Instruments and Observing Methods No. 67, Geneva, 88 pp.
- Grayson R. and Blöschl G. (2001). Spatial patterns in catchment hydrology: observations and modelling, Cambridge University Press, Cambridge
- Greuell W. and Böhm R. (1998). 2m temperatures along melting midlatitude glaciers, and implications for the sensitivity of the mass balance to variations in temperature. J. Glaciol., 44(146), 9–20.
- Gruber S. and Hoelzle M. (2001). Statistical modelling of mountain permafrost distribution: local calibration and incorporation of remotely sensed data. Perm. Periglac. Proc., 12, 69-77.
- Gruber S. (2007). A mass-conserving fast algorithm to parameterize gravitational transport and deposition using digital elevation models. Water Resour. Res., 43(W6), W06412.
- Gullett D.W., Vincent L. and Malone L.H. (1991). Homogeneity Testing of Monthly Temperature Series. Application of Multiple-Phase Regression Models with Mathematical Change points, CCC Report No. 91–10. Atmospheric Environment Service, Downsview, Ontario. 47 pp.
- Gupta Hoshin V., Kling H., Yilmaz K.K., and Martinez G.F. (2009). Decomposition of the Mean Squared Error and NSE Performance Criteria: Implications for Improving Hydrological Modelling. Journal of Hydrology 377 (1–2). Elsevier B.V.: 80–91. doi:10.1016/j.jhydrol.2009.08.003.
- Gurtz J., Lang H., Verbunt M., Zappa M. (2005). The Use of Hydrological Models for the Simulation of Climate Change Impacts on Mountain Hydrology. In Global Change and Mountain Regions (A State of Knowledge Overview)., Huber U.M., Bugmann H.K.M., Reasoner M.A. (eds). Springer, Dordrecht, 343-354.
- Hebeler F. and Purves R.S. (2008). The influence of resolution and topographic uncertainty on melt modelling using hypsometric sub-grid parameterization. Hydrological processes, 22(19), pp.3965-3979.
- Haeberli W. (1973). Die Basis Temperatur del winterlichen Schneedecke als möglicher Indikator für die Verbreitung von Permafrost in den Alpen. Zeit. Gletsch. Glazialgeol., 9, 221-227.
- Haeberli W. (1979). Holocene push- moraines in alpine permafrost. Geogr. Ann., 61 A, 43-48.
- Haeberli W. and Hölzle M. (1995). Application of inventory data for estimating characteristics of and regional climate-change effects on mountain glaciers: A pilot study with the European Alps. Annals of Glaciology 21, 206–212. Russian translation in „Data of Glaciological Studies 82.“ pp. 116–124. Moscow.
- Haeberli W., Hölzle M., and Suter S. (1998). Into the second century of worldwide glacier monitoring: Prospects and strategies. A contribution to the International Hydrological Programme (IHP) and the Global Environment Monitoring System (GEMS). UNESCO — Studies and Reports in Hydrology 56.
- Haeberli W., Frauenfelder R., Hoelzle M. and Zemp M. (2003). Glacier mass balance bulletin, Tech. Rep. 7, Int. Assoc. of Hydrol. Sci., Univ. of Zurich, Zurich, Switzerland.
- Haeberli W. (2005). Modelling the Response of Mountain Glacier Discharge to Climate Warming. In Global Change and Mountain Regions (A State of Knowledge Overview)., Huber U.M., Bugmann H.K.M., Reasoner M.A. (eds). Springer, Dordrecht, 169-175
- Haeberli W. (2006). Integrated perception of glacier changes: a challenge of historical dimensions. In: Knight, P. G. (ed): Glacier Science and Environmental Change. Blackwell, Oxford, 423-430.
- Haeberli W., Hoelzle M., Paul F. and Zemp M. (2007). Integrated monitoring of mountain glaciers as key indicators of global climate change: the European Alps. Ann. Glaciol., 46(1), 150-160.
- Hamon W. R. (1961). Estimating potential evapotranspiration. Journal of the Hydraulics Division, ASCE. 87(HY3):107-120.
- Hanssen-Bauer I., Forland E. (1994). Homogenizing long Norwegian precipitation series J. Climate, 7, 1001-1013.
- Hanzer F., Helfricht K., Marke T., and Strasser U. (2016). Multilevel spatiotemporal validation of snow/ice mass balance and runoff modeling in glacierized catchments. Cryosphere, 10(4), pp.1859–1881.

- Hargreaves G. H. and Samani Z. A. (1982). Estimating potential evapotranspiration Engineering – Journal of Irrigation and Drainage Division, ASCE Vol 108 No. IR3 September 1982, Technical Notes pag 225-230.
- Hargreaves G. H. and Samani Z. A. (1985). Reference crop evapotranspiration from temperature. – Applied Engineering in Agriculture, 1 (2) pag. 96-99.
- Harris S.A. and Pedersen D.E. (1998). Thermal regimes beneath coarse blocky material. Perm. Periglac. Proc., 9, 107–120.
- Hock R. (1999). A distributed temperature-index ice- and snowmelt model including potential direct solar radiation. J. Glaciol., 45(149), 101–111
- Hock R. and Jansson P. (2005). Modeling glacier hydrology. In “Encyclopedia of Hydrological Sciences”, M.G. Anderson and J.J. McDonnel ed., Wiley, England, 2647-2655.
- Hock R. (2005). Glacier melt: a review of processes and their modelling. Progr. Phys. Geogr., 29, 362-391.
- Hock R., Jansson P. and Braun L.N. (2005). Modelling the Response of Mountain Glacier Discharge to Climate Warming. In Global Change and Mountain Regions (A State of Knowledge Overview)., Huber U.M., Bugmann H.K.M., Reasoner M.A. (eds). Springer, Dordrecht, 243-252
- Hoelzle M., (1992). Permafrost occurrence from BTS measurements and climatic parameters in the eastern Swiss Alps. Perm. Periglac. Proc., 3, 143-147.
- Hoelzle M., Haeberli W. and Keller F. (1993). Application of BTS-measurements for modelling permafrost distribution in the Swiss Alps. Cheng, G. (ed.) Sixth International Conference on Permafrost. Proceedings.South China University Technology Press, pp. 272-277.
- Hoelzle M., Wegmann M. and Krummenacher B. (1999). Miniature temperature dataloggers for mapping and monitoring of permafrost in high mountain areas: first experience from the Swiss Alps. Perm. Periglac. Proc.., 10, 113–124.
- Hood E., Williams M. and Cline D. (1999) - Sublimation from a seasonal snowpack at a continental, mid-latitude alpine site. Hydrological Pro cesses, 13, 1781-1797.
- Hopkinson C. and Young G. (1998). The effect of glacier wastage on the flow of the Bow river at Banff, Alberta, 1951–1993. Hydrological Processes 12,
- Humlum O. (1998). The climatic significance of rock glaciers. Perm. Periglac. Proc., 9, 375–395.
- Huss M., Bauder A., Funk M. and Hock R. (2008)a. Determination of the seasonal mass balance of four Alpine glaciers since 1865. Journal of Geophysical Research, 113, F01015.
- Huss M., Farinotti D., Bauder A., and Funk M. (2008)b. Modelling runoff from highly glacierized alpine drainage basins in a changing climate, Hydrol. Processes, 22(19), 3888–3902, doi:10.1002/hyp.7055.
- Huss M. (2011). Present and future contribution of glacier storage change to runoff from macroscale drainage basins in Europe. Water Resources Research, 47(7), pp.1–14.
- Huss M. and Farinotti D., (2012). Distributed ice thickness and volume of all glaciers around the globe. Journal of Geophysical Research: Earth Surface, 117(4), pp.1–10.
- Huss M., Zemp M., Joerg,P.C. and Salzmann,N. (2014). High uncertainty in 21st century runoff projections from glacierized basins. Journal of Hydrology, 510, pp.35-48.
- Immerzeel W.W., Kraaijenbrink P.D.A., Shea J.M., Shrestha A.B., Pellicciotti F., Bierkens M.F.P. and De Jong S.M. (2014). High-resolution monitoring of Himalayan glacier dynamics using unmanned aerial vehicles. Remote Sensing of Environment, 150, 93-103.
- IPCC (2007). Climate Change 2007: Contribution of Working Group I to the Fourth Assessment Report of the IPCC , Technical report, Solomon S, Qin D, Manning M, Chen Z, Marquis M, Averyt KB, Tignor M, Miller HL (eds). Cambridge University Press.
- IPCC (2013). Summary for Policymakers. In: Climate Change 2013: The Physical Science Basis. Contribution of Working Group I to the Fifth Assessment Report of the Intergovernmental Panel on Climate Change [Stocker, T.F., D. Qin, G.-K. Plattner, M. Tignor, S. K. Allen, J. Boschung, A. Nauels, Y. Xia, V. Bex and P.M. Midgley (eds.)]. Cambridge University Press, Cambridge, United Kingdom and New York, NY, USA.
- IPCC. (2014). Climate Change 2014: Synthesis Report. Contribution of Working Groups I, II and III to the Fifth Assessment Report of the Intergovernmental Panel on Climate Change [Core Writing Team, R.K. Pachauri and L.A. Meyer (eds.)]. IPCC, Geneva, Switzerland, 151 pp.
- James M.R., Robson S. (2012). Straightforward reconstruction of 3D surfaces and topography with a camera: accuracy and geoscience application. Journal of Geophysical Research - Earth Surface 117:F03017.
- Jansson P., Hock R. and Schneider T. (2003). The concept of glacier water storage: A review. Journal of Hydrology, 282, 116-129
- Jones P.D., Raper S.C.B., Bradley R.S., Diaz, H.F., Kelly P.M. and Wigley T.M.L. (1986). Northern Hemisphere Surface Air Temperature Variations: 1851–1984, J. Climate Appl. Meteorol., 25, 161– 179.
- Junghans N., Cullmann J. and Huss M. (2011). Evaluating the effect of snow and ice melt in an Alpine headwater catchment and further downstream in the River Rhine. Hydrological sciences journal, 56(6), pp.981-993.
- Kääb A., Funk M. (1999). Modelling mass balance using photogrammetric and geophysical data: a pilot study at Griesgletscher, Swiss Alps. Journal of Glaciology 45(151): 575 – 583.
- Kääb A., Girod L., Berthling I. (2013). Surface kinematics of periglacial sorted circles using structure-from-motion technology. The Cryosphere Discussions 7(6): 6043 – 6074.
- Karpilo R.D. Jr. (2009). Glacier monitoring techniques. Geological Monitoring. Geological Society of America: Boulder, Colorado.141 – 162.
- Kaser G., Fountain A. and Jansson P. (2003). A Manual for Monitoring the Mass Balance of Mountain Glaciers (IHP-VI, Technical Documents in Hydrology, No. 59), UNESCO, Paris.
- Kaser G. (2007). Mountain Glaciers, in Glacier Science and Environmental Change (ed. P. G. Knight), Blackwell Publishing, Malden, MA, USA.
- Kendall, M.G. (1970). Rank Correlation Methods, 2nd Ed., New York: Hafner.
- Khodakov V.G. (1975). Glaciers as water resource indicators of the glacial areas of the USSR, IAHS Publ. No. 104, 22–29.
- Kjellström E., Nikulin G., Hansson U., Strandberg G., and Ullerstig A. (2011). 21st century changes in the European climate: Uncertainties derived from an ensemble of regional climate model simulations, Tellus Ser. A, 63, 24–40, doi:10.1111/j.1600-0870.2010.00475.x.

- Klok E.J. and Oerlemans J. (2002). Model study of the spatial distribution of the energy and mass balance of Morteratschgletscher, Switzerland. J. Glaciol., 48, 505–18.
- Kobysheva N. and Naumova L. (1979). Works of the Main Geophysical Observatory, 425, Saint Petersburg, Russia.
- Konz M. and Seibert J. (2010). On the value of glacier mass balances for hydrological model calibration. Journal of hydrology, 385(1), pp.238-246.
- Krimmel R. (2001). Water, ice, and meteorological measurements at South Cascade Glacier, Washington, 2000–01 balance years. U.S. Geological Survey, Water-Resources Investigations Report 02–4165.
- Kuhn M., and Batlogg N. (1998). Glacier runoff in Alpine headwaters in a changing climate. In "Hydrology, water resources and ecology in headwaters." (K. U. Kovar, N. Tappeiner, E. Peters, and R. G. Craig, Eds.), pp. 78–88. IAHS Publication 248.
- La Chapelle E. (1961). Snow Layer Densification. Alta Avalanche Study Center, Project F, Progress Report No. 1, US Department of Agriculture Forest Service, Wasatch National Forest, 8 pp.
- Lane S.N., Richards K.S., Chandler J.H. (1993). Developments in Photogrammetry – the Geomorphological Potential. Progress in Physical Geography 17(3): 306 – 328.
- Lane S.N., Westaway R.M., Murray Hicks D. (2003). Estimation of erosion and deposition volumes in a large, gravel-bed, braided river using synoptic remote sensing. Earth Surface Processes and Landforms 28:249 – 271.
- Lang H. (1986). Forecasting meltwater runoff from snow-covered areas and from glacier basins. In "River flow modelling and forecasting." (D. A. Kraijenhoff, and J. R. Moll, Eds.), pp. 99–127. D. Reidel Publishing, Dordrecht
- Legates D.R. (1987). A climatology of global precipitation. Publications in Climatology, 40(1), Newark, Delaware, 85 pp.
- Lehning M., Löwe H., Ryser M. and Radeschall N. (2008). Inhomogeneous precipitation distribution and snow transport in steep terrain. Water Resour. Res., 44(W7), W07404.
- Lemke P., Ren J., Alley R.B., Allison I., Carrasco J., Flato G., Fujii Y., Kaser G., Mote P., Thomas R.H. and Zhangt T. (2007). Observations: Changes in Snow, Ice and Frozen Ground. In: Climate Change 2007: The Physical Science Basis. Contribution of Working Group I to the Fourth Assessment Report of the Intergovernmental Panel on Climate Change, Cambridge University Press: 337-383.
- Levermann A. and 12 others. (2012). Potential climatic transitions with profound impact on Europe. Review of the current state of six 'tipping elements of the climate system'. Climatic Change 110: 845-878.
- Lim M., Petley D.N., Rosser N.J., Allison R.J., Long A.J., Pybus D. (2005). Combined digital photogrammetry and time – of-flight laser scanning for monitoring cliff evolution. The Photogrammetric Record 20:109 – 129.
- Luce C.H., Tarboton D.G. and Cooley K.R. (1998). The influence of the spatial distribution of snow on basin-averaged snowmelt. Hydrol. Process., 12(10–11), 1671–1683
- Machguth H., Eisen O., Paul F. and Hoelzle M. (2006a). Strong spatial variability of snow accumulation observed with helicopter-borne GPR on two adjacent Alpine glaciers. Geophys. Res. Lett., Vol. 33, L13503.
- Machguth H., Eisen O., Paul F. and Hoelzle M. (2006b). Strong spatial variability of snow accumulation observed with helicopter-borne GPR on two adjacent Alpine glaciers. Geophys. Res. Lett.,33(13), L13503.
- Machguth H., Purves R.S., Oerlemans J., Hoelzle M. and Paul F. (2008). Exploring uncertainty in glacier mass balance modelling with Monte Carlo simulation. The Cryosphere, 2(2), p.191.
- Majone, B. Villa F., Deidda R., Bellin A. (2016). Impact of climate change and water use policies on hydropower potential in the south-eastern Alpine region. Science of the Total Environment, 543, pp.965–980. Available at: http://dx.doi.org/10.1016/j.scitotenv.2015.05.009.
- Mann, H.B. (1945). Nonparametric tests against trend, Econometrica, 13,245–259.
- Martin Y., Church M. (2004). Numerical modelling of landscape evolution: geomorphological perspectives. Progress in Physical Geography 28(3): 317–339.
- Martinec, J. (1975). Snowmelt-Runoff Model for Stream Flow Forecasts. Nord Hydrol. 6. 145-154.
- Meier M.F. and Tangborn W.V. (1961). Distinctive characteristics of glacier runoff. U.S. Geological Survey Professional Paper 424-B, 14–16.
- Meier M.F. and Bahr D.B. (1996). Counting glaciers: Use of scaling methods to estimate the number and size distribution of the glaciers on the world. In „Glaciers, ice sheets and volcanoes: A tribute to Mark F. Meier." (S. C. Colbeck, Ed.), pp. 1–120, CRREL Special Report 27.
- Mestre O. and Caussinus H. (2001). A Correction Model for Homogenisation of Long Instrumental Data Series, in Brunet, M. and López, D., Detecting and Modelling Regional Climate Change, Springer, pp13- 19
- Michlmayr G., Lehning M., Koboltschnig G., Holzmann H., Zappa M., Mott R. and Schöner W. (2008). Application of the Alpine 3D model for glacier mass balance and glacier runoff studies at Goldbergkees, Austria. Hydrological processes, 22(19), pp.3941-3949.
- Moore R.J. and Clarke R.T. (1981). A distribution function approach to Rainfall runoff Modeling – Water Resources Research, vol.17, No.5 pag. 1367-1382, 1981.
- Moore R.J. (1985). The probability-distributed principle and runoff production at point and basin scales - Hydrological Sciences Journal 30,2,6/1985 pag 273-297.
- Nash J.E. and Sutcliffe J.V. (1970). River flow forecasting through conceptual models part I — A discussion of principles. Journal of Hydrology, 10(3), pp.282–290.
- Norbiato D., Borga M., Merz R., Blöschl G., Carton A. (2009). Controls on event runoff coefficients in the eastern Italian Alps. J. Hydrol., 375, 312-325.
- Nye, J.F., 1952. The mechanics of glacier flow. Journal of Glaciology 2, 82–93.
- Oerlemans J. (1994). Quantifying global warming from the retreat of glaciers. Science 264, 243–245.
- Oerlemans J., Anderson B., Hubbar, A., Huybrechts P., Johannesson T., Knap W. H., Schmeits M., Stroeven A. P., van de Wal R. S. W., Wallinga J. and Zuo Z. (1998). Modelling the response of glaciers to climate warming. Climate Dynamics 14, 261–214.
- Oerlemans J. (2001). Glaciers and climate change. Balkema Publishers, Rotterdam.
- Oke T.R. (1987). Boundary layer climates. Routledge Press, London
- Olafsdottir K.B., Geirsdóttir Á., Miller G.H. and Larsen D.J. (2013). Evolution of NAO and AMO strength and cyclicity derived from a 3-ka varve-thickness record from Iceland. Quaternary Science Reviews, 69, pp.142-154.

- Østrem G. (1964). Ice-cored moraines in Scandinavia. Geogr. Ann., 46A, 282–337.
- Østrem G. and Brugman M. (1991). Glacier mass-balance measurements, a manual for field and office work. N.H.R.I. Science Report, 4, 224 pp.
- Paul F., Kääb A., Maisch M., Kellenberger T.W. and Haeberli W. (2004). Rapid disintegration of Alpine glaciers observed with satellite data. Geophysical Research Letters, 31, L21402.
- Paul F., Kääb A., Haeberli W. (2007). Recent glacier changes in the Alps observed from satellite: consequences for future monitoring strategies. Glob. Planet. Change, 56(1–2), 111–122.
- Paul F. and Haeberli W. (2008). Spatial variability of glacier elevation changes in the Swiss Alps obtained from two digital elevation models. Geophysical Research Letters, 35, L21502.
- Paul F., Frey H., Le Bris R. (2011). A new glacier inventory for the European Alps from Landsat TM scenes of 2003: challenges and results. Annals of Glaciology, 52 (59), 144-152
- Pellicciotti F., Brock B., Strasser U., Burlando P., Funk M., Corripio J. (2005). An enhanced temperature-index glacier melt model including the shortwave radiation balance: development and testing for Haut Glacier d'Arolla, Switzerland. J. Glaciol., 51, 573-587.
- Peterson T.C., Easterling D.R., Karl T.R., Groisman P., Nicholls N., Plummer N., Torok S., Auer I., Böhm R., Gullett D., Vincent L., Heino R., Tuomenvirta H., Mestre, O., Szentimrey T., Salinger J., Førland E.J., Hanssen-Bauer I., Alexandersson H., Jones P., Parker D. (1998). Homogeneity adjustments of in situ atmospheric climate data: a review, Int. J. Climatol., 18, 1493-1517.
- Petersen L., Pellicciotti F., Juszak I., Carenzo M., Brock B. (2013). Suitability of a constant air temperature lapse rate over an Alpine glacier: testing the Greuell and Böhm model as an alternative. Ann. Glaciol., 54(63), 120-130.
- Pettitt AN (1979). A non-parametric approach to the change-point problem. Appl.Statist., 28, 126–135
- Piermattei L., Carturan L., Guarnieri A. (2015). Use of terrestrial photogrammetry based on structure from motion for mass balance estimation of a small glacier in the Italian Alps. Earth Surface Processes and Landforms, p.n/a–n/a
- Piermattei L., L. Carturan, F. de Blasi, P. Tarolli, G. Dalla Fontana, A. Vettore and N. Pfeifer (2016). Analysis of glacial and periglacial processes using structure from motion. "ESURFD doi:10.5194/esurfd-3-1345-2015.
- Plummer N., Lin Z., Torok S. (1995). Trends in the diurnal temperature range over Australia since 1951, Atmos. Res., 37, 79–86.
- Potter K.W. (1981). Illustration of a new test for detecting a shift in mean in precipitation series, Mon. Wea. Rev., 109, 2040–2045.
- Quadrelli R., Lazzeri M., Cacciamani C., and Tibaldi S. (2001). Observed winter Alpine precipitation variability and links with large-scale circulation patterns, Clim. Res., 17, 275–284, doi:10.3354/cr017275.
- Rhoades D.A. and Salinger M.J. (1993). Adjustment of temperature and rainfall records for site changes, Int. J. Climatol., 13, 899–913.
- Rolstad C., Haug T., Denby B. (2009). Spatially integrated geodetic glacier mass balance and its uncertainty based on geostatistical analysis: application to the western Svartisen ice cap, Norway. Journal of Glaciology, Vol. 55, No. 192
- Rott H. and Siegel A. (1999). Analysis of mass movement in alpine terrain by means of SAR interferometry. IEEE Geoscience and Remote Sensing Symposium, pp. 1933–1936. IGARSS'99.
- Saghafian B. and Bondarabadi S.R. (2008). Validity of regional rainfall spatial distribution methods in mountainous areas. Journal of Hydrologic Engineering, 13 (7), 531-540.
- Salvatore M.C., Zanoner T., Baroni C., Carton A., Banchieri F.A., Viani C., Giardino M., and Perotti L. (2015). The State of Italian Glaciers: A Snapshot of the 2006-2007 Hydrological Period. Geografia Fisica E Dinamica Quaternaria 38 (2): 175–98. doi:10.4461/GFDQ.2015.38.16.
- Schär C., Vidale P. L., Lüthi D., Frei C., Häberli C., Liniger M. A., and Appenzeller C. (2004). The role of increasing temperature variability in European summer heatwaves, Nature, 427, 332–336.
- Sevruk B. (1982). Methods of correction for systematic error in point precipitation measurement for operational use. Operational Hydrology Report 21 (WMO No. 589).
- Sevruk B. (1985). Correction of precipitation measurements: Swiss experience. Workshop on the correction of precipitation measurements, 1-3 April 1985, Zurich.
- Sevruk B. and Zahlavova L. (1994) - Classification system of precipitation gauge site exposure: evaluation and application. International Journal of Climatology, 14, 681-689.
- Shea J. M. and Moore R.D. (2010). Prediction of spatially distributed regional-scale fields of air temperature and vapor pressure over mountain glaciers, J. Geophys. Res., 115, D23107.
- Singh P. and Kumar N. (1997). Impact assessment of climate change on the hydrological response of a snow and glacier melt runoff dominated Himalayan river. Journal of Hydrology 193, 316–350.
- Small E.E. (1995). Hypsometric forcing of stagnant ice margins: pleistocene valley glaciers, San Juan Mountains, Colorado, Geomorphology, 14, 109–121.
- Smiraglia C., Sergio R., D Agata C, and Maragno D. (2015). The New Italian Glacier Inventory : A Didactic Tool for a Better Knowledge of the Natural Alpine Environment, no. June: 81–94. doi:10.4458/5196-08.
- Solbø S. and Storvold R. (2013). Mapping svalbard glaciers with the cryowing uas. ISPRS-International Archives of the Photogrammetry, Remote Sensing and Spatial Information Sciences XL-1 W, 2, 373-377,
- Solomon S. and 30 others. (2007). Technical Summary. In: Climate Change 2007: The Physical Science Basis. Contribution of Working Group I to the Fourth Assessment Report of the Intergovernmental Panel on Climate Change [Solomon S. and 7 others (eds.)], Cambridge University.
- Solow A. (1987). Testing for climatic change: an application of the two-phase regression model, J. Climate Appl. Meteorol., 26, 1401–1405.
- Stenborg T. (1970). Delay of runoff from a glacier basin. Geografiska Annaler 52A, 1–30.
- Stojic M., Chandler J., Ashmore P.E., Luce J. (1998). The assessment of sediment transport rates by automated digital photogrammetry. Photogrammetric Engineering and Remote Sensing 64(5): 387 – 395.
- Sturm M. and Wagner A.M. (2010). Using repeated patterns in snow distribution modeling: an Arctic example. Water Resour. Res., 46(W12), W12549.
- Szentimrey T. (1996). Statistical procedure for joint homogenization of climatic time series, Proceedings of the Seminar for Homogenization of Surface Climatological Data, Budapest, Hungary, pp. 47–62.

- Szentimrey T. (1999). Multiple Analysis of Series for Homogenization (MASH), Proceedings of the Second Seminar for Homogenization of Surface Climatological Data, Budapest, Hungary; WMO, WCDMP-No. 41, pp. 27-46.
- Szentimrey T. (2000). Multiple Analysis of Series for Homogenization (MASH). Seasonal application of MASH (SAM), Automatic using of Meta Data, Proceedings of the Third Seminar for Homogenization of Surface Climatological Data, Budapest, Hungary.
- Tonkin T.N., Midgley N.G., Graham D.J., Labadz J.C. (2014). The potential of small unmanned aircraft systems and structure-from-motion for topographic surveys: A test of emerging integrated approaches at Cwm Idwal, North Wales. Geomorphology, 226, 35-43.
- Van der Linden P., Mitchell JFB. (2009). ENSEMBLES: Climate Change and Its Impacts: Summary of Research and Results From the ENSEMBLES Project . Met Office Hadley Centre: UK; 160.
- Verbunt M., Gurtz J., Jasper K., Lang H., Warmerdam P., Zappa M. (2003). The hydrological role of snow and glaciers in alpine river basins and their distributed modeling. Journal of Hydrology 282 (2003) 36–55.
- Verhoeven G., Doneus M., Bries C., Vermeulen F. (2012). Mapping by matching: a computer vision-based approach to fast and accurate georeferencing of archaeological aerial photographs. Journal of Archaeological Science 39: 2060 – 2070.
- Vincent L. (1998). A technique for the identification of inhomogeneities in Canadian temperature series, J. Climate, 11, 1094–1104.
- Welch R., Howarth P.J. (1968). Photogrammetric measurements of glacial landforms. The Photogrammetric Record 6: 75 – 96.
- WGMS (World Glacier Monitoring Service) 1989: World glacier inventory – Status 1988, edited by: Haeberli, W., Bösch, H., Scherler, K., Østrem, G., and Wallén, C. C., IAHS (ICSI) / UNEP / UN- ESCO, World Glacier Monitoring Service, Zurich, Switzerland, 458 pp., 1989.
- WGMS (World Glacier Monitoring Service). (2008). Fluctuations of Glaciers 2000-2005 (Vol. IX), edited by: Haeberli, W., Zemp, M., Kääb A., Paul F., Hoelzle, M., ICSU (FAGS) / IUGG (IACS) / UNEP / UNESCO / WMO, World Glacier Monitoring Service, Zurich, Switzerland, 266 pp., 2008.
- WGMS (World Glacier Monitoring Service). (2011). Glacier Mass Balance Bulletin No. 11 (2008–2009), edited by: Zemp M., Nussbaumer S.U., Gärtner-Roer I., Hoelzle M., Paul F., Haeberli W., ICSU (WDS) / IUGG (IACS) / UNEP / UNESCO/ WMO, World Glacier Monitoring Service, Zurich, Switzerland, 102 pp.
- WGMS (World Glacier Monitoring Service). (2012). Fluctuations of Glaciers 2005-2010 (Vol. X). Zemp M. and 7 others (eds.), ICSU (WDS) / IUGG (IACS) / UNEP / UNESCO / WMO, World Glacier Monitoring Service, Zurich, Switzerland: 336 pp.
- Whitehead K., Moorman B.J., Hugenholtz C.H. (2013). Brief communication: Low-cost, on-demand aerial photogrammetry for glaciological measurement. The Cryosphere, 7(6), 1879-1884.
- Willis I.C., Anold N.S., Brock B.W. (2002). Effect of snowpack removal on energy balance, melt and runoff in a small supraglacial catchment. Hydrological Processes 16, 2721–2749.
- Yang D., Goodison B.E., Metcalfe J.R., Golubev V.S., Bates R., Pangburn T., Hanson C.L. (1998) Accuracy of NWS 8-inch standard non-recording precipitation gauge: results of WMO intercomparison. Journal of Atmospheric and Oceanic Technology, 15, 54-68.
  Yang D., Kane D.L., Hinzman L.D., Goodison B.E., Metcalfe J.R., Louie P.Y.T., Levesley G.H., Emerson D.G., Hanson C.L. (2000) An evaluation of the Wyoming gauge system for snowfall measurement. Water Resources Research, 36, 2665-2677.
- Zanon G. (1982). Recent glaciological research in the Ortles-Cevedale region (Italian Alps), GFDQ – Geografia Fisica e Dinamica Quaternaria, 5, 75–81.
- Zanon G. (1991) – Vent'anni di progresso dei ghiacciai 1965-1985, pp. 153–165. In Pinna M. (a cura di) - Le variazioni climatiche recenti(1800-1990) e le prospettive per il XXI secolo Atti del Convegno, Roma, 5-6 aprile 1990, Memorie Società Geografica Italiana, 46.
- Zanon G. (1992). Venticinque anni di bilancio di massa del ghiacciaio del Careser, 1966–67/1990–91, Geogr. Fis. Din. Quat., 15, 215–220.
- Zanoner T., Carton A., Seppi R., Carturan L., Baroni C., Salvatore M.C., Zumiani M. (2017). Little Ice Age mapping as a tool for identifying hazard in the paraglacial environment: The case study of Trentino (Eastern Italian Alps), In Geomorphology, Volume 295, 2017, Pages 551-562, ISSN 0169-555X,
- Zemp M., Paul F., Hoelzle M., Haeberli W. (2008). Glacier fluctuations in the European Alps 1850-2000: an overview and spatio-temporal analysis of available data. In: Orlove, B., Wiegandt, E., Luckman B. (eds.): The darkening peaks: Glacial retreat in scientific and social context. University of California Press, 152-167.

# Appendix

*Table 45: Temperature and precipitation raw series. With "+" the considered year has more than half of the data as available. With "-" the considered year has more than half of the data as gaps.*

| Temperature series | | | | Precipitation series | | | | | |
|---|---|---|---|---|---|---|---|---|---|
| *Years* | *Careser* | *Peio* | *Mendola* | *Careser* | *Peio* | *Malè* | *Tonale* | *Mendola* | *Years* |
| 1921 | | | | | + | + | | + | 1921 |
| 1922 | | | | | + | + | | + | 1922 |
| 1923 | | | | | + | + | + | + | 1923 |
| 1924 | | | | | + | + | + | + | 1924 |
| 1925 | | + | | | + | + | + | + | 1925 |
| 1926 | | + | + | | + | + | + | + | 1926 |
| 1927 | | + | + | | + | + | + | + | 1927 |
| 1928 | | + | + | | + | + | + | + | 1928 |
| 1929 | | + | + | | + | + | + | + | 1929 |
| 1930 | | + | + | + | + | + | + | + | 1930 |
| 1931 | | + | + | + | + | + | + | + | 1931 |
| 1932 | | + | + | + | + | + | + | + | 1932 |
| 1933 | | + | + | + | + | + | + | + | 1933 |
| 1934 | | + | + | + | + | + | + | + | 1934 |
| 1935 | | + | + | + | + | + | + | + | 1935 |
| 1936 | | + | + | + | + | + | + | + | 1936 |
| 1937 | | + | + | + | + | + | + | + | 1937 |
| 1938 | | + | + | + | + | + | + | + | 1938 |
| 1939 | | + | + | + | + | + | + | + | 1939 |
| 1940 | + | + | + | + | + | + | + | + | 1940 |
| 1941 | + | + | + | + | + | + | + | + | 1941 |
| 1942 | + | + | + | + | + | + | + | + | 1942 |
| 1943 | + | + | + | + | + | + | + | + | 1943 |
| 1944 | + | + | + | + | + | + | + | + | 1944 |
| 1945 | + | + | - | + | + | + | - | + | 1945 |
| 1946 | - | + | - | + | + | + | + | + | 1946 |
| 1947 | - | + | - | - | + | + | + | + | 1947 |
| 1948 | - | + | - | + | + | + | + | + | 1948 |
| 1949 | + | + | - | + | + | + | + | + | 1949 |
| 1950 | + | + | - | + | + | + | + | + | 1950 |
| 1951 | + | + | - | + | + | + | + | + | 1951 |
| 1952 | + | + | - | + | + | + | + | + | 1952 |
| 1953 | + | + | - | + | + | + | + | + | 1953 |
| 1954 | + | + | - | + | + | + | + | + | 1954 |
| 1955 | + | + | + | + | + | + | + | + | 1955 |
| 1956 | + | + | + | + | + | + | + | + | 1956 |
| 1957 | + | + | + | + | + | + | + | + | 1957 |
| 1958 | + | + | + | + | + | + | + | + | 1958 |
| 1959 | + | + | + | + | + | + | + | + | 1959 |
| 1960 | + | + | + | + | + | + | + | + | 1960 |

| | | | | | | | | | |
|---|---|---|---|---|---|---|---|---|---|
| 1961 | + | + | + | + | + | + | + | + | 1961 |
| 1962 | + | + | + | + | + | + | + | + | 1962 |
| 1963 | + | - | + | + | + | + | + | + | 1963 |
| 1964 | + | - | - | + | + | + | + | + | 1964 |
| 1965 | + | - | + | + | + | + | + | + | 1965 |
| 1966 | + | + | + | + | + | + | + | + | 1966 |
| 1967 | + | + | + | + | + | + | + | + | 1967 |
| 1968 | + | + | + | + | + | + | + | + | 1968 |
| 1969 | + | + | + | + | + | + | - | + | 1969 |
| 1970 | + | + | + | + | + | + | + | + | 1970 |
| 1971 | + | + | + | + | + | + | - | + | 1971 |
| 1972 | + | + | + | + | + | + | - | + | 1972 |
| 1973 | + | + | + | + | + | + | + | + | 1973 |
| 1974 | + | + | + | + | + | + | + | + | 1974 |
| 1975 | + | + | + | + | + | + | + | + | 1975 |
| 1976 | + | + | + | + | + | + | + | + | 1976 |
| 1977 | + | + | + | + | + | + | + | + | 1977 |
| 1978 | + | + | + | + | + | + | + | + | 1978 |
| 1979 | + | + | + | + | + | + | + | + | 1979 |
| 1980 | + | + | + | + | + | + | + | + | 1980 |
| 1981 | + | + | + | + | + | + | + | + | 1981 |
| 1982 | + | + | + | + | + | + | + | + | 1982 |
| 1983 | + | + | + | + | + | + | + | + | 1983 |
| 1984 | + | + | + | + | + | + | + | + | 1984 |
| 1985 | + | + | + | + | + | + | + | + | 1985 |
| 1986 | + | + | + | + | + | + | + | + | 1986 |
| 1987 | + | + | + | + | + | + | + | + | 1987 |
| 1988 | + | + | + | + | + | + | + | + | 1988 |
| 1989 | + | + | + | + | + | + | + | + | 1989 |
| 1990 | + | + | + | + | + | + | + | + | 1990 |
| 1991 | + | + | + | + | + | + | + | + | 1991 |
| 1992 | + | + | + | + | + | + | + | + | 1992 |
| 1993 | + | + | + | + | + | + | - | + | 1993 |
| 1994 | + | + | + | + | + | + | - | + | 1994 |
| 1995 | + | + | + | + | + | + | - | + | 1995 |
| 1996 | + | + | + | + | + | + | - | + | 1996 |
| 1997 | + | + | + | + | + | + | + | + | 1997 |
| 1998 | + | + | + | + | + | + | + | + | 1998 |
| 1999 | + | + | + | + | + | + | + | + | 1999 |
| 2000 | + | + | + | + | + | + | + | + | 2000 |
| 2001 | + | + | + | + | + | + | + | + | 2001 |
| 2002 | + | + | + | + | + | + | + | + | 2002 |
| 2003 | + | + | + | + | + | + | + | + | 2003 |
| 2004 | + | + | + | + | + | + | + | + | 2004 |
| 2005 | + | + | + | + | + | + | + | + | 2005 |
| 2006 | + | + | + | + | + | + | + | + | 2006 |
| 2007 | + | + | + | + | + | + | + | + | 2007 |
| 2008 | + | + | + | + | - | + | + | + | 2008 |

| | | | | | | | | | |
|---|---|---|---|---|---|---|---|---|---|
| 2009 | + | + | + | + | + | + | + | + | 2009 |
| 2010 | + | + | + | + | + | + | + | + | 2010 |
| 2011 | + | - | + | + | - | + | + | + | 2011 |
| 2012 | + | + | + | + | + | + | + | + | 2012 |
| 2013 | + | + | + | + | + | + | + | + | 2013 |
| 2014 | + | + | + | + | + | + | + | + | 2014 |
| 2015 | + | + | + | + | + | + | + | + | 2015 |

## Acknowledgements

I wish to thank all people that helped me during these PhD years concerning both research activities and my personal life.
Special thanks to Luca Carturan, which taught and helped me a lot about the different parts of my research program, also considering the field activities on La Mare and Careser glaciers. I want to thank Federico Cazorzi that was a very good teacher to develop a technical *forma mentis* and because he had an indispensable role concerning the development of the glacio-hydrological model. I thank Marco Borga's research group for the support and the suggestions on my PhD, and Alberto Carton's group for having made available some geomorfological datasets. A particular thought for my colleagues of Geomatica laboratory for suggestions and everyday. Finally, thanks to Giancarlo Dalla Fontana for his advice and for the supervision of my research.
I wish to thank the different organizations that supported this research; Meteotrentino for meteorological archive, PAT archive for hydrometric dataset and ENEL archive for meteorological and hydrometric old analogic measurements before the 1960s.
Thanks to Carlo Baroni and Roberto Dinale for their revision of my work.

I want to thank my family and friends for all their support.

Spinea, January 11, 2018

Fabrizio De Blasi